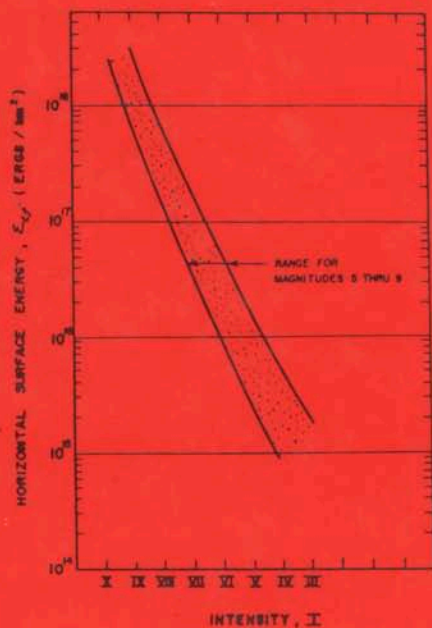


EARTHQUAKE ENGINEERING

Mechanism, Damage Assessment and Structural Design

(Second & Revised Edition)

S. F. Borg



World Scientific

EARTHQUAKE ENGINEERING

This page is intentionally left blank

EARTHQUAKE ENGINEERING

Mechanism, Damage Assessment and Structural Design

S. F. Borg

*Professor of Civil Engineering
Stevens Institute of Technology
Hoboken, New Jersey, USA*

(Second & Revised Edition)



World Scientific

Singapore • New Jersey • Hong Kong

Published by

World Scientific Publishing Co. Pte. Ltd.
P. O. Box 128, Farrer Road, Singapore 9128

U. S. A. office: World Scientific Publishing Co., Inc.
687 Hartwell Street, Teaneck NJ 07666, USA

EARTHQUAKE ENGINEERING — (Second & Revised Edition)

Copyright © 1988 by World Scientific Publishing Co Pte Ltd.

All rights reserved. This book, or parts thereof, may not be reproduced in any form or by any means, electronic or mechanical, including photocopying, recording or any information storage and retrieval system now known or to be invented, without written permission from the Publisher.

ISBN 9971-50-435-9

Printed in Singapore by General Printing Services Pte. Ltd.

*This book is for
Audrey and Rebecca Lynne
and for
Daniel*

This page is intentionally left blank

PREFACE AND INTRODUCTION TO THE SECOND EDITION

This book is an expanded version of the earlier (first edition) text, *Earthquake Engineering — Damage Assessment and Structural Design*, here called *EE-DA&SD*. Every chapter of the first edition has been altered and enlarged and new chapters have been added to include work done by the author and some of his graduate students, following publication of *EE-DA&SD*.

Some remarks concerning the modus operandi of the two texts may be in order.

In accordance with currently accepted methods of scientific inquiry, the procedures used in *EE-DA&SD* and in this book for developing the rational earthquake engineering theory are as follows:

1. Key experiments are performed and quantitative data from these are collected. (In the earthquake engineering field there are two basic sets of quantitative experimental data — (a), the accelerogram record and (b) the isoseismal contour chart).
2. Generalized relations (as simple and straightforward as possible) are looked for to describe the quantitative data of (1a) and (1b) above. The relations or equations or charts or invariants are given in terms of specifically earthquake engineering parameters — i.e., variables that are characteristic of earthquake engineering phenomena and very likely apply only to these phenomena. (It will be seen that such parameters and such invariants and resulting relations are, in fact, the bases for the rational theory of the text).
3. In addition to generalizing the experimental behaviour of (1) above, the relations should *predict* new quantitative results that may be verified experimentally. (It will be seen that a number of new quantitative relations are predicted using the new rational theory and these can be checked either in the field or in laboratories).

The coverage of *EE-DA&SD* included the entire earthquake event starting with the onset of the earthquake (the mechanism), then proceeding to the transmission of earthquake energy to the ground surface, then the damage assessment and finally the structural design.

The fundamental point of view of *EE-DA&SD* (and also of the present text) is that energy is the most important parameter of the entire earthquake happening. Energy is released by some underground mechanism (and this is the earthquake), energy causes the damage to structures and energy is the basic input in the structural design process.

Secondly, as noted earlier, it was accepted as a given fact that two basic sources of quantitative experimental (i.e. field) data were available and these are the foundations upon which the rational theory of earthquake engineering must be built.

The two sets of experimental data were:

- a) The accelerogram which, physically, must be related in some way to the variation, with *time*, of the ground energy at a *point* on the surface of the earth in the earthquake field.
- b) The isoseismal contour map which, physically, must be related in some way to the variation, with *distance*, of the ground energy over the *entire surface* of the earth affected by the earthquake.

The rational quantitative theories of *EE-DA&SD* were developed along three lines:

1. A closed-form mathematical solution for a theoretical mechanism was obtained, based upon a similarity solution for a plate rupture instability and an assumed underground superplastic-type material.
2. and 3. The accelerogram records and isoseismal maps referred to in (a) and (b) above were woven into a unified, comprehensive theory of energy transmission — timewise and spacewise — over the surface of the earthquake field.

The theory was then extended to include the major problems of damage assessment and structural design, both of which are developed in terms of the previously introduced isoseismal and accelerogram invariants and parameters. Various special topics related to these were also considered, including a brief discussion of model testing.

The present edition includes a postulated computation for an actual earthquake field, based upon a recent comprehensive geological test program, which can be related directly to the theoretical rupture instability mechanism. Because this analysis was not included in *EE-DA&SD* and because the author feels that

the rupture instability mechanism now has some physical justification for its derivational form, it was decided to expand the sub-title of the text. Hence, as indicated, the inclusion of the word *Mechanism* more completely describes the scope of the material contained herein.

One additional concept which is of fundamental importance in establishing a rational quantitative theory of earthquake engineering is the assumption of 'averageness' or the 'average condition'. Thus assumption lies at the base of all the various theories included in the comprehensive treatment presented — including the rupture instability mechanism. An especially illuminating discussion of this 'averageness' requirement occurs in Chapter 10, Section E in which the anomalous behaviours of the very destructive September 19, 1985 Mexican earthquake are directly related to this characteristic property. The application presented there emphasizes the important effect of deviating from averageness on the magnification or diminution of earthquake damage and how this relates, quantitatively and rationally, to the energy approach of this text.

Indeed, the key words in describing the intended coverage of the earlier and present texts are *rational* and *quantitative*. It was taken for granted that engineers deal with *numbers*. Qualitative materials, if these were to be included, were of secondary and only supportive importance. The basic requirement was that numbers must be generated in all phases of the theory and applications.

Furthermore, the theories must be rational. Certainly some reliance was and will continue to be placed upon engineering and physical intuitive considerations. But in all cases these must be reasonable and must lead to testable results that could be used by and would be of value to the average well-trained professional in the earthquake engineering field — including engineers, architects, code and specification writers and insurance and related workers.

The crucible for the definitive testing of theories and predictions in earthquake engineering is the earthquake itself. Some portions of a theory and possibly its predictions may perhaps be tested in laboratories and suggestions along these lines are included in later chapters of the book. But the difficulties of duplicating the required ground and energy absorption conditions of actual full size structures would seem to introduce problems related to model-prototype scaling that leave open to serious doubts the pertinence of the data generated by laboratory tests of reduced-size models.

A principal testing and checking procedure used in this text is the after-the-fact analyses and comparisons between results predicted by the derived rational theory and those actually obtained due to earthquakes. Furthermore, because an earthquake is one of nature's more traumatic experiences and because the perceptions of the physical and human damage done by an earthquake are quickly altered by the healing affects of time, the major sources of some actual earth-

quake damage data used in this text were the on-the-spot reports prepared by responsible professional major news gathering services all over the world. In effect, it was assumed that a description of the human and physical response prepared by reporters at the scene within hours after the onset of an earthquake, when this is available, is at least as reliable as that reported by a committee of observers who visit the site and question the inhabitants days and perhaps weeks after the actual event.

Wherever possible the results and predictions of the new theory were tested against quantitative earthquake data. Also, as was pointed out in *EE-DA&SD*, an essential step in the application of the theory is the calibration of various fundamental (and uniquely earthquake engineering) parameters. This is an ongoing process, quite common in all fields of engineering (although few of these encounter the evaluation difficulties of earthquake engineering) and work along these lines forms a part of the extension of materials included herein.

There is no doubt whatever in the author's mind that as more and more data are collected, the various equations, design charts and other engineering tools derived here will become more accurate, thereby enabling engineers and the other earthquake engineering professionals to use the theories with greater accuracy and confidence.

However, by the same token, the author suggests that even at this point, the new rational quantitative theories can be applied by these same professionals, subject to an awareness of the approximations involved in the applications. As most practicing engineers realize, approximations — some small and some large — occur in all engineering designs and analyses.

The author takes this opportunity to thank several of his graduate students who prepared reports on various aspects of the overall earthquake engineering problem using the rational methods described in this book. Some of these reports contained data and results that extend and expand the coverage of *EE-DA&SD*. Acknowledgement of this assistance is made at the appropriate points in the text.

CONTENTS

| | |
|--|-----|
| Preface and Introduction to the Second Edition | vii |
| Chapter 1 A Tensile Rupture Instability Similarity Earthquake Mechanism | 1 |
| Chapter 2 The Canonical Accelerogram and Its Parameters | 29 |
| Chapter 3 The Canonical Iseismal Chart and Its Parameters | 45 |
| Chapter 4 The Earthquake Engineering Damage Assessment and Structural Design Charts and Curves | 61 |
| A) The Temporal Variation of Energy at a Point | 65 |
| B) The Spacewise Variation of Energy Over the Entire Field | 67 |
| C) The Magnitude — $\Sigma(IS)_f - S_f$ — Geology Chart | 70 |
| D) The Magnitude-Intensity-Distance (MID) Chart | 84 |
| E) The Intensity — $\Sigma(a\Delta t)_f - t_f$ — Geology Chart | 86 |
| F) The Energy-Intensity Compatibility Relation | 88 |
| Chapter 5 Efficiency-Focal Depth and Figure 4.5 | 92 |
| Chapter 6 Superposition of Canonical Accelerograms | 100 |
| Chapter 7 Superposition of Canonical Iseismal Contour Maps | 126 |
| Chapter 8 Approximate Analytical Damage (Intensity Number) Assessment Procedures | 133 |

| | | |
|-------------------|--|------------|
| Chapter 9 | Special Topics in Earthquake Structural Engineering | 139 |
| | A) Equivalent or Effective Length and Equivalent or Effective Base Area | 140 |
| | B) Length-of-Time Effect for Tall Buildings | 142 |
| | C) Damping of Vibrational Building Oscillations Due to an Earthquake | 144 |
| | D) Model Scaling Requirements | 146 |
| Chapter 10 | Some Non-Structural Applications of the Rational Theory | 155 |
| | A) An Approximate Theoretical Predicted Iseisml Map for the Predicted $M = 6$ Parkfield Earthquake of 1988 | 156 |
| | B) The Earthquake-Code Zone of Bangladesh — A Comparison Analysis | 159 |
| | C) An Approximate Theoretical Method for Analyzing Rock Slope Stability Due to Earthquakes | 170 |
| | D) The Mexican Earthquake of September 19, 1985 | 191 |
| | E) Monitoring Underground Atomic Blasts | 208 |
| Chapter 11 | Some Structural Applications of the Rational Theory | 215 |
| | A) The Earthquake Engineering Analysis of the Supports for an Offshore Platform Structure (OPS) | 215 |
| | B) The Earthquake Engineering Analysis of a Building with an Open, Ground Level, Column-Supported Parking Area | 222 |
| | C) The Earthquake Engineering Analysis of a Short Squat Shear-Type Structure $l/w \lesssim 1/2$ | 233 |
| | D) The Earthquake Engineering Analysis of a Low to Intermediate Height Beam-Girder-Column Energy Absorbing Structure | 244 |
| | E) The Earthquake Engineering Analysis of a High Structure, $l/w \gtrsim 5$ | 264 |
| | F) A Concrete Dam Earthquake Analysis | 293 |
| Appendix | Earthquake Engineering and Applied Mechanics | 306 |
| Index | | 312 |

EARTHQUAKE ENGINEERING

This page is intentionally left blank

CHAPTER 1

A TENSILE RUPTURE INSTABILITY SIMILARITY EARTHQUAKE MECHANISM

INTRODUCTION

A mathematical-physical model of a particular earthquake will be derived. The model, which is a 'mechanism', is a mathematical formulation that may apply to earthquakes that originate within the mantle of the earth, say 50–800 km below the surface of the earth, or in regions of lesser depth providing the physical conditions are such that the necessary triggering relations are developed for the initiation of the earthquake. This last will be explained in more detail in a later section of this chapter.

This derived mechanism will have the following properties:

1. It will be a complete, closed form solution to the field equations and boundary conditions assumed for the event.
2. It will be based upon a reasonable, realistic, possible physical explanation for the development of the earthquake.
3. The instability, or trigger, for the initiation of the earthquake is included as a fundamental element in the solution.
4. It will account for the enormous amount of energy which, it is estimated, is released in a major earthquake. This energy shall be calculable using approximate relations.
5. It will account for the production of P and S waves that are generated in earthquakes.
6. It will predict a number of phenomena that may be subject to checks by geologists, rock scientists, and others working in this field.

The proposed mechanism requires the generation of relatively high stresses by ground surface standards. Although there may be doubt as to whether these could be generated on the surface of the earth, it is a fact that within the earth the rock may be subjected to enormous pressures and temperatures and these

affect the properties of the material in some, as yet, unknown ways. Thus, the required stresses and other properties (including the initiation of the triggering fracture, possibly by some phase change) may conceivably occur as required for the solution presented. Only a check of actual phenomena in the field can prove or disprove this point.

It is certainly a fact that enormous amounts of energy are released in earthquakes. Since these are probably generated by the release of 'locked-in' strain energy, it is conceivable that very high stresses acting on large volumes of material are involved. Both the high stresses and large volumes are part of the mechanism being discussed.

It seems clear that different tectonic earthquakes are caused by more than a single-type mechanism. There is little doubt that vertical near-surface fault slippage, such as occurs in many California quakes, is the mechanism for some earthquakes. But, it is also quite probable that this is not the only type of mechanism. Thus, as noted by Newmark and Rosenblueth,^{1*} some seismologists hold that earthquakes originate in phase changes of rocks, rather than by fault slippage. Those who favour the phase change (volume change) theory argue that there is little likelihood that geological faults exist below depths of a few hundred kilometres because of the high temperatures and confining pressures, and yet data have been interpreted to indicate that earthquakes have originated at depths exceeding 600 km and up to 800 km.

In addition, as will be shown, the mechanism derived herein may be an explanation for certain earthquakes which have foci relatively close to the surface of the earth, under special geological conditions — also characteristic of some California earthquakes.

Some additional insight into the question of possible earthquake mechanisms appears in an article in *Science*² which reported on a meeting of geologists, seismologists, and engineers held in Knoxville, Tennessee in September, 1981. Among other activities, various speculations concerning possible mechanisms were presented. Quoting from the reference: 'John Armbruster and Leonardo Seeber of Lamont Doherty Geological Observatory, in particular, in discussing the major 19th-century earthquake in Charleston, South Carolina, favoured a nearly horizontal fault separating an upper thin sheet of rock from the crust beneath the fault. They argue that the most violent effects of the 1886 Charleston earthquake covered too large an area to have resulted from a break on a nearly vertical fault. A break on a horizontal fault, on the other hand, could have directed its seismic energy over a much larger area of surface. A horizontal break could be caused by a tendency of the thrust sheet to backslide off the continent . . .'

* Numbering shown refers to references at end of chapter.

The mechanism developed in this chapter is generally consistent with the Armbruster-Seeber view, although it is not a unique representation or solution for the assumed phenomena. It will, however, represent a broad, particular explanation of an earthquake which, by extension and generalization, may give some insight and knowledge of the actual details behind the build-up to and occurrence of certain earthquakes. In this way, some important leads and hints may emerge relating to the two most important problems in earthquake engineering, still unsolved:

1. How to predict when an earthquake will occur.
2. How to 'defuse' an earthquake that is about to occur.

Finally, in the Appendix to this chapter, the derived mechanism will be related to four fundamentally different types of earthquake happenings.

NOMENCLATURE FOR THIS CHAPTER

- C = velocity of small disturbance in the solid (velocity of sound)
- p = pressure of superplastic material
- P = pressure of ruptured area material
- r = radial distance coordinate
- t = time
- u = particle velocity
- U_I = initial strain energy of element
- U_F = final strain energy remaining in element following rupture
- ξ = similarity coordinate
- θ = angular variation
- ρ = density
- σ = stress, positive when tension
- ν = Poisson's ratio
- μ = viscosity
- o = subscript, outer
- i = subscript, inner

PHYSICAL ASSUMPTIONS

Some distance below the surface of the earth, where the earthquake is assumed to originate, we have a condition of hydrostatic stress, which is shown below in Fig. 1.1 on a membrane or strip of thickness t . We assume this is a zero, initial condition, just as such a strip on the surface of the earth is subjected

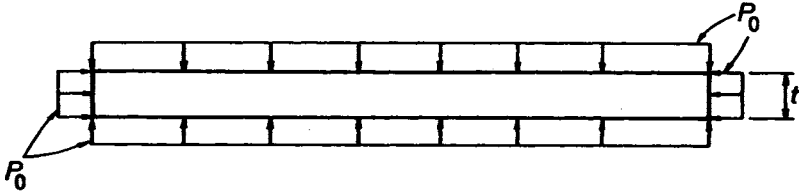


Figure 1.1

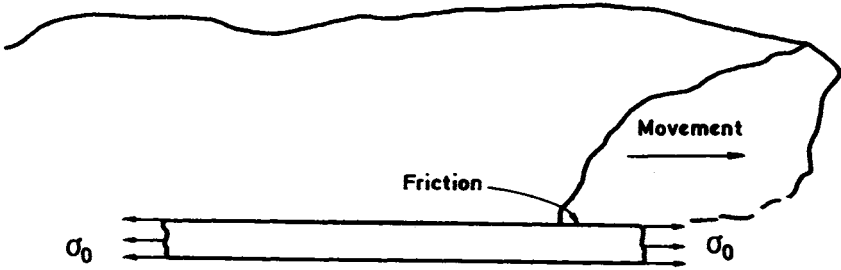


Figure 1.2

to a hydrostatic atmospheric pressure. Due to tectonic plate movement of the crust of the earth mantle, or due to an inner build-up of pressure (see the later section in this chapter in which the California Caldera earthquakes are discussed) or due to some other physically realizable effect, a tensile stress σ_0 is added to the above strip of mantle (see Figures 1.1 and 1.2). This stress is assumed to be uniform along the edge of an enclosed area of indefinite extent and we consider the effect of σ_0 alone. Thus the layer, initially subjected to the hydrostatic pressures, now has the stresses σ_0 applied to it uniformly around the boundary and these stresses introduce a strain energy in the layer caused by stretching. See Figure 1.2 in which an upper sliding movement and the resultant friction cause a stress, σ_0 , which gradually increases and builds up as the tectonic plate or other movement action proceeds. There are other ways by which this stress σ_0 may be generated, as shown later in this chapter. In any case, finally, a value of σ_0 is reached that, in conjunction with the initial state of the layer and a possible phase change, leads to a 'rupture' or 'fracture' initiated at a single point, A (see Figure 1.3). (It is interesting to note that Benioff³ has suggested, on the basis of observed wave forms from three earthquakes, that a class of deep earthquakes may arise when a phase transition occurs through a region of rock, causing a sudden change in volume.) This failure at a point A spreads radially throughout the layer, so that at a time t after initiation of the rupture, conditions are shown in Figure 1.4.

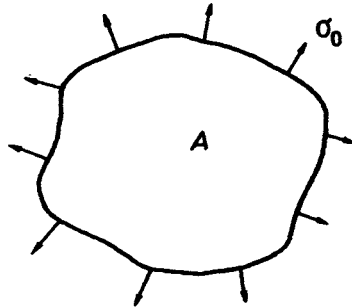


Figure 1.3

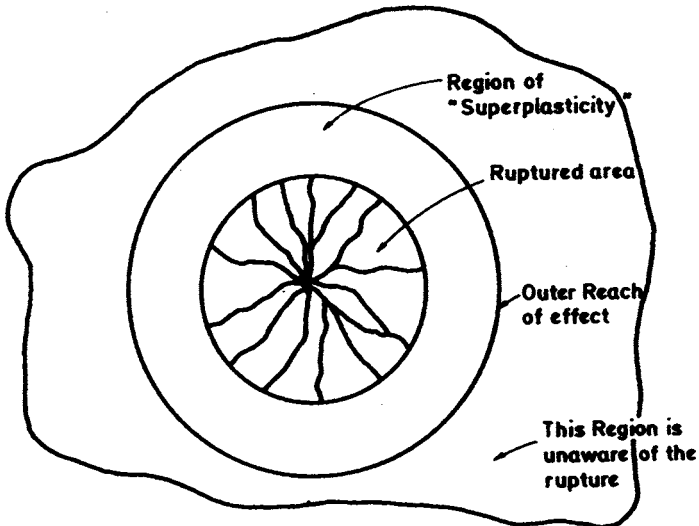


Figure 1.4

The mathematical development governing the event follows⁴.

MATHEMATICAL ANALYSIS

For the dynamic phenomenon being investigated in this chapter, the material may be assumed to have the properties of a border region fluid-solid, a so-called 'superplastic' material. Therefore the analysis will be based upon the conservation equations of continuum fluid mechanics instead of the somewhat uncertain relations of combined dynamic elasticity-plasticity action, as is usually done in

analysing fracture phenomena. Thus the rupturing strip must satisfy the following equations (given in the two-dimensional symmetrical polar coordinate form).

Mass conservation:

$$\frac{\partial \rho}{\partial t} + \frac{\partial(\rho u)}{\partial r} + \frac{\rho u}{r} = 0 . \quad (1)$$

Momentum conservation (Navier-Stokes equation):

$$\frac{\partial u}{\partial t} + u \frac{\partial u}{\partial r} = - \frac{1}{\rho} \frac{\partial p}{\partial r} + 4/3\mu \left(\frac{\partial^2 u}{\partial r^2} + \frac{1}{r} \frac{\partial u}{\partial r} - \frac{u}{r^2} \right) . \quad (2)$$

Also, an equation for the velocity of small disturbances (since the effect of the point rupture spreads radially and reaches a finite distance from the centre of rupture),

$$C = C(p, \rho) . \quad (3)$$

In the foregoing equations, p is the negative mean value of the principal diagonal elements of the stress tensor, i.e.,

$$p = -1/3(\sigma_r + \sigma_\theta + \sigma_z) \quad (4)$$

so that for the uniform strip stress field we have ($\sigma_r = \sigma_\theta$, $\sigma_z = 0$),

$$p = - \frac{2\sigma_r}{3} . \quad (5)$$

Physically, the phenomenon may be described in the following manner (this explanation will justify the assumed boundary conditions for the foregoing mathematical formulation of the field equations): (A) For $t < 0$, the entire strip is in a uniform tensile stress state, σ_0 ; (B) At $t = 0$, a small puncture is introduced at some interior station. We may think of this as the sudden introduction, along the arc of a small circle (the puncture point) of an equal and opposite, i.e. compressive, stress, $-\sigma_0$. Hence at this inner circle we have

$$\begin{aligned} \sigma_\theta &= \sigma_{\theta F} \\ \sigma_r &= 0 \end{aligned}$$

$$\sigma_z = 0$$

$$p = \frac{-\sigma_{\theta F}}{3} \quad (6)$$

$\sigma_{\theta F}$ is the 'fracture' or 'tearing' stress for the material, i.e. the tensile stress that will just cause the strip to fracture; and (C) For $t > 0$, conditions are as shown in Figure 1.5, which is the physical (r, t) plane. Note there are an infinite number of sketches Fig. 1.5 corresponding to all the different times $t > 0$.

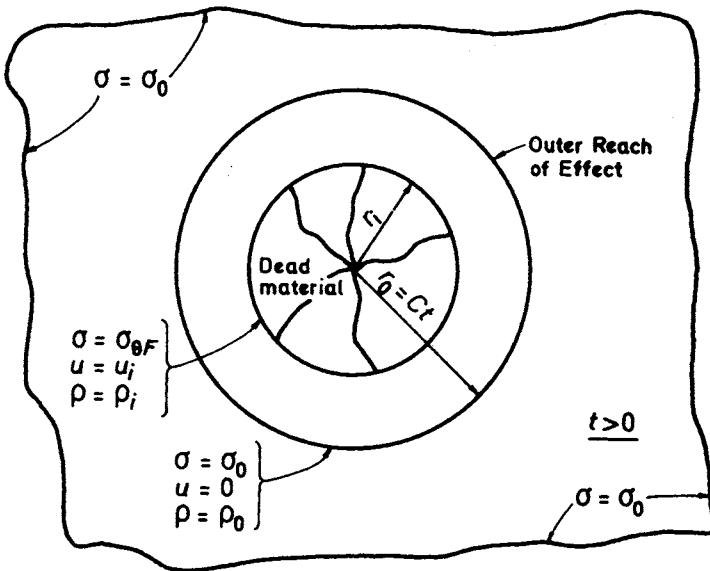


Figure 1.5

1. The punctured region now has a radius r_i moving with an assumed constant velocity, the velocity of fracture. The stress along the circle bounding this region is

$$\sigma_{\theta} = \sigma_{\theta F}$$

$$\sigma_r = 0$$

$$\sigma_z = -P_i$$

(7)

$$p = -\frac{\sigma_{\theta F}}{3} + \frac{P_i}{3}$$

in which P_i is the final pressure on the entire ruptured strip (see Eq. 16 for an approximate value of this stress) due to the swelling of the ruptured layer that has been relieved of stress. Furthermore, P_i almost certainly decays to zero in a boundary layer,⁵ i.e. a very thin layer in the neighbourhood of r_i . Hence, it is not unreasonable to assume the region $r_i < r < r_0$ has $\sigma_z = 0$ and this will be done.

2. The material density at $r_i = \rho_i$.
3. Within the radius r_i is a region of 'dead' material with cracks and fractures as required.
4. The outer reach of the effect is at a radius $r_0 = Ct$. The particle velocity at r_0 is zero and the stress at r_0 is

$$\begin{aligned} \sigma_\theta &= + \sigma_0 \\ \sigma_r &= + \sigma_0 \\ \sigma_z &= 0 \\ p &= -\frac{2\sigma_0}{3} . \end{aligned} \tag{8}$$

The material density is ρ_0 , the initial stressed strip density.

5. For $r_i < r < r_0$, the particle velocity, strip density, and stress condition have some variable values as required by the field equations and boundary conditions given above.

Because of the constant velocities of the outer and inner boundaries, and the constant stress $\sigma_{\theta F}$ at the inner boundary, an essential and fundamental simplification is involved by introducing the similarity coordinate

$$\xi = r/t . \tag{9}$$

Since (based upon dimensional considerations) u must be linear in ξ , it follows that when

$$\frac{\mu}{t\xi_0^2} \ll 1 \tag{10}$$

we may neglect the viscosity term in the Navier-Stokes equation. We will assume this is so, and we shall neglect this quantity in our subsequent analysis. Then Eqs. (1), (2), and (3) become:

Mass Conservation:

$$-\xi \frac{d\rho}{d\xi} + \frac{d(\rho u)}{d\xi} + \frac{\rho u}{\xi} = 0 . \quad (1a)$$

Momentum conservation:

$$-\rho \xi \frac{du}{d\xi} + \rho u \frac{du}{d\xi} = -\frac{dp}{d\xi} . \quad (2a)$$

State:

$$C = \left(\frac{dp}{d\rho} \right)^{1/2} . \quad (3)$$

Now, the phenomenon which is represented by an infinite number of different maps in the physical (r, t) plane for each time t , is shown by a single field in the ξ -plane which holds for all times t , Figure 1.6. Note $\xi_0 = C$ is the velocity of sound of small disturbances in the stressed strip and is the outer reach of affect, ξ_i is the velocity of the fractured boundary and hence also the fracture velocity in the strip.

The solution to these equations, which satisfies all of the physical and boundary conditions as previously given in (A), (B), and (C), are

$$u = \xi_0 - \xi \quad (11)$$

$$\rho = \rho_0 \frac{\xi_0}{\xi} \quad (12)$$

$$2\sigma_0 + 3p = 6\rho_0 \xi_0 (\xi_0 - \xi) - 3\rho_0 \xi_0^2 \ln \frac{\xi_0}{\xi} \quad (13)$$

On physical grounds, Eq. (11) implies that the velocity, ξ_i , of the inner fracture surface is bounded by $\xi_0/2 < \xi_i < \xi_0$.*

* The boundary condition $\sigma_{r_i} = 0$ at ξ_i implies that the fracture velocity ξ_i is just equal to u_i . Only then will $\sigma_{r_i} = 0$ despite the radial expansion of the ruptured plate due to the Poisson ratio effect. This may, in fact, be the necessary condition for the uniqueness of the solution. The two fundamental material properties involved in this plate instability — the velocity of sound, ξ_0 , in the σ_0 stressed plate and the fracture velocity ξ_i of the region of dead material, determine the velocity u_i and the stress compatibility solution for the phenomenon. Thus,

if $u_i = \xi_0/2$, then $\xi_i = \xi_0/2$ and $\sigma_{r_i} = 0$.

if $u_i > \xi_0/2$ then $\xi_i < \xi_0/2$ and the two regions separate at ξ_i which is physically impossible.

If $u_i < \xi_0/2$ then $\xi_i > \xi_0/2$ and the fractured region presses against the unfractured plate — i.e. $\sigma_{r_i} \neq 0$. This is a possible condition and, if true, leads to the lack of uniqueness of the solution.

ing to note that Mott⁶ found that the velocity of travel for a linear fatigue crack in metals is given by approximately

$$\xi_i = 0.38C \tag{14}$$

as compared to the value

$$\frac{C}{2} \leq \xi_i < C \tag{15}$$

assumed in the foregoing.

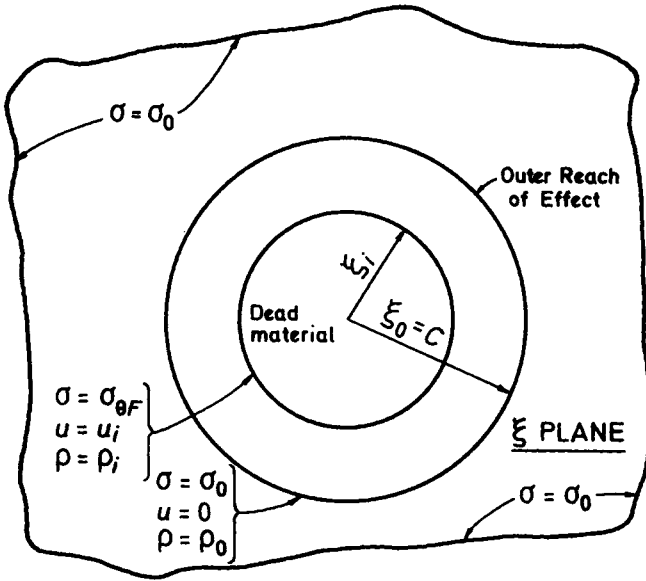


Figure 1.6

Also, a value for velocity of rupture of about 2 to 3.5 km s⁻¹ has been inferred for a few earthquakes from seismograms,⁷ although these are probably slip-fault ruptures.

The solutions of Eqs. (11), (12), and (13) imply certain restrictions on the field quantities for the particular solution obtained.

1. As noted above, ξ_i is given by $\xi_0/2 < \xi_i < \xi_0$
2. The conditions of the inner, ruptured material may be represented as in Figure 1.7, where a unit cube is shown. P_i causes a unit deflection just equal

to that caused by σ_0 in Figures 1.2 and 1.3. Therefore

$$P_i = 2\nu\sigma_0 \quad (16)$$

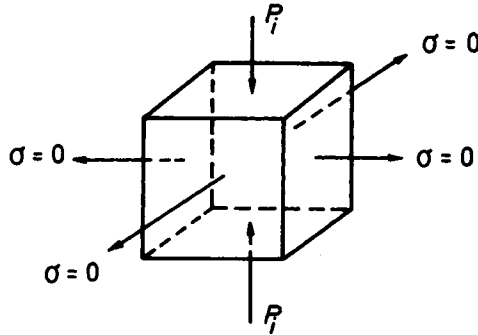


Figure 1.7

and from Eq. 13 and the boundary conditions

$$\sigma_0 = \frac{3\rho_0 \xi_0^2}{(1 + \nu)} \left[1 - \frac{\xi_i}{\xi_0} - \frac{1}{2} \ln \frac{\xi_0}{\xi_i} \right] + \frac{\sigma_{\theta F}}{2(1 + \nu)} \quad (17)$$

This is the stress compatibility condition for the given solution.

The gross energy of the earthquake is just the net strain energy released in the 'dead material' layer. We may obtain an approximate expression for this in terms of σ_0 , P_i and the properties of the dead material layer as follows, using the equations of elasticity

$$\begin{aligned} U_{\text{INITIAL}} &= \text{strain energy in the unruptured layer} \\ &= \frac{\sigma_0^2}{E} (1 - \nu) (\text{volume}) \end{aligned} \quad (18)$$

After failure, the dead material has

$$\begin{aligned} \sigma_z &= P_i = 2\nu\sigma_0 \quad (\text{compression}) \\ \sigma_0 &= 0 \end{aligned} \quad (19)$$

and the strain energy

$$U_{\text{FINAL}} = \frac{2\nu^2 \sigma_0^2}{E} (\text{volume}) . \quad (20)$$

(If P_i is assumed ‘suddenly applied’ $U_{\text{FINAL}} = \frac{4\nu^2 \sigma_0^2}{E}$.)

Then the energy released by the earthquake is

$$U_{\text{EARTHQUAKE}} = U_{\text{INITIAL}} - U_{\text{FINAL}} = \frac{\sigma_0^2}{E} (1 - \nu - 2\nu^2) (V_{\text{DM}}) \quad (21)$$

in which V_{DM} is the volume of dead material. A portion of this energy is then ‘lost’ in fracturing the dead material region, in thermodynamic and, probably, chemical reactions as well.

The earthquake mechanism is then as shown in Figure 1.8. The fracture or rupture, caused when σ_0 reaches the value given in Eq. 17, is a sudden one brought about by the extremely high stress and (possibly) a sudden phase change at a point. The dead material releases net strain energy and develops a pressure $P_i (= 2\nu\sigma_0)$ which, very likely, pulsates as it pushes against the overlaying and underlying material, introducing P and S waves and transfers the energy released by the fractured layer to, ultimately, the surface region affected by the earthquake.

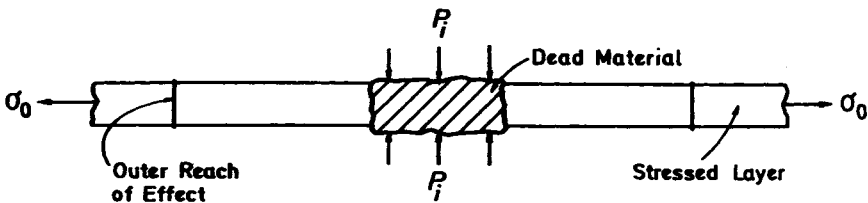


Figure 1.8

To indicate approximate values for energy and deflection of P_i , if we assume the fracture area is 5000 ft in diameter and 100 ft thick, and using assumed values that follow:

$$\sigma_0 = 200,000 \text{ psi}$$

$$P_i = 2\nu\sigma_0 = 120,000 \text{ psi}$$

$$E = 3 \times 10^6 \text{ psi}$$

$$\nu = 0.3 \quad (22)$$

Assume the energy lost in fracturing = 10 per cent ($U_1 - U_F$), we find

$$U_{\text{EARTHQUAKE}} = 2 \times 10^{15} \text{ in lb} \quad (23)$$

and a maximum deflection of P_i of about 10 in.

The energy value obtained is not unreasonable.¹ Also, following the initial rupture, the enormous temperatures and pressures 'heal' the fracture region. More movement and phase change in a vulnerable or weakened layer may be an explanation for aftershocks.

SUMMARY TO THIS POINT

Before proceeding to an analysis of a field condition which appears to be consistent with the development of the proposed mechanism, we summarize the theoretical formulations up to this point.

A mathematical-physical model of a particular underground earthquake mechanism was derived. The model utilized equations of fluid flow as well as those of linear elasticity theory and a basic similarity transformation. In a sense, the analysis (which leads to a closed form solution) assumes a so-called 'super-plastic' material.

Summarizing the key physical requirements, hypotheses, and results for the proposed mechanism:

1. A plate subjected to a uniform tensile stress field.
2. A critical value for this stress, σ_0 .
3. A puncture or a phase change or an occlusion or whatever, at any rate, a rupture at a point A.
4. Which causes
 - (a) A circular region centered at A of zero in-plane stresses surrounded by
 - (b) A circular ring subject to the conservation equations of mechanics, in terms of r, t . These equations can be transformed by introducing the similarity coordinate $\xi = r/t$, so that the infinite number of time-dependent maps of the phenomenon in the r, t plane collapse to a single map of the ξ plane.
5. The rupture at point A causes a 'tearing or fracture' stress σ_{θ_F} at the inner boundary of 4(b), the rupture boundary, so that the rupture is self-sustaining and

6. The region 4(a) grows uniformly with time and this is the earthquake energy-producing region whose outer boundary moves with the constant velocity ξ_i , the rupture velocity.
7. ξ_i is also the constant velocity of the inner boundary of region 4(b). The outer boundary of this region moves with the constant velocity ξ_0 , which is the velocity of sound in the stressed region, i.e., the velocity of small disturbances.
8. On physical grounds, because $u_i = \xi_0 - \xi_i$

$$\frac{\xi_0}{2} < \xi_i < \xi_0 \quad (24)$$

so that

9. σ_0 , the critical stress, which must be less than $\sigma_{\theta F}$ is given by

$$\frac{\sigma_{\theta F}}{2(1 + \nu)} < \sigma_0 < \sigma_{\theta F} \quad (25)$$

and therefore

$$\sigma_{\theta F} > \frac{3\rho_0 \xi_0^2 (1 - \ln 2)}{1 + 2\nu} \quad (26)$$

The mechanism summarized above includes predictions of earthquake behaviour and parameters. Such of these can only be checked in the field with actual earthquakes. Others may be checked in laboratory experiments in which material properties, temperatures and pressures simulate the field conditions.

APPLICATION OF THE MECHANISM TO THE LONG VALLEY, CALIFORNIA, CALDERA EARTHQUAKES

During recent years, a comprehensive three-dimensional mapping program has been carried out at Long Valley Caldera in California as the focus of geological studies by various private corporations, government agencies and universities. The region in question is shown in Figure 1.9 redrawn from Ref. 9.

The testing indicates the presence of a molten magma chamber at least eight miles wide and six miles deep that is clearly the source of the volcanic and earthquake activity in the area. The tests indicate that the chamber may come within two miles of the ground surface and, in addition, they chart the geologic features between the magma chamber and the surface.

Especially significant from the point of view of the mechanism considered in this chapter, is the fact that there appears to be a continuous swelling of the caldera surface due to magma flowing into the chamber and causing a pressure which has caused a central region of the caldera floor six miles in diameter to have risen as much as three feet, as shown in the inset sketch of Figure 1.9.

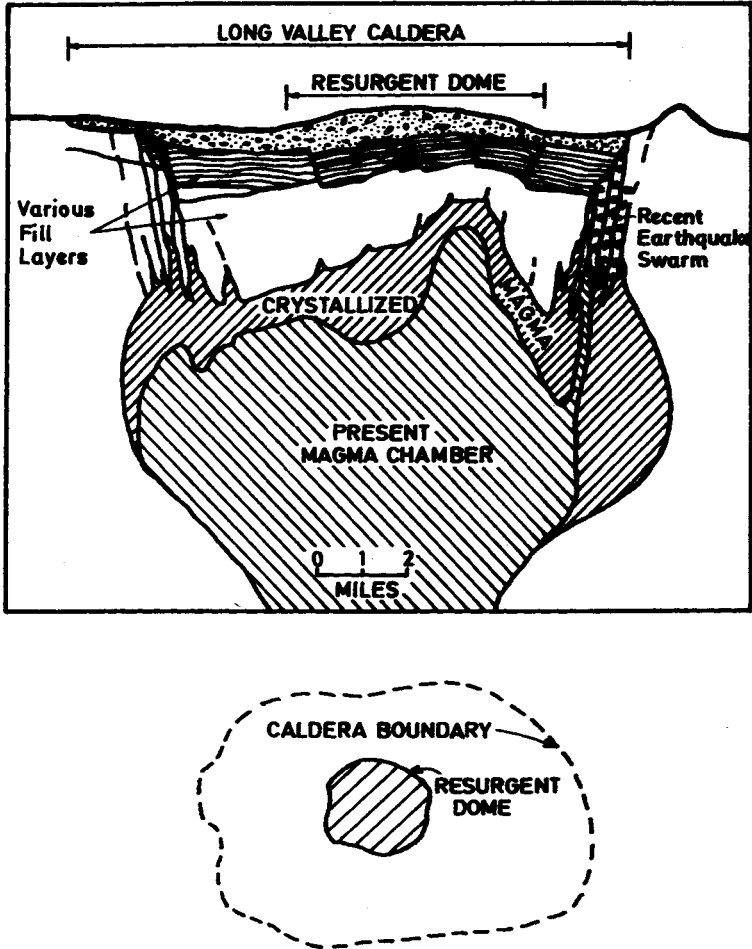


Figure 1.9

The swelling and rising of the earth's surface can be related directly to the proposed mechanism. Simple plate and membrane theories (based upon reasonable dimensioning assumptions) when combined with the mechanism theory of the previous sections, give rise to a number of quantitative results and predictions. Most of these may be checked either in the field or by means of carefully controlled laboratory experiments in which pressure and temperature and material corresponding to the field conditions are simulated.

For convenience sake, the previously shown Figure 1.6 is reproduced below. Also given for clarity in connection with the caldera mechanism are other forms of the definitions of the various terms and regions shown in this figure, as follows:

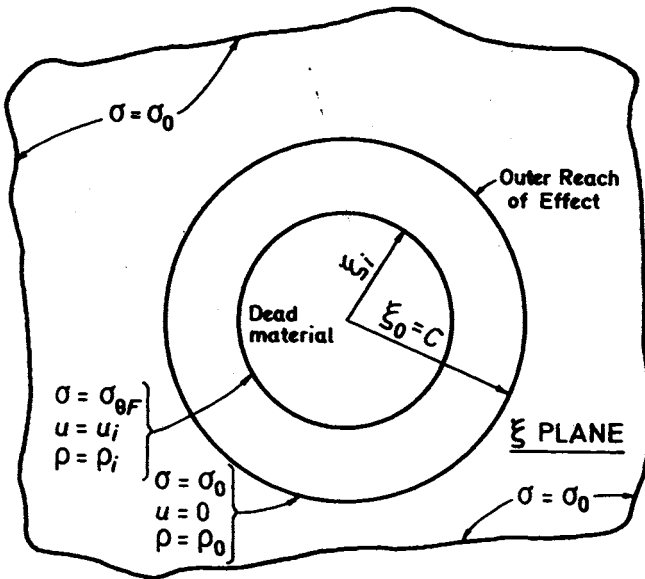


Figure 1.6

$\sigma_0 =$ The uniform initial tensile stress to which the plate is subjected. When σ_0 reaches a critical value, the plate ruptures, starting at a point shown in the figure as the centre of the region of 'dead material'.

Region of 'dead material' — This area, growing with time, is the fracture region caused by the critical value of σ_0 and is triggered by an occlusion or other physically possible source. The outer boundary of this expanding area is shown as ξ_f . Within this region, the material is fractured and is subjected to a zero in-plane stress condition.

ξ plane = a single map which holds for all time $t > 0$ during the lifetime of the earthquake. ξ is the 'similarity' coordinate, $\xi = r/t$, which transforms the infinite number of time dependent maps governing the phenomenon into a single map (Figure 1.6) as shown, thus permitting a closed-form analytic solution for the phenomenon.

$\sigma_{\theta F}$ = The tensile fracture stress at the outside boundary of the dead material (and the inside boundary of the stressed material shown in the doughnut shaped area). This stress will just cause the material to fracture or tear and by virtue of the similarity behavior, it is a self-sustaining (i.e., continual) stress that 'fuels' the mechanism, which releases energy from the stress-relieved plate. It is this energy which is the earthquake.

$\xi_0 = C$, The velocity of sound (i.e., velocity of small disturbances) in the stressed plate and this represents the outer reach of the earthquake mechanism solution. That is, the plate region outside of ξ_0 is unaware of the fractured region and hence of the earthquake until it receives signals (pressure waves) from the energy released by the region of dead material.

ρ, u = The density and velocity of the plate material.

This mechanism will now be considered in conjunction with conditions at the Long Valley Caldera area.

It must be stated at the outset of this portion of the analysis, that of necessity, various assumptions had to be made concerning dimensions of different elements involved in the proposed mechanism. However, in all cases, these appear to be consistent with the known geologic profile and do lead to numerical results that appear to be reasonable. Furthermore, the assumptions involved in the application of the mechanics also seem to be reasonable and consistent with the geological and physical profile of the Long Valley Caldera area.

Following is a step-wise listing of the assumptions involved in the analysis (see also Figure 1.9):

1. A molten magma sphere 30,000 ft (approximately six miles) in diameter surrounded by a band region of crystallized magma topped with other materials and sediments up to the earth's surface.
2. The earth's surface has bulged in a 'resurgent dome', a circular area of maxi-

mum rise equal to three feet.

3. This dome is caused by an increase in internal pressure in the molten magma sphere which in turn causes a bulge of the molten magma sphere, an increase in its diameter as it pushes against the crystallized magma which in turn pushes against the overlying material until the surface is reached and the 'resurgent dome' is formed.
4. The increase in internal pressure is assumed to be 20 psi and this is assumed to cause an increase in the molten magma sphere radius of 10 feet which deformation decreases through the overlaying material until it is three feet at the surface. The intermediate variation is of no interest in this analysis.
5. The increase in molten magma diameter causes an increase in the diameter of a spherical band of crystallized magma adjacent to the molten magma, causing a uniform stress in this band. The thickness of stressed band is assumed to be 500 feet.
6. As the pressure builds up in the molten magma sphere, the uniform tension increases in the crystallized magma band. At a critical value of this stress, σ_0 , a tensile rupture instability occurs, and this self-sustaining rupture (which is the earthquake) continues over a radius of 1000 feet, releasing energy due to the 'fracturing' of the crystallized magma. That is, the 500 feet thickness of crystallized magma is assumed to be at a pressure and temperature condition which — in conjunction with the uniform stress σ_0 — is at the rupture instability condition that requires a slight perturbing trigger to initiate the growth of the region of dead material — i.e., the earthquake. Otherwise stated — according to this model of the mechanism, the earthquake originates in an expanse of the crystallized magma adjacent to the molten magma sphere.
7. A sketch (approximately to scale) of the assumed profile, including the ruptured plate ('dead material' area of Figure 1.6) is shown in Figure 1.10. Note, in particular that for all practical purposes, the ruptured plate is essentially a flat plate and furthermore this plate (earthquake source) can probably occur at any point on the upper half of the sphere, thereby leading to possible multiple or swarms of earthquakes following a first triggering.

The mathematical-physical analysis follows, see Figures 1.10 and 1.11

THE MECHANISM

In Figure 1.11,

$$\sigma_0 = \frac{pR}{2h} \text{ psf} \quad (27)$$

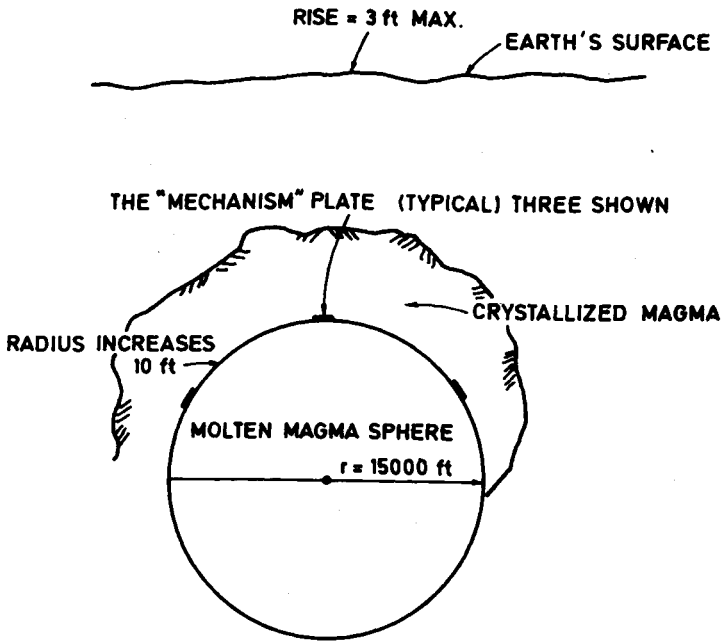


Figure 1.10

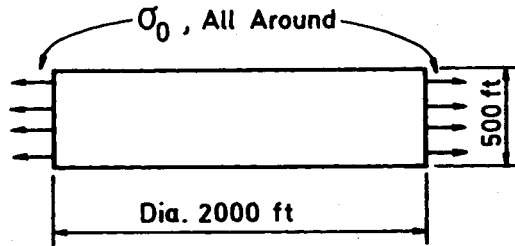


Figure 1.11

in which

σ_0 = the critical value of the uniform tensile stress

p = internal pressure increase in the molten magma sphere

$$= 20 \text{ psi or } 3000 \text{ psf}$$

$$r = 15,000 \text{ ft}$$

$$h = 500 \text{ ft}$$

$$\text{Hence } \sigma_0 \cong 45,000 \text{ psf.} \quad (28)$$

We assume the internal pressure causes a 10 feet increase in the band radius.

Hence the circumference of a one foot strip of the band is increased by 60 feet, and

$$E = (1 - \nu) \frac{\sigma_0}{\epsilon} \quad (29)$$

in which

E = modulus of elasticity

ν = Poisson ratio, assumed as 0.3

ϵ = unit strain

$$= \frac{60}{2\pi(15,000)}$$

$$= \frac{1}{1500}$$

$$\text{Thus } E \cong 300,000 \text{ psi.} \quad (30)$$

It was shown previously in this chapter that the approximate energy released by the earthquake is given by

$$U_E = U_{\text{EARTHQUAKE}} = \frac{\sigma_0^2}{2E} (\text{Volume of rupture material}) . \quad (31)$$

This becomes, using the above numbers

$$U_E = 6 \times 10^{17} \text{ ergs} . \quad (32)$$

One of the relations listed in the literature for the energy released by an earthquake is

$$\log_{10} E = 11.4 + 1.5 M \text{ ergs} \quad (33)$$

in which

E = energy of the earthquake

M = magnitude of the earthquake

For an $M = 4$, which is a representative magnitude for a Long Valley earthquake, this gives

$$E = 10^{17.4} \text{ ergs} . \quad (34)$$

Other predictions involving the stress σ_0 are given in earlier sections of the chapter.

To summarize the Long Valley Caldera analysis:

Using what appear to be realistic *assumptions* and *numbers*, computations indicate the possible development of earthquakes of the proper magnitude at the Long Valley Caldera. The mechanism used is essentially a tensile rupture instability of a plate or membrane and is based upon a similarity representation utilizing the Navier-Stokes equation as well as the elementary relations of elasticity theory. Thus, in effect, the solution is a combined plastic-viscous-elastic material phenomenon.

For the *assumptions* and *numbers* used, certain stresses and material properties are predicted in the analysis, including those given in the earlier sections of the chapter. These stresses and material properties are capable of experimental check.

Clearly, an exact check on these would be an unrealistic expectation since different (reasonable) initial *assumptions* and *numbers* would lead to other values for the predicted stresses and material properties.

However, if actual values for the stresses and material properties (which in this proposed mechanism are fundamental parameters of the Long Valley Caldera earthquake event) are determined, it would be a simple task to determine the corresponding consistent *assumptions* and *numbers* which could then, in turn, be checked.

Finally, even an approximate check-if obtained—would represent an important verification for a given earthquake mechanism, for which, to the best of

the author's knowledge, no other actual experimental verification has been given.

CONCLUSION

This chapter was in two main parts:

- 1) A derivation of a particular theoretical rational earthquake mechanism. Included in the derivation were a number of predictions dealing with material properties and bounding-stress values.
- 2) An application of the rational mechanism to an actual earthquake generating geological condition — this being the situation prevailing at the Long Valley Caldera in California. The analysis required a priori dimensioning assumptions for different parts of the proposed mechanism. What appear to be reasonable numbers were assumed and what appear to be reasonable results were obtained although field and/or laboratory checks on these are needed.

The application, (2) above, was to a relatively shallow focus horizontal plate mechanism.

It is suggested the same or a similar mechanism may be appropriate for deep focus earthquakes, although this too requires (much more difficult) field and/or laboratory verification.

In addition to the above, a number of future activities are desirable insofar as the proposed model is concerned:

1. Values of the physical constants that occur should be determined. These will have to come from some of the centres working in deep-earth research, such as the one, for example, at Cornell University.⁸
2. Is there any evidence — geologic, seismograph, accelerogram, observations — that tends to confirm or contradict the proposed model, for shallow focus and/or deep focus earthquakes?
3. Among the behaviours to look for are:
 - (a) A 'pulsating' loading due to P_i , with the corresponding P and S waves (Figure 1.8).
 - (b) An enormous release of energy in a matter of seconds (Eq. 22–23 and the assumed 5000 ft diameter ruptured area).
 - (c) Energy release from either a layer or area a mile (miles) in extent or a thicker strip of lesser area.
 - (d) Surface or interior movement which leads to the build-up of the stress σ_0 .
 - (e) A phase change or other unusual behaviour or configuration of the material which, in conjunction with σ_0 , results in a triggering instability.

fracture or rupture.

- (f) A 'healing' of (e) due to the high pressures and temperatures involved.
 - (g) Any clues in the proposed mechanism that would lead to a prediction of a possible earthquake, such as the raised mound in the Caldera analysis.
 - (h) Any means for triggering or defusing an earthquake due to the suggested mechanism. Once again, for the Caldera analysis — if the mechanism is, in fact, as indicated herein, would it be possible to artificially increase the pressure in the molten magma chamber until the critical stress is attained?
4. Finally, can the proposed mechanism be connected with the Richter scale?

REFERENCES

1. Nanthan M. Newmark and Emilio Rosenblueth, *Fundamentals of Earthquake Engineering*, Prentice Hall, Inc. Englewood Cliffs, N.J. 1071, Ch. 7.
2. Richard A. Kerr, Assessing the risk of Eastern U.S. earthquakes, *Science*, Vol. 214, 9 Oct. 1981, p 169–171.
3. H. Benioff. Source wave forms of three earthquakes, *Bull. Seism. Soc. Am.*, 53, 893, 1963.
4. S.F. Borg. Rupture instability of plane membranes and solids, *Journal of Applied Mechanics*, (ASME), Sept. 1960.
5. S.F. Borg. A note on Boundary Layer Type Solutions in Applied Mechanics, *Journal of Aeronautical Sciences*, April 1950.
6. N.F. Mott. Brittle fracture of mild steel plates, *Engineering (British)*, 164, 1947; 165, 1948.
7. Bruce A. Bolt. Causes of Earthquakes, in *Earthquake Engineering*, Robert L. Weigel, Coordinating Editor, Prentice-Hall, Inc., Englewood Cliffs, N.J. 1970, Ch. 2.
8. See Materials at ultrahigh pressures, *Engineering, Cornell Quarterly*, 14, No. 1, Summer 1979.
9. Walter Sullivan, *Mapping Technique Produces Image of Magma Chamber Near Yosemite*, N.Y. Times, June 11, 1985, C3.

APPENDIX

Introduction

The previously derived thin plate (membrane) tensile rupture instability solution will now be suggested as the mechanism governing four different types of earthquake events which are known to occur.

- a) The 'plains' type earthquake, typically, the New Madrid quake of 1811.
- b) The caldera type earthquake, as at Long Valley earlier described in this chapter.
- c) The mini-quakes that occasionally occur under the lakes formed behind high dams and
- d) The tectonic earthquakes that frequently accompany erupting volcanos.

It will be shown that all four may have the tensile rupture instability phenomenon as the common factor.

Some very preliminary quantitative data will be discussed.

The self-sustaining similarity mechanism which is taken as the earthquake model in this chapter corresponds physically to a plate which is subjected, through some simple easily accounted for physical process, to a transverse pressure loading thereby leading to a deformed stretching which in turn introduces a uniform tensile stress field into an essentially flat plate. This plate has a thickness to length ratio which corresponds approximately to 'thin plate' or 'membrane' action.

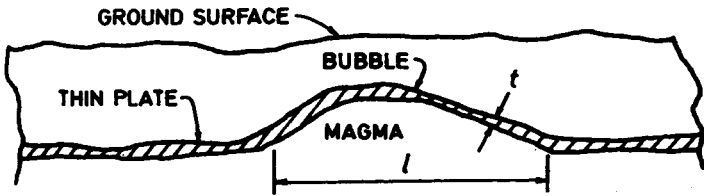
As the pressure increases (for whatever reason) the uniform tensile stress and strain energy stored in the plate increase until the critical value of the stress is reached. At this point some non-uniformity triggers the initiation of the rupture instability failure.

The similarity solution developed for this instability indicates that the rupture is self-sustaining involving a progressive radially expanding shattering of the plate which in turn releases the stored strain energy in an explosive form — which is, physically, the earthquake.

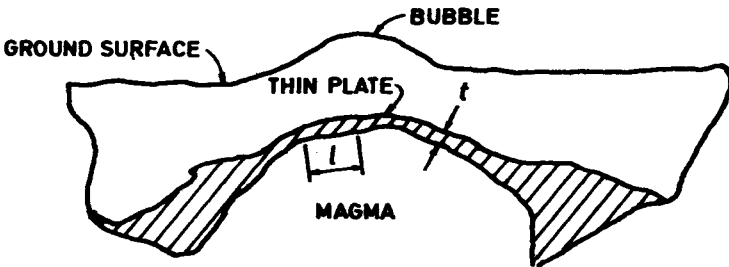
This physical picture over the extent of plates of various sizes is shown in Figure 1.12 for the four different types of earthquakes considered in the Appendix. These four, radically different in their outward manifestations and appearances are, it is suggested, identical in the fundamental mechanism involved in the earthquake.

Analysis

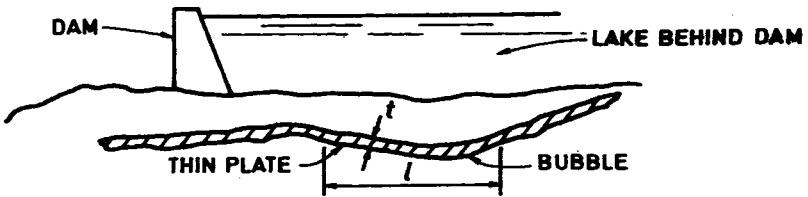
The similarity solution for the mechanism implies that the rupture (i.e., earthquake) will continue expanding and releasing energy as long as the plate and stress condition are maintained without interruption. If, for example, the edge of the expanding rupture field reaches a discontinuity of some sort (such as the boundary edge of the uniformly stressed plate or the edge of the uniformly stressed field or some other physical change) the solution will no longer be valid and the earthquake will stop. Thus, a critical factor in limiting the magnitude (i.e., energy) of an earthquake is a boundary of the stretched plate.



(A) The 'Plains' Earthquake-Typically New Madrid — Dec. 16 1811



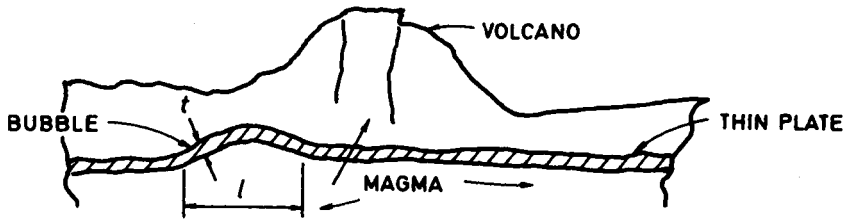
(B) At a Caldera-Typically Long Valley



(C) Under Lake Behind a High Dam

(continued on following page 26)

(continued from previous page 25)



(D) Under a Volcano

Figure 1.12 The Four Earthquake Types (No Scale-Schematic)

In our present discussion for the four cases, of energy, physical dimensions, variables and similar terms that enter into the mechanism theory, we will of necessity have to make assumptions concerning most of the quantities. The information concerning these — the hard data — simply is not available at this time. However, the general theory postulated herein does indicate, in detail, exactly how the computations should be performed and what quantitative results may be obtained. Simple computations will be shown, using what appear to be reasonable, representable values of the required variables. However, the author must state that what may seem to be reasonable could in fact, be very much in error, since our knowledge of rock and soil properties deep within the earth is in a most rudimentary state.

The Richter-Gutenberg equation for earthquake energy, U , as a function of earthquake magnitude, M , will be assumed as

$$\log_{10} U = 11.4 + 1.5 M \text{ ergs} \tag{A1}$$

or

$$U = 10^{11.4 + 1.5 M} \text{ ergs.}$$

This equation has the advantage of simplicity and furthermore is probably at least as accurate as other published expressions.

The energy released by the ruptured plate, as derived earlier and which corresponds to the energy of Eq. A1 is given approximately by

$$U = \frac{\sigma_0^2}{2E} (\text{volume of stretched plate}) \tag{A2}$$

- in which U = energy released
 σ_0 = critical stress (tensile) in the plate
 E = modulus of elasticity in the plate
 l = diameter of ruptured plate
 t = thickness of ruptured plate
 $t/l \ll 1$, for this plate, membrane action
 $l^2 t \cong$ volume of ruptured plate

At this time, it appears likely that the maximum earthquake magnitude which may occur anywhere in the world corresponds to $M = 9$. Thus, one of the largest recorded is the New Madrid, 1811 earthquake which is rated as $M = 8.7$. See Figure 1.12A.

On the other hand, tectonic earthquakes at Calderas, behind dams and those associated with volcanic eruptions appear to have maximum magnitudes of about 3 to 4.

We shall use the bounds $4 < M < 9$ in our approximate quantitative formulation.

Insofar as type D earthquakes are concerned, it should be noted that we are considering the so-called 'tectonic' earthquake and not the 'volcanic' event. Both forms are equally likely to occur in connection with volcanos. The volcanic form is associated with massive expenditures of energy associated with violent magma explosive movements which are in addition to the tectonic effect of Figure 1.12D.

As shown in Eq. A1, we have for the two limiting magnitudes

$$U_4 = 10^{17.4} \text{ say } 10^{18} \text{ ergs}$$

$$U_9 = 10^{25} \text{ ergs} . \tag{A3}$$

For no reason other than it seems a reasonably high value for a stress in a probably highly viscous rock-like material, we shall assume

$$\sigma_0 = 30,000 \text{ psi} \tag{A4}$$

and, similarly $E = 500,000$ psi
 and assuming, for thin plate behaviour, that

$$\frac{t}{l} = \frac{1}{100} \ll 1 \tag{A5}$$

we have

$$\begin{aligned} \text{for } M = 9, & & l &= 14 \text{ mi} \\ & & t &= .14 \text{ mi} \end{aligned} \tag{A6}$$

$$\begin{aligned} \text{and for } M = 4, & & l &= 350 \text{ ft.} \\ & & t &= 3.5 \text{ ft.} \end{aligned}$$

Clearly, other values for l and t will be obtained for different combinations of Equations (A4), (A5), (A6).

Conclusion

A particular earthquake mechanism is considered in connection with four different, but related, types of earthquake phenomena.

The mechanism — a tensile thin plate rupture instability solution which is a self-sustaining continuing event — in all four cases is tied in directly with a physically possible related cause. Pressures on an underground thin plate or membrane-like plate cause a uniform expanding circular stretching which in turn leads to storage of strain energy in the plate. Ground surface movements may or may not be associated with this phase of the developing earthquake. As the pressure on the plate increases the deformation and stress and strain energy storage increase until a critical value of the stress is reached and the rupture is initiated.

Typical computations are made for two limiting cases using assumed values for the plate properties. These represent predictions that should be at least partially capable of checking.

Finally — many of the ground surface features which occur in connection with tectonic plate-fault earthquakes (in the circumpacific belt, for example) can be accounted for by the mechanism described in this report.

CHAPTER 2

THE CANONICAL ACCELEROGRAM AND ITS PARAMETERS

INTRODUCTION

One of the more important and useful records of an earthquake is the accelerogram. This data, which is a printout of acceleration in a given direction, as a function of time, at a given locality, is utilized by earthquake scientists to assist in the analyses of the earthquakes that developed the particular accelerograms, and also in the design of structures for future earthquakes. Because of the important role played by the accelerogram in many areas of earthquake engineering, it was considered crucial that a unifying concept or invariant relation for this fundamental data be obtained. The invariant, to be most useful, should be one that is generated by a rigorous mathematical and physical hypothesis capable of being checked experimentally and, furthermore, should be one that can be utilized in extended analyses of earthquake engineering phenomena in ordinary engineering design offices.

In particular, a 'canonical' form of the accelerogram will be considered and analyzed. Physically, it will be assumed that the canonical accelerogram is one which is generated by a single-shock earthquake with a point focus. Those accelerograms which are not canonical, as will be shown in Chapter 6 can invariably be represented by a superposition of canonical accelerograms which — again physically — will be assumed as being caused by a superposition (or sequence or cluster) of earthquake shocks. While these two assumptions are reasonable on physical grounds (and, in fact, may offer a most useful rational explanation for the various shapes of earthquake accelerograms, as shown in a later chapter), a check of these fundamental assumptions for the canonical accelerogram is one of the several major tasks insofar as the rational theory of this text is concerned.

In any event, the canonical accelerogram and its invariant relations and its parameters will be utilized as major tools in the damage assessment and struc-

tural design phases of the present theory. In particular, insofar as the canonical accelerogram is concerned, it will be shown

1. such an accelerogram does exist.
2. The canonical accelerogram may be related to an invariant relation (equation) which holds, approximately, for all canonical accelerograms.
3. Various properties of the canonical accelerogram will be determined, including a timewise variation of ground energy at a point due to an earthquake.
4. The fundamental parameters of the canonical accelerogram will be obtained and their physical connection to the earthquake event will be considered.
5. In a later chapter, the superposition theory for canonical accelerograms will be derived and
6. Also in later chapters, the invariant and parameters will be utilized as basic tools in
 - a) The development of a 'damage criterion'.
 - b) The proposed method of structural analysis in earthquake engineering.

It must be emphasized that, as is true for practically every event that occurs in earthquake engineering, the hypothesized canonical accelerogram invariant does not represent an exact relation. It can only be considered as an 'average' for typical earthquakes with a spread depending upon a number of parameters. One of these important parameters must almost certainly be the 'average geology' of the region affected by the earthquake. Among other factors that we shall include in the general term 'average geology' or 'average geologic region' are (a) the depth of the focus, (b) the overall configuration (i.e. boundary of continent or mountainous or plains region), and (c) the frequencies of the accelerations.

The invariant analysis developed herein is reasonable and consistent with one of the fundamental characteristics of the earthquake phenomenon, namely that all phases of it, starting from its initiation (the mechanism) to its final destructive effect, are variable and appear to be of uncertain and erratic form. One can make very few absolutely positive statements in dealing with earthquake phenomena. One can only speak of 'averages', 'probabilities', and similar terms in attempting to obtain a basic understanding of a particular event, as is the case in this and later chapters.

One additional consideration is that whereas the canonical accelerograms and the relations derived from them in this chapter refer only to the horizontal ground accelerations, it is probable that an invariant (i.e., canonical) accelerogram relation also holds for vertical accelerograms. This matter will not be pursued further in this text. However see the discussion of vertical ground energy in Chapter 5.

NOMENCLATURE FOR THIS CHAPTER

Following are the terms used in this chapter. They will be defined also when they are introduced.

- a = ordinate to accelerogram envelope
- f = subscript final
- k, K = dimensionless constants
- n = dimensionless constant
- t = time
- A, B = numerical constants
- ϵ_{t_f} = SHE = the total surface horizontal energy per unit area supplied by the earthquake at the site where acceleration is recorded
- T = SHE per unit area per unit time supplied by the earthquake at the site where the acceleration is recorded
- θ = angle between a ray from focus to location of accelerograph and the direction of the accelerograph

MATHEMATICAL-PHYSICAL ARGUMENT

A typical canonical accelerogram is shown in Figure 2.1. Note in particular the following properties of the accelerogram which are characteristic of all canonical accelerograms.

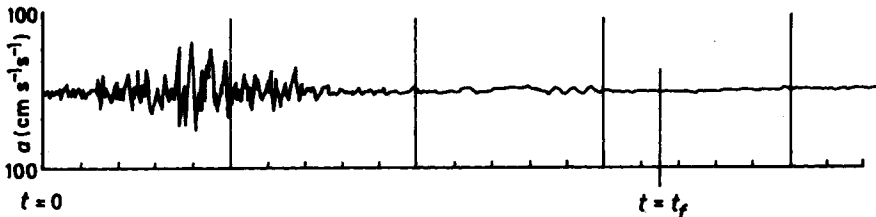


Figure 2.1

1. The acceleration starts at, essentially zero corresponding to $t = 0$. It then increases to a maximum and finally decreases to zero, corresponding to $t = t_f$.
2. The chart is approximately symmetric with respect to the time axis, so that positive and negative accelerations are assumed to be mirror images of each other.

In developing the canonical accelerogram invariant, we form an envelope of the positive portion of the curve, as shown in Figure 2.2. The positive portion

only is used because of (2) above, and in view of the following mathematical development and of the uses to which the canonical accelerogram-envelope is put. In essence, an approximate combined curve (positive and negative accelerations) is accounted for in what follows.

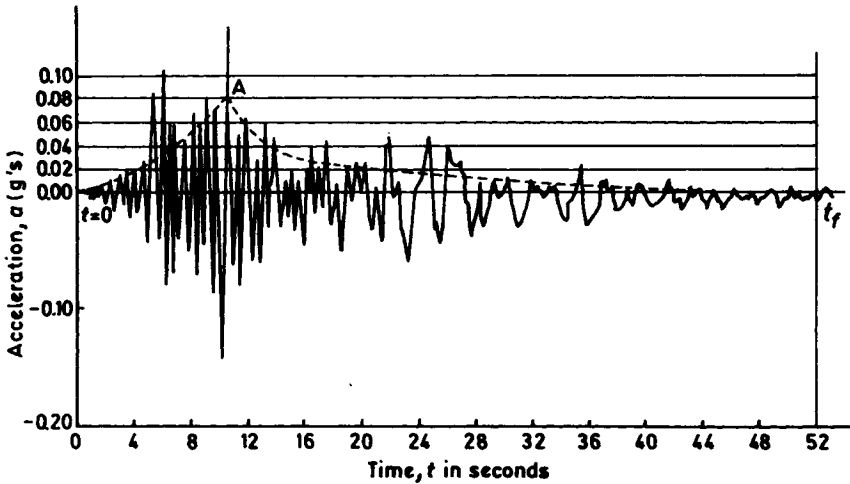


Figure 2.2

Starting at the initiation of acceleration increase ($t = 0$) and proceeding to the final time (t_f) of acceleration change, and using the area under the envelope curve, we assume, considering two points, subscripts 1 and 2, a distance Δt apart,

$$\sum_{t=0} (a\Delta t)_2 = \sum_{t=0} (a\Delta t)_1 + \Delta(\Sigma a\Delta t) \quad (1)$$

in which a is the ordinate (i.e. acceleration) to the envelope at the point considered. Eq. (1) is mathematically and physically reasonable.

The next statement is a key assumption in the mathematical formulation¹. Based upon dimensional as well as physically reasonable arguments we assume that

$$\Delta(\Sigma a\Delta t) = k \sum_{t=0}^{t_1} (a\Delta t)_1 \frac{t_f^n}{t^{n+1}} \Delta t \quad (2)$$

in which k and n are non-dimensional constants whose values are to be determined.

Proceeding,¹ we obtain after integrating

$$\frac{\Sigma(a\Delta t)}{\Sigma(a\Delta t)_f} = e^{K[1 - (t_f/t)^n]} \quad (3)$$

an equation which satisfies the initial and final conditions and which must be tested against the realities of actual canonical accelerograms.

For clarity, we list again the definitions of the terms in Eq. (3).

$\Sigma(a\Delta t)$ = area under the canonical accelerogram envelope between $t = 0$ and $t = \text{any time, } t$

$\Sigma(a\Delta t)_f$ = total area under the canonical accelerogram envelope between $t = 0$ and $t = t_f$

K, n = numerical constants to be determined

Eq. (3) is the postulated 'invariant' of the canonical earthquake accelerogram. We shall also refer to it on occasion, as the 'acceleration index'. To test this hypothesis, the accelerograms of the following earthquakes were utilized:

- (a) Tolmezzo, 1976²
- (b) Taft, 1952³
- (c) Lima, 1966⁴
- (d) San Fernando, 1971⁵
- (e) Bucharest, 1977⁶

It was found that a best fit for the data from the five earthquakes is given by (see Figure 2.3 and the Appendix to this chapter) the approximate relation

$$\frac{\Sigma(a\Delta t)}{\Sigma(a\Delta t)_f} = e^{0.12[1 - (t_f/t)^{1.8}]} \quad (4)$$

In Eq. 4, t_f and $\Sigma(a\Delta t)_f$ vary for each earthquake, and the values for these two quantities are listed in Table 2.1.

As pointed out above, K and n are constant. The significance of this is related to a postulated uniqueness-existence hypothesis which was formulated elsewhere⁷ and the details of which will not be discussed further in this textbook although the tentative conclusions obtained from it will be used later in this chapter and the next chapter.

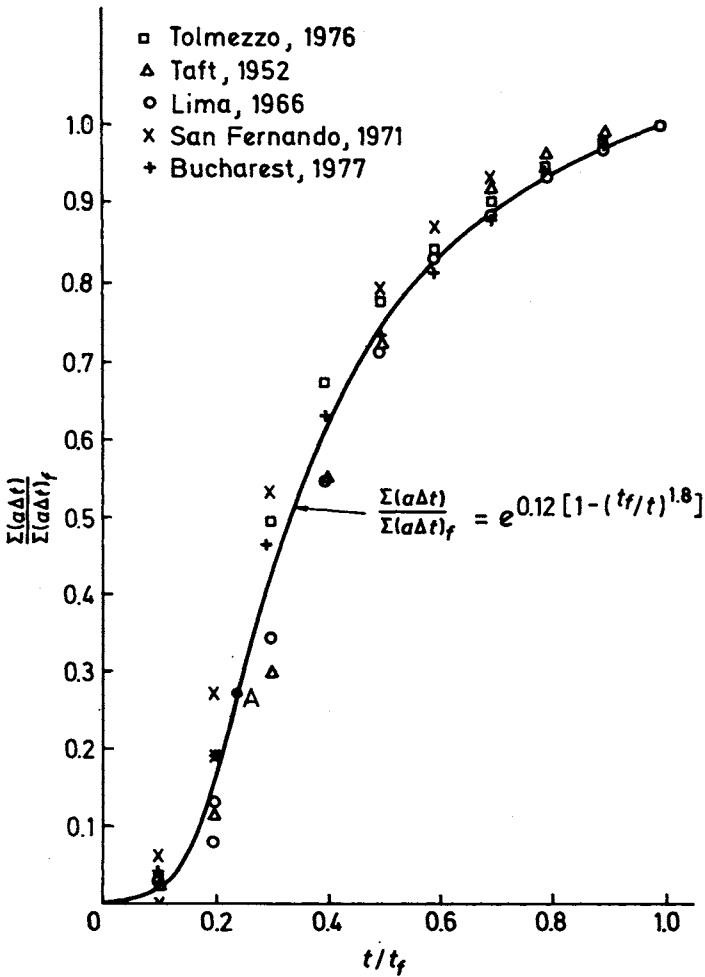


Figure 2.3

Table 2.1 t_f and $\Sigma(a\Delta t)_f$ for five earthquakes

| Earthquake | t_f sec | $\Sigma(a\Delta t)_f$ 'g' sec |
|--------------------|-----------|-------------------------------|
| Tolmezzo, 1976 | 20 | 0.98 |
| Taft, 1952 | 20 | 0.96 |
| Lima, 1966 | 20 | 1.84 |
| San Fernando, 1971 | 48 | 1.06 |
| Bucharest, 1977 | 14 | 0.72 |

DETAILED ANALYSIS OF THE INVARIANT EQUATION 4

As indicated in Figure 2.3 a plot of the invariant, Eq. 4, is a typical S or growth curve. The point A, which is the point of zero curvature, corresponds to the point A on Figure 2.2 which is the maximum positive (and assumed negative) acceleration on the envelope curve of the accelerogram. This point occurs at approximately

$$\left(\frac{t}{t_f}\right)_A = 0.25 \tag{5}$$

One additional approximate property of the canonical accelerogram curve which will be used in later sections follows from the area relation for parabolic curves.

$$\sum(a\Delta t)_f = \frac{a_{\max} t_f}{3} \tag{6}$$

The values given in Eqs. 4, 5, and 6 will at this time be assumed as fixed average values for typical canonical earthquake accelerograms subject to verification, possible change, or modification as a more detailed study and analysis of accelerograms throughout the world requires.

Once more it is emphasized that particular accelerograms, subject to special conditions, will not conform to the invariant form of Eq. 4. Thus, the accelerogram of the Pacoima Dam, Figure 2.4, which represents conditions almost directly over the focus, probably includes a number of shock-clusters and reflection-refraction effects and perhaps even dam vibration effects that do not, in general, occur in canonical accelerograms. However, the accelerogram of Figure 2.4 can very easily be approximated by the sum of two canonical accelerograms, as shown in Figure 2.5, indicating the likelihood of two successive shocks occurring at and during the times shown. The combined effect may then be taken by considering the separate canonical accelerogram effects, as will be discussed in Chapter 6.

Finally, based upon the analysis here presented, it seems clear that the two fundamental parameters of the accelerogram are t_f and $\sum(a\Delta t)_f$, i.e. the total time of the accelerogram and the area under the envelope of the accelerogram.

THE PHYSICAL VARIABLES RELATED TO THE CANONICAL ACCELEROGRAMS

It was stated earlier in this chapter that a tentative uniqueness-existence hypothesis which related to Eq. 4 was developed⁷. According to this tentative

hypothesis, there are two physical variables upon which the two fundamental parameters t_f and $\Sigma(a\Delta t)_f$ depend.

SAN FERNANDO EARTHQUAKE 2/9/71 0600 PST PACOIMA DAM, CALIFORNIA S16° E COMPONENT

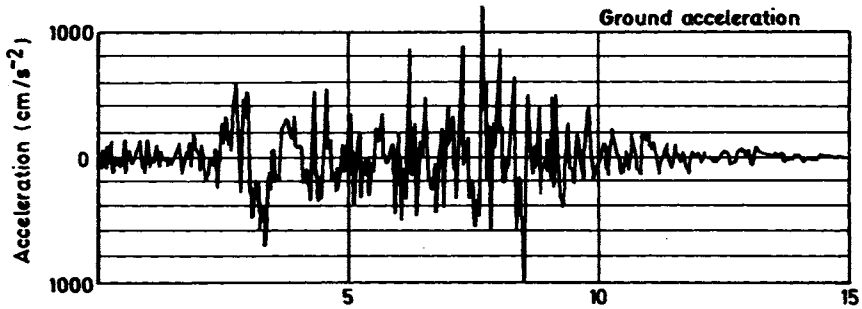


Figure 2.4

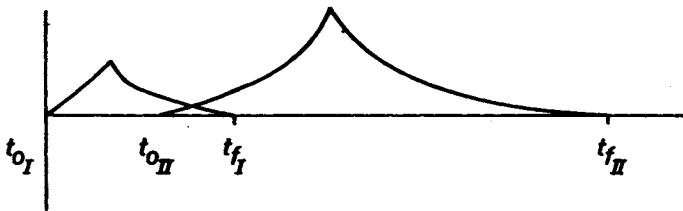


Figure 2.5

An analysis of the earthquake phenomenon suggests that these two variables are:

1. Soil or geological conditions at the point where the accelerogram is obtained.
2. The total surface horizontal energy — SHE — per unit ground area developed by the earthquake at the site where the accelerogram is obtained. SHE is the energy which reaches the surface of the earth and which causes the horizontal vibration and damage of structures. A fundamental assumption in the development of the rational procedures of this book is that in one form or another it is this quantity which must be determined if a rational method of structural analysis is to be obtained for structures subject to earthquake effects. SHE can be expressed in terms of an 'efficiency, η ' in which η converts the total focal earthquake energy into the destructive surface energy. Bolt⁸ discusses an efficiency to convert source energy to seismic energy but as he notes very little is known about the value of η . See Chapter 5 in this connection.

SHE is a key physical quantity insofar as this textbook is concerned. It will be directly related to both the canonical accelerogram and the canonical iso-seismal chart (Chapter 3) and is the basis for the structural design procedure as

well as the damage assessment analyses described in later chapters. Furthermore — and once more based upon physical arguments — we shall assume that:

- 1a. t_f is the factor influenced by the local soil or geological conditions.
- 2a. $\Sigma(a\Delta t)_f$ is the factor influenced by the total SHE per unit area at the site.

Note that the form of the parameters indicates a likely cross-correlation.

Among the indicated topics for future research which this chapter suggests are studies to check the two major correlations hypothesized above. Some checks along these lines are described in later chapters.

As an approximation, we hypothesize that the determination of 'maximum canonical accelerogram effect', i.e. $\{\Sigma(a\Delta t)_f\}_{max}$ may be obtained from

$$\{\Sigma(a\Delta t)_f\}_{max} = \frac{\{\Sigma(a\Delta t)_f\}_{actual}}{\cos \theta} \quad (7)$$

in which

$\{\Sigma(a\Delta t)_f\}_{actual}$ is the value obtained from a single available canonical accelerogram, and θ is the angle between a ray from the focus of the location of the accelerograph and the actual direction of the accelerograph.

Admittedly, Eq. 7 may be a poor approximation (or it may be a very good one) depending upon local soil conditions, and also upon geological features between the focus and the accelerograph. But these difficulties are inherent in the earthquake phenomenon. One looks for correlation and generalizations that apply 'on the whole'.

THE TIMEWISE VARIATION OF SHE AT A POINT

Eq. 4, which is an invariant of the canonical accelerogram, enables one to obtain an approximate expression for the SHE as a function of time, supplied by the earthquake, at the ground site of the accelerogram. This is accomplished by postulating a parallel (although different) physically-based mathematical relation for the $\Sigma(a\Delta t)$ term which is assumed to be a basic parameter of the accelerogram record. The procedure is as follows. Assume

$$\frac{\Delta[\Sigma(a\Delta t)]}{\Delta t} = A \frac{T}{8t_f} \Sigma(a\Delta t) \quad (8)$$

in which A is a numerical constant* and

ε_{t_f} is a physical constant related to the canonical accelerogram response, say the total surface horizontal energy, SHE, per unit area supplied by the earthquake at the site where the acceleration is recorded. And, based upon dimensional as well as physical requirements,

T is the derivative of SHE per unit area with respect to time t , supplied by the earthquake at the site where the acceleration is recorded.

Now, comparing Eq. 8 above and Eq. 2, and equating equivalent terms, we find

$$T = B\varepsilon_{t_f} \frac{t_f^{1.8}}{t^{2.8}} \quad (9)$$

in which B is a numerical constant. This expression, which has a singularity at $t = 0$, will be analysed further in Chapter 4, and will be used in that and later chapters in the damage assessment and structural analysis procedures.

CONCLUSION

One of the major sources of field (experimental) data connected with earthquakes — the accelerograph record — is analysed with particular emphasis on the determination of the invariant relating thereto. Based upon a physical-mathematical-dimensional line of reasoning, a canonical accelerogram is postulated and an invariant for it is obtained. Two basic parameters are also postulated and define the invariant. These in turn are related to two physical variables

* Concerning the parallel acceleration index representations: In Eq. 2, it is postulated that

$$\frac{\Delta \Sigma(a\Delta t)}{\Delta t} = f(\Sigma(a\Delta t), t) .$$

The alternate formulation, Eq. 8 is

$$\frac{\Delta \Sigma(a\Delta t)}{\Delta t} = g(\Sigma a\Delta t, \text{SHE}(t)) .$$

In both the particular variables and parameters of earthquake engineering are used.

See Chap. 3 pp. 51 and 54 in which a very similar analysis is used for the isoseismal index. Note also the symmetries in accelerogram-time and isoseismal-space in these and other equations and curves given in the text.

variables of the earthquake event. Various properties of the canonical invariant are derived and the invariant itself is also related to the single most important quantity involved in the earthquake phenomenon — the energy. The equations, relations, and results obtained in this chapter will be utilized in later chapters dealing with damage assessment and also with structural design analyses.

REFERENCES

1. S.F. Borg. *Similarity Solutions in the Engineering, Physical-Chemical, Biological-Medical and Social Sciences*, Proceedings of Symposium 'Symmetry, Similarity, and Group Theoretic Methods in Mechanics', P.G. Glockner and M.C. Singh (eds.), University of Calgary, August 1974.
2. CNEN-ENEL. *Commission of Seismic Problems Associated with the Installation of Nuclear Plants*, Contribution to the Study of Friuli Earthquake of May, 1976, Figure 4, p. 52.
3. Robert L. Wiegel. *Earthquake Engineering*, Figure 4.2, p. 78, Prentice-Hall, Inc., Englewood Cliffs, N.J. 1970.
4. Robert L. Wiegel, *Earthquake Engineering*, Figure 4.19, p. 89, Prentice-Hall, Inc. Englewood Cliffs, N.J. 1970.
5. I.M. Idress. *Characteristics of Earthquake Ground Motions*, Specialty Conference on Earthquake Engineering and Soil Dynamics, ASCE, Pasadena, California, June 19–21, 1978, p. 18.
6. Fattal *et al.* Observations on the Behaviour of Buildings in the Romania Earthquake of March 4, 1977, NBS SP 490, Sept. 1977.
7. S.F. Borg, *Generalized Tensors and Matrices*, Proc. Second International Conference on Mathematical Modeling, St. Louis, Missouri, July 1979.
8. Robert L. Wiegel. *Earthquake Engineering*, Chap. 2 written by Bruce A. Bolt, Prentice-Hall, Inc., Englewood Cliffs, N.J. 1970.

APPENDIX

Tables 2.2 to 2.6 and the accompanying accelerograms show the values that were used in preparing Figure 2.3.

Table 2.2 Tolmezzo, 1976 (see Figure 2.6): $t_f = 20$ s, $\Sigma(a\Delta t)_f = 0.98$, $\cos \theta = 45^\circ$

| t/t_f | $\Sigma(a\Delta t)/\Sigma(a\Delta t)_f$ | $e^{0.12[1-(t_f/t)^{1.8}]}$ |
|---------|---|-----------------------------|
| 0 | 0 | 0 |
| 0.1 | 0.03 | ~ 0 |
| 0.2 | 0.19 | 0.13 |
| 0.3 | 0.49 | 0.40 |
| 0.4 | 0.67 | 0.60 |
| 0.5 | 0.77 | 0.74 |
| 0.6 | 0.84 | 0.83 |
| 0.7 | 0.90 | 0.90 |
| 0.8 | 0.94 | 0.94 |
| 0.9 | 0.98 | 0.98 |
| 1.0 | 1.00 | 1.00 |

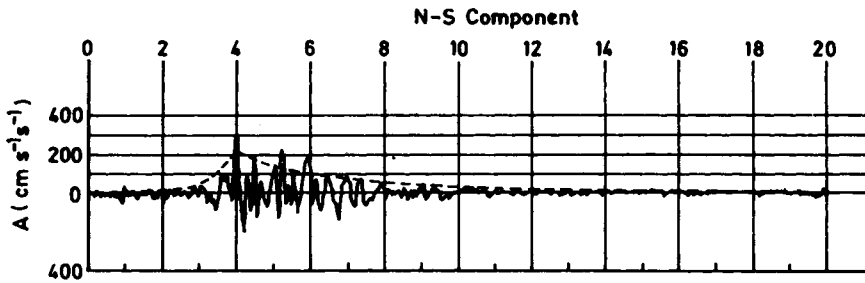


Figure 2.6

Table 2.3 Taft, 1952 (see Figure 2.7): $t_f = 20$ s, $\Sigma(a\Delta t)_f = 0.96$, $\cos \theta = \text{Unknown}$

| t/t_f | $\Sigma(a\Delta t)/\Sigma(a\Delta t)_f$ | $e^{0.12[1-(t_f/t)^{1.8}]}$ |
|---------|---|-----------------------------|
| 0 | 0 | 0 |
| 0.1 | 0.03 | ~ 0 |
| 0.2 | 0.11 | 0.13 |
| 0.3 | 0.30 | 0.40 |
| 0.4 | 0.55 | 0.60 |
| 0.5 | 0.72 | 0.74 |
| 0.6 | 0.83 | 0.83 |
| 0.7 | 0.92 | 0.90 |
| 0.8 | 0.96 | 0.94 |
| 0.9 | 0.99 | 0.98 |
| 1.0 | 1.00 | 1.00 |

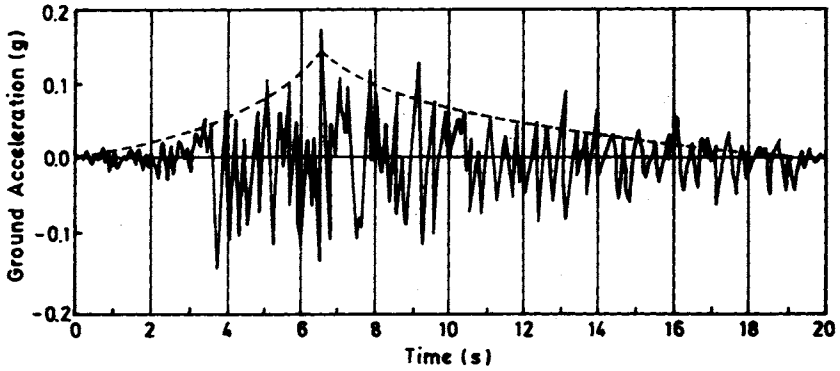


Figure 2.7

Table 2.4 Lima, 1966 (see Figure 2.8): $t_f = 20$ s, $\Sigma(a\Delta t)_f = 1.84$, $\cos \theta = \text{Unknown}$

| t/t_f | $\Sigma(a\Delta t)/\Sigma(a\Delta t)_f$ | $e^{0.12[1-(t_f/t)^{1.8}]}$ |
|---------|---|-----------------------------|
| 0 | 0 | 0 |
| 0.1 | 0.03 | ~0 |
| 0.2 | 0.13 | 0.13 |
| 0.3 | 0.34 | 0.40 |
| 0.4 | 0.54 | 0.60 |
| 0.5 | 0.71 | 0.74 |
| 0.6 | 0.82 | 0.83 |
| 0.7 | 0.90 | 0.90 |
| 0.8 | 0.95 | 0.94 |
| 0.9 | 0.98 | 0.98 |
| 1.0 | 1.00 | 1.00 |

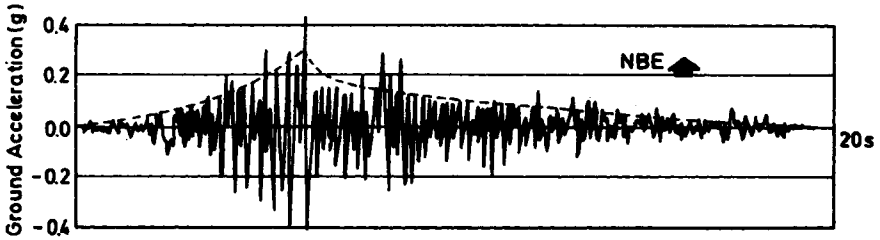


Figure 2.8

Table 2.5 San Fernando, 1971 (see Figure 2.9): $t_f = 48$ s, $\Sigma(a\Delta t) = 1.06$, $\cos \theta = \text{Unknown}$

| t/t_f | $\Sigma(a\Delta t)/\Sigma(a\Delta t)_f$ | $e^{0.12[1-(t_f/t)^{1.8}]}$ |
|---------|---|-----------------------------|
| 0 | 0 | 0 |
| 0.1 | 0.06 | ~ 0 |
| 0.2 | 0.27 | 0.13 |
| 0.3 | 0.53 | 0.40 |
| 0.4 | 0.67 | 0.60 |
| 0.5 | 0.79 | 0.74 |
| 0.6 | 0.87 | 0.83 |
| 0.7 | 0.93 | 0.90 |
| 0.8 | 0.96 | 0.94 |
| 0.9 | 0.98 | 0.98 |
| 1.0 | 1.00 | 1.00 |

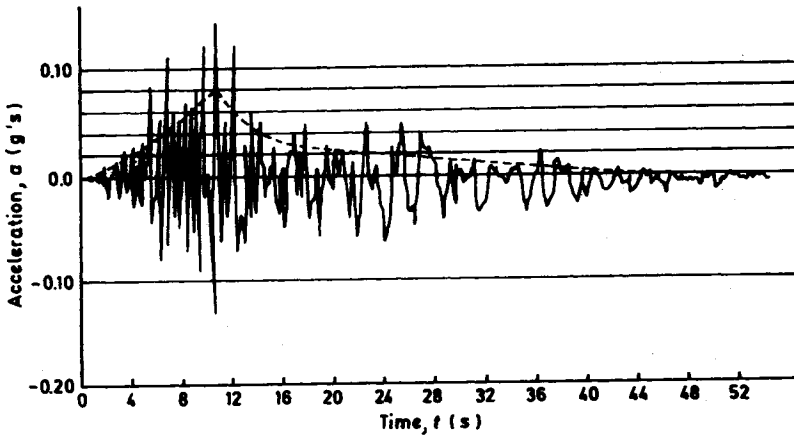


Figure 2.9

Table 2.6 Bucharest, 1977 (see Figure 2.10): $t_f = 14$ s, $\Sigma(a\Delta t)_f = 0.72$, $\cos \theta = 36^\circ$

| t/t_f | $\Sigma(a\Delta t)/\Sigma(a\Delta t)_f$ | $e^{0.12[1-(t_f/t)^{1.8}]}$ |
|---------|---|-----------------------------|
| 0 | 0 | 0 |
| 0.1 | 0.04 | ~ 0 |
| 0.2 | 0.19 | 0.13 |
| 0.3 | 0.46 | 0.40 |
| 0.4 | 0.63 | 0.60 |
| 0.5 | 0.73 | 0.74 |
| 0.6 | 0.81 | 0.83 |
| 0.7 | 0.88 | 0.90 |
| 0.8 | 0.93 | 0.94 |
| 0.9 | 0.97 | 0.97 |
| 1.0 | 1.00 | 1.00 |

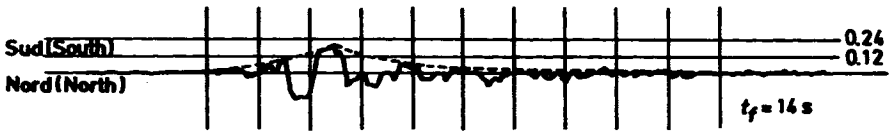


Figure 2.10

CHAPTER 3

THE CANONICAL ISOSEISMAL CHART AND ITS PARAMETERS

INTRODUCTION

One of the problems inherent in the development of rational theories in earthquake engineering is the uncertainty as to which parameters are important for the various phenomena observed in the field. The aim of the present approach to the analysis of the two sets of experimental data which are included in this textbook is to recognize, if possible, these significant parameters. In all cases, this required initial hypotheses or postulates which then had to be checked out against actual observed phenomena.

The basic parameters could be particular physical quantities or they could be invariant models or equations. Both sets are considered and utilized in this text. The previous chapter presented the results of this approach when applied to the accelerogram, which is one of the two sets of field data. This chapter discusses the procedure as it is applied to the second set of experimental data — the isoseismal intensity contour chart. Data from twenty-eight different earthquakes are used to check the basic postulates and the derived expressions.

The intensity contour scale is generally given in descriptive terms, indicating damage or the effects on humans corresponding to different intensities of the earthquakes. The most common intensity scale is the Modified Mercalli Scale (MM) going from 1 to 12 as indicated in the following, reprinted with permission from *Elementary Seismology*, by Charles F. Richter, W. H. Freeman and Company, San Francisco, Copyright © 1958. The scale is also shown in Appendix 2 of Newmark and Rosenblueth.¹

To eliminate many verbal repetitions in the original scale, the following convention has been adopted. Each effect is named at that level of intensity at which it first appears frequently and characteristically. Each effect may be found less strongly, or in fewer instances, at the next lower grade of intensity, more strongly or more often at the next higher grade. A few effects are named at two successive levels to indicate a more gradual increase.

Masonry A, B, C, D. To avoid ambiguity of language, the quality of masonry, brick or otherwise, is specified by the following lettering (which has no connection with the conventional Class A, B, C construction).

Masonry A. Good workmanship, mortar, and design; reinforced, especially laterally, and bound together by using steel, concrete, etc.; designed to resist lateral forces.

Masonry B. Good workmanship and mortar; reinforced, but not designed in detail to resist lateral forces.

Masonry C. Ordinary workmanship and mortar; no extreme weakness like failing to tie in at corners, but neither reinforced nor designed against horizontal forces.

Masonry D. Weak materials, such as adobe; poor mortar; low standards of workmanship; weak horizontally.

Modified Mercalli Intensity Scale of 1931 (Abridged and rewritten †)

- I.* Not felt. Marginal and long-period effects of large earthquakes (for details see text).
- II.* Felt by persons at rest, on upper floors, or favorably placed.
- III.* Felt indoors. Hanging objects swing. Vibration like passing of light trucks. Duration estimated. May not be recognized as an earthquake.
- IV.* Hanging objects swing. Vibration like passing of heavy trucks; or sensation of a jolt like a heavy ball striking the walls. Standing motor cars rock. Windows, dishes, doors rattle. Glasses clink. Crockery clashes. In the upper range of IV wooden walls and frame creak.
- V.* Felt outdoors; direction estimated. Sleepers wakened. Liquids disturbed, some spilled. Small unstable objects displaced or upset. Doors swing, close, open. Shutters, pictures move. Pendulum clocks stop, start, change rate.
- VI.* Felt by all. Many frightened and run outdoors. Persons walk unsteadily. Windows, dishes, glassware broken. Knick knacks, books, etc., off shelves. Pictures off walls. Furniture moved or overturned. Weak plaster and masonry D cracked. Small bells ring (church, school). Trees, bushes shaken (visibly, or heard to rustle — CFR).
- VII.* Difficult to stand. Noticed by drivers of motor cars. Hanging objects quiver. Furniture broken. Damage to masonry D, including cracks. Weak chimneys broken at roof line. Fall of plaster, loose bricks, stones, tiles, cornices (also unbraced parapets and architectural ornaments — CFR). Some cracks in masonry C. Waves on ponds; water turbid with mud. Small slides and caving in along sand or gravel banks. Large bells ring. Concrete irrigation ditches damaged.

† The author takes full responsibility for this version, which, he believes, conforms closely to the original intention. He requests that, should it be necessary to specify it explicitly, the reference be 'Modified Mercalli Scale, 1956 version,' without attaching his name. The expression 'Richter scale' is popularly attached to the magnitude scale; this is desirable to forestall confusion between magnitude and intensity.

- VIII.** Steering of motor cars affected. Damage to masonry C; partial collapse. Some damage to masonry B; none to masonry A. Fall of stucco and some masonry walls. Twisting, fall of chimneys, factory stacks, monuments, towers, elevated tanks. Frame houses moved on foundations if not bolted down; loose panel walls thrown out. Decayed piling broken off. Branches broken from trees. Changes in flow or temperature of springs and wells. Cracks in wet ground and on steep slopes.
- IX.** General panic. Masonry D destroyed; masonry C heavily damaged, sometimes with complete collapse; masonry B seriously damaged. (General damage to foundations — CFR). Frame structures, if not bolted, shifted off foundations. Frames racked. Serious damage to reservoirs. Underground pipes broken. Conspicuous cracks in ground. In alluviated areas sand and mud ejected, earthquake fountains, sand craters.
- X.** Most masonry and frame structures destroyed with their foundations. Some well-built wooden structures and bridges destroyed. Serious damage to dams, dikes, embankments. Large landslides. Water thrown on banks of canals, rivers, lakes, etc. Sand and mud shifted horizontally on beaches and flat land. Rails bent slightly.
- XI.** Rails bent greatly. Underground pipelines completely out of service.
- XII.** Damage nearly total. Large rock masses displaced. Lines of sight and level distorted. Objects thrown into the air.

A further basic premise in our analysis of the separate (but related) research areas being discussed was that the key element in all phases of the earthquake engineering happening is the 'energy'. The different topics consider energy from the alternate points of view relevant for the particular subject involved. Thus,

1. Chapter 1 is a study of a new earthquake mechanism in which a closed form non-unique solution is obtained for a possible earthquake-producing occurrence. An approximate value of the energy developed by this mechanism is calculable. The mechanism is consistent with a horizontal rupture failure, a type of action which is here suggested as a possible deep focus mechanism. In Chapter 1 it is also shown as a mechanism which is consistent with a shallower focus in conjunction with a particular geological condition (the caldera) as well as three other different types of earthquake happenings.
2. Chapter 2 represents a hypothesized theory, founded on the canonical accelerogram record, for the timewise distribution of energy created by an earthquake mechanism.
3. The present chapter discusses a postulated theory of spacewise distribution of energy from the earthquake, based upon a particular canonical isoseismal record.
4. The following chapters will develop superposition theories for the canonical accelerograms and the canonical isoseismal charts (Chapter 6 and 7), and also a set of design curves and similar aids which will be utilized in the rational

studies of damage assessment (Chapters 4 and 8) and also in the design-analysis process (Chapters 10 and 11).

5. One of the principal design curves developed in Chapter 4 will introduce a direct connection between the qualitative (descriptive) MM intensity designation and the *quantitative* energy field produced by an earthquake. The combination of qualitative and quantitative statements will expand the definition of intensity and will enable engineers to provide more scientific measures of damage assessment as well as structural design procedures.

NOMENCLATURE FOR THIS CHAPTER

- I = Modified Mercalli Scale intensity
 S = distance from epicentre to centre of constant intensity region on the surface of the earth
 k, n = non-dimensional constants
 f = subscript for final
 A, B = numerical constants
 H = the total SHE, surface horizontal energy, generated by the earthquake between the epicentre and the radius S_f
 Y = derivative with respect to the radius S of the SHE between the epicentre and any distance S

THE MATHEMATICAL THEORY

An important consideration involved in this text is the attempt to determine the significant parameters connected with rational earthquake engineering analyses. This chapter is concerned with the canonical form of isoseisms or the canonical isoseismal map. The isoseismal map (see Figure 3.1 which shows the isoseisms of the earthquake which occurred in the Udine region of Italy on June 29, 1873) is a map of the region affected by an earthquake, in which areas of equal intensity are shown. An interesting (and occasionally ignored) aspect of the intensity map is mentioned by Espinosa *et al.*², wherein they emphasize the rather arbitrary and selective (and frequently incorrect) nature of the intensity contours which are used for many earthquakes*.

* This is very graphically illustrated by the data shown in the following figure (bottom of p. 49) which is a chart of the response obtained from some hundreds of Japanese residents of an area struck by a recent earthquake. Each point represents some human perception of intensity vs. distance from the focus for the Japanese intensity scale which differs somewhat but is similar to the MM scale. See in this connection Tech. Rept. No. COE-85-4, "The Tockaki-Oki $M = 7.9$ Earthquake of May 16, 1968 — A Rational Comparison Analysis of the Main Shock Isoseismal Field", Dept. of Civil and Ocean Engineering, Stevens Institute of Technology, Hoboken, N.J. Sept. 1985.

Their comments must surely be appropriate for an earthquake in 1873 shown in Figure 3.1).**

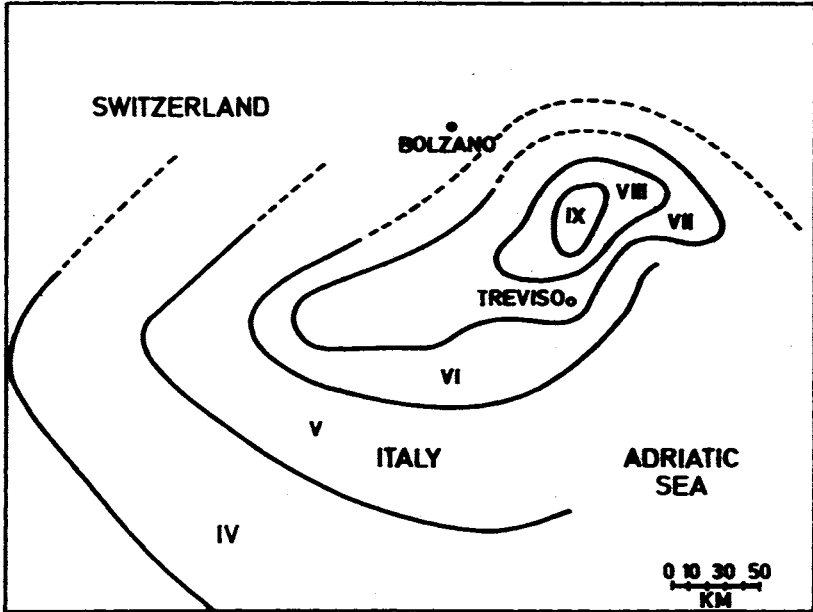


Figure 3.1 Isoseisms of the earthquake occurring on June 29, 1873 in the Udine region of Italy

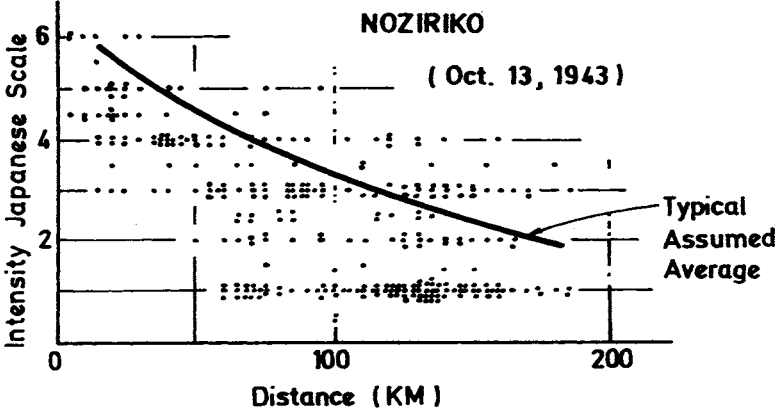


Figure for footnote* (Pg 48)

** Indeed, as shown in Chapter 7 in which the superposition of canonical isoseismal maps is discussed, according to the present rational theory there is a strong likelihood of Figure 3.1 being representative of at least two shocks separated by about 100 km along, roughly, an east-west axis and possibly by some unknown period of time.

On purely physical grounds it would seem reasonable that a measure of the earthquake strength — or of its energy — is connected with the intensity number and the area over which this intensity number acts. Thus, as a first step in the development of a model, it was assumed that the isoseismal curves are *canonical* and may be represented by circles*. Deep-focus earthquakes as well as many shallow point-focus quakes probably generate nearly circular isoseisms. In any case, an average circular representation can be taken as a first step and its validity checked against the realities of actual earthquakes, including the undeniable discrepancies and differences inherent in the determination of accurate isoseisms. Having made the initial 'circular assumption', it is then assumed that a basic parameter for the canonical isoseismal analysis (Figure 3.2) is the product of 'intensity \times average radius to the region of constant intensity.

Physically, this is plausible. The product (IS_{AV}) or simply (IS) is one measure of the energy generated by the earthquake. We shall call this term the Intensity Index. Note that $S = 0$ at the epicentre and increases as one moves into regions of smaller intensity.

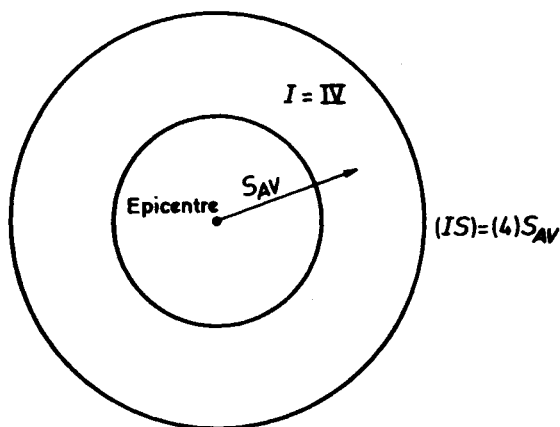


Figure 3.2

* Physically, as was the case for the canonical accelerograms, this probably corresponds most nearly to a single point-focus earthquake response. Admittedly, some of the isoseismal representations are highly unsymmetric. It will be shown in Chapter 7, in which a superposition hypothesis for canonical isoseismal maps will be developed, that the unsymmetric maps may be generated by a superposition of canonical isoseismal curves. These, physically, are very likely due to a series or sequence or cluster of separate point-focus shocks (possibly separated by a time interval in addition to a spatial separation). The long surface fault earthquake may be considered as a 'distributed' shock and the distinction between point-focus and distributed shocks is similar to that between 'concentrated' loads and 'distributed' loads in structural theory. See the lengthy discussion of this, with an example in Chapter 10.

The mathematical development which follows also is reasonable, on mathematical as well as physical bases. We assume

$$\sum_{S=0}^{S=S_{j+1}} (IS) = \sum_{S=0}^{S=S_j} (IS) + \Delta (IS) \Big|_j^{j+1} \quad (1)$$

The next step is a critical one in the mathematical formulation. We assume (note that this preserves dimensional homogeneity and also is physically reasonable),

$$\Delta (IS) = k \sum_{S=0}^{S=S_j} (IS) \frac{S_f^n}{S^{n+1}} \Delta S \quad (2)$$

in which k and n are non-dimensional terms assumed constant. For clarity, the terms in Eqs. (1) and (2) are defined herewith:

- I = Modified Mercalli Scale intensity
- S = distance from epicentre to centre of constant intensity doughnut shaped region
- k, n = non-dimensional constants
- f = subscript for 'final'. $I = III$ represents a suitable final value and this will be assumed to be the case in this analysis and throughout the text.

Now, substituting Eq. (2) in Eq. (1) and proceeding as in Ref. 3, we obtain finally

$$\frac{\sum_{S=0}^{S=S_j} (IS)}{\sum_{S=0}^{S=S_f} (IS)_f} = e^{k[1 - (S_f/S)^n]} \quad (3)$$

This equation must be tested against the realities of actual isoseismals.

Eq. 3 is the postulated 'invariant' of the canonical representation. It presents a correlation between the Intensity Index and distance from the epicentre of the earthquake. To test this hypothesis, the published isoseismals of twenty-eight different earthquakes were utilized. These earthquakes occurred all over the world during the past 500 years. It was found that the best fit for the data from these earthquakes is given by, approximately,

$$\frac{\sum_{S=0}^{S=S_j} (IS)}{\sum_{S=0}^{S=S_f} (IS)_f} = e^{2[1 - (S_f/S)^{1/3}]} \quad (4)$$

At this time it will be assumed that this equation applies to those earthquakes of magnitude equal to or greater than five for intensities equal to and greater than III.

For simplicity, Eq. 4 and the results of five earthquakes only are shown on Figure 3.3. The five earthquakes (which are quite typical) are:

- (a) San Fernando, February 9, 1971⁴
- (b) Friuli, May 6, 1976⁵
- (c) Udine region, June 29, 1873⁶
- (d) Washington State, December 14, 1872⁷
- (e) Imperial Valley, May 18, 1940⁸

and, as indicated in the Appendix to this chapter, all of the twenty-eight earthquakes satisfy the invariant relation, Eq. 4, satisfactorily.*

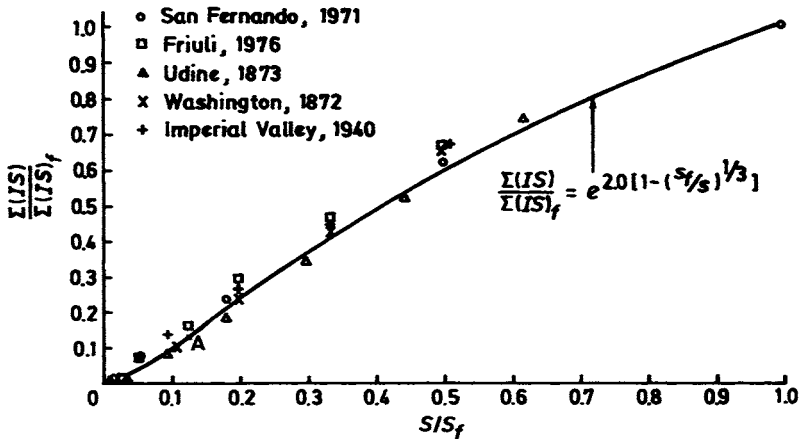


Figure 3.3

* When one considers that the canonical (i.e. circular) assumption was applied to the maps of all 28 earthquakes and that some of these were surely due to multiple quakes which introduced at least some distortion to the circular form, the check on Eq. 4 must be considered as acceptable for engineering design purposes.

ANALYSIS OF THE INVARIANT — EQUATION 4

As is clear from Figure 3.3, a plot of the invariant, Eq. 4 is a typical S or growth curve. The point A, which is the point of zero curvature corresponds, physically, to the point at which the rate of change of the sum of the Intensity Index with distance changes from positive to negative. The full importance of this point is not clear at this time. In any case, it occurs at approximately

$$\frac{S}{S_f} = 0.125 \quad (5)$$

and therefore, from Eq. 4 at the point A

$$\frac{\sum(IS)}{\sum(IS)_f} = 0.135 \quad (6)$$

At this time the values given in Eqs. 4, 5, and 6 will be assumed as fixed average values for typical earthquakes, subject to further check, possible change, or modification as required by a more detailed study of isoseisms for earthquakes throughout the world.

THE PHYSICAL VARIABLES AND THE INVARIANT — EQUATION 4

In Eq. 3, S_f and $\sum(IS)_f$ vary for each earthquake, k and n are, in fact, constants. The significance of these two statements is related to a tentative uniqueness-existence hypothesis which was formulated in Ref. 9, and which will not be discussed in detail in this book, although the conclusions which follow from it were utilized in Chapter 2 and will now be applied to the canonical isoseismal invariant.

It follows from the hypothesis that there are two fundamental parameters involved in the canonical isoseismal chart analysis. By inspection, it is clear that these are S_f and $\sum(IS)_f$, and that these terms vary for different earthquakes. In addition, the tentative theory assumes that this variation of the basic parameters depends upon two physical variables directly related to the canonical isoseismal chart. An analysis of the phenomenon suggests that the two variables quantities are:

1. The average of soil or geological conditions between the epicentre and the distance S_f .
2. The total surface horizontal energy, SHE, between the epicentre and the distance S_f . SHE is the energy which reaches the surface of the earth and which causes the horizontal vibration and damage of structures. In one form

or another it is this quantity which must be determined if rational methods of damage assessment and structural analysis are to be developed for structures subject to earthquake effects. SHE can be expressed in terms of an 'efficiency, η ' in which η converts the total focal earthquake energy into the destructive surface energy. Bolt, as pointed out earlier¹⁰, discusses an efficiency to convert source energy to seismic energy. However, he notes that little is known about the value of η .

Furthermore, and once more based upon physical arguments, we shall assume (subject to further verification) that

- 1a. S_f is the factor influenced by soil or geological conditions.
- 2a. $\Sigma(IS)_f$ is the factor influenced by the total (SHE) of the earthquake. This factor, as noted above, can also be related directly to the magnitude, M , or total focal energy of the earthquake.

The form of the parameters strongly suggests a cross-correlation. Among the indicated topics for future research which this analysis suggests are studies leading either to a confirmation or rejection of the two major correlations hypothesized above.

In any case, the derived invariant, Eq. 4, and the two postulated relations presented above, imply that S_f and $\Sigma(IS)_f$ vary and that these vary depending primarily upon the geological conditions of the region affected by the earthquake and the total SHE or magnitude, M of the earthquake.

It will be seen (Chapter 4) that this conclusion is consistent with the form taken by one of the major design charts developed as part of this rational theory.

THE SPACEWISE VARIATION OF SHE

It is possible to develop an expression for SHE per unit radius at a point on the earth's surface where the Intensity Index is $\Sigma(IS)$. This is done by considering a parallel (although different) physically-based mathematical relation for the variation of the $\Sigma(IS)$ term. The procedure is as follows. Assume

$$\frac{\Delta [\Sigma(IS)]}{\Delta S} = A \frac{Y}{H} \Sigma(IS) \quad (7)$$

in which

A is a numerical constant

H is a physical constant, related to the canonical isoseismal map, say 'the

total SHE generated by the earthquake between the epicentre and the radius S_f' .

and, based upon dimensional as well as physical requirements,

Y is the derivative with respect to the radius S , of the SHE between the epicentre and any radius S .

Now comparing Eq. 7 above and Eq. 2 and equating equivalent terms, we find

$$Y = BH \frac{S_f^{1/3}}{S^{4/3}} \quad (8)$$

in which B is a constant. Note that Eq. 8 has a singularity at $S = 0$, i.e. at the epicenter. The equation will be analysed further in Chapter 4 and will be used in that chapter, and in later chapters, in the damage assessment and structural analysis sections of the textbook. See the footnote on p 38 for the similar accelerogram-time formulation.

CONCLUSION

The second fundamental source of earthquake experimental data, the canonical isoseismal chart, is analysed and an invariant for this phenomenon is obtained. Two basic parameters are also determined in connection with this analysis, these being the distance S_f and Intensity Index, $\Sigma(IS)_f$. Various properties of the invariant are obtained and it is shown that — subject to the accuracy of the field data — twenty-eight earthquakes throughout the world over the past 500 years conform to the derived relation. The parameters are also related to the energy of the earthquake and the results obtained in this chapter will be utilized in later chapters dealing with the damage assessment and structural analysis problems in earthquake engineering.

REFERENCES

1. Nathan M. Newmark and Emilio Rosenblueth. *Fundamentals of Earthquake Engineering*, Prentice-Hall, Inc., Englewood Cliffs, N.J. 1971.
2. A. F. Espinosa, Jose Austurias and A. Quesada. *Applying the Lessons Learned in the 1976 Guatemala Earthquake to Earthquake-Hazard-Zoning Problems in Guatemala*, International Symposium on the Feb. 4, 1976 Guatemalan Earthquake and the Reconstruction Process.

3. S. F. Borg. *Similarity Solutions in the Engineering, Physical-Chemical, Biological-Medical and Social Sciences*, Proceedings of Symposium 'Symmetry, Similarity and Group Theoretic Methods in Mechanics', P. G. Glockner and M. E. Singh (Eds.), Univ. of Calgary, August 1974.
4. Karl V. Steinbrugge *et al.* *San Fernando Earthquake, Feb. 9, 1971*, Pacific Fire Rating Bureau, 465 California St., San Francisco, Calif. 1971.
5. F. Giorgetti. Isoleismal map of the May 6, 1976 Friuli earthquake, *Boll. Geof. Teor. Appl.*, XIX, No. 72, Fig. 1, Udine, Dec. 4–5, 1976.
6. Proceedings of the Specialist Meeting on *The Friuli Earthquake and the Antiseismic Design of Nuclear Installations*, 1, 114, OE CD-NEA/CSNI Rept. No. 28, Rome, Italy, 11–13 October, 1977.
7. Neville C. Donovan. *Let's Be Mean*, NSF Seminar — Workshop on Strong Ground Motion, San Diego, Feb. 1978.
8. Frank Neumann. *Earthquake Intensity and Related Ground Motion*, Univ. of Wash. Press, 1954, as reproduced in Giorgetti,⁵ p. 219, Fig. 7.1.
9. S. F. Borg. *Generalized Tensors and Matrices*, Proc. Second International Conference on Mathematical Modeling, St. Louis, Missouri, July, 1979.
10. Robert L Wiegel (Ed. *Earthquake Engineering*, Chap. 2 written by Bruce A. Bolt, Prentice-Hall, Inc., Englewood Cliffs, N.J., 1970.
11. S. F. Borg. *An Isoleismal-Energy Correlation for Use in Earthquake Structural Design*, Seventh World Conf. on Earthquake Engineering, Istanbul, Turkey, Sept 8–13, 1980. Also Technical Report ME/CE-792 Dep't of Mechanical Engineering (Civil Engineering), Stevens Institute of Technology, Hoboken, N.J., Dec. 1979.
12. F. Machado. *Seismology-Portugal: Curso de Sismologia*, Imprimarte SARL, Losboa 1970.
13. National Academy of Sciences. *Seismology, Responsibilities and Requirements of a Growing Science*, Part II, 1970.
14. M. Bath. *Introduction to Seismology*, Berkhauser Verlag, Basil, Borton, Stuttgart, Germany, 1979.
15. K. E. Bullen. *New Zealand Seismology*, Methuen, London, 1954.
16. Australian Congress. *Earthquake Engineering Symposium*, Melbourn, 1969.
17. E. J. Ramirez. *Historia de los Terremotos en Colombia*, Institute Geografico Agustin Godazzi, Bogota, 1969.
18. AISI. *The Agadir Morocco Earthquake*, American Iron and Steel Institute, N.Y. 1962.
19. Indonesia Earthquakes. *Lembaga Meteorolog dan Geofisika*, Ministry of Communications, Meteorological and Geophysical Institute, Jakarta, 1971.
20. G. L. Berlin. *Earthquakes and the Urban Environment*, Vol. II, CRC Press Inc., West Palm Beach, Fla. 1978.

21. James M. Gere and Hareesh C. Shan. *Tangshan rebuilds after mammoth earthquake*, Dec. 1980, Civil Engineering.
22. The New York Times, Feb. 16, 1981.
23. S. F. Borg. *Extended Analysis of Isoseismal-Magnitude-Intensity Index Correlations in Earthquake Engineering*, Technical Report ME/CE-81-1, Department of Mechanical Engineering (Civil Engineering), Stevens Institute of Technology, Hoboken, N.J., May, 1981.

APPENDIX

Eqs. (4) and Figure 3.3 were checked against twenty-eight different earthquakes in various parts of the world that had occurred in the past five hundred years. Detailed computations are shown for four of these. References and a summary of all twenty-eight are shown in the Summary Table 3.5.

The model was brought down to intensity III, which agrees with the other checks made and appears to be about the smallest intensity that can usually be observed or felt. For the Friuli data, since the map⁵ only went down to intensity VII, the lower intensity values were obtained from a line drawn on the Neumann curve⁸ parallel to the lines previously drawn for the California earthquakes. This appears to be reasonable since the higher intensity values (obtained from Figure 3.3) do fall on this assumed line.

A final statement concerning Figure 3.3. It is clearly possible to obtain a closer fit of the data by choosing other values for k and n . Also, k and n are not unique (although there is little variation possible in these for a close fit). It is not deemed worthwhile to belabour the point concerning k , n values. It must be remembered that the data itself — the isoseismal maps — are extremely subjective and representations of the same event by different investigations would result in more variation than shown in Figure 3.3. Eq. 4 may be pointed to as just one of a number of different equations that could be used to represent the variation. This is true — but Eq. 4 is useful in several respects. It is dimensionally sound, it has reasonable physical and mathematical bases, and, furthermore, it permitted an extension corresponding to Eq. 8.

It is a hypothesized equation. It must be checked out further. But it appears to be a very promising first step in the direction of developing a rational, analytical knowledge of a particular phase of the earthquake problem and it does lend itself to extended applications to the damage assessment and structural design problems. In all cases the applications give reasonable numerical results that checked well against available data.

Table 3.1 San Fernando, February 9, 1971^{4,11}

| <i>I</i> | Distance to Outer Reach (miles) | S_{AV} | (IS) | $\frac{S_f}{S}$ | $\frac{S}{S_f}$ | $\frac{\Sigma(IS)}{\Sigma(IS)_f}$ |
|-----------------------|---------------------------------------|----------|----------|-----------------|-----------------|-----------------------------------|
| Epicentre | 0 | 0. | 0 | ∞ | 0 | 0 |
| VIII-IX | 5 | 2.5 | 21.3 | 72 | 0.014 | 0.018 |
| VII | 15 | 10 | 70 | 18 | 0.06 | 0.08 |
| VI | 50 | 32.5 | 195 | 5.5 | 0.18 | 0.24 |
| V | 130 | 90 | 450 | 2 | 0.50 | 0.62 |
| I-IV (SAY. II 1/2) | 250 | 190 | 450 | 1 | 1.0 | 1.00 |

Table 3.2 Friuli, May 6, 1976^{5,11}

| <i>I</i> | Distance to Outer Reach (km) | S_{AV} | (IS) | $\frac{S_f}{S}$ | $\frac{S}{S_f}$ | $\frac{\Sigma(IS)}{\Sigma(IS)_f}$ |
|-----------|------------------------------------|----------|----------|-----------------|-----------------|-----------------------------------|
| Epicentre | 0 | 0 | 0 | ∞ | 0 | 0 |
| X | 8 | 4 | 40 | 125 | 0.01 | 0.008 |
| IX | 17 | 12.5 | 112 | 40 | 0.02 | 0.032 |
| VIII | 38 | 27.5 | 220 | 18 | 0.06 | 0.08 |
| VII | 85 | 62 | 434 | 8 | 0.12 | 0.17 |
| VI | 120 | 102 | 612 | 5 | 0.20 | 0.30 |
| V | 205 | 162 | 810 | 3 | 0.33 | 0.47 |
| IV | 300 | 252 | 1008 | 2 | 0.50 | 0.68 |
| III | 700 | 500 | 1500 | 1 | 1.0 | 1.00 |

Table 3.3 Udine Region, June 29, 1973^{6,11}

| <i>I</i> | Distance to Outer Reach (km) | S_{AV} | (IS) | $\frac{S_f}{S}$ | $\frac{S}{S_f}$ | $\frac{\Sigma(IS)}{\Sigma(IS)_f}$ |
|----------|------------------------------------|----------|----------|-----------------|-----------------|-----------------------------------|
| X | 0 | 0 | 0 | ∞ | 0 | 0 |
| IX | 12 | 6 | 54 | 34 | 0.03 | 0.02 |
| VIII | 27 | 19 | 152 | 10.8 | 0.09 | 0.09 |
| VII | 45 | 36 | 252 | 5.7 | 0.18 | 0.19 |
| VI | 80 | 63 | 378 | 3.3 | 0.30 | 0.35 |
| V | 100 | 90 | 450 | 2.3 | 0.43 | 0.53 |
| IV | 160 | 130 | 520 | 1.6 | 0.63 | 0.75 |
| III | 250 | 205 | 615 | 1.0 | 1.00 | 1.00 |

Table 3.4 Imperial Valley, May 18 1940^{8,11}

| <i>I</i> | Distance to outer reach (km) | S_{AV} | (IS) | $\frac{S_f}{S}$ | $\frac{S}{S_f}$ | $\frac{\Sigma(IS)}{\Sigma(IS)_f}$ |
|----------|------------------------------------|----------|--------|-----------------|-----------------|-----------------------------------|
| X | 0 | 0 | 0 | ∞ | 0 | 0 |
| IV | 3 | 1.5 | 14 | 50 | 0.02 | 0.02 |
| VIII | 5 | 4 | 32 | 18.8 | 0.05 | 0.07 |
| VII | 9 | 7 | 49 | 10.7 | 0.09 | 0.14 |
| VI | 20 | 15 | 90 | 5 | 0.20 | 0.27 |
| V | 30 | 25 | 125 | 3 | 0.30 | 0.45 |
| IV | 50 | 40 | 160 | 1.9 | 0.53 | 0.68 |
| III | 100 | 75 | 225 | 1.0 | 1.00 | 1.00 |

Table 3.5 Summary data for twenty-eight earthquakes

| Designation | Earthquake | S_f km | $\frac{\Sigma(IS)_f}{S}$ in km | Ref. |
|-------------|------------------------|----------|-----------------------------------|------|
| a | San Fernando, 1971 | 300 | 2360 | 4 |
| b | Friuli, 1976 | 500 | 5000 | 5 |
| c | Udine, 1873 | 205 | 2420 | 6 |
| d | Washington State, 1872 | 900 | 8000 | 7 |
| e | Imperial Valley, 1940 | 75 | 700 | 8 |
| f | Valparaiso, 1906 | 1100 | 15000 | 1 |
| g | Mexico, 1962 | 390 | 4700 | 1 |
| h | S. Miguel, 1522 | 115 | 1620 | 12 |
| i | Lisbon, 1755 | 1500 | 23350 | 12 |
| j | S. Jorge, 1757 | 125 | 1970 | 12 |
| k | Charleston, 1886 | 1500 | 23200 | 13 |
| l | San Francisco, 1906 | 550 | 4420 | 14 |
| m | Messina, 1908 | 335 | 4430 | 12 |
| n | Benavente, 1909 | 340 | 3450 | 12 |
| o | Hawke's Bay, 1921 | 440 | 4380 | 15 |
| p | Faial, 1926 | 100 | 1160 | 12 |
| q | Wairoa, 1932 | 250 | 2600 | 15 |
| r | Madeira, 1946 | 1150 | 14500 | 12 |
| s | Wewak, 1946 | 280 | 2450 | 16 |
| t | Orleanville, 1954 | 95 | 1375 | 12 |
| u | Arboledos, 1950 | 80 | 1040 | 17 |
| v | Agadir, 1960 | 30 | 460 | 18 |
| w | Madjene, 1969 | 65 | 760 | 19 |
| x | Agadir, 1969 | 50 | 725 | 12 |
| y | Bantarkawung, 1971 | 75 | 730 | 12 |
| z | Lice, 1975 | 80 | 780 | 20 |
| aa | Tangshan, 1976 | 700 | 9770 | 21 |
| bb | Corinth, 1981 | 95 | 1040 | 22 |

In Table 3.5, on page 59, are shown the key values for twenty-eight different earthquakes which have occurred in the past 500 years all over the world. Each of these has a canonical isoseismal map which corresponds to Eq. 4 and Figure 3.3, subject to the probable accuracy of the data as reported in the references and also to the possibility that the published isoseismal data actually corresponds to more than a single-shock earthquake. In this table are shown values for $\Sigma(IS)_f$, S_f and the references from which the data are obtained. The detailed tabulations for those earthquakes not shown in Tables 3.1 to 3.4 are given in Ref. 23.

CHAPTER 4

THE EARTHQUAKE ENGINEERING DAMAGE ASSESSMENT AND STRUCTURAL DESIGN CHARTS AND CURVES

INTRODUCTION

As noted previously, the main thrust and purpose of this textbook is to develop earthquake theories and procedures that can be used by engineering design offices and others involved with the damage assessment and structural design aspects of the event. Furthermore, it was pointed out that derived invariants and parameters were to be utilized and these in conjunction with energy, since energy in one form or another is at the core of all phases of the earthquake phenomena.

In the previous two chapters, the canonical accelerogram and the canonical isoseismal chart were analysed from the invariant-parameter point of view and it was shown that these can be represented, to an acceptable degree of engineering accuracy, by means of suitable invariants in terms of particular parameters which hold for the two basic sets of data.

In this chapter, these results are extended and a group of six engineering design tools will be described. These six (and the two canonicals) represent the body of engineering design data that are included in this rational theory. Briefly, they are (each will be described in more detail as it is introduced and discussed later in the chapter):

- A) The temporal variation of energy per unit area at a point.
- B) The spacewise variation of energy over the entire field.
- C) The Magnitude — $\Sigma(IS)_f - S_f$ — Geology chart.
- D) The Magnitude-Intensity-Distance (MID) chart.
- E) The Intensity — $\Sigma(a\Delta t)_f - t_f$ — Geology chart.
- F) The Energy-Intensity Compatibility relation.

These charts, whose parameters are those previously described as well as other well-known variables of earthquake engineering such as focal depth and efficiency

of earthquake, will be the basic design tools for analysing earthquake damage assessment and structural design.

Those to be used for damage assessment will be discussed further in Chapter 8. Those that are to be used for structural and related analyses and design will be utilized in Chapters 10 and 11.

Some additional comments are in order concerning the accuracy of the two basic sources of data. In the first place, it must be recognized that the accelerogram and isoseismal are two major sources of direct data available for the effect of an earthquake. Some of the uncertainty has been pointed out: 'Following a strong earthquake, different stations report magnitudes often differing more than one degree from each other. Within 8 hours these values are unified to within 0.2 degrees, giving the impression of great precision. The spread in intensities assessed by different observers is even greater'.¹

The charts and curves developed in this and earlier chapters are not 'exact' (even if we assume that exactness is possible in any engineering analysis).

However, it must also be recognized that the theories and developments presented here do have sound physical, mathematical, and dimensional bases. In their entirety, they form a rational, interrelated, coherent theory of the earthquake response, suitable for engineering design and related purposes (such as damage assessment) by the average engineering office. The charts are self-correcting, in the sense that in their present, early forms they are subject to revision and greater precision should follow as more data is collected and correlated with derived expressions.

For completeness, very brief statements concerning the canonical accelerogram and canonical isoseismal chart are repeated from Chapters 2 and 3.

NOTATION FOR THIS CHAPTER

The different terms in this chapter are collected and presented below:

- a = ordinate to accelerogram envelope
- f = subscript, final
- i = subscript, small lower value or 'initial'
- t = time
- B = a numerical constant
- D = distance
- E = energy, in ergs, of earthquake at the focus. This term is related to the magnitude, M , of the earthquake
- G = a numerical constant
- H = total surface horizontal energy of the earthquake between the radius S_i and up to and including the Intensity = III radius, S_f

- I = Intensity of the earthquake at a point
- K = a constant
- M = magnitude of the earthquake
- \mathcal{R}_m = designation for geological region m
- S_j = distance from epicentre to mid-radius of the j th intensity band
- T = derivative of the surface horizontal energy (due to the earthquake) with respect to the time, t , at the accelerogram location
- W = total surface horizontal energy between the small inner radius, S_f , and the radius S
- Y = derivative of the surface horizontal energy with respect to the radial distance S
- ϵ_t = surface horizontal energy per unit area between the times t_f and t at the accelerogram location
- θ = angle made by accelerograph direction and a ray from the epicentre
- η = efficiency of the earthquake, i.e. $H = \eta E$

THE CANONICAL ACCELEROGRAM CHART AND PARAMETERS

As noted in Chapter 2, a canonical invariant can be derived for the accelerogram in terms of a bounding envelope and the two fundamental parameters $\Sigma(a\Delta t)$, the Acceleration Index, and t_f for this canonical accelerogram. The resulting invariant is given by Eq. 1 and Figure 4.1 which follow (these have been reproduced from Chapter 2).

$$\frac{\Sigma(a\Delta t)}{\Sigma(a\Delta t)_f} = e^{0.12[1 - (t_f/t)^{1.8}]} \tag{1}$$

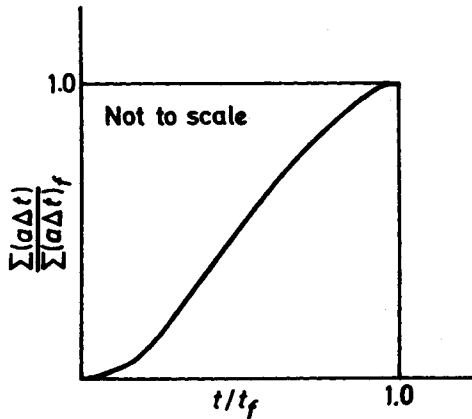


Figure 4.1

THE CANONICAL ISOSEISMAL CHART AND ITS PARAMETERS

As indicated in Chapter 3, if the 'circular approximation' assumption is made, then canonical isoseismal charts for $M > 5$ earthquakes can be represented by the following equation and the curve in Figure 4.2, these being the invariant for this very important source of field data. Note, Eq. 2 and Figure 4.2 are given in terms of the basic parameters for this quantity, these being $\Sigma(IS)$, the Intensity

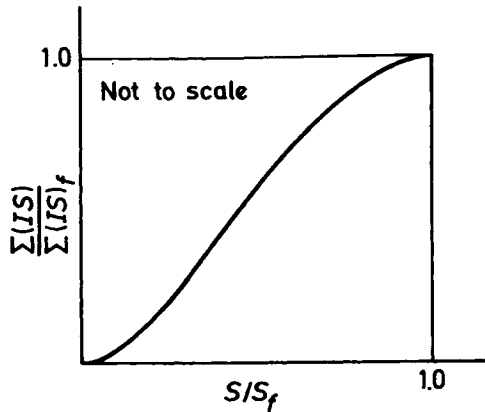


Figure 4.2

Index and S , the distance from the epicentre to the midpoint of the $I = \text{constant}$ intensity band.

$$\frac{\Sigma(IS)}{\Sigma(IS)_f} = e^{2.0[1 - (S_f/S)^{1/3}]} \quad (2)$$

THE 'GEOLOGY' OF A REGION

We must assume that the effect of an earthquake on structures is related to (among other variables) the mechanism and also to the depth of focus of the earthquake as well as to the overall geological character of the earthquake field. To attempt an exact analysis including these as variables (in addition to other possible 'geological' factors) would be an impossible task. We can, however, assume initially three separate, different geological regions as an approximation to the effect of geology on the engineering response.

A three-region classification is given in terms of (in Ref. 10),

1. The Circumpacific Belt,
2. The Alpine Belt,
3. The Low Seismicity Region.

In this chapter and in later sections of the text we shall use a somewhat different scheme mentioned in *EE-DA&SD* with designations as noted:

1. Surface Fault Region, \mathcal{R}_1 .
2. Mountain Region, \mathcal{R}_2 .
3. Plains Region, \mathcal{R}_3 .

In a very rough way, the focal depth increases with the number designation given above and therefore the effect of focal depth, for simplicity, will at this time be assumed as accounted for in the geologic region designation. In the next chapter a different approximate analysis is developed, based upon energy considerations, to account for the effect of focal depth. The frequencies of the accelerations also will be assumed as roughly correlated with the geology and accounted for in the designation. See, in this connection, the discussion in Section D of Chapter 10.

Also, the three-region classification of Ref. 10 is considered as, roughly, equivalent to the $\mathcal{R}_1, \mathcal{R}_2, \mathcal{R}_3$ designations given above.

Finally, if it is found to be necessary for engineering purposes, more (or less) than three geologies can be introduced — in each of which conditions are approximately invariant for all earthquakes.

Now we consider the six design tools mentioned previously.

A) THE TEMPORAL VARIATION OF ENERGY AT A POINT

In Chapter 2, it was shown in Eq. 9, that

$$T = B \epsilon_{t_f} \frac{t_f^{1.8}}{t^{2.8}} \quad (3)$$

in which

T = derivative of the surface horizontal energy per unit area with respect to the time, t , due to the earthquake at the accelerogram location

B = a numerical constant

ϵ_{t_f} = the total surface horizontal energy per unit area supplied by the earthquake as the point where the accelerogram is obtained

t, t_f = any time t and the total time, t_f , of the accelerogram record

Using Eq. 3 we can determine the value of B by integrating over the interval

$\int_{t_i \rightarrow 0}^{t_f}$, in which t_i is a very small time, and it is introduced in order to surmount the infinity at $t = 0$.

Then

$$\int_{t_i}^{t_f} B \epsilon_{t_f} \frac{t_f^{1.8}}{t^{2.8}} dt = \int_{t_i}^{t_f} T dt = \epsilon_{t_f} \quad (4)$$

and therefore

$$T = \frac{\epsilon_{t_f} t_f^{1.8}}{1.8 \left[\left(\frac{t_f}{t_i} \right)^{1.8} - 1 \right] t^{2.8}} \quad (5)$$

Also

$$\begin{aligned} \int_{t_i}^t T dt &= - \frac{1.8 \epsilon_{t_f}}{1.8 \left[\left(\frac{t_f}{t_f} \right)^{1.8} - 1 \right]} \left(\frac{t_f}{t} \right)^{1.8} \Big|_{t_i}^t \\ &= \epsilon_{t_f} \frac{\left[\left(\frac{t_f}{t} \right)^{1.8} - \left(\frac{t_f}{t_i} \right)^{1.8} \right]}{\left[1 - \left(\frac{t_f}{t_i} \right)^{1.8} \right]} \\ &= \epsilon_t \end{aligned} \quad (6)$$

where ϵ_t = surface horizontal energy per unit area between the times t_i and the t at the accelerogram location.

Thus finally

$$\frac{\epsilon_t}{\epsilon_{t_f}} = \frac{\left[\left(\frac{t_f}{t} \right)^{1.8} - \left(\frac{t_f}{t_i} \right)^{1.8} \right]}{\left[\left(\frac{t_f}{t_i} \right)^{1.8} - 1 \right]} \quad (7)$$

and clearly as t goes from $t_i \rightarrow t_f$, this ratio goes from 0 to 1 as required.

The question which must be answered now, is — ‘What is the value of t_i ’? An inspection of typical canonical accelerograms indicates that if we take

$$\frac{t_f}{t_i} \cong 10 \quad (8)$$

the results (at least initially) appear to be acceptable for engineering purposes. Subject to revision as more data indicates, we shall use this value, from which, finally, the temporal variation of surface horizontal energy at a point is given by

$$\frac{\epsilon_t}{\epsilon_{t_f}} = \frac{63 - \left(\frac{t_f}{t}\right)^{1.8}}{62} \quad (9)$$

which plots as shown on Figure 4.3. Also shown on this figure are curves corresponding to other values of t_f/t_i . Figure 4.3 may be used in design applications, subject to revision as more data is collected.

Insofar as engineering applications of Eq. 7 are concerned, the most important fact is that for all reasonable values of t_f/t_i , the analysis indicates that practically *all* of the earthquake energy at the accelerogram location is applied at the ground surface (and hence to the structure at the given location) in a very short time period after initiation of the ground motion. This phenomenon is utilized in the structural analysis portion of the rational theory which will be presented in a later chapter and also in the damage assessment analysis of superposed multiple canonical shocks.

B) THE SPACEWISE VARIATION OF ENERGY OVER THE ENTIRE FIELD

In Chapter 3, it was shown that the variation of surface horizontal energy with distance over the area affected by a single-shock earthquake is given by

$$Y = BH \frac{S_f^{1/3}}{S^{4/3}} \quad (10)$$

The various terms are defined as follows:

Y = derivative with respect to the radius, S , of the SHE generated by the earthquake.

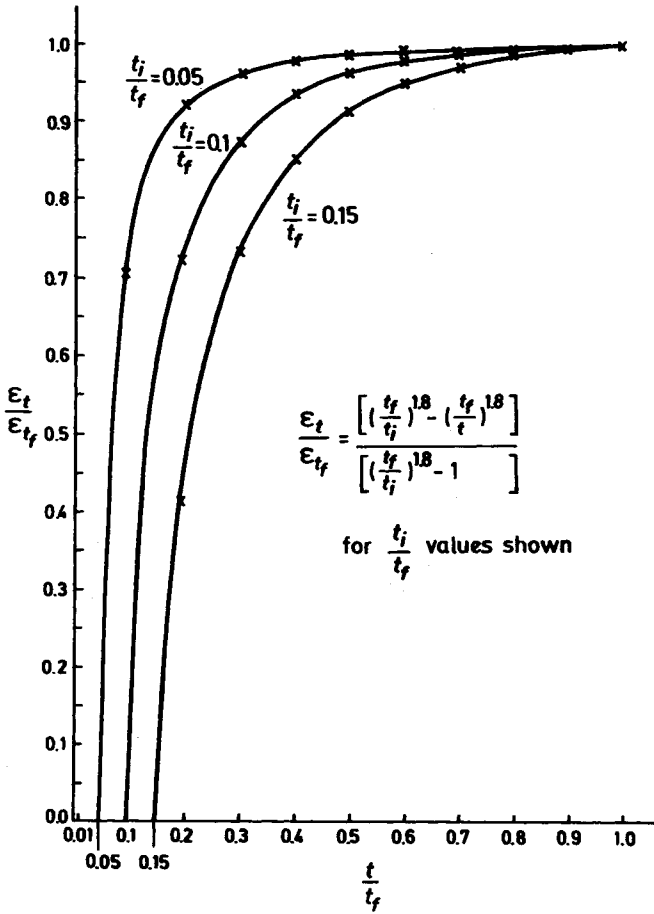


Figure 4.3

B = a constant

S_i = a small radial distance, lower limit of the integration to remove the singularity at $S = 0$

S = radial distance in the earthquake field

S_f = radial distance to the centre of the $I = III$ field, the maximum distance in this analysis

H = total surface horizontal energy of the earthquake between S_i and the Intensity = III radius, S_f

W = total surface horizontal energy between the small inner radius S_i and the radius S

If we integrate Eq. 10 between the limits $S_i \rightarrow S$ we obtain

$$W = KH \left[\left(\frac{S_f}{S_i} \right)^{1/3} - \left(\frac{S_f}{S} \right)^{1/3} \right] \quad (11)$$

K = a constant which we evaluate by noting that $W = H$ when $S = S_f$, so that

$$K = \frac{1}{\left[\left(\frac{S_f}{S_i} \right)^{1/3} - 1 \right]} \quad (12)$$

and therefore

$$\frac{W}{H} = \frac{\left[\left(\frac{S_f}{S_i} \right)^{1/3} - \left(\frac{S_f}{S} \right)^{1/3} \right]}{\left[\left(\frac{S_f}{S_i} \right)^{1/3} - 1 \right]} \quad (13)$$

Consider the S values and, in particular, the fact that they have a dual nature, i.e.

- (1) in the canonical isoseismal invariant, Eq. 2, they have discrete values, S_{III} , S_{IV} , etc.
- (2) in the energy variation over the field equation, Eq. 13, they have continuous values, i.e. energy = $f(S)$.

This behaviour is not unknown in applied mechanics. The performance of S noted above is similar to (but not the same as) the eigenvalue conduct of, say, the column buckling problem in which a term kx/R has the values $\pi, 2\pi, \dots, n\pi$ for determining the critical buckling loads, P_{cr} , although the deflection of the member, as a function of x is continuous for $0 < x < \ell$.

In this earthquake engineering analysis, the analogous procedure is that in (1) above, S_j has the values S_{III} , S_{IV} , etc. for determining the isoseismal index relation, but the energy throughout the earthquake regions as a function of S is continuous for $S_i < S < S_f$, as of course, it must be.

The question arises concerning the value of S_i , the 'small' inner radius. Because of the $1/3$ power, the choice is somewhat insensitive to most reasonable assumptions. To indicate one form of the variation, Table 4.1 which follows

shows values of W/H for several values of S_f/S_i and a particular value of S_f/S . Considering the uncertainty in the value of H , the numbers shown in the last column represent an acceptable spread.

Table 4.1 Values of W/H

| S_f/S_i | $(S_f/S_i)^{1/3}$ | (W/H) for $(S_f/S)^{1/3} = 2$ |
|-----------|-------------------|---------------------------------|
| 1,000,000 | 100 | 0.99 |
| 1,000 | 10 | 0.89 |
| 125 | 5 | 0.75 |

For preliminary, tentative design purposes, subject to revision, we shall assume that $S_f/S_i = 1000$ or Eq. 13 becomes

$$\frac{W}{H} = \frac{10 - \left(\frac{S_f}{S}\right)^{1/3}}{9} \quad (14)$$

for $S_i < S < S_f$. See also Figure 4.4, a plot of Eq. 14 and also of several other curves corresponding to the S_i/S_f values shown.

C) THE MAGNITUDE — $\Sigma(IS)_f$ — S_f — GEOLOGY CHART

Introduction

One of the basic tools in the present rational theory of earthquake engineering is a curve or chart showing the relation between the canonical isoseismal quantities (intensity and distance from earthquake centre), geology and magnitude of the earthquake.

This curve is the source for determining the values of two of the fundamental parameters used in structural design and damage assessment in the new theory, these being $\Sigma(IS)_f$ and S_f .

As is the case in all newly emergent engineering theories, an essential step in establishing the relationship is a 'calibration' or determination of 'allowables' for the key parameters. Furthermore, this calibration can generally be obtained only by resorting to experimental measurement. In this case the 'experiment' must be an actual earthquake.

A first primitive form of the chart was presented in *EE-DA&SD* at which time the tentative and approximate nature of the data was emphasized — although it

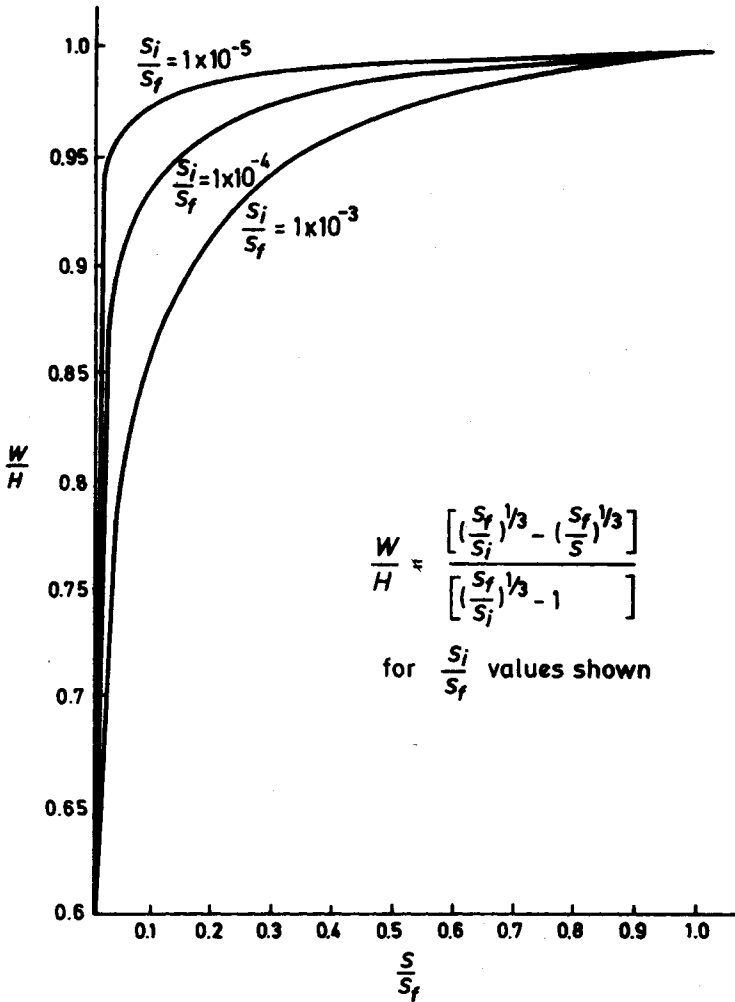


Figure 4.4

was pointed out that it could probably be used for initial design purposes subject to an appreciation of its approximate nature. Such applications were in fact made and the analyses indicated that some slight adjustment is desirable for several points in the original chart.

In this section a study is made of a number of recent earthquakes (in addition to those used in the original analysis) and on the basis of this study, a slight modification is made in the data as presented on the original chart which will be referred to, in this text, as the 'first chart'.

The revised chart is an improvement (which is almost certainly merely one step in an ongoing process) that will enable professionals in the earthquake engineering field to use the new theory with greater accuracy and confidence.

Insofar as the calibration process in engineering is concerned, it must be emphasized that this is dependent entirely upon the accuracy of the experimental (i.e., field) data. In the case at hand (earthquake engineering) it is unfortunate (but true) that the numbers obtained from the two experimental sources are frequently of questionable accuracy. Thus, the 'magnitude' of a given earthquake (one of two or three major parameters) frequently varies by up to a factor of thirty in the total energy depending upon the source of the information. Another extremely important parameter is the 'intensity number', which is a fundamental quantity in the present rational theory, occurring in nearly all of the equations, charts and measurements of damage as well as in the structural design charts. The intensity values reported after an earthquake are suspect in two major respects (see also the discussion on this point in Chapter 3):

1. They are frequently based upon (occasionally long time) after-the-fact remembrances of inhabitants of the region effected. They are thus highly subjective in content and subject to wide variations in quantitative value depending upon the person reporting.
2. They are frequently dependent upon the effects of large after shocks and clustered shocks which tend to distort the (assumed) circular shape of the canonical isoseismal contours, thereby introducing an effect not considered in the original theory which was based upon a single focus shock. However, it may be noted that it is possible to consider the effects of multiple and clustered shocks by utilizing a superposition procedure to be described in Chapter 7 and this can in effect de-couple the several shocks and allow the application of the canonical rational procedure.

The approximations and limitations noted above are consistent with others introduced at various stages in the development of the complete theory as given in *EE-DA&SD*. Otherwise stated, it is unlikely that an 'exact' theory of earthquake engineering can ever be developed given the inevitable limitations in the accuracy attainable in the experimental determinations.

In *EE-DA&SD*, a limited number of earthquake events were referred to and an initial primitive form of the 'first chart' was obtained. It was noted there that the values shown were, in all probability, tentative and subject to possible revision as more and more actual earthquake data were analyzed and included within the framework of the new theory.

Furthermore, again it is pointed out that the process is a continuing one. More and more data will surely lead to more and more refinement and accuracy.

The present discussion describes one such additional step in the calibration of one major design chart of the theory — this being the Magnitude — $\Sigma(IS)_f - S_f$ — Geology chart.*

The field data used are those for a number of earthquakes in various parts of the world.

Procedure

One of the main problems with the region-magnitude relationships in the 'first chart' is that they are based on a relatively small number of data points (only 8 earthquakes where magnitude, region type, and isoseismal contours are known). The eight earthquakes and the data utilized were the following:

Table 4.2

| Earthquake | Region | $\Sigma(IS)_f$, km | M, Richter | S_f , km |
|---------------------|--------|---------------------|------------|------------|
| San Fernando, 1971 | R_1 | 2360 | 6.5 | 300 |
| S. Jorge, 1970 | R_2 | 1970 | 7.4 | 125 |
| San Francisco, 1906 | R_1 | 4420 | 8.2 | 550 |
| Orleanville, 1954 | R_3 | 1375 | 6.75 | 95 |
| Agadir, 1960 | R_3 | 460 | 5.75 | 30 |
| Lice, 1975 | R_2 | 780 | 6.70 | 80 |
| Tangshan, 1976 | R_3 | 9970 | 7.8 | 700 |
| Corinth, 1981 | R_3 | 1040 | 6.6 | 95 |

In an effort to improve the applicability of this chart additional well-documented earthquakes were researched and analyzed so that more data points could be obtained and used to refine the magnitude-region relationship**.

The additional earthquakes analyzed and the resulting data include the following:

* Note that the chart does in fact correlate the two theoretical parameters ($\Sigma(IS)_f$ and S_f) with the two physical variables (earthquake magnitude and average regional geology) as the theory predicted in Chapter 3.

** The author wishes to thank George B. Bakun, who analyzed the new and old data and prepared the revised chart included in this section.

Table 4.3

| Earthquake | Region | $\Sigma(JS)_f$ (km) | M (Richter) | S_f (km) |
|-------------------------------|-----------------|------------------------|------------------|---------------|
| Santiago, Chile — 3/3/85 | \mathcal{R}_1 | 7000 | 7.4–7.6 | 550 |
| Managua, Nicaragua — 12/23/72 | \mathcal{R}_1 | 1600 | 6.25 | 130 |
| Anchorage, Alaska — 3/27/64 | \mathcal{R}_1 | 18000 | 8.3–8.6 | 1400 |
| Skopje, Yugoslavia — 7/26/63 | \mathcal{R}_2 | 1300 | 5.4–6.6 | 110 |
| Al Asnam, Algiers — 10/10/80 | \mathcal{R}_2 | 3000 | 7.5 | 250 |
| Guatemala, Guatemala — 2/4/76 | \mathcal{R}_1 | 6000 | 7.5 | 470 |

Several existing data points were modified in the development of the new region-magnitude relationships based on additional information found in references. Also, several additional earthquake data points were added when references were found which identified magnitudes for earthquakes where the isoseismal map characteristics had previously been evaluated and used to develop the first chart (e.g., the 1908 Messina earthquake and the 1755 Lisbon earthquake).

The resulting revised chart is not considered an exact tool. Some difficulties exist with refining it. The two most important are that wide ranges in magnitudes are often reported for an earthquake, and insufficient data usually is reported to permit a meaningful analysis. As a result, to make the revised chart a useful engineering design tool, some degree of conservatism was used so that the resulting magnitude-region relationships bounded most of the earthquakes with smaller values of S_f than predicted by this chart. However, there should be few with values significantly greater.

Detailed Description of the Earthquakes of Table 4.3

Following are detailed descriptions of the six earthquakes of Table 4.3 which were used to revise the 'first chart'.

SANTIAGO, CHILE EARTHQUAKE — 3/3/85

Table 4.4 summarizes the data for the isoseismal contour map which was developed based on using the rational theory and actual damage reports from news dispatches. The supporting calculations and information for this analysis are contained in Reference 1. Essentially, the isoseismal map which was developed based on the rational theory gave an excellent correlation with the reported damage.

Richter magnitudes of 7.4 to 7.8 were reported for this earthquake by several sources. For the purposes of this study, it was decided — for two reasons, —

use a value of 7.6. First, the value of 7.6 was reported by the University of Chile Seismology Institute, which regularly records Chile earthquakes and thus should have better capabilities of measuring a local earthquake. The 7.4 value was recorded by the Honolulu Tsunami Centre. Secondly, based on a comparison of the magnitude values predicted by the 'first chart' for this earthquake, a higher magnitude was expected than recorded. Thus, the decision to use the higher value based on the experiences with other earthquakes.

Region \mathcal{R}_1 is considered to be the most appropriate earthquake region for this case. Region \mathcal{R}_1 represents faulted areas located primarily along the Circumpacific Belt. It is possible that Region \mathcal{R}_1 should be primarily for the deeper faulted earthquakes which occur due to plate movements (i.e., horizontal faults), as opposed to shallower earthquakes due to vertical fault movements (i.e., California type earthquakes), but this is a question which will not be considered here at this time.

Table 4.4 Analysis Results of 3/3/85 Chile Earthquake (1)-Theoretical Values

| Intensity Level | S (km) | (IS) (km) | $\Sigma(IS)$ (km) | Distance to Outer Reach (km) |
|-----------------|----------|-------------|-------------------|------------------------------|
| XI | 0 | 0 | 0 | 0 |
| X | 10 | 100 | 100 | 23 |
| IX | 35 | 315 | 415 | 50 |
| VIII | 65 | 520 | 935 | 85 |
| VII | 105 | 735 | 1670 | 137 |
| VI | 160 | 960 | 2630 | 205 |
| V | 250 | 1250 | 3880 | 310 |
| IV | 370 | 1480 | 5360 | 465 |
| III | 550 | 1650 | 7010 | 640 |

Use $S_f = 550$ km Use $\Sigma(IS)_f = 7000$ km

NOTE (1): See Reference 1 for supporting data and calculations.

MANAGUA, NICARAGUA EARTHQUAKE — 12/23/72

On December 23, 1972, a Richter magnitude 6.25 earthquake occurred with an epicentre located within the Nicaraguan city of Managua. Because of the epicentre location and the shallow focal depth of 6 km, the damage was unusually high for the magnitude level.

Since Nicaragua is located in the seismically active Circumpacific Belt, this earthquake can be classified as a Region \mathcal{R}_1 earthquake for the purposes of this study.

The canonical isoseismal map characteristic values developed for this analysis are $S_f = 130$ km and $\Sigma(IS)_f = 1600$ km. The S_f value is based on a review of isoseismal contour maps which were presented in Ref. 2. The value was determined assuming that distortions in the reported isoseismal maps were due to both local fault activity and the effects of an elongated belt of many after shocks associated with the main shock. This analysis is only concerned with the effects of the main shock. Table 4.5 presents a comparison of the S values which were extrapolated from the isoseismal maps in Ref. 2 and the S values developed following the procedure shown in Section D using $S_f = 130$ km and a value of $\Sigma(IS)_f = 1600$ km from the 'first chart'.

The actual $\Sigma(IS)_f$ value based on the reported information was not used so that the magnitude of any differences predicted by the theory could be reviewed. Essentially, the theory compared well with the extrapolated values for the lower intensity values (III, IV, and V), but overpredicted the effects of the earthquake near the epicentre. This discrepancy may be related to the occurrence of a superposed sequence or cluster of earthquake effects.

Table 4.5 Analysis Results for the 12/23/62 Managua Earthquake

| Intensity Level | S | | IS | | $\Sigma(IS)$ | |
|-----------------|-------------|-------------|-------------|-------------|--------------|-------------|
| | Ref. 2 (km) | Theory (km) | Ref. 2 (km) | Theory (km) | Ref. 2 (km) | Theory (km) |
| X | 0 | 2 | 0 | 20 | 0 | 20 |
| IX | 1 | 7 | 9 | 63 | 9 | 83 |
| VIII | 2 | 14 | 16 | 112 | 25 | 195 |
| VII | 5 | 24 | 35 | 168 | 60 | 363 |
| VI | 15 | 37 | 90 | 222 | 150 | 585 |
| V | 59 | 58 | 295 | 290 | 445 | 875 |
| IV | 98 | 88 | 392 | 352 | 837 | 1227 |
| III | 130 | 130 | 390 | 390 | 1227 | 1617 |

NOTE: Theory values of S_f were calculated using $S_f = 130$ km from Ref. 2 and $\Sigma(IS)_f = 1600$ km from the 'first chart' which corresponds to a value of $S_f = 130$ km in the 'first chart'.

ANCHORAGE, ALASKA EARTHQUAKE — 3/27/64

On March 27, 1964, at about 5:36 p.m., an earthquake of unusual severity struck the Prince William Sound and the Aleutian area. Fortunately, the economic losses were relatively minor compared to the severity of the earthquake because the area is sparsely populated.

This area is one of the world's most seismically active regions. It is located along the Circumpacific Belt. Because of this, the earthquake was classified as

Region \mathcal{R}_1 . The mechanism for this earthquake is believed to be large horizontal plate movements.

The magnitude of the earthquake was estimated to range from 8.3 to 8.6. For the purposes of this analysis, an intermediate value of 8.5 was selected because it is most commonly cited in the earthquake literature. It should be noted that the magnitude of the earthquake was estimated from teleseismic records because there were no seismic instruments in Alaska capable of recording strong ground motion at the time of this earthquake.

Because the area is so sparsely populated, in-depth damage assessments were not conducted to the point that the isoseismal map was prepared. However, References 3 and 4 did report the areas of significant damage so that an isoseismal map could be prepared by estimating the value of S_f and using an appropriate value of $\Sigma(IS)_f$ from the 'first chart'. The final isoseismal values which were selected for this earthquake give reasonably comparative intensity values for areas of significant damage. The theoretical isoseismal values are summarized in Table 4.6 and are based on $S_f = 1400$ km and $\Sigma(IS)_f = 18,000$ km.

Table 4.6 Analysis Results of 3/27/64 Alaska Earthquake-Theoretical Values

| Intensity Level | S (km) | IS (km) | $\Sigma(IS)$ (km) | Outer Reach (km) | Damage Reports (1) |
|-----------------|----------|-----------|------------------------|------------------|--------------------|
| X | 33 | 330 | 330 | 60 | |
| IX | 93 | 837 | 1167 | 123 | Major Landslides |
| VIII | 168 | 1344 | 2511 | 206 | Severe Damage Area |
| VII | 272 | 1904 | 4415 | 347 | |
| VI | 422 | 2532 | 6947 | 532 | |
| V | 642 | 3210 | 10157 | 803 | |
| IV | 963 | 3852 | 14009 | 1182 | |
| III | 1400 | 4200 | 18209 | 1620 | Shock Felt |
| | | | $\Sigma(IS)_f = 18000$ | | |

NOTE: (1) Damage shown falls within the outer reach of the respective intensity level area.

SKOPJE, YUGOSLAVIA EARTHQUAKE — 7/26/63

In the early morning hours of July 26, 1963, the Yugoslavian city of Skopje was struck by a catastrophic earthquake. Damage within the city limits of Skopje was severe, but the total area affected by the earthquake was small and the magnitude of the earthquake was not great. In many respects, this earthquake is thus very similar to the 1960 Agadir earthquake which despite its relatively small magnitude, created a significant amount of economic loss in a relatively small

area. One reason for the extensive damage at Skopje is that the epicentre was located only 15 km northwest of the city. The focal depth was calculated as being 10–15 km.

The magnitude of the earthquake has been reported as ranging from 5.4 to 6.6 on the Richter scale, depending where on the earth the reading was recorded. For the purposes of this report, the maximum value of 6.6 was used because of the damage which was done and because of a comparison of the isoseismal contours which were developed with other earthquakes.

The region for this earthquake was assumed to be Region R_2 . Yugoslavia is in a seismically active region and is in the vicinity of the Alpide Belt region.

The available data on the effects of the earthquake outside the city of Skopje is minimal. However, an isoseismal map was developed covering the intensity levels within the city limits of Skopje and was presented in Reference 5. Based on the information presented and using the rational theory approach, data for a detailed isoseismal map were extrapolated for the entire earthquake. The result is presented in Table 4.7. This data is based on values of $S_f = 110$ km and $\Sigma(IS)_f = 1300$ km.

The damage reported was concentrated within the city limits of Skopje. The maximum intensity reported within Skopje was Intensity VIII (MM). Slight cracks in the ground were found. Extensive damage to homes of adobe construction resulted. Also, several large masonry structures were fractured, became dislodged or collapsed. Damage which would result from the theoretical isoseismal contours presented in Table 4.7 would probably have been very similar. The Intensity VIII contour predicted was found to agree almost perfectly with the one reported in Ref. 5. Thus, the theoretical isoseismal contours are considered representative of the effects expected over the entire earthquake affected region and suitable for the revision of the 'first chart'.

Table 4.7 Analysis Results of 7/26/63 Skopje Earthquake-Theoretical Values

| Intensity Level | S (km) | IS (km) | $\Sigma(IS)$ (km) | Outer Reach (km) | Comments |
|-----------------|----------|-----------|-----------------------|------------------|--------------------|
| IX | 3 | 27 | 27 | 7 | |
| VIII | 11 | 88 | 115 | 15 | Matches Isoseismal |
| VII | 19 | 133 | 248 | 25 | |
| VI | 30 | 180 | 428 | 39 | |
| V | 47 | 235 | 663 | 60 | |
| IV | 73 | 292 | 955 | 92 | |
| III | 110 | 330 | 1285 | 130 | |
| | | | $\Sigma(IS)_f = 1300$ | | |

AL ASNAM, ALGERIA EARTHQUAKE — 10/10/80

On October 10, 1980, two earthquakes struck northwestern Algeria, destroying most of the city of Al Asnam. The magnitude of the first earthquake was recorded as 7.5 on the Richter scale and was the larger of the two. The second earthquake occurred about 4 hours later and had a recorded Richter magnitude of 6.5. This study concerns itself primarily with the first earthquake which is considered the main shock and cause of damage.

The damage data used to develop the isoseismal contours for this earthquake was extrapolated from References 6 and 7. The contours were developed by applying the rational approach to values of $S_f = 250$ km and $\Sigma(IS)_f = 3000$ km. The resulting isoseismal contours are shown in Table 4.9 and compare favorably with the effects of the earthquake which were reported. Essentially, severe damage is restricted to the Intensity IX area and reports of distant regions where the shock was felt fall within the Intensity III contour.

Table 4.8 Analysis Results of the 10/10/80 Algeria Earthquake-Theoretical Values

| Intensity Level | S (km) | IS (km) | $\Sigma(IS)$ (km) | Outer Reach (km) | Damage Reports |
|-----------------|----------|-----------|-------------------|------------------|----------------|
| IX | 13 | 117 | 117 | 19 | Severe Damage |
| VIII | 26 | 208 | 325 | 35 | |
| VII | 44 | 308 | 633 | 57 | |
| VI | 70 | 420 | 1053 | 89 | |
| V | 109 | 545 | 1507 | 138 | |
| IV | 167 | 668 | 2175 | 210 | Shock Felt |
| III | 250 | 750 | 2925 | 300 | |

$\Sigma(IS)_f = 3000$

GUATEMALA, GUATEMALA EARTHQUAKE — 2/4/76

On February 4, 1976, a major earthquake hit Guatemala. The epicentre was located about 45 km south of the capital city of Guatemala, and the effects of the earthquake were felt as far away as Honduras and El Salvador. The earthquake resulted in major damage to homes of adobe construction as far away as the capital city. Buildings in wealthier neighborhoods of the area were not affected except for some cracks which were reported in high rise condominiums. Based on this data, an isoseismal contour study was completed for use in refining the region-magnitude relationships used in the 'first-chart'.

The damage data used to develop the isoseismal contours for this earthquake were extrapolated from Reference 8. The contours were developed by applying

the rational approach to values of $S_f = 470$ km and $\Sigma(IS)_f = 6000$ km. The resulting isoseismal contours are shown in Table 4.9 and compare favorably with the effects of the earthquake which were reported. Based on a comparison of the damage reports with the resulting isoseismal contours, adobe homes were destroyed if located in the Intensity IX contour and damaged if located within the Intensity VIII contour. Reports of the shock being felt in distant locations are verified by falling within the Intensity III contour.

Additional related analyses of this earthquake are presented in Chapter 7 and in Chapter 10 (in which our rational theory is applied to the analysis of a destructive rockslide caused by this earthquake). As shown in Chapter 7, the published isoseismal map almost certainly corresponds to a superposition of several widely separated large earthquakes.

Table 4.9 Analysis Results of the 2/4/76 Guatemala Earthquake-Theoretical Values

| Intensity Level | S (km) | IS (km) | $\Sigma(IS)$ (km) | Outer Reach (km) | Damage Reports |
|-----------------------|----------|-----------|-------------------|------------------|-----------------------|
| X | 13 | 130 | 130 | 25 | |
| IX | 36 | 324 | 454 | 44 | Adobe Homes Destroyed |
| VIII | 51 | 408 | 862 | 68 | Adobe Homes Damaged |
| VII | 85 | 595 | 1457 | 110 | |
| VI | 134 | 804 | 2261 | 171 | |
| V | 207 | 1035 | 3296 | 262 | |
| IV | 317 | 1268 | 4564 | 395 | |
| III | 470 | 1410 | 5974 | 550 | Shock Felt |
| $\Sigma(IS)_f = 6000$ | | | | | |

ADDITIONS AND MODIFICATIONS TO EXISTING DATA POINTS OF THE 'FIRST CHART'

In addition to obtaining new data points, the need to modify several of the existing data was reviewed to ensure that they were suitably represented. The following earthquakes were found to have conflicting or additional information to that used to prepare the 'first chart'.

San Fernando, 1971. Reference 2 reports the magnitude of the 1971 San Fernando earthquake as 6.6 and not as the value of 6.5 used in the 'first chart' and shown in Table 4.10.

Agadir, 1960. Based on the discussion presented in Reference 1, it may be more appropriate to consider the Agadir earthquake as a Region \mathcal{R}_2 earthquake,

as opposed to \mathcal{R}_3 which was used to develop the 'first chart'. Although Agadir did not suffer significant earthquakes for a long period prior to 1960 (and thus may have been considered to be in a low seismicity zone characteristic of Region \mathcal{R}_3) it is located at the end of the so-called, 'Alpide Belt'. Thus, even though the earthquakes may not be frequent, it is likely that the mechanism is very similar to other earthquake areas more commonly classified as Region \mathcal{R}_2 . Also, it does not seem likely that the 1960 Agadir earthquake can be considered characteristic of a low seismicity area since the 1969 Agadir earthquake was even larger in magnitude and intensity.

Messina, 1908. Reference 9 identifies this earthquake as having a magnitude of 7.5. The isoseismal values have been previously calculated for use in preparing the 'first chart'. The region classification can be either \mathcal{R}_2 or \mathcal{R}_3 , although it is likely \mathcal{R}_2 since Messina is located in the vicinity of the Alpide Belt.

San Francisco, 1906. The magnitude of the 1906 San Francisco Earthquake was estimated as being 7.8 in Reference 6, as opposed to the value of 8.2 used in the 'first chart'.

Valparaiso, 1906. The magnitude of the 1906 Valparaiso, Chile earthquake was estimated to be about 8.2 in one reference based on a review of the isoseismal contour map. The Valparaiso earthquake should be classified as Region \mathcal{R}_1 .

Lisbon, 1755. Reference 9 identifies this earthquake as having a magnitude of about 8.9–9.0. The isoseismal values have been previously calculated for use in preparing the 'first chart'. The region classification can be treated either as \mathcal{R}_2 or \mathcal{R}_3 , but it is probably \mathcal{R}_2 since Lisbon is located in the vicinity of the Alpide Belt.

THE REVISED FORM OF THE 'FIRST CHART'

Utilizing the new and modified data points, the existing 'first chart' was modified. The revised chart is shown in Figure 4.5. The data used is summarized in Tables 4.10 and 4.11. Table 4.10 shows existing data points which were either modified or to which data was added to permit their application to the development of Figure 4.5. Table 4.11 summarizes the data for the six additional earthquakes which were analyzed for use in developing Figure 4.5. The S_f vs. $\Sigma(IS)_f$ relationship of the 'first chart' was not changed, as this relationship checked the new data fairly well. However, the region-magnitude relationships were modified slightly.

CHART SHOWING RELATION BETWEEN
 $S_f - \Sigma(ZS)_f$ - MAGNITUDE - GEOLOGY

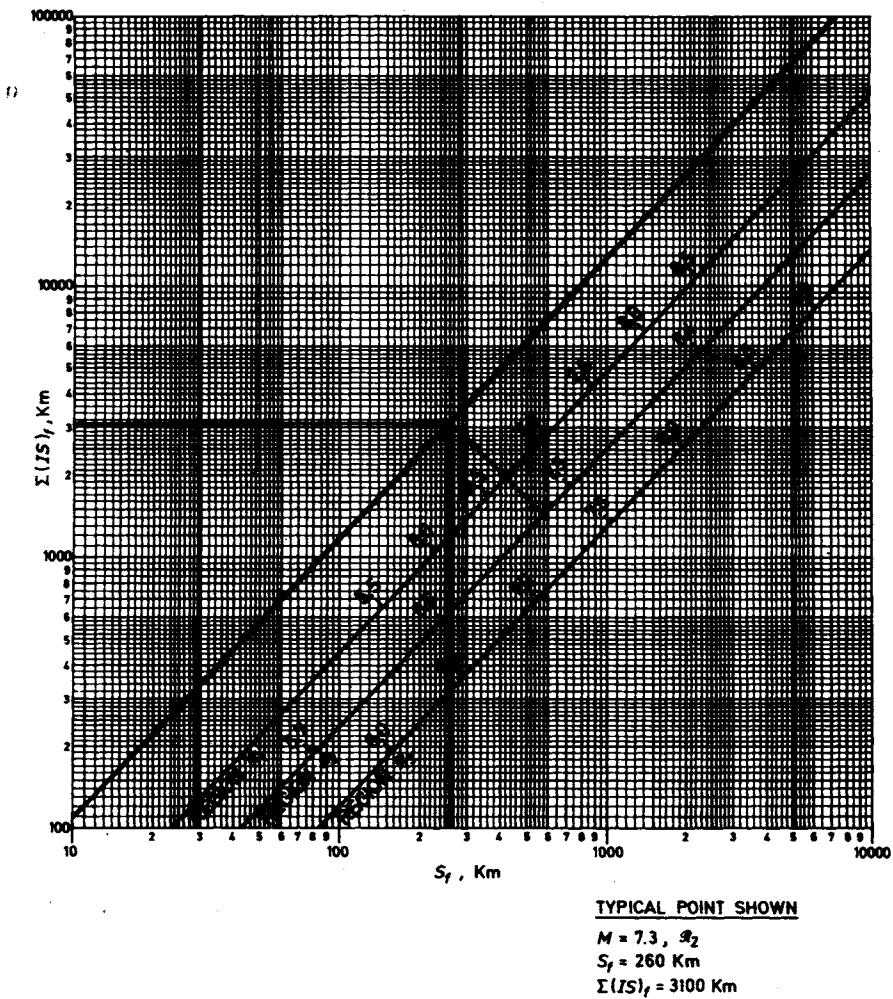


Figure 4.5

Table 4.10 Existing data points used to develop the 'first chart' region — magnitude relationships

| Earthquake | $\Sigma(IS)_f$ (km) | S_f (km) | M | Region |
|---------------------|------------------------|---------------|--------|---------------------|
| San Fernando, 1971 | 2360 | 300 | 6.5(1) | \mathcal{R}_1 |
| S. Jorge, 1757 | 1970 | 125 | 7.4 | \mathcal{R}_2 |
| San Francisco, 1906 | 4420 | 550 | 8.2(2) | \mathcal{R}_1 |
| Orleanville, 1954 | 1375 | 95 | 6.75 | \mathcal{R}_3 |
| Agadir, 1960 | 460 | 30 | 5.75 | \mathcal{R}_3 (3) |
| Lice, 1975 | 780 | 80 | 6.7 | \mathcal{R}_2 |
| Tangshan, 1976 | 9770 | 700 | 7.8 | \mathcal{R}_3 |
| Corinth, 1981 | 1040 | 95 | 6.6 | \mathcal{R}_3 |
| Valparaiso, 1906 | 15000 | 11000 | (4) | \mathcal{R}_1 |
| Lisbon, 1755 | 25350 | 1500 | (5) | (5) |
| Messina, 1908 | 4430 | 335 | (6) | (6) |

- NOTES: (1) Magnitude reported in Reference 2 as 6.6 with a focal depth of 13 km.
(2) Magnitude reported as 7.8 in Reference 6.
(3) Region \mathcal{R}_3 is reported in Reference 9 for the Agadir area.
(4) Magnitude reported as 8.2 in one reference based on a review of the isoseismal contour map.
(5) Reference 9 identifies the magnitude as 8.9–9.0. The region is located immediately outside of the Alpide Belt and can be either \mathcal{R}_2 or \mathcal{R}_3 .
(6) Reference 9 identifies the magnitude as 7.5. The region is located immediately outside of the Alpide Belt and can be either \mathcal{R}_2 or \mathcal{R}_3 .

Table 4.11 New data points used to modify the 'first chart' region — magnitude relationships

| Earthquake | $\Sigma(IS)_f$ (km) | S_f (km) | M | Region | Focal Depth (km) |
|-----------------|------------------------|---------------|---------|-----------------|---------------------|
| Santiago, 1985 | 7000 | 550 | 7.4–7.6 | \mathcal{R}_1 | 50 |
| Managua, 1972 | 1600 | 130 | 6.25 | \mathcal{R}_1 | 6 |
| Anchorage, 1964 | 18000 | 1400 | 8.3–8.6 | \mathcal{R}_1 | 60 |
| Skopje, 1963 | 1300 | 110 | 5.4–6.6 | \mathcal{R}_2 | 10–15 |
| Al Asnam, 1980 | 3000 | 250 | 7.5 | \mathcal{R}_2 | — |
| Guatemala, 1976 | 6000 | 470 | 7.5 | \mathcal{R}_1 | — |

Finally, and once more, it is pointed out that the use of Figure 4.5 in future designs and analyses should be done with care. Unfortunately, the data used to develop Figure 4.5, although the best available, is still open to scrutiny. Magnitude values reported for earthquakes often vary, sometimes considerably. For example, as noted, magnitude values reported for the 1963 Skopje earthquake varied from 5.4 to 6.6. Values depend on where they are taken, local conditions

which may affect readings, and the accuracy of machines to record such information. Furthermore, damage reports which are used to develop isoseismal contours are often exaggerated and always subjective. Even when isoseismal maps are reported after long studies, they must be applied with care. Often they include the effects of local faults and of after shocks (see, for example, the later superposition study of Chapter 7) and are thus not directly applicable to the main shock which is being analyzed. In spite of this, Figure 4.5 is considered to be applicable to most earthquakes of concern to designers.

It is believed that Figure 4.5 is suitable for conservative engineering design and analysis work. In some cases, points were not incorporated into the final curves (e.g., the 1906 San Francisco earthquake) because it was felt that using these points could result in an unconservative design or analysis. The final points which are recommended were based on developing a relationship between region and magnitude which would encompass most earthquakes and would be slightly conservative for the unusual occurrences.

In other words, Figure 4.5 must not be considered as the final form for this chart. As more and more earthquakes are analysed using the rational theory, it is a virtual certainty that Figure 4.5 will be revised and modified as required by the normal ongoing calibration process.

D) THE MAGNITUDE-INTENSITY-DISTANCE (MID) CHART

In the previous Section C it was shown that for an earthquake of a given magnitude occurring in a given geological region, approximate values of the basic canonical isoseismal map parameters $\Sigma(IS)_f$ and S_f , may be determined.

It will now be shown how, having $\Sigma(IS)_f$ and S_f for the canonical map, the entire canonical isoseismal map may be constructed by rational means.

In the present theory, the canonical isoseismal map is one of the more important tools in the damage assessment as well as the structural design and analysis parts of the overall rational treatment. This will be shown in detail in later chapters, from which it will be clear that the construction of a rational MID chart will be of value to insurers, engineers, architects, preparers of codes and other professionals in the earthquake engineering field.

In a typical engineering office the canonical charts will consist of a series of circular curves similar to the ones shown in Figure 4.6. All three geologic regions will be represented with magnitudes going from, say, 5 to 8.5, in increments of 0.1 to 0.2. Values of $\Sigma(IS)_f$ and S_f will be obtained from Figure 4.5 as this chart is continuously revised and refined and made more accurate.

In addition, values of ϵ_{tf} , the surface horizontal energy per unit area for each intensity band will be shown, where ϵ_{tf} is determined as in Section F of this chapter.

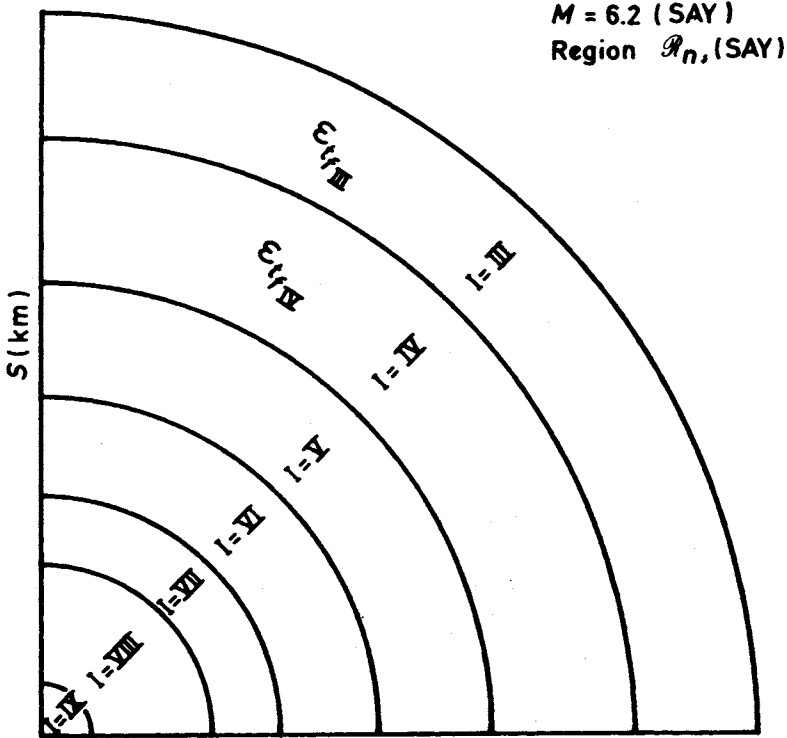


Figure 4.6 Typical MID Chart

A particular chart is prepared as follows:

1. Assume a value of M for a given geological region
2. From Figure 4.5, knowing M and the geology, determine the canonical $\Sigma(IS)_f$ and S_f values
3. From Eq. 2, with known $\Sigma(IS)_f$ and S_f , start with Intensity = III and S_f , so that

$$\frac{\Sigma(IS)_f - 3S_f}{\Sigma(IS)_f} = e^{2[1 - (S_f/S_{IV})^{1/3}]} \quad (16)$$

and determine S_{IV} the only unknown in this equation.

4. Repeat step 3 for $S_V, S_{VI} \dots S_X$, reducing the numerator of the left hand side by, successively, $4S_{IV}, 5S_V \dots 9S_{IX}$.
5. Having determined the S_f values, the approximate widths of the bands, w_j , for I_j is obtained as follows:

$$w_{III} = \frac{S_{III} - S_{IV}}{2} + \frac{S_{III} - S_{IV}}{2}, \quad I_j = III \tag{17}$$

$$w_j = \frac{S_{j-1} - S_j}{2} + \frac{S_j - S_{j+1}}{2}, \quad I_j > III$$

E) THE INTENSITY – $\Sigma(a\Delta t)_f$ – t_f – GEOLOGY CHART

t_f and $\Sigma(a\Delta t)_f$ are assumed to be the fundamental parameters in our formulation of the canonical accelerogram invariant. On physical grounds, it seems reasonable to assume that the damage inflicted on a structure at a given location is related to the acceleration of the ground at the location. It appears reasonable therefore to assume that the parameters $\Sigma(a\Delta t)_f$ and t_f are in some way connected with the intensity of an earthquake at the location of the accelerogram instrument, subject to possible anomalous variations due to local geological conditions.

A first, primitive form of the correlation was presented in *EE-DA&SD* in which the points for five canonical accelerograms were utilized. The data for the five points are shown in Table 4.12 repeated from the earlier text. The angle θ is defined in the ‘Notation for this Chapter’ section.

Figure 4.7 shows a modified form of the earlier chart in accordance with minor calibration modifications.

Table 4.11 $\Sigma(a\Delta t)_f$ and t_f

| Earthquake | t_f, s | $\Sigma(a\Delta t)_f, 'g' s$ | θ | $\frac{\Sigma(a\Delta t)_f}{\cos \theta}$ | Intensity I^* |
|--------------------|----------|------------------------------|----------|---|-----------------|
| Tolmezzo, 1976 | 20 | 0.98 | 45° | 1.39 | IX |
| Taft, 1952 | 20 | 0.96 | unknown | 0.96 | VIII |
| Lima, 1966 | 20 | 1.84 | unknown | 1.84 | >IX |
| San Fernando, 1971 | 48 | 1.06 | unknown | 1.06 | VIII |
| Bucharest, 1977 | 14 | 0.72 | 36° | 0.89 | VIII |

* At the accelerogram location.

Note, the regions $\mathcal{R}_1, \mathcal{R}_2, \mathcal{R}_3$ are assumed average geologies at the locations where the accelerograms were recorded. Obviously, anomalous geological conditions at the accelerogram location (such as occurred, for example, in central Mexico City for the September 19, 1985 earthquake) will require special consideration and are not covered by the $\mathcal{R}_1, \mathcal{R}_2, \mathcal{R}_3$ designations on Figure 4.7. The author is unaware of anomalies for the five points shown and – tentatively – assumed these were obtained at ‘average’ geologies for the respective regions.

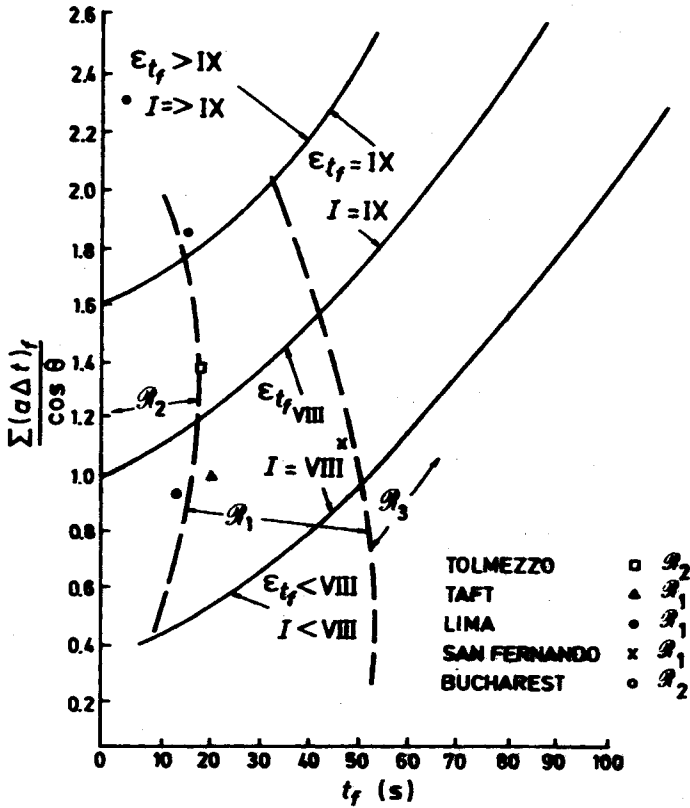


Figure 4.7 $\Sigma(a\Delta t)_f - t_f$ Damage Contour Chart

See, in this connection Figure 10.17, Table 10 and Table 11 of Chapter 10 and the accompanying discussion. The 'average' geology region designation on the chart is a secondary feature. When it is appropriate it serves as a rough check on the points and also as a means for obtaining a quick approximate correlation between intensity number (i.e., damage and surface energy) and the possible combination values of the two canonical accelerogram parameters, $\Sigma(a\Delta t)_f$ and t_f .

In Chapter 6 it is shown how this same chart can be used for superposed canonical accelerograms which correspond to a sequence or series of shocks forming a single accelerogram record, again for average, non-anomalous geologies for the region designations shown.

Shown on Figure 4.7 are the general ϵ_{t_f} values for each intensity band. The numerical value for this extremely important quantity is discussed in the next Section F of this chapter.

The effect of frequency of the accelerations is assumed as approximately accounted for in the geological region designation. That is, similar geologies are assumed to generate approximately similar mechanisms and hence approximately similar frequency patterns. If this assumption is found to be too approximate for engineering design purposes, then it may be necessary that additional geology regions (i.e., \mathcal{R}_4 -) and intensity contours are needed to account for the frequency effect. This may be the case especially for anomalous geologies.

Clearly, more points are needed in order to establish the validity of Figure 4.7 as well as its accuracy. This requires an ongoing analysis of canonical accelerograms (or superposed canonical accelerograms as described in Chapter 6) at locations where the local intensity numbers are known, and especially where the possibility of anomalous geologies is a factor.

As more of such points are obtained and plotted on the figure corresponding to Figure 4.7, the correlation will become more accurate. For the available data, it appears that the interdependence between the two fundamental parameters, $\Sigma(a\Delta t)_f$ and t_f and the two physical variables, local geology and local ground energy per unit area predicted in Chapter 2 has been established.

F) THE ENERGY-INTENSITY COMPATIBILITY RELATION

As pointed out earlier a fundamental premise in the present rational theory is that energy is the key parameter of the entire earthquake event.

Energy is released at the focal point (the mechanism), energy is transmitted through the earth until it reaches the surface and finally energy — horizontal and vertical — is applied to the structure on the surface of the earth. If the structure can absorb the applied energy, it will remain undamaged. Damage will occur if the applied surface energy is greater than the elastic energy absorption capacity of the structure.

The commonly accepted measure of damage in the United States is the Modified Mercalli (MM) intensity number*. This *qualitative* description of damage is independent of the magnitude and location of the earthquake, that is, the geology. Because of this, the engineer — whose primary concern is *numbers* — must look for a *quantitative* measure of intensity (other than the MM intensity number which is of negligible design and analysis value) that can be used in

* There are other intensity scales used in various countries. All are similar although they may differ in numerical scales and descriptive details. See, for example, the discussion concerning the Japanese scale in Chapter 3.

engineering damage and structural analysis applications. And — once again — this should be an energy related quantity.

In this section such an energy measure of intensity will be derived. And because of its universal position in the theory, the relation is here called the 'energy-compatibility relation'.

The procedure in developing this compatibility relation will be as follows:

- 1) An accepted form of an energy-magnitude equation is assumed, such as $E = K_1 + K_2 M$, K_1 and K_2 are numerical constants. From this, the energy E will be known for a given magnitude, M .
- 2) From (1) above, the total surface horizontal energy, H , will be known for a given efficiency, η , since

$$H = \eta E$$

- 3) From Eq. 13 the total surface horizontal energy, W_j , between $S = S_j$ and $S = S_{j+1}$ can be determined. j is any intensity numbers $> III$.
- 4) From (3), using Eq. 13, we can determine

$$W_{j+1} - W_j$$

- 5) and therefore

$$\epsilon_{rj} = \frac{W_{j+1} - W_j}{2\pi S_j} \quad (18)$$

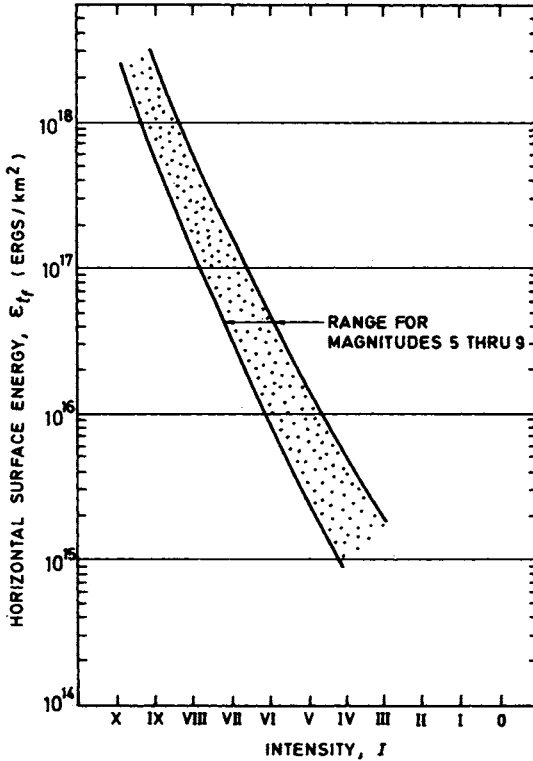
ϵ_{rj} is the value of the energy per unit area at the distance S_j . It can be taken as the average value for the j band, or if desired its variation over the band can be determined by computing its value at any S as in (3), (4), and (5) above.

In any case, for any M it is possible to obtain values for ϵ_{rj} at each intensity band from which curves of ϵ_{rj} vs intensity may be drawn.

If this is done for, say $5 < M < 9$, using a fixed equation in (1) and a fixed efficiency in (2), it will be found that curves do not coincide, as they must for all magnitudes. An adjustment in the curves must be made and this had been done, noting that

- a) It is likely that for different geologies a different form of E vs M equation holds for each magnitude, requiring different values of K_1 and K_2
- b) It is likely that the efficiency, η , is different for each magnitude, M .
- c) It is likely that consistent values of S_j are different for each magnitude, M and,
- d) there are other possible variations as well.

In any case, proceeding as in (1) through (5) above, using values of efficiency, η , corresponding to those shown in Chapter 5 and adjusting the curves in a reasonable manner, it is found that — at this time — a first suggested ϵ_{tf} vs intensity compatibility curve is as shown in Figure 4.8.



Earthquake Intensity vs. Horizontal Surface Energy

Figure 4.8

- 1) As shown in Figure 4.8, it is suggested that a 'band' rather than a 'line' may be more appropriate until additional checks on the curve are obtained.
- 2) Applications of the curve to a series of practical problems (as described in Chapters 10 and 11) indicate that the values for ϵ_{tf} are reasonable. Fair to good results (i.e., numbers) are obtained when this curve is used and checked against after-the-fact experimental results.
- 3) Just as for the design charts Figures 4.5 and 4.7, this curve will almost certainly be adjusted and altered, as required, as more and more experimental (i.e. field analysis and check designs) data are obtained.

However, at this time, it is suggested that the curve, Figure 4.8, can be used as a *conservative* design tool in engineering designs and analyses subject to the comments given above.

Finally, an important property of the energy — intensity compatibility curve shown in Figure 4.8 is that the change in energy for a unit increase in intensity is roughly by a factor of five. In view of the approximate and subjective nature of the canonical isoseismal map, this means that the *combined directional* energy of-say-an intensity VIII region, ϵ_{VIII} , and-say-an intensity VII region, ϵ_{VII} , is for all practical approximate purposes equal to ϵ_{VIII} . This property is the basis for the superposition assumptions utilized in connection with non-canonical accelerogram and isoseismal maps as shown in Chapters 6 and 7.

REFERENCES

1. G. B. Bakun, '*Analysis of Santiago, Chile Earthquake — March 3, 1985*', CE 226 Paper, Stevens Institute of Technology, April, 1985.
2. ANON, *Managua, Nicaragua Earthquake of Dec. 23, 1972*, Earthquake Engineering Research Institute, Conference Proceeding Vols. 1 and 2, San Francisco, Calif. Nov., 1973.
3. ANON, *The Great Alaska Earthquake of 1964 — Oceanography and Coastal Engineering*, National Academy of Sciences, Wash., D.C., 1972.
4. W. R. Hansen, *Effects of the Earthquake of March 27, 1964 at Anchorage, Alaska*.
5. G. V. Berg, *The Skopje, Yugoslavia Earthquake — July 26, 1963*, American Iron and Steel Institute, New York, 1964.
6. ANON, Earthquake in Algeria Said to Devastate City and to Kill Thousands, N.Y. Times, Oct. 11, 1980.
7. ANON, *At Least 17000 Dead in Algeria's Quake, Relief Agency Says*, N.Y. Times, Oct. 12, 1980.
8. S. F. Borg, J. Ayala and J. S. Chang, *A Rational Isoseismal Map Superposition Analysis for the February 4, 1976 Guatemala Earthquake*, COE-84-7, Department of Civil and Ocean Engineering, Stevens Institute of Technology, July 1984, Rev. Sept. 1984. Also International Symposium on Engineering Geology, Bari, Italy, 1986.
9. ANON, *The Agadir, Morocco Earthquake — February 29, 1960*, American Iron and Steel Institute, 1962.
10. N. Newmark and E. Rosenblueth, *Fundamentals of Earthquake Engineering*, Prentice-Hall, Inc. Englewood Cliffs, N. J. 1971.
11. E. Rosenblueth (Ed.), *Design of Earthquake Resistant Structures*, John Wiley and Sons, New York, Toronto, 1980.

CHAPTER 5

EFFICIENCY-FOCAL DEPTH AND FIGURE 4.5

INTRODUCTION

In Section C of the previous chapter, Figure 4.5, one of the more important rational design charts was developed. This chart related the canonical isoseismal parameters to earthquake magnitude, M , and to 'average geology'. It was stated at the time that the average regional geology is assumed to include — approximately — the effect of focal depth — i.e., for each of the three assumed geologies, the focal depth is taken to be approximately the same. Also stated was the suggestion that, if necessary, additional geologies could be specified. Examination of actual earthquake data would indicate whether this is necessary and, if so, how these should be accounted for.

In this chapter an approximate rational analysis is developed which connects the three geologies of Figure 4.5 (and others, if these are needed). The connecting element is the earthquake efficiency, η (defined as $\eta = H/E$) and an approximate volume-related partition of earthquake energy for an assumed homogeneous isotropic earth. This will permit a rough check on the geology scales of Figure 4.5 and will also assist in rational damage and structural analysis applications of the theory for other possible geologies, as described in previous and later chapters.

PROCEDURE

In strain energy applications for various solids (beams, plates etc.) it is found that the energy capacity (and transmission) properties are dependent upon the stress (and strain) and also on the volume of the stressed-strained body. We assume, in this approximate rational approach, that the energy is proportional to the volume and that the overall conservation of energy requirement implies that the removal of a portion of the volume transfers the removed energy to

the surface of the earth in the form of surface horizontal energy and surface vertical energy.

Figure 5.1 is the key to the rational determination of approximate focal depth-efficiency effects. It shows the approximate partitioning of the earthquake energy among the different parts of the idealized sphere assumed to be affected by the earthquake.

As noted above, this theoretical approach is approximate. The efficiency relations do, however, satisfy end conditions with a reasonable continuous variation between the two end points. For engineering purposes in rational earthquake analyses it is suggested that this is acceptable.

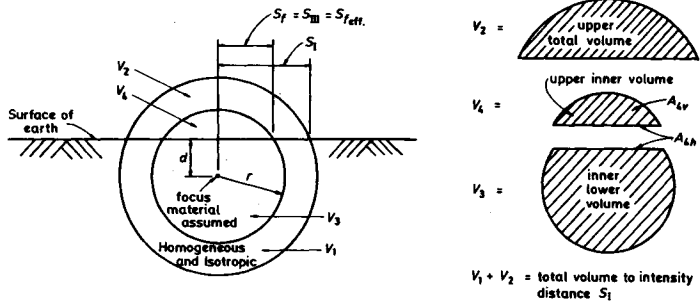
With further reference to Figure 5.1, note

1. The d/r term introduces the focal depth effect.
2. V_2/V_4 introduces the geology effect and the earthquake magnitude effect. The numerical values of this parameter are not known at this time and they will have to be assumed. As an initial assumption, the number 1.75 is suggested.
3. The efficiency, η , expressions are consistent for $d = 0$ and $d = r$ and are continuous for $0 < d < r$.
4. A simplified, approximate volume-related partition of earthquake energy, E , is developed. This connects, in a simple form, the canonical energy analysis of Section B, Chapter 4.
5. A simplified, approximate expression is given for the connection between vertical and horizontal ground energy.

Figure 5.2 is a set of curves representing the η vs d/r solution of Figure 5.1. Since at this time, as noted above, the values of the ratio V_2/V_4 are unknown (indeed, this ratio may be different for different geologies or regions — thus, California may have one value, Venezuela may have a second value, etc.), the curves are drawn for typical representative values of this ratio. As more and more data is collected, this important ratio will be established with sufficient accuracy for engineering design purposes for different regions, although as pointed out earlier it is suggested that the value 1.75 be used at this time.

Figure 5.3 is an approximate curve for checking Figure 4.5 values of $\Sigma(IS)_f - S_f$ against the magnitude and focal depth variation. Its use will be shown in the illustrative example that follows.

The complete procedure is included in the four charts and figures, Figures 4.5, 5.1, 5.2 and 5.3. As more and more data are collected, these figures may be revised and improved. It is suggested that they can be used in their existing forms subject to an awareness of their approximate nature.



$$\log_{10} E = K_1 + K_2 M, \\ = 11.4 + 1.5 M$$

$$H = \eta E$$

E = Energy of Earthquake at Focus, Ergs
 M = Magnitude of Earthquake (Richter)
 K_1, K_2 = Constants for a given Region
 H = Horizontal Ground Energy over A_{4h}
 η = Efficiency of Earthquake

Vertical Ground Energy over A_{4h} is given by V , where

$$V = \frac{A_{4v}}{A_{4h}} H$$

$d = 0$ is surface fault condition, assumed \mathcal{R}_1 geology.

$d = r$ is maximum depth of focus for S_f indication of earthquake on the surface

| $d = 0$ | | | $0 < d < r$ | |
|--|--------|---------------------|--|----------------------|
| $\eta = \frac{1}{2} \frac{V_4}{V_2} \left(\frac{A_{4h}}{A_{4h} + A_{4v}} \right)$ | | | $\eta = \frac{V_4}{V_1 + V_2} \left(\frac{A_{4h}}{A_{4h} + A_{4v}} \right)$ | |
| V_4/V_2 | η | $S_1/S_f = S_{III}$ | as $d \rightarrow r$, | $V_4 \rightarrow 0$ |
| 1 | .33 | 1 | | $\eta \rightarrow 0$ |
| 1/2 | .16 | 1.2 | | |
| 1/10 | .03 | 2.1 | | |
| 1/27 | .01 | 3 | as $d \rightarrow 0$, | we approach |
| 1/64 | .005 | 4 | | $d = 0$ value |

Figure 5.1 The Efficiency-Focal Depth Analysis

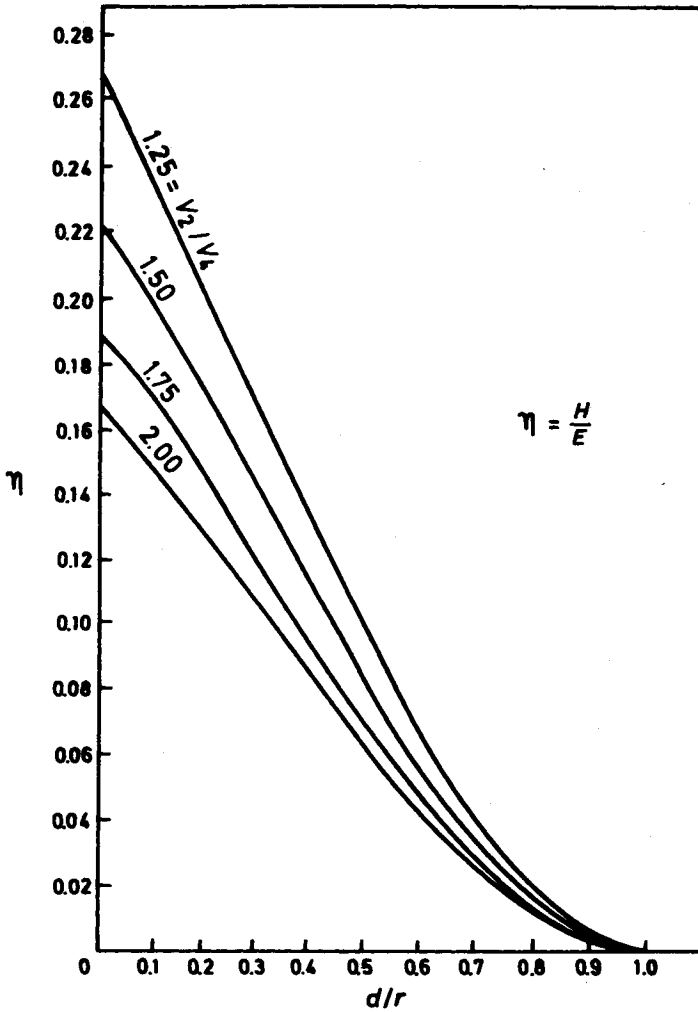


Figure 5.2 Efficiency vs. d/r vs. V_2/V_4

Illustrative Example

There are three ways, all approximate in varying degrees, in which we can account for the effect of depth of focus in our rational earthquake engineering analyses. In order to illustrate the three different procedures and to indicate the differences in the results obtained we solve the following typical example.

Example

Consider a magnitude $M = 7$ earthquake in an unknown \mathcal{R} average geology region, with a focal depth equal to 175 km. This is the information generally reported by the seismological station. What is the M_{eff} (See Figure 5.3) and the canonical $\Sigma(IS)_{f_{eff}}$ and $S_{f_{eff}}$ of this earthquake as determined by the three different approximate methods? Also what is the probable \mathcal{R}_j region as given by Figure 4.5?

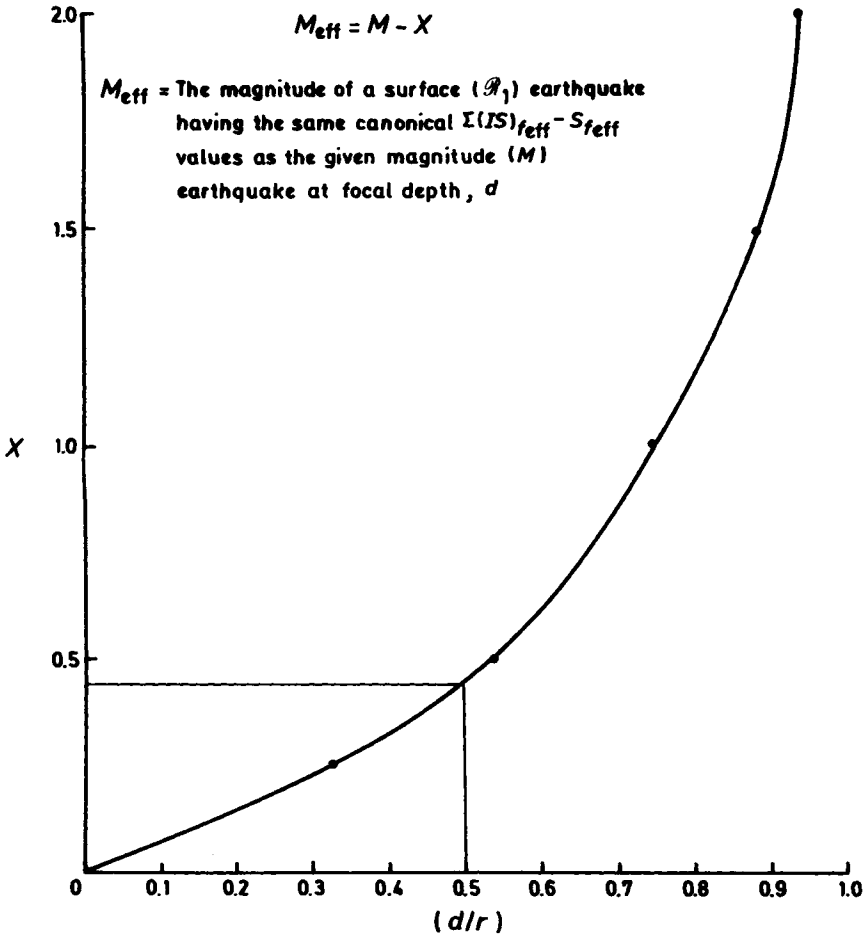


Figure 5.3 The Earthquake Magnitude Decrement vs d/r

Solution**First Approximate Method**

For the \mathcal{R}_1 , $M = 7$ values of Figure 4.5, assuming this is the surface fault earthquake condition (i.e., $d = 0$) we find

$$\left. \begin{aligned} S_f &= 350 \text{ km} \\ &= r \\ \Sigma(IS)_f &= 4200 \text{ km} \end{aligned} \right\} \quad (1)$$

Then from Figure 5.1,

$$\left. \begin{aligned} S_{f_{eff.}} &= r \sqrt{1 - (d/r)^2} \\ &= 350 \sqrt{0.75} \\ &= 303 \text{ km} \end{aligned} \right\} \quad (2)$$

and using this value in conjunction with the \mathcal{R}_1 line, Figure 4.5,

$$\left. \begin{aligned} M_{eff.} &= 6.8 \\ \Sigma(IS)_{f_{eff.}} &= 3700 \text{ km} \end{aligned} \right\} \quad (3)$$

Second Approximate Method

From the η vs. d/r chart, Figure 5.2, assuming $V_2/V_4 = 1.75$, we find

$$\left. \begin{aligned} \text{For } d/r = 0, \quad \eta &= 0.19 \\ \text{For } d/r = \frac{1}{2}, \quad \eta &= 0.07 \end{aligned} \right\} \quad (4)$$

Using $\log_{10} E = 11.4 + 1.5 M$, we find (for an earthquake occurring on the earth's surface)

$$\left. \begin{aligned} \frac{d}{r} &= 0 \\ \eta &= 0.19 \\ M &= 7 \end{aligned} \right\} \left. \begin{aligned} E_7 &= 8 \times 10^{21} \text{ ergs} \\ H &= 0.19 (8 \times 10^{21}) \text{ ergs} \end{aligned} \right\} \quad (5)$$

Therefore (for the 'effective' surface values of the actual earthquake)

$$\left. \begin{aligned} \eta &= 0.07 \\ \frac{d}{r} &= 0 \\ M &= 7 \end{aligned} \right\} \begin{aligned} H &= 0.07 (8 \times 10^{21}) \text{ ergs} \\ &= H_{eff} \end{aligned} \quad (6)$$

and

$$\eta = \frac{H_{eff}}{E_{eff}} = 0.19 \quad (7)$$

or

$$\left. \begin{aligned} E_{eff} &= \frac{0.07}{0.19} (8 \times 10^{21}) \text{ ergs} \\ &= 10^{21.47} \text{ ergs} \end{aligned} \right\} \quad (8)$$

from which

$$11.4 + 1.5 M_{eff} = 21.47$$

and

$$M_{eff} = 6.7 \quad (9)$$

Therefore from the \mathcal{R}_1 line

$$\left. \begin{aligned} S_{f\,eff} &= 280 \text{ km} \\ \Sigma(IS)_{f\,eff} &= 3300 \text{ km} \end{aligned} \right\} \quad (10)$$

Third Approximate Method

In this method we use the 'Decremental Curve', Figure 5.3 which is an average of the $\eta - d/r$ curve.

Thus for $d/r = 0.5$, we have a decrement of, approximately, 0.4 therefore, $M_{eff} = 6.6$ and from the \mathcal{R}_1 line of Figure 4.5 we get

$$\left. \begin{aligned} S_{eff} &= 250 \text{ km} \\ \Sigma(IS)_{f\,eff} &= 3300 \text{ km} \end{aligned} \right\} \quad (11)$$

We list the results in the following Table 1.

Table 1

| Method | 1 | 2 | 3 |
|-----------------------|---------|---------|---------|
| M_{eff} | 6.8 | 6.7 | 6.6 |
| $S_{f\,eff}$ | 303 km | 280 km | 250 km |
| $\Sigma(IS)_{f\,eff}$ | 3700 km | 3300 km | 3000 km |

It should be noted that reported magnitudes of earthquake frequently differ by the amounts shown above (and more).

Finally, from Figure 4.5, we can only state at this time that the earthquake occurred in an \mathcal{R}_2 or \mathcal{R}_3 region. As more data are collected and included in the calibration of Figure 4.5 it will be possible to pinpoint the region more specifically.

CONCLUSION

Three different approximate engineering procedures are given for determining the effect of 'depth of focus' of an earthquake on the response on the surface of the earth.

Effective values are obtained for the resulting efficiency, intensity field, magnitude, extent of observed response and procedures for determining damage assessment as well as structural design.

The approximate analysis presented in the above sections implies that depth of focus effects on $S_f - \Sigma(IS)_f - M$ become significant when $d/r > 1/2$. That is, for values of d/r within the range (say)

$$0 < \frac{d}{r} < \frac{1}{4} \text{ to } \frac{1}{2} \quad (9)$$

it is suggested that the \mathcal{R}_j lines of Figure 4.5 be used directly as shown on Figure 4.5, without correcting for depth of focus.

CHAPTER 6

SUPERPOSITION OF CANONICAL ACCELEROGRAMS

INTRODUCTION

In this chapter, we examine one of the hypothesis formulated in Chapter 2 in connection with the accelerogram portion of the theory — i.e. those accelerograms which cannot be represented directly by the single 'canonical' form, can generally be approximated by a superposition of canonical accelerograms. Furthermore, this superposition very likely corresponds to the actual physical occurrence in which a cluster or sequence of shocks occurs due to multiple fault slippages or other mechanism behaviours. This approach, therefore, opens a new window on the connection between superposed accelerograms and earthquakes mechanisms — an approach which may be checked by studies of accelerograms for the same event obtained at different stations and correlating these with isoseismal contour maps.

A number of accelerograms will be examined insofar as the superposition hypothesis is concerned. It will be found that — approximately — the superposition hypothesis is valid based upon the charts considered*.

Some remarks will also follow from the connection between local 'intensity' and the accelerograms and the discussion of the intensity — energy compatibility relations in Chapter 5.

In particular, we shall consider the connection between the superposed accelerograms and the local intensity-compatibility-damage theory.

In the body of the chapter, only the results will be given. The detailed superposed canonical accelerogram charts, tables etc. will be included in the Appendix to the Chapter.

* The author wishes to thank George Roussey, a graduate student in Civil Engineering at Stevens Institute for assistance in analyzing the various data included in this chapter.

**BRIEF REVIEW OF THE CANONICAL ACCELEROGRAM RELATIONS
(CHAPTERS 2 AND 5)**

An analysis and study of a number of accelerograms, and physical considerations, suggest that $\sum_{t=0}^t (a\Delta t)$ and t are the important variables in this phenomenon, and in particular $\Sigma(a\Delta t)_f$ and t_f are the fundamental parameters. a is the accelerations, t is the time between $t = 0$ and any intermediate value of time, t , t_f is the final time corresponding to a return to zero acceleration. $\Sigma(a\Delta t)$ is the area under the top envelope to the accelerogram.

A mathematical derivation leads to an invariant expression which holds for 'canonical' accelerograms, this being (see Chapter 2)

$$\frac{\sum_{t=0}^t (a\Delta t)}{\sum_{t=0}^{t_f} (a\Delta t)_f} = e^{0.12[1 - (t_f/t)^{1.8}]} \tag{1}$$

As will be shown, for those accelerograms that are not 'canonical' we can generally superpose two or more canonical accelerograms.

By utilizing an alternate, but equivalent postulated mathematical formulation, equating equal terms, and integrating we obtain an equation for the *time-wise* variation of horizontal ground energy at the *point* where the canonical accelerogram was obtained, Eq. 2: (See Chapter 5),

$$\frac{\epsilon_t}{\epsilon_{t_f}} = \frac{\left[\left(\frac{t_f}{t}\right)^{1.8} - \left(\frac{t_f}{t_i}\right)^{1.8} \right]}{\left[1 - \left(\frac{t_f}{t_i}\right)^{1.8} \right]} \tag{2}$$

ϵ_t = surface horizontal energy per unit effective area between the times t_f and t at the accelerogram location.

ϵ_{t_f} = same for $t \rightarrow t_f$

For two or more superposed canonical records we account for the energy expressions as indicated later in the chapter.

THE GEOLOGY OF THE REGION

Physically, we must assume that the 'geology' of a region affects the ground behaviour and structural response. We assume in this text, 3 'geologies' similar to but different from the regions described by Newmark and Rosenblueth, N-R. These are:

- \mathcal{R}_1 = Surface Fault Region
(The Circumpacific Belt) N-R
- \mathcal{R}_2 = Mountain Region
(The Alpine Belt) N-R
- \mathcal{R}_3 = Plains Region
(The Low Seismicity Region) N-R

In a general way, frequency of the accelerogram record (as well as focal depth) are assumed to be accounted for in this classification. These geological designations are used in the mathematical, physical and technical formulations throughout the text. If necessary and desirable other or additional (or fewer) geologies may be specified. This determination will be made as more actual earthquake data permits a finer calibration of the charts utilizing the geology parameter. In particular, as pointed out in Chapter 10, the effects of anomalous or non-average regional geologies may also be related to the superposed accelerograms.

THE SUPERPOSED ACCELEROGRAMS

A study was made of a relatively large number of texts and papers covering earthquake topics including accelerograms. Not surprisingly, a small amount of data was obtained which connected accelerograms with local intensity (a desirable correlation in the present rational theory). Also, there appeared to be some fairly obvious inconsistencies in some of the accelerograms — a behaviour probably related to the fact that many accelerograms tell the observers more about the accelerograph (the recording machine) than they do about the ground acceleration.

In any case, data was obtained from References 1-8 and this was analyzed with results as shown in this chapter.

Figure 6.1 shows the original data from Chapter 2 for the five canonical accelerograms.

Figure 6.2 shows a typical two-fold superposition of canonical accelerograms.

As a preliminary exercise, canonical accelerograms (single forms) from two earthquake will be examined. The accelerograms are in the references noted

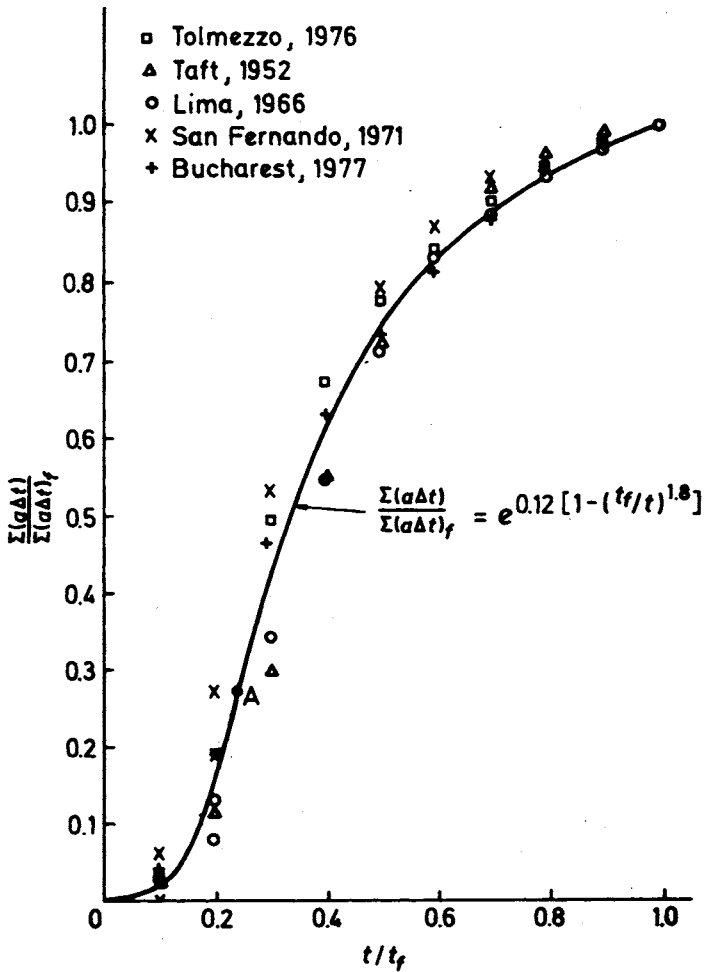


Figure 6.1

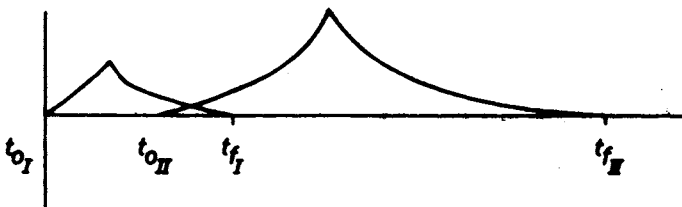


Figure 6.2

previously. Some of the difficulties involved in accelerogram analyses will be indicated.

The accelerograms are for the El Alamo, Baja California earthquake of February 9, 1956 and the Helena, Montana earthquake of October 31, 1935.

The El Alamo Quake accelerogram was measured at the El Centro site in the Imperial Valley, California. Unfortunately, the graph was started late as shown in Figure 6.3.

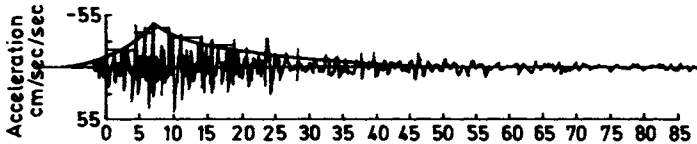


Figure 6.3

From the recorded data the canonical accelerogram was drawn and estimated to be at -4.6 sec. from the start of the graph. The final time was taken as 42.4 sec. Although the graph continues on, the remainder is probably noise. This is a judgement decision and may be an error although it seems reasonable. The table of t/t_f and $\Sigma(a\Delta t)_f$, Table 1A of the Appendix*, shows that this quake follows Eq. 1 as do the points plotted on the $\Sigma(a\Delta t)/\Sigma(a\Delta t)_f$ plot as shown in Figure 1A.

The Helena earthquake accelerogram Figure 6.4 appears to have a poorly defined t_f value. This may be an instrumental peculiarity or due to some other noise effect. An assumed $t_f = 10$ seconds obtained a reasonable fit. If $t_f = 9$ had been chosen (and this is a possible value) then a better agreement would have been obtained. See Figure 1A and Table 2A.

The first multiple canonical accelerogram considered is of the May 18, 1940 Imperial Valley California quake, recorded at the El Centro site. The accelerogram, as shown in Figure 6.5, consists of four canonicals. They were drawn to be fairly symmetrical with the bottom halves. For each separate canonical a $\Sigma(a\Delta t)/\Sigma(a\Delta t)_f = t/t_f$ table was constructed as shown in Tables 3A–6A. These points were then plotted on the same graph, shown in Figure 6.6. As can be seen each canonical plotted well with respect to the invariant curve, which agrees with the superposition assumption.

The second quake of this genre which was examined is the Managua, Nicaragua earthquake of December 23, 1972.

* The letter A refers to Tables, Charts and Figures in the Appendix to this chapter.

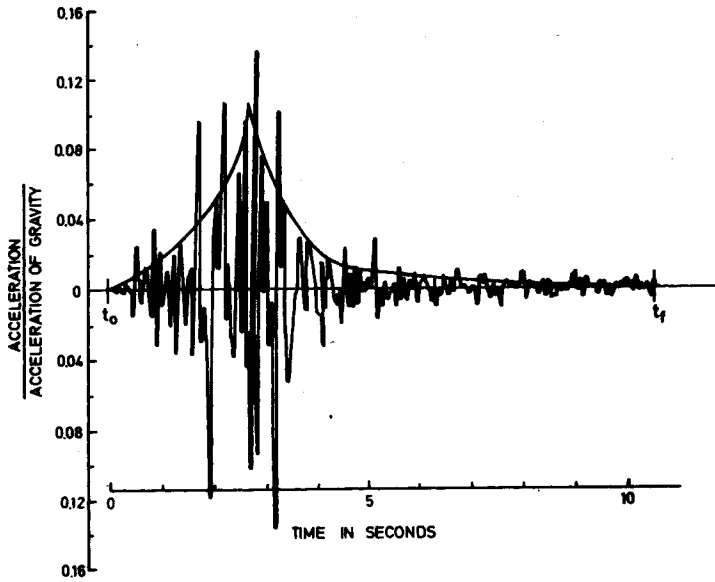


Figure 6.4 Helena Accelerogram

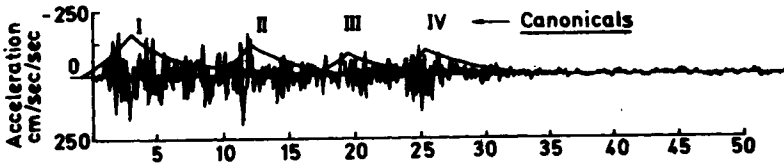


Figure 6.5

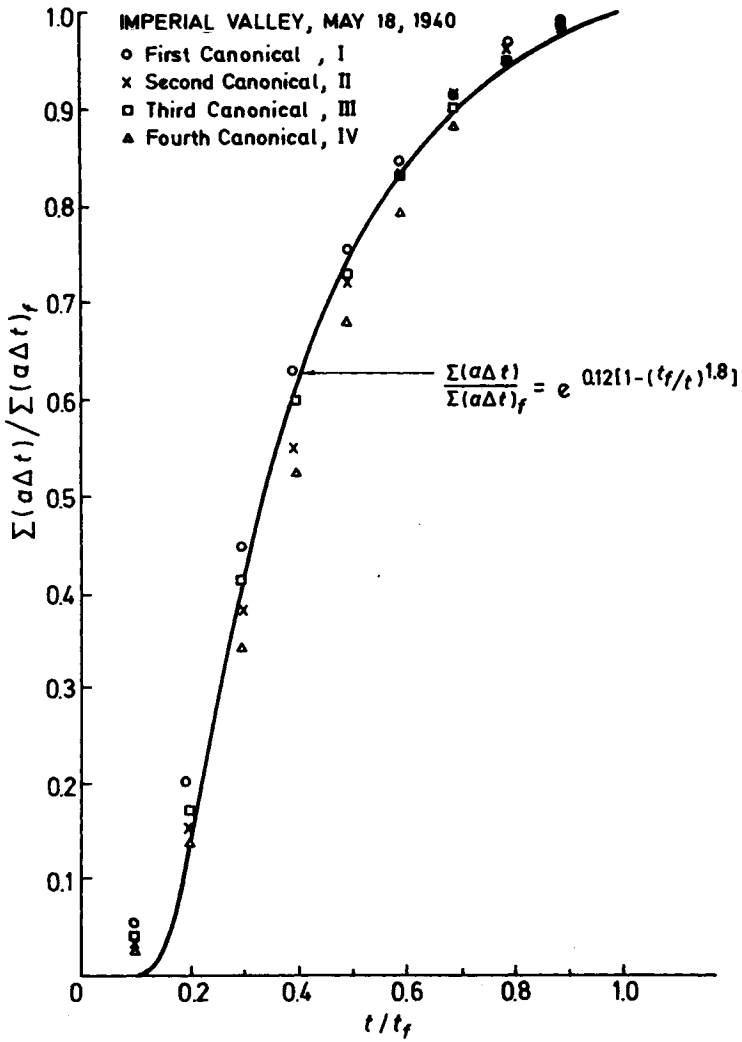
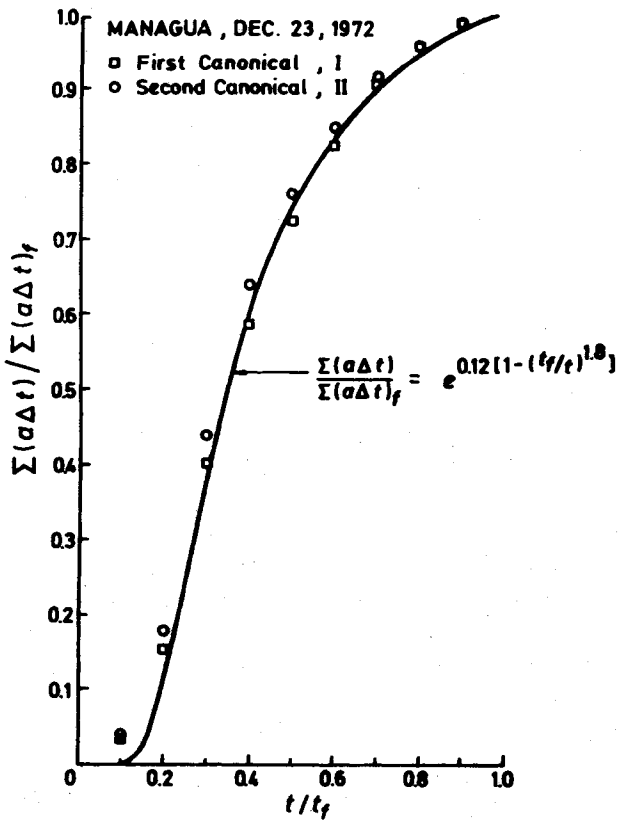
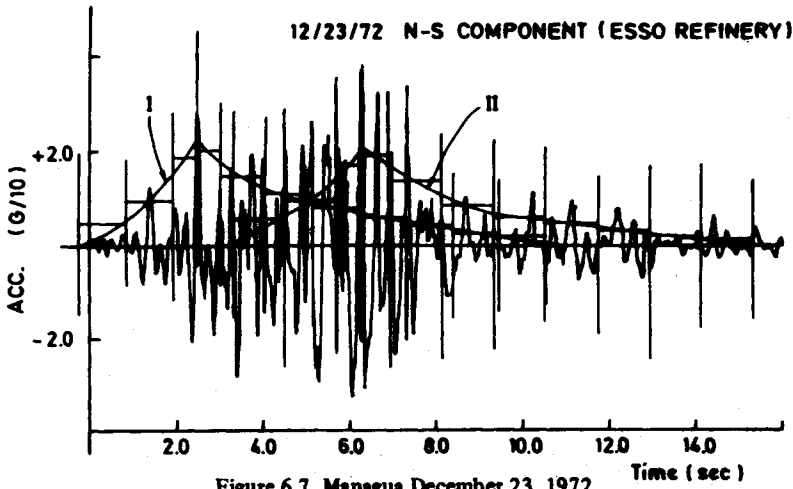


Figure 6.6

As seen in Figure 6.7, the accelerogram consists of two canonicals. It was rather difficult to determine the shape of the first canonical. The bottom half of the accelerogram was examined to help in this determination. The tables for each



canonical are shown in Tables 7A and 8A. As can be seen in Figure 6.8 the two canonicals plotted follow the invariant equation curve. Other information on this earthquake includes a magnitude of $M = 6.2$ and the intensity at the location of the accelerogram of $I = VI$. For this accelerogram it must be noted that t_0 had to be estimated from the shape of the graph.

The Olympia Washington earthquake of April 13, 1949 was a rather complex accelerogram to relate to the canonicals, as it was difficult to determine how many peaks there were as shown in Figure 6.9.

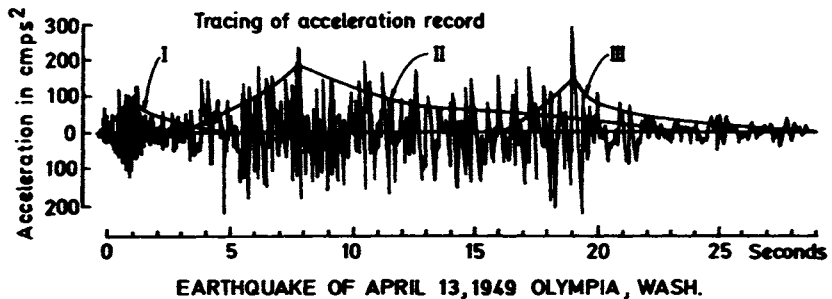


Figure 6.9

Table 9A–11A give the values for each canonical. The plot of the points can be seen in Figure 6.10. All three follow the invariant curve fairly well although the second canonical is slightly off. The magnitude of the quake was $M = 7$ and the intensity at the epicentre was $MM = VIII$ but it is not known where the accelerogram was taken.

For the accelerogram for the Lima, Peru earthquake of May 31, 1970 it was very difficult to determine whether or not there was a second canonical. The height for the top of the main peak was determined by comparing the top half to the bottom half. A small second canonical was estimated toward the end but this may not be reasonable. The accelerograms and their canonicals for both the 1970 and 1974 Lima earthquakes are shown in Figure 6.11. Tables 12A and 13A and Figure 6.12 show the check against the invariant relation which is good. The magnitude was $M = 7.7$. The highest intensity was $MM = VIII$, but the intensity in Lima where the accelerogram was taken was $MM = VI$.

As noted, the accelerogram for the Lima, Peru earthquake of October 3, 1974 was also examined, Figure 6.11. The canonicals were estimated as shown for I, II and III. Not enough of the accelerogram was given so that the fourth canonical, which seems to be of the longest duration was not used, although a reasonable choice of t_f for this canonical would have indicated a good check. Figure

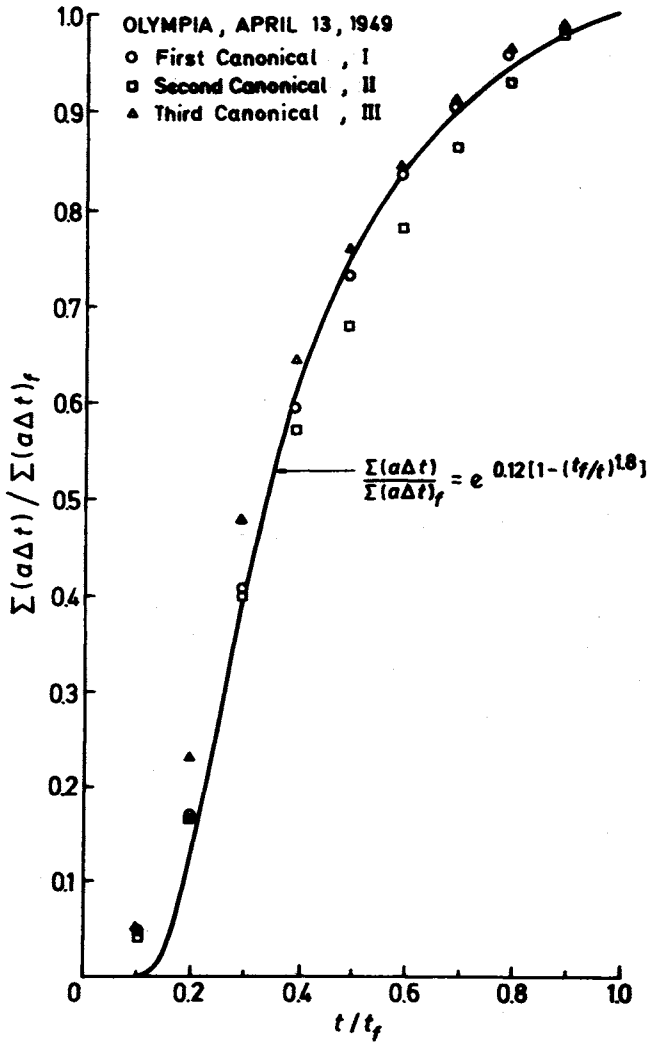
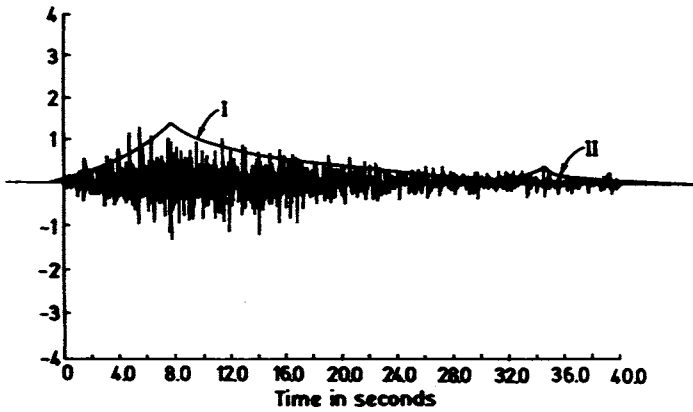


Figure 6.10



Accelerogram records of the October 3, 1974 Peru Earthquake. Upper is from the Geophysical Institute and lower is from residence of Dr. Huaco in Lima.



Accelerogram record of May 31, 1970 Peru earthquake recorded at the Geophysical Institute of Lima.

Figure 6.11

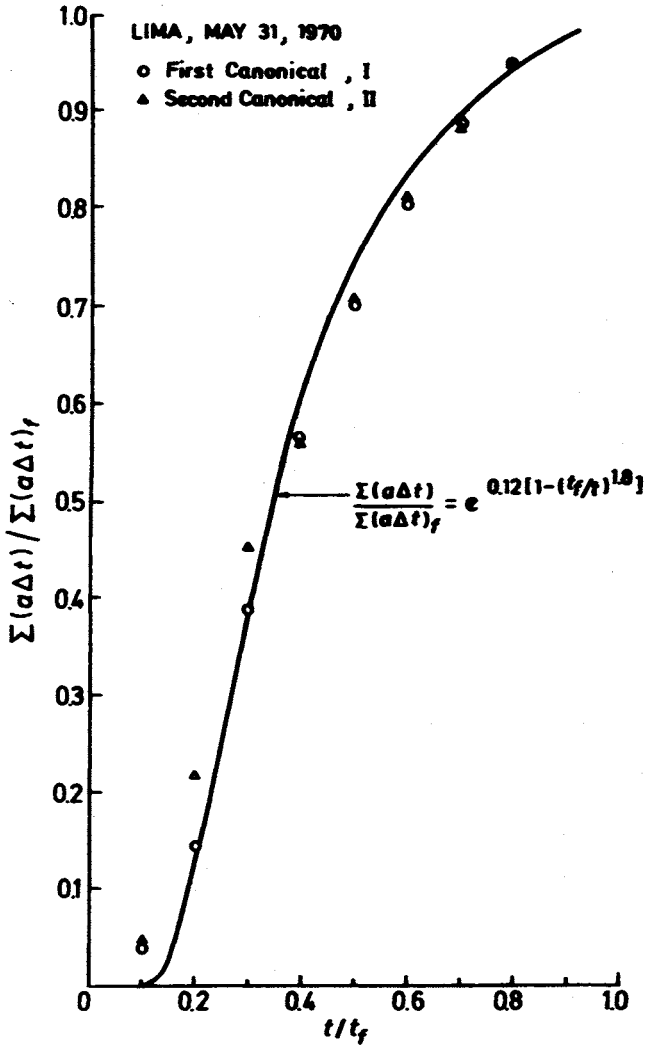


Figure 6.12

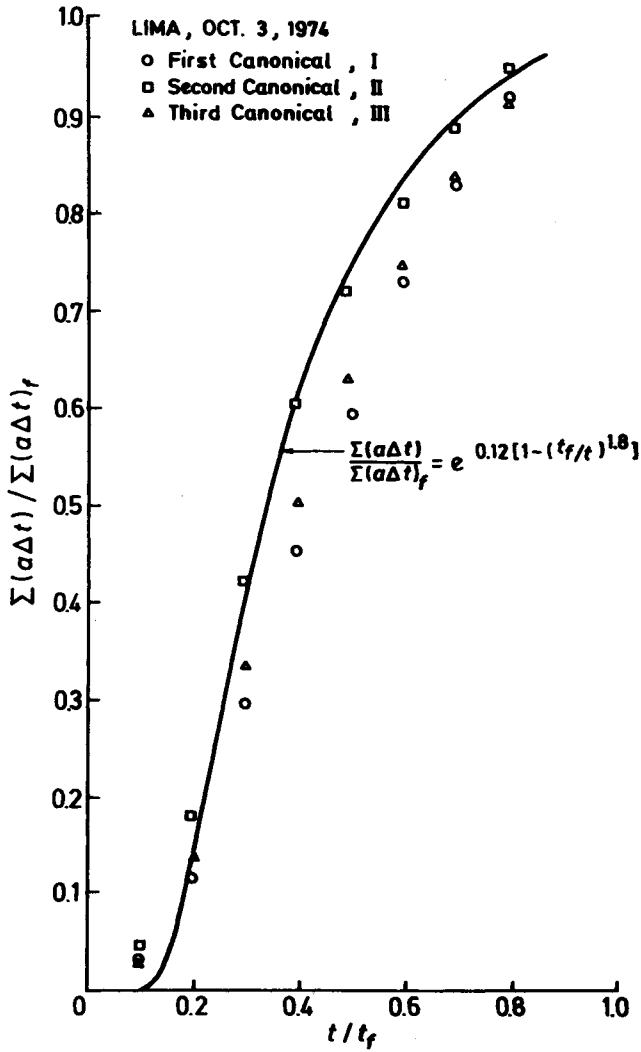


Figure 6.13

6.13 shows the check for the canonicals I, II and III, with the numerical values shown in Tables 14A, 15A and 16A. Concerning the magnitude of the earth-

quake, the USGS put it at $M = 7.6$ while the Geophysical Institute of Peru put it at $M = 6$ which is probably more correct.

The intensity maximum was VIII but the intensity ranged from VI–VII in Lima so that it is not known what the intensity was at the location of the accelerogram.

Another piece of information that can be used for the five original accelerograms, is for the 1966 Lima earthquake. The magnitude was $M = 7.5$ and the intensity in Lima where the accelerogram was taken was MM = VII. However, in view of the magnitude spread indicated above for the 1974 earthquake, some question may rise concerning the $M = 7.5$ value, as well as the intensity.

THE SUPERPOSED ACCELEROGRAM-DAMAGE CORRELATION

In Chapter 5 a correlation is hypothesized connecting the accelerogram and the damage (as measured by the MM intensity scale) at a point on the surface of the earth.

The correlation is based upon the assumptions that

1. The accelerogram at a point on the earth's surface must be related to the variation with time of the horizontal energy per unit effective area at that point.
2. Damage is related to the ability of the structure to absorb this energy.

Thus, regardless of the location, earthquake magnitude or other parameter values, a given accelerogram should be related to the expected intensity, and hence damage at the location where the accelerogram was recorded.

Certainly, the geology of a region, the epicentre or focal depth, the earthquake magnitude and other fundamental parameters will be correlated with the damage. But, just as certainly, these will be correlated with the accelerogram, and the correlation is assumed to be through the two fundamental accelerogram parameters, $\Sigma(a\Delta t)_f$ and t_f , as well as through the 'geology' which as shown previously in this chapter is simplified to *three* basic 'regions' or 'geologies' as shown in Figure 6.14. As noted in Chapter 4, Figure 6.14 is an approximate form of the given correlation. More points are needed, more data on earthquake accelerograms must be analyzed in the light of the rational theory and — very likely — as noted in the earlier sections dealing with geology, it is possible that more than three basic regions will be required. This can only be determined following a continuing determination of actual earthquake data.

The question which will now be addressed is: 'How is the Damage Contour Chart, Figure 6.14 to be used when we have superposed canonical accelerogram?'

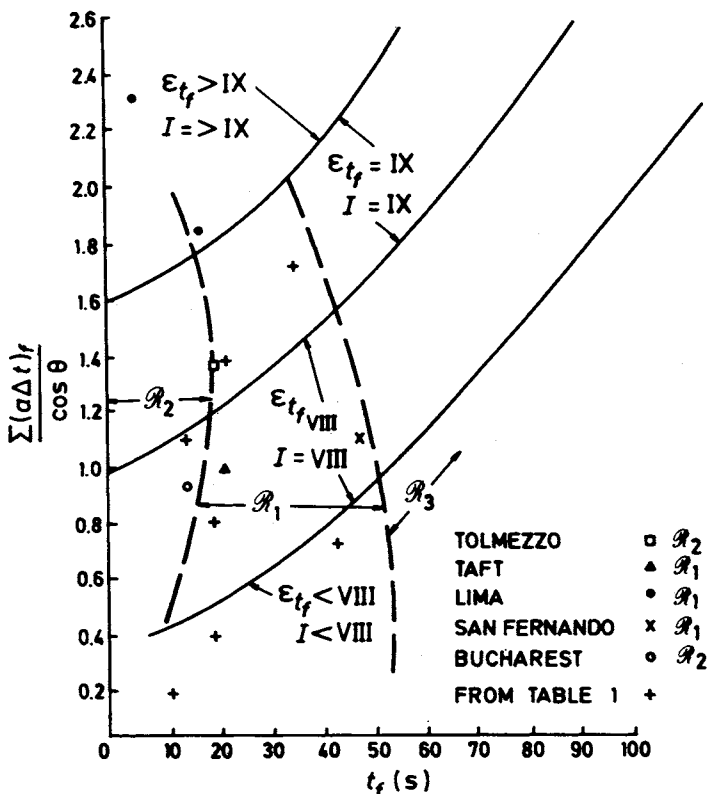


Figure 6.14 R_1 , R_2 and R_3 are assumed 'average geological' regions. Anomalous geological effects at particular accelerogram locations (such as for the Central Mexico City area in the September 19, 1985 earthquake) are not accounted for in this chart. It is conceivable, however, that special regions, R_N , could be determined for particular anomalous ground behaviours. See also Section D of Chapter 10.

Although the first mention of this chart, in *EE-DA&SD* suggested a procedure for handling the multiple accelerograms, further study since publication of the text suggests a somewhat different approach.

According to recent studies, the intensity-ground energy compatibility requirement indicates that the resultant intensity (i.e., damage or ground energy) at a point where several isoseismal maps superpose or overlay, can be taken approximately as the *maximum* intensity of the various superposed maps.

Thus, if we have a series or cluster or sequence of earthquake shocks — such as that due to a sequence of superposed canonical accelerograms, then the

damage — or the intensity — or the ground energy — at the point where the accelerograms are taken can be approximated by the value corresponding to the maximum-effect canonical. That is, the combination of $\Sigma(a\Delta t)_f - t_f$ for each of the canonicals is determined, and the pair which — on Figure 6.14 — corresponds to maximum intensity governs the structural damage and design.

Therefore, for the accelerograms considered in this chapter the key parameters of the various canonicals are as indicated in the following Table 1. Also shown is the canonical which governs for each earthquake as well as the intensity indicated by Figure 6.14. Where available, the intensity value at the accelerograph location (as reported in the literature) is also listed. See, however, the remark under Table 1.

There does not appear to be sufficient information in the literature to check the predictions of the theory as given in the table. As more and more data is collected and recorded, the curves of Figure 6.14 will be altered, modified or revised as required. Ultimately, it is suggested, a single map (or set of maps, each corresponding to a single region or 'geology') will be available, from which the engineer-designer, damage and insurance professionals and others concerned with earthquakes will be able to determine probable damage as well as ground energy for different possible accelerograms.

Furthermore, it is possible that the new theory, which postulates a rational, quantitative explanation for clusters and sequenced earthquakes, when used in conjunction with carefully prepared isoseismal maps for the same events (see the next chapter) may give some fundamental insights into the basic mechanics and predictability of earthquakes.

CONCLUSION

The rational theory of earthquake engineering is applied to a study of the interpretation of accelerograms.

Starting with a previously defined 'canonical' accelerogram, a postulate involving superposition of canonical accelerograms leads to a quantitative analysis suggesting a connection with clustered or sequenced shocks or multiple shocks.

The literature was culled for various accelerograms and the theory applied to analysis of these. The original reports themselves, in a number of cases, indicated inconsistencies and possibly errors in the reported data. However, in spite of these, the results obtained by the analyses show good agreement.

As more and more data of the required form is obtained, and checked as suggested by the theory, more accurate design charts and curves will be obtained. This in turn will enable professionals in the earthquake engineering field to use the theories with greater certainty.

Table 1

| Earthquake | Canonical (governs indicated by*) | $\Sigma(a\Delta t)_f$ g-Sec. | t_f seconds | Intensity from Fig. 6.14 | Intensity Reported |
|-----------------------------|---|---------------------------------|------------------|--------------------------------|-----------------------|
| El Alamo, 1956 | I* | 0.7 | 47 | VIII | |
| Helena, 1935 | I* | 0.2 | 10 | < VIII | VII |
| Imperial Valley, 1940 | I* | 1.1 | 15 | VIII | |
| | II | 0.6 | 10 | VIII | |
| | III | 0.5 | 12 | VIII | |
| | IV | 0.5 | 8 | VIII | |
| Managua, 1972 | I | 0.8 | 11 | VIII | VI |
| | II* | 0.8 | 12 | VIII | |
| Olympia, 1949 | I | 0.2 | 5 | < VIII | |
| | II* | 1.4 | 20 | IX | |
| | III | 0.6 | 12 | VIII | |
| Lima, 1970 | I* | 1.7 | 34 | IX | |
| | II | 0.2 | 13 | < VIII | |
| Lima, 1974 | I | 0.1 | 9 | < VIII | |
| | II | 0.3 | 14 | < VIII | |
| | III* | 0.4 | 15 | < VIII | |

In the above chart, it is assumed that all accelerogram records were taken at non-anomalous or 'average geologies'. If any of the accelerograms were, in fact, taken at anomalous geological locations, then the corresponding average geological regions of Figure 6.14 may not be applicable. See the discussion of the September 19, 1985 Mexican Earthquake, Section D of Chapter 10.

REFERENCES

1. Earthquake Engineering Research Institute, *Managua Nicaragua Earthquake December 23, 1972*, Conference Proceedings, Oakland, 1973.
2. Earthquake Engineering Research Institute, *Managua, Nicaragua Earthquake of December 23, 1972*, Reconnaissance Report. Oakland, Calif. 1973.
3. Earthquake Engineering Research Institute, *Engineering Aspects of the Lima, Peru Earthquake of October 3, 1974*. Prepared by EERI Reconnaissance Team, 1975.

4. Earthquake Engineering Research Institute, Earthquake design criteria, structural performance and strong motion records. Series of lectures held in Gaithersburg, Md. Sept. 7-8, 1977.
5. Neumann, Frank, *Earthquake intensity and related ground motion*, Seattle, 1954.
6. U.S. Environmental data service, *Earthquake history of the U.S.* J.L. Coffman and C.A. vanHake, Eds., Rev. Ed. (through 1970) Washinton, 1973.
7. Hudson, D.E., *Reading and Interpreting Strong Motion Accelerograms*, EERI, 1979.
8. Chang, Mark, et. al., *ARMA Models for Earthquake ground motions*, EERI, 1979.

APPENDIX

The appendix contains the numerical Tables used in the canonical accelerogram analyses.

Table 1A El Alamo, 1956: t_0 (est) = -4.59 sec, t_f = 42.43 sec,
 $\Sigma(a\Delta t)_f = 737.62$ cm/sec = .753g-sec

| t/t_f | $\Sigma(a\Delta t)/\Sigma(a\Delta t)_f$ | $e^{0.12[1 - (t_f/t)^{1.8}]}$ |
|---------|---|-------------------------------|
| 0 | 0.000 | 0.000 |
| 0.1 | 0.035 | 0.001 |
| 0.2 | 0.149 | 0.128 |
| 0.3 | 0.380 | 0.395 |
| 0.4 | 0.577 | 0.604 |
| 0.5 | 0.720 | 0.742 |
| 0.6 | 0.828 | 0.834 |
| 0.7 | 0.905 | 0.896 |
| 0.8 | 0.955 | 0.942 |
| 0.9 | 0.990 | 0.975 |
| 1.0 | 1.000 | 1.000 |

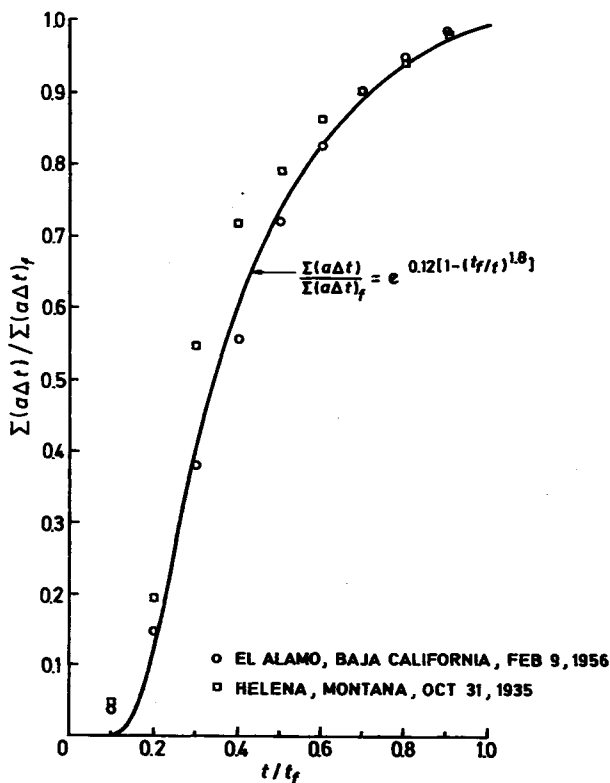


Figure 1A

Table 2A Helena, 1935: $t_0 = 0$, $t_f = 10.0$ sec, $\Sigma(a\Delta t)_f = .24$ g-sec

| t/t_f | $\Sigma(a\Delta t)/\Sigma(a\Delta t)_f$ | $e^{0.12[1-(t/t_f)^{1.8}]}$ |
|---------|---|-----------------------------|
| 0 | 0.000 | 0.000 |
| 0.1 | 0.047 | 0.001 |
| 0.2 | 0.195 | 0.128 |
| 0.3 | 0.55 | 0.395 |
| 0.4 | 0.72 | 0.604 |
| 0.5 | 0.79 | 0.742 |
| 0.6 | 0.87 | 0.834 |
| 0.7 | 0.91 | 0.896 |
| 0.8 | 0.94 | 0.942 |
| 0.9 | 0.99 | 0.975 |
| 1.0 | 1.00 | 1.000 |

Intensity $M = VII$

Table 3A Imperial Valley, 1940 — First Canonical, I: $t_0(\text{est}) = -.75 \text{ sec}$,
 $t_f = 14.25 \text{ sec}$, $\Sigma(a\Delta t)_f = 1084.52 \text{ cm/sec} = 1.107 \text{ g-sec}$

| t/t_f | $\Sigma(a\Delta t)/\Sigma(a\Delta t)_f$ | $0.12[1 - (t_f/t)^{1.2}]$ |
|---------|---|---------------------------|
| 0 | 0.000 | 0.000 |
| 0.1 | 0.055 | 0.001 |
| 0.2 | 0.204 | 0.128 |
| 0.3 | 0.448 | 0.395 |
| 0.4 | 0.629 | 0.604 |
| 0.5 | 0.754 | 0.742 |
| 0.6 | 0.845 | 0.834 |
| 0.7 | 0.916 | 0.896 |
| 0.8 | 0.971 | 0.942 |
| 0.9 | 0.994 | 0.975 |
| 1.0 | 1.000 | 1.000 |

Table 4A Imperial Valley, 1940 — Second Canonical, II: $t_0 = 9.5 \text{ sec}$
 $t_f = 19.67 \text{ sec}$, $\Sigma(a\Delta t)_f = 609.38 \text{ cm/sec} = .622 \text{ g-sec}$

| t/t_f | $\Sigma(a\Delta t)/\Sigma(a\Delta t)_f$ | $0.12[1 - (t_f/t)^{1.2}]$ |
|---------|---|---------------------------|
| 0 | 0.000 | 0.000 |
| 0.1 | 0.033 | 0.001 |
| 0.2 | 0.154 | 0.128 |
| 0.3 | 0.380 | 0.395 |
| 0.4 | 0.571 | 0.604 |
| 0.5 | 0.720 | 0.742 |
| 0.6 | 0.832 | 0.834 |
| 0.7 | 0.916 | 0.896 |
| 0.8 | 0.963 | 0.942 |
| 0.9 | 0.991 | 0.975 |
| 1.0 | 1.000 | 1.000 |

Table 5A Imperial Valley, 1940 — Third Canonical, III: $t_0 = 16.42$ sec,
 $t_f = 28.42$ sec, $\Sigma(a\Delta t)_f = 477.27$ cm/sec = .487 g-sec

| t/t_f | $\Sigma(a\Delta t)/\Sigma(a\Delta t)_f$ | $e^{0.12[1-(t_f/t)^{1.8}]}$ |
|---------|---|-----------------------------|
| 0 | 0.000 | 0.000 |
| 0.1 | 0.043 | 0.001 |
| 0.2 | 0.171 | 0.128 |
| 0.3 | 0.414 | 0.395 |
| 0.4 | 0.600 | 0.604 |
| 0.5 | 0.729 | 0.742 |
| 0.6 | 0.830 | 0.834 |
| 0.7 | 0.901 | 0.896 |
| 0.8 | 0.951 | 0.942 |
| 0.9 | 0.987 | 0.975 |
| 1.0 | 1.000 | 1.000 |

Table 6A Imperial Valley, 1940 — Fourth Canonical, IV: $t_0 = 23.13$ sec,
 $t_f = 31.04$ sec, $\Sigma(a\Delta t)_f = 482.58$ cm/sec = .492 g-sec

| t/t_f | $\Sigma(a\Delta t)/\Sigma(a\Delta t)_f$ | $e^{0.12[1-(t_f/t)^{1.8}]}$ |
|---------|---|-----------------------------|
| 0 | 0.000 | 0.000 |
| 0.1 | 0.026 | 0.001 |
| 0.2 | 0.138 | 0.128 |
| 0.3 | 0.342 | 0.395 |
| 0.4 | 0.526 | 0.604 |
| 0.5 | 0.679 | 0.742 |
| 0.6 | 0.791 | 0.834 |
| 0.7 | 0.883 | 0.896 |
| 0.8 | 0.949 | 0.942 |
| 0.9 | 0.985 | 0.975 |
| 1.0 | 1.000 | 1.000 |

Table 7A Managua, 1972 — First Canonical, I: $t_0(\text{est}) = -0.23 \text{ sec}$, $t_f = 10.58 \text{ sec}$
 $\Sigma(a\Delta t)_f = .829 \text{ g-sec}$

| t/t_f | $\Sigma(a\Delta t)/\Sigma(a\Delta t)_f$ | $e^{0.12[1-(t_f/t)^{1.2}]}$ |
|---------|---|-----------------------------|
| 0 | 0.000 | 0.000 |
| 0.1 | 0.030 | 0.001 |
| 0.2 | 0.151 | 0.128 |
| 0.3 | 0.398 | 0.395 |
| 0.4 | 0.588 | 0.604 |
| 0.5 | 0.725 | 0.742 |
| 0.6 | 0.825 | 0.834 |
| 0.7 | 0.903 | 0.896 |
| 0.8 | 0.956 | 0.942 |
| 0.9 | 0.988 | 0.975 |
| 1.0 | 1.000 | 1.000 |

Table 8A Managua, 1972 — Second Canonical, II: $t_0 = 3.32 \text{ sec}$, $t_f = 15.27 \text{ sec}$,
 $\Sigma(a\Delta t)_f = .811 \text{ g-sec}$

| t/t_f | $\Sigma(a\Delta t)/\Sigma(a\Delta t)_f$ | $e^{0.12[1-(t_f/t)^{1.2}]}$ |
|---------|---|-----------------------------|
| 0 | 0.000 | 0.000 |
| 0.1 | 0.041 | 0.001 |
| 0.2 | 0.179 | 0.128 |
| 0.3 | 0.440 | 0.395 |
| 0.4 | 0.639 | 0.604 |
| 0.5 | 0.760 | 0.742 |
| 0.6 | 0.845 | 0.834 |
| 0.7 | 0.913 | 0.896 |
| 0.8 | 0.956 | 0.942 |
| 0.9 | 0.988 | 0.975 |
| 1.0 | 1.000 | 1.000 |

Table 9A Olympia, 1949 — First Canonical, I: $t_0 = 0$, $t_f = 5.2$ sec,
 $\Sigma(a\Delta t)_f = 191.03$ cm/sec = .195 g-sec

| t/t_f | $\Sigma(a\Delta t)/\Sigma(a\Delta t)_f$ | $e^{0.12[1 - (t_f/t)^{1.8}]}$ |
|---------|---|-------------------------------|
| 0 | 0.000 | 0.000 |
| 0.1 | 0.046 | 0.001 |
| 0.2 | 0.168 | 0.128 |
| 0.3 | 0.403 | 0.395 |
| 0.4 | 0.597 | 0.604 |
| 0.5 | 0.730 | 0.742 |
| 0.6 | 0.832 | 0.834 |
| 0.7 | 0.903 | 0.896 |
| 0.8 | 0.959 | 0.942 |
| 0.9 | 0.989 | 0.975 |
| 1.0 | 1.000 | 1.000 |

Table 10A Olympia, 1949 — Second Canonical, II: $t_0 = 3.42$ sec, $t_f = 23.63$,
 $\Sigma(a\Delta t)_f = 1408.67$ cm/sec = 1.44 g-sec

| t/t_f | $\Sigma(a\Delta t)/\Sigma(a\Delta t)_f$ | $e^{0.12[1 - (t_f/t)^{1.8}]}$ |
|---------|---|-------------------------------|
| 0 | 0.000 | 0.000 |
| 0.1 | 0.040 | 0.001 |
| 0.2 | 0.164 | 0.128 |
| 0.3 | 0.395 | 0.395 |
| 0.4 | 0.572 | 0.604 |
| 0.5 | 0.690 | 0.742 |
| 0.6 | 0.781 | 0.834 |
| 0.7 | 0.862 | 0.896 |
| 0.8 | 0.932 | 0.942 |
| 0.9 | 0.979 | 0.975 |
| 1.0 | 1.000 | 1.000 |

Table 11A Olympia, 1949 — Third Canonical, III: $t_0 = 16.63$ sec,
 $t_f = 28.79$ sec, $\Sigma(a\Delta t)_f = 577.74$ cm/sec = .59 g-sec

| t/t_f | $\Sigma(a\Delta t)/\Sigma(a\Delta t)_f$ | $e^{0.12[1 - (t_f/t)^{1.8}]}$ |
|---------|---|-------------------------------|
| 0 | 0.000 | 0.000 |
| 0.1 | 0.049 | 0.001 |
| 0.2 | 0.229 | 0.128 |
| 0.3 | 0.479 | 0.395 |
| 0.4 | 0.644 | 0.604 |
| 0.5 | 0.761 | 0.742 |
| 0.6 | 0.840 | 0.834 |
| 0.7 | 0.909 | 0.896 |
| 0.8 | 0.965 | 0.942 |
| 0.9 | 0.988 | 0.975 |
| 1.0 | 1.000 | 1.000 |

Table 12A Lima, 1970 — First Canonical, I: $t_0(\text{est}) = -.8$ sec,
 $t_f = 33.33$, $\Sigma(a\Delta t)_f = 1.66$ g-sec

| t/t_f | $\Sigma(a\Delta t)/\Sigma(a\Delta t)_f$ | $e^{0.12[1 - (t_f/t)^{1.8}]}$ |
|---------|---|-------------------------------|
| 0 | 0.000 | 0.000 |
| 0.1 | 0.038 | 0.001 |
| 0.2 | 0.154 | 0.128 |
| 0.3 | 0.385 | 0.395 |
| 0.4 | 0.568 | 0.604 |
| 0.5 | 0.701 | 0.742 |
| 0.6 | 0.803 | 0.834 |
| 0.7 | 0.889 | 0.896 |
| 0.8 | 0.949 | 0.942 |
| 0.9 | 0.987 | 0.975 |
| 1.0 | 1.000 | 1.000 |

**Table 13A Lima, 1970 – Second Canonical, II: $t_0 = 30.6$ sec,
 $t_f = 43.93$ sec, $\Sigma(a\Delta t)_f = .194$ g-sec**

| t/t_f | $\Sigma(a\Delta t)/\Sigma(a\Delta t)_f$ | $e^{0.12[1-(t_f/t)^{1.8}]}$ |
|---------|---|-----------------------------|
| 0 | 0.000 | 0.000 |
| 0.1 | 0.044 | 0.001 |
| 0.2 | 0.219 | 0.128 |
| 0.3 | 0.453 | 0.395 |
| 0.4 | 0.560 | 0.604 |
| 0.5 | 0.708 | 0.742 |
| 0.6 | 0.810 | 0.834 |
| 0.7 | 0.883 | 0.896 |
| 0.8 | 0.949 | 0.942 |
| 0.9 | 0.985 | 0.975 |
| 1.0 | 1.000 | 1.000 |

**Table 14A Lima, 1974 – First Canonical, I: $t_0(\text{est}) = -1.07$ sec,
 $t_f = 7.53$ sec, $\Sigma(a\Delta t)_f = .125$ g-sec**

| t/t_f | $\Sigma(a\Delta t)/\Sigma(a\Delta t)_f$ | $e^{0.12[1-(t_f/t)^{1.8}]}$ |
|---------|---|-----------------------------|
| 0 | 0.000 | 0.000 |
| 0.1 | 0.029 | 0.001 |
| 0.2 | 0.116 | 0.128 |
| 0.3 | 0.295 | 0.395 |
| 0.4 | 0.455 | 0.604 |
| 0.5 | 0.600 | 0.742 |
| 0.6 | 0.731 | 0.834 |
| 0.7 | 0.833 | 0.896 |
| 0.8 | 0.920 | 0.942 |
| 0.9 | 0.978 | 0.975 |
| 1.0 | 1.000 | 1.000 |

Table 15A Lima, 1970 — Second Canonical, II: $t_0 = 3.33$ sec,
 $t_f = 17.33$ sec, $\Sigma(a\Delta t)_f = .301$ g-sec

| t/t_f | $\Sigma(a\Delta t)/\Sigma(a\Delta t)_f$ | $e^{0.12[1 - (t_f/t)^{1.8}]}$ |
|---------|---|-------------------------------|
| 0 | 0.000 | 0.000 |
| 0.1 | 0.044 | 0.001 |
| 0.2 | 0.181 | 0.128 |
| 0.3 | 0.422 | 0.395 |
| 0.4 | 0.608 | 0.604 |
| 0.5 | 0.725 | 0.742 |
| 0.6 | 0.814 | 0.834 |
| 0.7 | 0.892 | 0.896 |
| 0.8 | 0.951 | 0.942 |
| 0.9 | 0.985 | 0.975 |
| 1.0 | 1.000 | 1.000 |

Table 16A Lima, 1974 — Third Canonical, III: $t_0 = 7.53$ sec,
 $t_f = 23.07$ sec, $\Sigma(a\Delta t)_f = .428$ g-sec

| t/t_f | $\Sigma(a\Delta t)/\Sigma(a\Delta t)_f$ | $e^{0.12[1 - (t_f/t)^{1.8}]}$ |
|---------|---|-------------------------------|
| 0 | 0.000 | 0.000 |
| 0.1 | 0.027 | 0.001 |
| 0.2 | 0.127 | 0.128 |
| 0.3 | 0.331 | 0.395 |
| 0.4 | 0.504 | 0.604 |
| 0.5 | 0.635 | 0.742 |
| 0.6 | 0.750 | 0.834 |
| 0.7 | 0.838 | 0.896 |
| 0.8 | 0.915 | 0.942 |
| 0.9 | 0.977 | 0.975 |
| 1.0 | 1.000 | 1.000 |

CHAPTER 7

SUPERPOSITION OF CANONICAL ISOSEISMAL CONTOUR MAPS

INTRODUCTION

We shall describe a rational solution to the problem of the highly asymmetric isoseismal intensity chart, such as usually occurs in the case of surface fault earthquakes or clustered earthquakes.*

The procedure is based upon a superposition of canonical isoseismal contour charts which are characteristic of single shock earthquakes as described in Chapter 3.

Also made use of is the energy-intensity compatibility relation of Section F in Chapter 4.

A comparison is made between the rational map and the published map for a recent large earthquake and it is shown that similar contour fields are obtained.

The procedure will enable professionals in the field of earthquake engineering to determine probable approximate damage and energy fields required for structural analysis for combinations of specified earthquakes.

PROCEDURE

In Section F of Chapter 4 a ground energy-intensity compatibility relation was derived for canonical isoseismal maps. This curve indicates approximate values of the ground energy throughout regions of constant intensity and it indicates that a unit increase in intensity corresponds roughly to a five-fold increase in ground energy.

Thus, if for two canonical isoseismal maps we superpose two intensity bands (say $I = VIII$ and $I = VII$), then, for all practical purposes, the resulting intensity

* The author wishes to thank Jose Ayala and Ja-Shian Chang, graduate students in Civil Engineering at Stevens Institute for assistance in collecting the data for the study described in this chapter.

is, approximately, still $I = VIII$. This behaviour is even more plausible when one accounts for the superposition of directional effects at a point due to separate foci. This very useful approximate property of the compatibility condition derived in the theory, permits us to superpose canonical isoseismal maps for several nearby earthquakes or foci — whether these occur nearly simultaneously (as they probably do in the case of surface fault slippages) or with some time lapse as also frequently happens in many earthquake fields.

Clearly, when an isoseismal map is prepared after the event, and when this isoseismal map is so assymetric that there is a strong probability of superposed earthquakes, it is difficult to ascertain the time lags involved and these are usually not considered in the preparation of the isoseismal contours. Thus, the superposition procedure described above is a reasonable one on both physical and practical grounds.

It is true that in some cases damage may be cummulative due to a series of earthquakes with close foci, in which case the damage criterion might indicate a higher intensity than the highest of each earthquake, but this may be assumed as an unusual and isolated phenomenon.

Thus, in this chapter, using the theory previously derived, we shall superpose earthquakes $E_1, E_2, \dots E_n$, each event having its own magnitude, depth and location of focus and canonical isoseismal chart. The superposed chart will then show layered or lapped intensity regions and the resulting intensity value at any point will be taken as the maximum intensity of the superposed maps at that point.

This procedure will be followed for the Guatemala earthquake of February 4, 1976 and compared with the published isoseismal chart for this earthquake, Ref. 1. The comparison will indicate overall qualitative and quantitative agreement in the two maps.

THE EARTHQUAKE

On February 4, 1976 central Guatemala (according to published reports) experienced an earthquake of 7.5 magnitude with numerous aftershocks. Damage due to the earthquake and aftershocks extended over an approximate area of 100 square km.

The earthquake was due to a rupture along the Motagua Fault with an average displacement of about 100 centimetres. Secondary faulting also occurred (probably associated with the earthquake as a trigger effect) on the areas near the Motagua Valley.

An epicentre location of the main shock was determined to be near Los Amates, within the Motagua Valley, about 157 km northeast of Guatemala City.

The depth of focus d , was assigned as 5 kilometres. For practical purposes we will use $d = 0$ since for a near surface fault earthquake this assumption does not introduce a significant error, see Chapter 5.

THE PUBLISHED ISOSEISMAL MAP

The published isoseismal map, Ref. 1 is shown in Figure 7.1. There are certain features on the map for which we shall attempt to obtain a rational explanation. These are:

1. Two areas of intensity IX approximately 160 km apart (actually there are three areas of intensity IX but one of them is most unrealistic).
2. Two areas of intensity VIII approximately 80 km apart.
3. The intensity curves tend to follow an asymmetric shape along the Motagua Fault.

THE ANALYSIS

Refer to previous chapters for a full explanation of the following notation, equations and procedures.

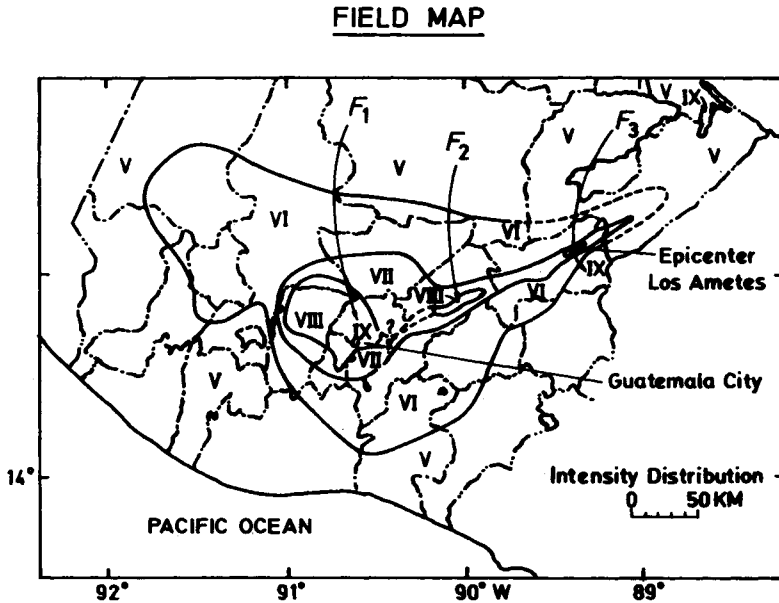


Figure 7.1 Isoseismal Map showing Modified Mercalli intensity distribution in Guatemala from the February 4, 1976 earthquake. F_j indicates epicentre location. (From USGS PP1002)

The fault is essentially a surface fault. Therefore we assume an \mathcal{R}_1 geologic region. Also we assume the depth of all foci equals zero.

Initially, possible earthquakes of magnitudes 8, 7.5, 7, 6.5 and 6.0 were considered. Of these, three separate shocks of magnitudes 7.0, 6.5 and 6.0 were chosen as shown later. Then, from Figure 4.5 and using the derived equation

$$\frac{\sum(IS)}{\sum(IS)_f} = e^{2[1 - (S_f/S)^{1/3}]} \tag{1}$$

we obtain the following values for the $M = 7.0$ and 6.5 earthquakes, Table 1.

Table 1

| Intensity | Km. distance to outer reach, $S_{O.R.}$ | |
|-----------|---|-----------|
| | $M = 7.0$ | $M = 6.5$ |
| III | 315 | 224 |
| IV | 216 | 156 |
| V | 130 | 99 |
| VI | 85 | 63 |
| VII | 52 | 39 |
| VIII | 30 | 23 |
| IX | 15 | 12 |

Assuming 3 separate shocks (or earthquakes) as indicated below with foci and magnitudes as shown at F_1 , F_2 and F_3 in Figure 7.1, the isoseismal contours are then superposed,

| Location | Magnitude |
|----------|-----------|
| F_1 | 7.0 |
| F_2 | 6.5 |
| F_3 | 6.5 |

and Figure 7.2 shows the result of this superposition. That is, it shows the combined or net MID isoseismal map. This may be compared to the actual or field map that was determined shortly after the earthquake, as shown in Figure 7.3, in which the same scale is used for both maps.

Finally, as may be verified, the earthquake energies of the single $M = 7.5$ event and the triple $M = 7.0, 6.5, 6.5$ events are approximately equal.

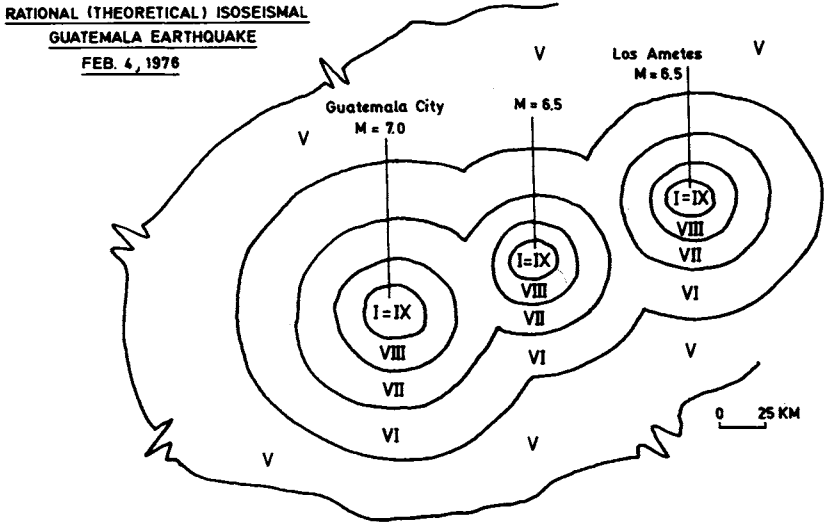


Figure 7.2

CONCLUSION

The very asymmetric field determined isoseismal map for the February 4, 1976 Guatemala earthquake was modelled using the new rational earthquake engineering theory of this text. The model, following the directions indicated by the theory, utilizes superposed theoretical canonical isoseismal fields for three earthquakes of approximate magnitudes 7.0, 6.5 and 6.5 with foci at locations indicated on the field map.

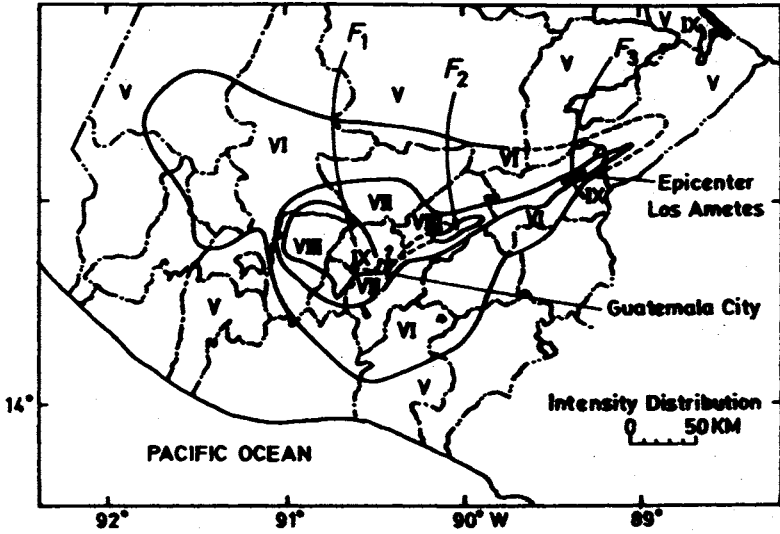
The theoretical map is shown in Figure 7.2 and the field-determined map is shown in Figure 7.1.

A comparison of Figures 7.2 and 7.2 shown on Figure 7.3 indicates a reasonable qualitative and quantitative agreement between the rational theoretical map and the actual field map.

Some considerations relating to the differences between the two isoseismal representations are the following:

1. The lower intensity, outer portion of the field chart, covering the less populated areas must surely be considered as fairly approximate (as, indeed, is true for the entire chart).

FIELD MAP



NATIONAL (THEORETICAL) ISOSEISMAL
GUATEMALA EARTHQUAKE
FEB. 4, 1976

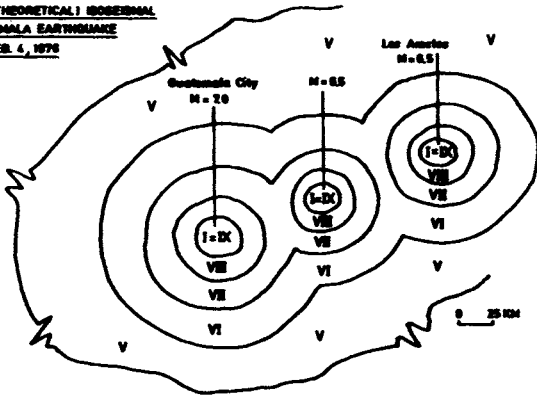


Figure 7.3

2. Slight changes in the assumed theoretical magnitude and foci would change the extent and locations of the different intensity regions and make for a closer check.
3. There are many uncertainties and difficulties involved in the field observations and interrogations — after the fact — and the transfer of this data to office mapping. Some of these are shown by the dotted line designations on the field map, Figure 7.1.

Thus, it would appear reasonable to assume that the technique described may be used to account for highly asymmetric specified surface fault earthquake combinations, quantitatively as well as qualitatively.

In addition, the derived energy-intensity compatibility correlation offers a tool which permits the engineer to design structures and to check and assess damage in the highly asymmetric field.

One final comment — the study suggests that the published isoseismal map for the event described as 'The February 4, 1976 earthquake of magnitude 7.5' was quite possibly a map corresponding to *three* separate earthquakes of magnitudes and foci locations approximately as determined in this analysis. A study of accelerograms of the event would help to answer the question as to whether there were in fact, separate happenings (of the same approximate total focal energy as the single shock) as described here.

REFERENCE

1. A. F. Espinosa 'The Guatemala Earthquake of February 4, 1976 a Preliminary Report', Geological Survey Professional Paper 1002, 1976.

CHAPTER 8

APPROXIMATE ANALYTICAL DAMAGE (INTENSITY NUMBER) ASSESSMENT PROCEDURES

INTRODUCTION

In this short and largely descriptive chapter the charts, curves, and equations derived from the basic invariant relations are utilized to assess probable approximate damage due to an earthquake. The measure of damage is the 'intensity number' which, by virtue of the Modified Mercalli (MM) Scale (see Chapter 3) will describe greater degrees of damage for different structures as the numbers increase. Once more, it must be emphasized, the results can only be considered as approximate. Quantitatively, some of the theoretical intensity values are probably no better than ± 20 per cent although others are possibly more accurate. However, in view of the usual accuracy in earthquake engineering analyses, this is perhaps as good as one can expect for engineering design and analysis purposes.*

The information may be required, for example, for preliminary engineering design purposes. Or an insurer may be interested in probable damage at a given location due to an earthquake (or cluster of earthquakes) of given magnitudes — or due to a canonical accelerogram (or series of canonical accelerograms) with given parameter values. Or preparers of codes (including governmental agencies) may wish to determine probable earthquake damage in a given area based upon historical records for the area in question. And there are other possible reasons for requiring this data.

The basic equations, curves, and charts are presented first. Following this several of the different approaches that may be used are described. Basically,

* Furthermore — and this is an extremely important and useful consideration from the civil engineering point of view — the theory has developed (Figure 4.8) a *quantitative* connection between the MM *intensity number* (which is of negligible design value) and the *energy* (either in the form of strain or kinetic energy) which the structure or other engineering element must absorb. See example D of this chapter.

one must assume a particular initial set of conditions and from that point various approximate damage-intensity data may be determined, depending upon the needs of the user. In all cases, the invariants and parameters obtained in Chapters 2 and 3 and the design data charts derived from these are the fundamental tools used.

THE BASIC EQUATIONS, CHARTS, AND FIGURES

In our analysis we shall utilize the following previously developed equations and charts:

From Chapter 2:

1. The invariant

$$\frac{\sum(a\Delta t)}{\sum(a\Delta t)_f} = e^{0.12[1 - (t_f/t)^{1.8}]} \quad (1)$$

and the plot of Eq. 1, shown quantitatively in Figure 2.3.

2. The point A of maximum acceleration, from Figure 2.3.

$$\left(\frac{t}{t_f}\right)\Big|_A \cong 0.25 \quad (2)$$

3. The value of the ordinate on Figure 2.3 corresponding to point A,

$$\frac{\sum(a\Delta t)}{\sum(a\Delta t)_f}\Big|_A \cong 0.27 \quad (3)$$

From Chapter 3:

1. The invariant

$$\frac{\sum(IS)}{\sum(IS)_f} = e^{2.0[1 - (S_f/S)^{1/3}]} \quad (4)$$

and the plot of Eq. 4, shown quantitatively in Figure 3.3.

2. The point A of zero curvature on Figure 3.3.

$$\left(\frac{S}{S_f}\right)\Big|_A = 0.125 \quad (5)$$

3. The value of the ordinate on Figure 3.3 corresponding to this point A.

$$\left. \frac{\sum(IS)}{\sum(IS)_f} \right| = 0.135 . \quad (6)$$

From Chapter 4:

1. The intensity-canonical accelerogram-geology chart, shown in Figure 4.7.
2. The magnitude — $\Sigma(IS)_f - S_f$ — geology canonical isoseismal chart shown in Figure 4.5.
3. The magnitude-intensity-distance (MID) chart shown typically in Figure 4.6.
4. The intensity-ground energy correlation curve shown in Figure 4.8.

With these curves and charts it is possible to determine, relatively quickly, various data of interest to earthquake engineering professionals. Some typical examples follow.

APPROXIMATE DAMAGE (INTENSITY) ESTIMATES

The damage which a building sustains due to an earthquake depends upon (in addition to other things) magnitude of earthquake, geology of the region, the acceleration record and distance from epicentre. These factors will be included in the damage assessment analysis which will be described in this section. But it must be pointed out that there are other important factors that are extremely difficult (or impossible) to include in a prior determination of overall damage to a particular structure. These include the orientation of the structure. Many structures have strong axes and weak axes and damage depends upon how these are located with reference to the direction of the energy shock. Also the soil-foundation interaction, which depends upon the type of building foundation in addition to soil conditions, affects the overall damage to a building. Finally, the building design (type of construction) affects the damage.

In the later analysis chapter methods will be described that account for, approximately, these different conditions. In this chapter, however, the damage criteria will be based upon the intensity as measured by the Mercalli Scales and is approximate to this degree in addition to the other approximations involved.

We shall consider some of the different initial conditions which may be assumed by design engineers, code-makers, insurers, and other involved in damage assessment, and how these are then utilized with the invariant relations and charts to determine approximate intensity numbers and, therefore, probable damage.

A. Assume a given magnitude M for a single shock, geological region, and distance from the epicentre.

- Procedure: 1. From Figure 4.5, the $M - \Sigma(IS)_f - S_f$ correlation, determine $\Sigma(IS)_f$ and S_f .
2. Prepare the MID chart, Figure 4.6, for the given M and $\Sigma(IS)_f$ and S_f .
3. From this chart, with the given S , determine the approximate intensity and hence the damage.

B. Assume a_{\max} and t_f for a canonical accelerogram and the geology are specified, based upon previous experience and code requirements.

- Procedure: 1. From Eq. 2, determine $t_A = 0.25 t_f$.
2. Based upon an analysis of several canonical accelerograms, the following parabolic area relation is approximately true,

$$\Sigma(a\Delta t) \Big|_A = \frac{a_{\max} t_A}{2.8} \quad (7)$$

3. From Eq. 3 and Eq. 7 we obtain

$$\Sigma(a\Delta t)_f \cong \frac{a_{\max} t_f}{3} \quad (8)$$

which is Eq. 6 of Chapter 2.

4. Having t_f and $\Sigma(a\Delta t)_f$ (and a check on the geology) from Figure 4.8 determine the approximate intensity, and hence the damage.

C. Assume that a composite accelerogram, consisting of several superposed canonical accelerograms each one similar to (B) above is given. Also the geology.

- Procedure: If the accelerogram which is specified consists of a series (summation) of canonical accelerograms as in Figure 2.5 of Chapter 2, then it is recommended that each canonical part be considered separately insofar as the $\Sigma(a\Delta t)_f - t_f -$ Intensity Damage Chart is concerned. That is, use Figure 4.7 for each separate canonical part and determine the worst case approximate intensity and hence the damage.

This is justified by the physical fact that many of the canonical segments are entirely or very nearly independent of each other with, at most, a slight overlap at the head and tail (low acceleration) ends of each. Thus insofar as local effect (intensity)

is concerned, each part is essentially independent. If the superposed accelerogram consists of segments which overlap more completely, a modification of the procedure will be indicated.

Another form of design information that may be related to a particular earthquake and region is the following.

- D. Assume a structure is designed so that it is capable of absorbing a given amount of energy about major and minor axes. What are the possible parameter combinations such that damage will not occur.

Procedure: 1. From the MID charts (essentially a handbook of M , ϵ_f , $\Sigma(IS)_f$, \mathcal{R} and S_f values), it is possible to determine the total energy, $\epsilon_{tf} \times (Ae)$ that a structure must absorb. Ae is the 'effective area' about which more will be written in later chapters. It is thus possible to determine various combinations of M , $\Sigma(IS)_f$, S_f , geology, and S corresponding to required total energy correlated with the possible orientations of the building. If the orientation is unknown then prudence would require that the weak axis direction be required to absorb the entire energy supplied by the earthquake.

There are other combinations of the variables and the charts that can be used as the basis for a given engineering or damage or code analysis. This depends upon the needs of the person making the study. The four examples given above are typical and indicate the procedures that may be used.

Other more detailed applications to a number of specific problems of engineering interest are described in Chapters 10 and 11.

CONCLUSION

The invariants of the canonical accelerogram and canonical isoseismal charts and the different extended relations, curves, and figures that follow from these which were developed in previous chapters are used as the basic tools for determining — analytically — approximate damage to structures due to an earthquake.

The damage criterion is the Mercalli (MM) Scale intensity number and most of the more important variables involved in damage phenomena are accounted for. The procedures are approximate and depend upon a compilation of damage data from previous earthquakes, i.e. basically a calibration of the curves and charts. As more and more data is collected and recorded, the basic design tools will become more accurate. As pointed out in Table A.2 of the Appendix,

p. 311 the determination of this data (which has a specialized form differing markedly from more familiar experimental structural design data) is entirely consistent with procedures used in other fields of applied mechanics and has its special form because of the fundamental uniqueness of earthquake engineering within the overall field of applied mechanics.

Finally, other combinations of input and output data than those given as examples in this chapter are possible and may be obtained. These depend upon the needs of the engineers, insurers, code-makers, and others who may find these data of interest.

CHAPTER 9

SPECIAL TOPICS IN EARTHQUAKE STRUCTURAL ENGINEERING

INTRODUCTION

Before proceeding to the discussion of various applications to particular problems (Chapter 10) and a detailed outline of the various structural design procedures (Chapter 11), it is desirable to introduce four special topics that are related to the analysis and design and have important connections with these subjects. The four topics are:

1. Equivalent or effective length and equivalent or effective base area.
2. Length-of-time effect.
3. Damping.
4. Model-prototype relations.

The connections of the four with structural analysis of buildings will be emphasized and in common with all other sections of the book, arguments will be based primarily upon engineering and physical considerations.

Several new concepts will be introduced. These also will have engineering-physical bases and will be significant elements in the overall theory to be described in the remaining chapters.

NOMENCLATURE FOR THIS CHAPTER

Following is a list of the terms used in this chapter. They will also be defined when they are introduced.

- A_e = equivalent or effective area
 g = acceleration of gravity
 l = equivalent or effective length
 l' = actual length

- t = time
- w = width of building
- w_o = inertia loading on structure
- x = lateral deflection of structure
- y = distance along axis of structure
- A = average uni-material area of building
- E = modulus of elasticity
- F = subscript 'framing'
- G = modulus of rigidity (shear modulus)
- I = moment of inertia
- M = bending moment
- P = load acting on base of building
- S = subscript 'shell'
- U = strain energy
- V = velocity of shear wave
- ϵ_{t_f} = total horizontal ground energy per unit effective area
- σ = stress
- ρ = density
- ω = frequency

EQUIVALENT (OR EFFECTIVE) LENGTH AND EQUIVALENT (OR EFFECTIVE) BASE AREA

In Chapter 11, the structural analysis procedure for buildings will describe *three* different methods of solution for earthquake loadings depending upon the geometry (i.e. height to width ratio) of the building structure. It will be assumed that

1. for high or tall buildings (i.e. $l/w \gtrsim 5$), the entire building will be assumed to vibrate essentially as a beam in bending and the energy will be absorbed accordingly.
2. for intermediate beam and girder and column buildings (i.e., $1 \lesssim l/w \lesssim 5$) the building will be taken as constructed of beam and girder and column elements that deform separately as the building vibrates to and fro about a vertical equilibrium position. The energy will be absorbed in the deforming beams and girders and columns.
3. for short, squat buildings, (i.e., $l/w \lesssim 1$) the building will be assumed as a shear structure and will be assumed to vibrate to and fro entirely in shear deformation. The energy will be absorbed as shear energy. Intermediate buildings of type 2 above constructed entirely of masonry-type walls may also be shear designed.

For the high building, of type 1 above, an important part of the energy absorption of the structures is accounted for in the soil-foundation interaction effect. In addition to transferring energy from the vibrating building to the adjacent soil (which in effect means that the soil is a part of the building system insofar as energy absorption is concerned), the deformation of the high building introduces a translation-rotation effect at the soil-foundation junction. The approximate method of analysis described later accounts for this in addition to the beam-vibration motion. To do this, it is necessary that an 'equivalent length' of structure be used.

For illustrative purposes in this chapter we will consider a building 100 ft x 100 ft in cross-sectional area having an 'actual' length l' , as shown in Figure 9.1. Note that l' is the true physical length of the building from roof to bottom of footings:

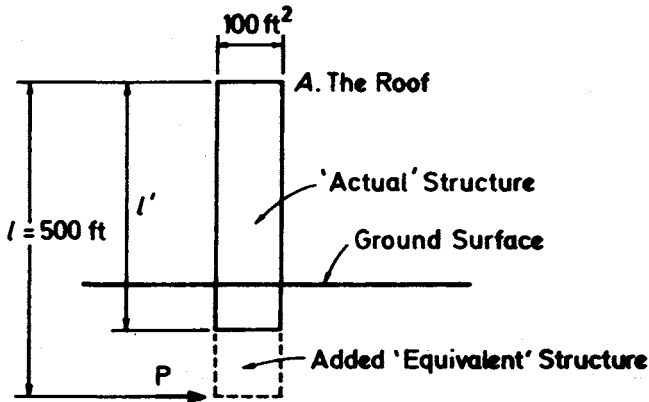


Figure 9.1

$l = 500$ ft is the 'equivalent' length (height) of the building, assumed known; l is the length actually used in the computations and is the length that accounts for the soil-foundation interaction as well as for the translation and rotation of the actual base of the building. This is an important (and frequently neglected) aspect of the structural response of a building¹.

In this text, by using l instead of l' , the translation and rotation of the actual base are introduced as normal elements of the design procedure. The determination of the distance l is based upon the judgement and experience of the designing engineer as well as upon an empirical relation for the period of the building as discussed in the next chapter. Note also, the earthquake loading (shown in Figure 9.1 as P) is applied at the base of the equivalent structure, l . The portion

of the structure, $l-l'$ accounts for the soil-foundation interaction corresponding to the actual structure beneath the ground surface. This also is clearly an item strongly dependent upon engineering judgement.

A second important consideration in the response analysis is the 'equivalent base area', A_e , which when multiplied by ϵ_{t_f} (see Figure 4.8) determines the amount of energy from the earthquake which the structure must absorb.

In *EE-DA&SD* it was suggested that the overall building base area be used for A_e . Since publication of the first edition, a number of applications (including some described in Chapter 11) strongly indicate that the actual *foundation area* be used for A_e . This, in fact, is probably a more realistic assumption than the earlier one and (until more data is available which suggest otherwise) it will be used.

This point must be emphasized — values of l and A_e , initially, will be based upon the experience and judgement of the designer as are the evaluations of various terms that occur in earthquake codes throughout the world. Perhaps the specifications will suggest a suitable range of values for these. As more data is stored and accumulated, it will be possible to determine more accurate and reasonable values for these two important design parameters. As of this time it is suggested that the recommendations of this book be used.

LENGTH-OF-TIME EFFECT FOR TALL BUILDINGS

Referring to Figure 9.1, note that l is the equivalent length, i.e. the length used in the analysis. The earthquake load is shown as P acting on the base of the l structure. Also shown are the dimensions considered for illustrative purposes.

We assume the velocity of sound (i.e. the velocity of, in this case, shear stress and displacement effects), is 10,000 fps in steel and 5000 fps in brick, mortar, and concrete. These could vary depending upon several factors, but in any case there will be, roughly, a factor of two between the steel and brick-concrete values. We assume further that the load due to the earthquake is initially, the force P .

The effect of P will travel up the building and will be felt at the roof, A , in about $1/20$ s, insofar as the steel frame is concerned.

1. We assume for the high structure that the structure of equivalent length, l , vibrates as a free-free beam (see Chapter 11). We shall assume, therefore, that the entire building of length l , vibrates as a free-free beam for time periods, t_3 , given by, roughly

$$\frac{l}{20} \text{ s} < t_3$$

This time period, therefore, is called the period of overall effect.

2. If the building cross-section is assumed to be 100 ft \times 100 ft then the force, P , applied as shown, will require approximately 1/100 s to traverse the building width, i.e. to be felt at the far side of the building. That is, for approximately

$$0 < t_1 < \frac{1}{100} \text{ s}$$

the stress and deformation characteristics of the earthquake loading are predominantly localized (in floor slabs, beams, girders, wall panels in the neighbourhood of the load application point) and can only be accounted for by considering the separate effects on these structural elements and, very likely, the three dimensional equations of dynamic elasticity. The problem in this last case is an extremely complicated one and can be solved, if at all, only for very simplified, idealized structures.

The approximate time period

$$0 < t_1 < \frac{1}{100} \text{ s}$$

is, for the reasons stated, called the period of localized effect.

3. The intermediate time period, approximately

$$\frac{1}{100} \text{ s} < t_2 < \frac{1}{20} \text{ s}$$

is called the period of transition in this book. During this time interval, the entire building is still not aware of the earthquake. Furthermore, for those buildings with a steel skeleton framing and a brick outside wall, it is possible that severe damage and wall cracking can occur during this time period because of the difference in the velocity of sound in the two materials as explained in the following:

Suppose $t = 1/50$ s. During this time, the wave will have travelled roughly, 200 ft up the steel framing portion of the building, see Figure 9.2, with the corresponding shear deformation. On the other hand, the wave through the brick will only have travelled about 100 ft, so that in the upper 100 ft there is deformation of the steel without any deformation of the brick. This could lead to serious cracking and damage problems unless the two materials can deform independently of each other.

In effect, the portion of the building shown shaded in Figure 9.2 is aware of the earthquake (i.e. is deforming, is being stressed). The portion AB of the building is unaware of any earthquake loading to point O.

For tall buildings the three time periods described above appear to be the significant ones in earthquake response analyses. They will be utilized in this book's consideration of the effect of earthquakes on high structures in Chapter 11.

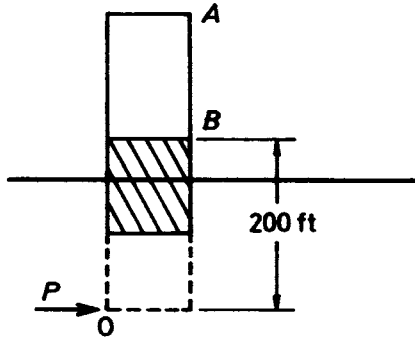


Figure 9.2

DAMPING OF VIBRATIONAL BUILDING OSCILLATIONS DUE TO AN EARTHQUAKE

When a building or other structure is subjected to a sudden impulse-type earthquake loading, it is set in vibratory motion. A convenient way of examining the response of the structure is to introduce energy considerations, that is, to assume that the vibrations are due to an energy input of known calculated value, which in turn induces kinetic and potential (strain) energy in this structure. This is the method utilized in this text (see Chapter 11) and the same considerations may be utilized in investigating the damping behaviour of the structure.

In this book therefore, we conceive of an earthquake as a mechanism for introducing energy into the system (the structure, including soil-substructure interaction). If damping were absent, the resulting vibrations would exist for all time. Because of damping, energy is withdrawn from the system, which in turn reduces the amplitude of vibration until the final stationary state is reached.

As a first step it is necessary that the damping mechanism be described as completely as possible. There seem to be three possible major modes of damping involved in the dissipation of energy from a vibrating structure, as follows:

1. Energy lost, due to internal friction, in the vibrating building shell, frame, partitions, floors etc. subjected to alternating stress cycles.
2. Energy lost, due to friction and slip, in the lap and butt riveted-bolted joints of the vibrating structure as well as other frictions between contiguous parts.
3. Energy lost as internal friction in (and in doing work against) subsurface soil by the foundation and subsurface portion of the structure.

Item (1)² and (2)³ have been studied in the past in simplified forms. Item (3), however, has been only briefly investigated. In this book an approximation for energy lost in soil-structure interaction is introduced by assuming an 'equivalent length', l , of structure greater than the actual length (height) as shown in Figures 9.1 and 9.2. The equivalent length procedure as pointed out before enables us to accomplish in an approximate way the following two tasks which are of some importance in earthquake structural analyses:

- a. By assuming an equivalent length structure we introduce translation and rotation of the actual foundation. These motions may be important or even critical in certain cases and should not be overlooked.
- b. By considering an equivalent length we introduce an added energy loss in the vibration cycle. This loss (damping) is assumed to represent the effect of the soil-substructure effect on damping.

The difficulty with item (3) analyses is the determination of l , the 'equivalent' length. This obviously must depend — among other things — on the type of soil, the type and size of foundation, and the intensity of the shock. One suggested approach will be to analyse structures utilizing variable equivalent lengths, preparing tables and charts, and attempting to correlate these with actual behaviour. If such a correlation can be obtained and this is sufficiently accurate for engineering design purposes, then a relatively simple technique will be available for including soil-substructure interaction effects in the design of structures subjected to earthquake loads.

Until this information is available, the author suggests that the equivalent length be determined by using the empirical period of vibration relation as outlined in Chapter 11, modified, if deemed necessary, by engineering judgement and experience. See also Eqs. 13, 14 and 15 of the next section, dealing with model scaling requirements.

MODEL SCALING REQUIREMENTS

Introduction

The earthquake phenomenon is an extremely complicated one involving, as it does, dynamic as well as elastic (possibly plastic) effects. In connection with the model testing of structures subjected to earthquake loadings, the questions to be answered initially are what the scaling requirements of model to prototype must be in order that the results be meaningful.

To answer these questions, it is necessary that the complex behaviour of the structure be categorized or separated into phenomena that can be analysed. This section reports on a study along these lines.

It must be stated at the outset, that in this analysis we are concerned with the overall scaling requirements for the *tall* structure. We do not consider details such as connections or isolated members. Many studies have been reported along these lines and the scaling requirements for such cases have been established. Our concern is with a set of requirements that are less well known, generally ignored and therefore lead to questions concerning the validity of the results of model tests.

We begin by discussing the basic technique to be utilized in the analysis. Following this, the separate effects which are to be considered are introduced and, in general, given in their dimensional form. This, in turn, leads directly to the required scaling parameters. We include a brief discussion of the scaling factors involved in vibrational damping. Finally, the question — ‘Is it possible to simultaneously satisfy all the scaling parameters?’ is discussed briefly.

Procedure

One method which is very fruitful in model and scaling analyses utilizes the concept of ‘ratio of effects’. That is, we may say that a model will behave the same as a prototype if the ‘ratio of two effects’ is the same. For example, in classical fluid dynamics, this approach leads to the following:

1. If, for a prototype, inertia and viscous effects (forces) are the important elements in the phenomenon, then, for model results to be meaningful, we require that the ratio of inertia effects to viscous effects be equal for both model and prototype. That is, we require that the Reynolds number be the same.
2. Or, if for model and prototype, we require that the ratio of compressibility effects to inertia effects be equal, then we require that the Mach number be the same.

3. Or, if for model and prototype, we require that the ratio of surface-wave effects to inertial effects be equal, then we require that the Froude numbers be the same.

And so on for other 'ratio of effect' combinations.

We shall use this concept in our analysis of the earthquake model-prototype relationship. The significant 'effects' in our problem shall be assumed to be the following geometric, elastic, and dynamic terms. In all cases we are dealing with a tall building.

1. The shear-bending wave transmission characteristics of the building — both steel framing and brick or concrete or other outer covering.
2. The lateral wave (vibratory wave) characteristics of the building.
3. The 'effective length-actual length' effect.
4. The time-loading history of the earthquake load.
5. The strain energy absorbed by the structure.
6. The total energy supplied to the structure by the earthquake.
7. The maximum stress induced in the structure.
8. The maximum allowable stress (modulus of rupture or yield stress) of the structure.

Our criterion is the following: in order that the model be scaled properly with respect to the prototype insofar as overall, major earthquake effects are concerned, it will be necessary that the 'ratio of effects' of various pairs of the foregoing quantities be the same for model and prototype.

We take the point of view that we wish to scale our model in such a way that its complex behaviour under an earthquake loading will be similar to that of the prototype. In this way, by means of model studies, we will be able to predict how a structure will behave in an earthquake and also be able to test the validity and applicability of any theory for the effects of earthquakes on structures.

The first four of the above effects are important, because they mean that the various phase relations of the lateral deflection wave, bending wave, earthquake loading time-history, and so on, for the model should be as nearly the same as possible as those of the prototype. To illustrate, in a purely physical and phenomenological way, the significance of the various relations, let us examine the behaviour of a typical building structure subject to a short-pulse earthquake loading, Figure 9.3.

First, based upon soil-substructure interaction and other pertinent data, an effective length, l , is assumed for the building. In a very short time after the earthquake load $P(t)$ is applied, a shear deflection occurs as indicated by the

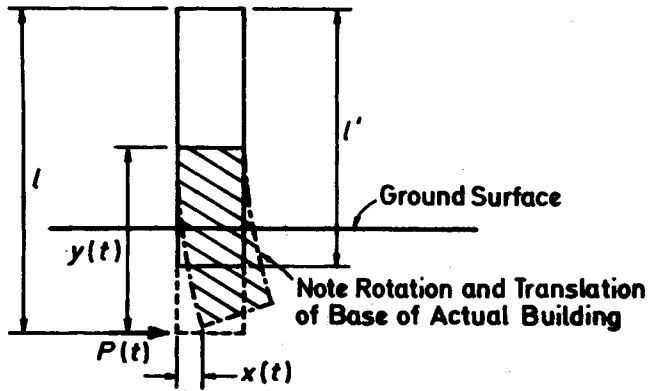


Figure 9.3

distance $x(t)$. If the model is to behave in a manner similar to the prototype, then it is necessary that (for the overall behaviour):

1. The ratio l'/l must be the same for model and prototype.
2. The ratios of the different distances $y(t)$ for steel framing and for brick shell (say) must be the same for model and prototype.
3. The ratio of the shear deformation, $x(t)$, to distance of shear wave travel, $y(t)$, must be the same for both model and prototype for a given ratio $y(t)/l$.
4. The ratio of the critical frequency of the applied load to the frequency of lateral vibration must be the same for model and prototype. 'Critical' frequency will be discussed in the following paragraphs.

In addition to the above ratios, the following also must hold for model and prototype:

5. The ratio of maximum strain energy in the structure to total energy applied to the structure by the earthquake must be the same in the model and in the prototype.
6. The ratio of the maximum stress in the structure to the modulus of rupture (or yield stress) must be the same for model and prototype.
7. The damping ratio must be the same for model and prototype.

The above seven geometric, elastic, and dynamic scaling requirements should be satisfied if the model test results are to represent a true picture of the prototype structure. They show clearly that one common method of testing, i.e. using a 'shaking machine' on the roof or some other floor of a model (or, indeed, prototype) cannot possibly give results corresponding to what actually occurs

during an earthquake, since the earthquake load — of necessity — is applied by the ground and the base of the building almost certainly rotates and translates during the time of loading. Unless these last noted motions are introduced — in both test or analytical solution — an important (possibly critical) element of the phenomenon has been omitted.

We now discuss the seven scaling requirements in more detail. The number headings conform to those used above.

1. This requires that

$$\left(\frac{l'}{l}\right)_{\text{model}} = \left(\frac{l'}{l}\right)_{\text{prototype}} \tag{1}$$

2. The velocity of a shear wave is given by

$$V = k \left(\frac{Gg}{\rho}\right)^{1/2} \tag{2}$$

in which G = shear modulus of elasticity, g = acceleration of gravity, and ρ = density of material.

The scaling requirements are therefore

$$\left| \frac{\left(\frac{Gg}{\rho}\right)^{1/2}_{\text{shell}}}{\left(\frac{Gg}{\rho}\right)^{1/2}_{\text{framing}}} \right|_{\text{model}} = \left| \frac{\left(\frac{GG}{\rho}\right)^{1/2}_{\text{shell}}}{\left(\frac{Gg}{\rho}\right)^{1/2}_{\text{framing}}} \right|_{\text{prototype}} \tag{3}$$

or

$$\left(\frac{G_s \rho_f}{G_f \rho_s}\right)_{\text{model}} = \left(\frac{G_s \rho_f}{G_f \rho_s}\right)_{\text{prototype}} \tag{4}$$

3. It is assumed in this analysis that the deformation during the period of transition is a pure shear translation only. That is, bending effects have not been introduced until the lateral vibration of the structure begins. (This point will be discussed in more detail in Chapter 11). Thus, in Figure 9.3, the distance $x(t)$ is given by

$$K \frac{Py}{AG} \quad (5)$$

in which

K = a numerical factor to account for suddenness of load, form factor, etc.

P = constant pulse load.

y = distance of shear wave travel.

A, G = average uni-material area and modulus of rigidity.

Then, for a given $y(t)/l$, the scaling requirement is that

$$\left(\frac{Py}{AG/y} \right) = \left(\frac{P}{AG} \right)_{\text{model}} = \left(\frac{P}{AG} \right)_{\text{prototype}} \quad (6)$$

Subject to

$$\left(\frac{y}{l} \right)_{\text{model}} = \left(\frac{y}{l} \right)_{\text{prototype}} \quad (7a)$$

or

$$\left\{ \frac{Gt^2}{\rho l^2} \right\}_{\text{model}} = \left\{ \frac{Gt^2}{\rho l^2} \right\}_{\text{prototype}} \quad (7b)$$

4. The frequency equation for the free-free beam modes of vibration (which is the assumed condition for the equivalent building in this formulation, see Chapter 11) is given by⁴

$$\omega = K \left[\frac{EIg}{\rho A l^4} \right]^{1/2} \text{ rad s}^{-1} \quad (8)$$

in which

ω = frequency in rad s^{-1}

E = tension-compression modulus of elasticity of uni-material building

I = moment of inertia of equivalent uni-material building cross-section

g = acceleration of gravity

ρ = density of equivalent uni-material building

- A = cross-section area of equivalent uni-material building
- ℓ = equivalent length of building

In Chapter 2, the study of earthquake accelerograms showed that, for many earthquakes, the accelerogram can be represented in an invariant canonical form when analysed between envelopes and for suitable choice of invariant-form variables. Furthermore, for those accelerograms not directly representable by the canonical invariant, a superposition of these may be utilized to represent the more complicated accelerograms.

It will be assumed in this book that a possible loading on the building due to the earthquake consists of a series of short pulses, acting in alternate directions, bounded by the shape of the envelopes of the accelerograms and having a most critical frequency insofar as the response of the structure is concerned. The pulses, the envelopes, and a typical simplified accelerogram is shown in Figure 9.4.

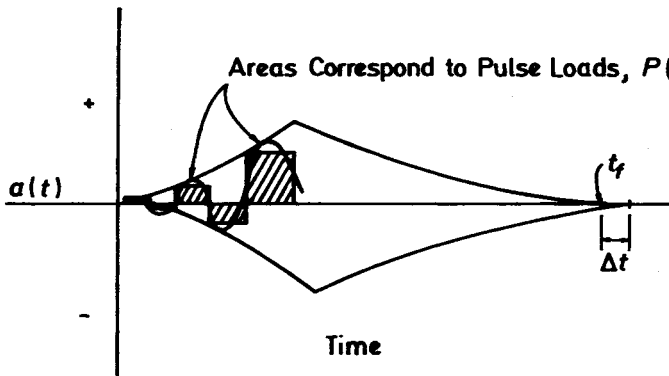


Figure 9.4

Note the pulse loads have a particular frequency (which may or may not be assumed constant). There is one frequency spectrum which is probably critical for a given building, in that it will cause the most damage to the building. Let us call this frequency ω_{crit} . Therefore the scaling requirement for load application requires that the ratio of critical load frequency to transverse vibration frequency be the same for model and prototype, i.e.:

$$\left(\frac{EI_g}{\rho A \ell^4 \omega_{crit}^2} \right)_{model} = \left(\frac{EI_g}{\rho A \ell^4 \omega_{crit}^2} \right)_{prototype} \quad (9)$$

5. The maximum bending strain energy in the vibrating structure, see Chapter 11, will be given by an expression of the form

$$\int \frac{M^2 dx}{2EI} \tag{10}$$

in which M = bending moment at any point on the vibrating structure due to the potential (inertia) load, E , I are as defined in Eq. 8, and the integration is taken over the entire free-free vibrating structure.

The total energy, due to the earthquake, that must be absorbed by the structure is given by $\epsilon_{t_f} Ae$, in which

ϵ_{t_f} = total horizontal ground energy per unit effective area supplied by the earthquake.

Ae = effective base area of the structure.

The model-prototype requirement is, therefore,

$$\left[\frac{\int \frac{M^2 dx}{EI}}{\epsilon_{t_f} Ae} \right]_{\text{model}} = \left[\frac{\int \frac{M^2 dx}{EI}}{\epsilon_{t_f} Ae} \right]_{\text{prototype}} \tag{11}$$

As noted above, this relation assumes bending energy alone (which is a reasonable assumption for a tall building) is the significant quantity. Depending, for example, upon the geometry of the structure (as pointed out earlier in this chapter) it is possible that shear energy alone or a combination of shear and bending energy are important and the relation Eq. 11 would therefore be modified accordingly.

A complication that arises in connection with this requirement has to do with the major-minor axes directions of the structure versus the direction of the ground motion (which, in this text, is assumed to be in a radial direction from the epicentre to the structure).

The most reasonable procedure might be to consider the direction of maximum effect and to look for an approximate equality for Eq. 11.

6. The stress requirement becomes

$$\left[\frac{w_0 l^2 d}{I} \right]_{\text{model}} = \left[\frac{w_0 l^2 d}{I} \right]_{\text{prototype}} \quad (12)$$

in which w_0 = maximum vibratory inertia loading on the structure, d = depth of the structure, and α_r or α_y = the modulus of rupture or yield stress of the structure.

7. Next, we consider the question, 'What are the scaling requirements in order that damping of the model be equivalent to damping of the prototype?' We shall consider lateral vibrational damping only since this is very likely the major source of damping and — in addition — damping due to soil-substructure interaction is accounted for approximately, in this theory, as added vibrational damping due to the additional length in the equivalent length formulation.

In discussing vibrational damping,² it is shown that the energy damped per cycle is given by

$$\Delta U = 2\pi\delta U \quad (13)$$

in which ΔU = energy lost per cycle, U = maximum strain energy in the vibrating structure, i.e. when the structure is at its maximum deflection, and δ = damping factor.

Furthermore, it is shown² that although δ is dependent upon a number of factors, its main dependence, for our purposes, for any given material is upon ω , the frequency of vibration. Also — and this may be important for model-scaling purposes — it is shown that ω is frequently a double-valued function, i.e. any given value of δ will occur at two different values of ω .

There are a number of approximate relations giving the period of vibration for actual building structures.⁵ Hence, if we define equivalent damping to mean

$$\left(\frac{\Delta U}{U} \right)_{\text{model}} = \left(\frac{\Delta U}{U} \right)_{\text{prototype}} \quad (14)$$

then we require (if model and prototype are constructed of the same material that

$$\omega_{\text{model}} = \omega_{\text{prototype}} \quad (15)$$

in which we have the leeway presented by the double-valued nature of the damping-function.

The final question — ‘Is it possible to satisfy all of the above requirements simultaneously?’ The answer to this question is dependent upon such a large mix of geometric, vibratory and elastic properties, and physical parameters, that it is unlikely all can be satisfied. Some contradictions almost certainly will arise. The best one can do is to assume some of the requirements are more important than others and attempt to satisfy these.

CONCLUSION

Four special topics dealing with earthquake engineering analyses and experimental work are considered in this chapter.

1. The concepts of equivalent length and equivalent base area are of major importance in the structural procedure developed in later chapters.
2. The length-of-time effect may help to explain one of the primary causes of some building damage — a differential deformation of adjoining parts of the structure.
3. The damping of a structure is a basic element in its vibratory behaviour, and one of the more difficult factors to quantify. Some approximate procedures are suggested to account for the responses of structures to earthquakes.
4. Experimental model work in earthquake engineering is an important area of activity. The difficulty with the use of models is that one must be certain that the model response is, in fact, a reasonable indication of the full-size structure response. One means for assuring this is by utilizing the ‘ratio of effect’ concept and this is carried through to determine various geometric, elastic, vibratory, and stress requirements.

REFERENCES

1. Nathan M. Newmark and Emilio Rosenblueth. *Fundamentals of Earthquake Engineering*, Prentice-Hall, Inc., Englewood Cliffs, N. J., 1971, p. 94.
2. C. Zener. *Elasticity and Anelasticity of Metals*, University of Chicago Press, Chicago, Ill., 1948.
3. E. L. Gayhart, ‘An investigation of the Behavior and of the Ultimate Strength of Riveted Joints Under Load’, *Trans. SNAME*, 34, 1926.
4. N. W. McLachlan. *Theory of Vibrations*, Dover Publications, Inc., New York, N.Y. 1951.
5. Robert L. Wiegel. *Earthquake Engineering*, Prentice-Hall, Inc., Englewood Cliffs, N.J. 1970, p. 88.

CHAPTER 10

SOME NON-STRUCTURAL APPLICATIONS OF THE RATIONAL THEORY

INTRODUCTION

In the previous chapters a complete comprehensive rational theory of earthquake engineering was developed. Various equations, invariants, parameters, design charts and curves were obtained and these may be applied to a number of different problems connected with the engineering aspects of the earthquake event, including the mechanism, damage assessment and structural design.

In this and the next chapter several different example-applications will be presented. In all cases, since *engineering* applications are our main concern, *numbers* will be obtained — values of stresses, deflections, intensities and other numerical results which are of interest and concern to engineers. Also, all of the analyses will utilize *rational* approaches. By 'rational' we mean that the previously derived theories are the bases for all of the procedures which will be employed. We will not use any of the empirical approaches which are the principal means employed by engineer-designers in current earthquake engineering practice.

A separation of sorts will be made, in the following respects: This chapter will be concerned only with non-structural (not building oriented) applications, whereas in the next chapter several different applications of the structural effects of earthquake will be presented.

An additional comment — the examples which follow in this and the next chapter are *not* the only possible applications. They are merely representative of the scope of rational analyses which may be made using the theory.

The problems (or applications) to be considered in this chapter are:

- A) An approximate theoretical predicted isoseismal map for the predicted Parkfield earthquake of 1988.
- B) The earthquake — code zones of Bangladesh — a comparison analysis.
- C) An approximate theoretical method for analyzing rock slope stability due to earthquake.

- D) The Mexican earthquake of September 19, 1985.
- E) The monitoring of underground atomic blasts.

A) AN APPROXIMATE THEORETICAL PREDICTED ISOSEISMAL MAP FOR THE PREDICTED $M = 6$ PARKFIELD EARTHQUAKE OF 1988

In early April of 1985 the U. S. Geological Survey announced that the National Earthquake Prediction Evaluation Council (NEPEC) and the California Earthquake Prediction Council have endorsed studies that indicate a moderate earthquake is likely to strike near Parkfield, in central California within several years of 1988 — and, in fact, is most likely in 1988. Each of the recent earthquakes (which have struck Parkfield about every 22 years with the most recent in 1966) was of magnitude 5.5 to 6 and each ruptured the same 20 kilometres of the San Andreas fault, thus leading to a magnitude and location prediction as well as the time.

We shall use the parameters for the given Parkfield earthquake and the methods outlined in previous chapters to develop a predicted isoseismal field for the event.

Procedure

The elements of the theory which are utilizing directly in the determination of the rational (theoretical) isoseismal chart are the following:

1. The canonical isoseismal index or invariant, Chapter 3.
2. The $S_f - \Sigma(IS)_f$ -Magnitude chart Chapter 4.
3. The magnitude-intensity-distance (MID) relation, Chapter 4.
4. The intensity-energy compatibility relations, Chapter 4, and finally,
5. The isoseismal superposition procedures, Chapter 7.

The analysis consists of the following steps:

- a. A surface rupture earthquake of magnitude 6 distributed along a 20 km rupture length (References 1, 2) is the input data.
- b. The total energy of this *distributed* earthquake will be determined using a Richter-type equation,
- c. The distributed (20 km) length of earthquake will be replaced by an energy-equivalent series of separate concentrated earthquakes. Ten such earthquakes, each 2 km apart, will be used.

We shall assume that the approximate energy magnitude relation is

$$\log_{10} E = 15.0 + 1.0 M$$

in which E is in ergs. This expression is approximately the same as the commonly used form, $11.4 + 1.5 M$ and simplifies the computation.

Thus, for $M = 6$ we have $E = 10^{21}$ ergs. and this is the total energy distributed along the 20 km line.

It will be more convenient to utilize a superposition of 'concentrated' earthquakes, of the same total energy as that of the distributed earthquake.

Toward this end, we shall assume 10 concentrated earthquakes, of approximate magnitude $M = 5$, with foci 2 km apart on the 20 km line. The total energy of these 10 earthquakes is the same as that of the $M = 6$ earthquake.

Then from Figure 4.5 we have, approximately, for each of the 10 canonical isoseismal maps,

$$S_f = 22 \text{ km}$$

$$\Sigma(IS)_f = 205$$

Using these values and the procedure outlined in Chapter 4, we can determine S_f , these being the distances to the centres of the (assumed) circular bands of constant intensity for the given $M = 5$, earthquake. These values are shown in Table 1. Other data which are used in this study and shown in Table 1 are the values of ϵ_{t_f} at S_f , the energy per unit area that is to be absorbed by a structure, which it is suggested is a true measure of earthquake 'intensity'.

Note, these values of ϵ_{t_f} are generally in the lower portion of the band curve of Figure 4.8

Table 1 $M = 5$, Approx., $S_f = 22\text{km}$, $\Sigma(IS)_f = 205$,
 $\log_{10} E = 15 + 1.0(5) = 20$

| Intensity | $S_f(\text{km})$ | $\epsilon_{t_f}(\text{ergs}/\text{km}^2)$ at S_f |
|-----------|------------------|--|
| III | 22 | 2.4×10^{14} |
| IV | 12.9 | 8.1×10^{14} |
| V | 7.6 | 2.7×10^{15} |
| VI | 4.4 | 9.1×10^{15} |
| VII | 2.40 | 3.4×10^{16} |
| VIII | 1.07 | 1.8×10^{17} |

Having S_j , it is possible to prepare an approximate MID diagram, which is essentially the theoretical rational canonical isoseismal map for the $M = 5$ earthquake.

We do this by using our S_j values to determine S_{OR} distance, as shown in Table 2 (S_{OR_j} is the distance to the outer range of the circular band of constant intensity j).

Table 2

| Intensity | S_{OR} , km | ϵ_{t_f} (ergs/km ²) at S_j |
|-----------|---------------|---|
| VIII | 1.8 | 1.8×10^{17} |
| VII | 3.5 | 0.3×10^{17} |
| VI | 6.1 | 0.09×10^{17} |
| V | 10.4 | 0.03×10^{17} |
| IV | 17.6 | 0.008×10^{17} |
| III | 26.6 | 0.002×10^{17} |

Noting that the ϵ_{t_f} values shown are approximate and represent the values at the centre of the constant intensity band (so that ϵ_{t_f} is higher when it is closer to the focus for any band), it is clear, for example, that a superposition of energy for, say, an Intensity = VIII band and an Intensity = VI band is, for all practical energy purposes, still an $I = VIII$ band. Similar reasoning applies to other superposed bands.

Thus, in the present case, we superpose ten $M = 5$ earthquakes, spaced 2 km apart, using the values shown in Table 2.

The result of the superposition is shown in Figure 10.1.

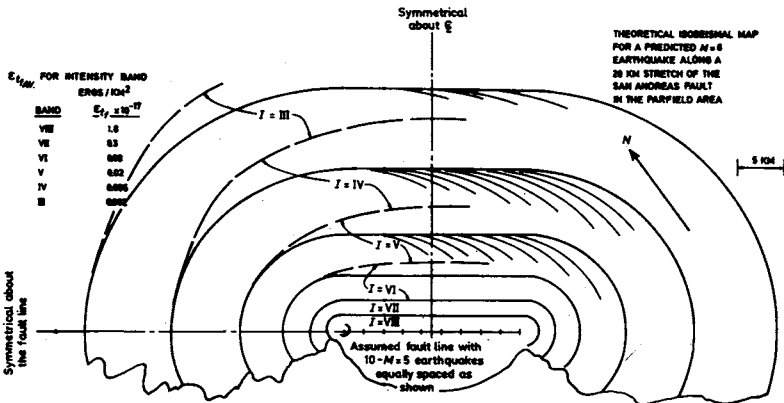


Figure 10.1

Note, for the lower intensities III, IV and V, the overlay of several of the earthquakes results in an energy value corresponding roughly to the next higher intensity. This is because of the distributed earthquake assumption and the (relatively) large number of equivalent smaller concentrated earthquakes. To account for this in an approximate manner an adjustment has been introduced as shown by the broken lines. For the most part, the author suggests this adjustment will be suitable for the usual qualitative purposes, particularly when one considers the subjective judgements involved in the determination of the *MM* numbers of the isoseismal chart. For actual engineering design purposes, by using the known locations and magnitudes of the concentrated earthquakes and the theoretical intensity bands for each, the engineer can determine actual values for the theoretical ground energy at any point in the field, including the directional effects introduced by different focal locations. It is this ground energy which is the significant parameter in the structural analyses.

Conclusion for This Section A

Because of the apparent temporal as well as physical regularity involved in earthquake events occurring at Parkfield on California's San Andreas fault, two governmental agencies have predicted (1985) the strong possibility of the occurrence in 1988 of an $M = 6$ earthquake along a 20 km stretch of the fault near Parkfield.

In this section the previously developed approximate rational quantitative theory is applied to the predicted Parkfield quake. In particular, the isoseismal contour map (the damage chart) is predicted using the superposition technique which utilizes those parameters which should be involved in a rational earthquake theory.

Because of the stated repeat property of the Parkfield earthquakes it should be possible to check the predicted isoseismal chart by referring to previous earthquake behavior in the several 22 year cycles.

Finally, it may be noted that the technique and procedure applied herein may be used to determine the isoseismal field even when these are highly asymmetric as shown in Chapter 7. It is only necessary (as must be expected in a rational procedure) that the earthquakes parameters that are involved in a particular event be known or capable of estimation.

B) THE EARTHQUAKE-CODE ZONE OF BANGLADESH

— A COMPARISON ANALYSIS

Introduction

Bangladesh, an Asian country having an area of approximately 55,000 square miles is located roughly at 25°N and 90°E.

It is surrounded by West Bangal (India) on the west, Nepal and Tibet on the northwest, Assam and Meghalaya on the north, Tripura on the east, Burma on the southeast and the Bay of Bengal and Indian Ocean on the south.

Although Bangladesh is not considered as being in an active earthquake zone, several recorded earthquakes in the region during the past hundred years have caused widespread damage. Typical of these was the 'Great Earthquake' of 1897 which had its epicentral track in the Shillong Plateau, situated north of Bangladesh. Other major earthquakes, such as the 'Bengal Earthquake' of 1885 and the 'Srimangal Earthquake' of 1918 caused severe damage only in local areas surrounding the epicentres.

The known geological data do not indicate the existence of seismically active faults within the country. However, in India and Burma, north and east of Bangladesh, there are regions of severe seismic activity and earthquakes originating in these areas have affected adjacent regions in Bangladesh.

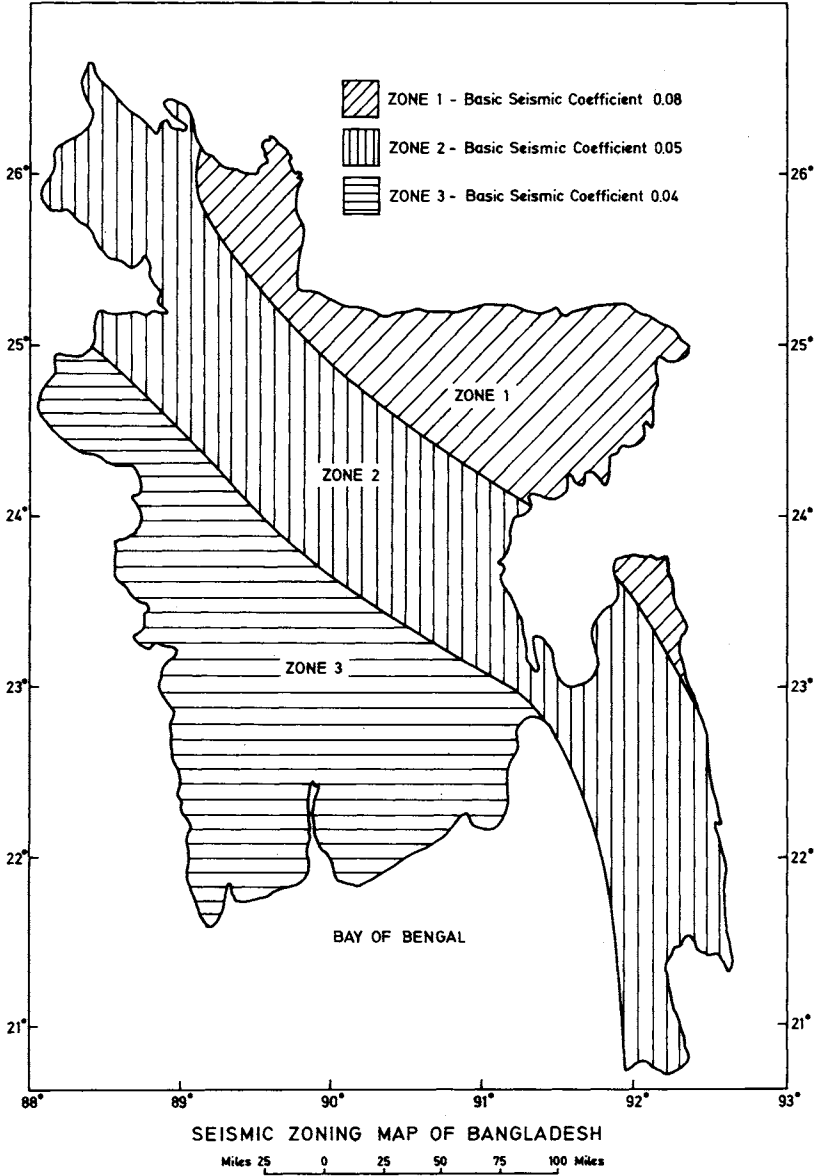
Because of this there is an earthquake engineering-seismic activity code for Bangladesh which divides the country into broad bands of roughly uniform seismic risk correlated with 'damage'. These are as indicated on Map 1, Map 2 and Map 3. For design purposes, the code assigns to these zones equivalent 'seismic factors' which are, in turn, included in empirical formulas given in the general code.

In this section, we apply the theory and results of the previous chapters to determine, analytically, damage zones for the entire country. These will then be compared to those shown on the maps. In order to perform the analysis we shall utilize the published data (admittedly vague and approximate) of a number of major earthquakes which have caused damage in Bangladesh during the past one hundred years. This published 'experimental' data will be considered in the context of the theory and a quantitative analysis will be made from which the comparison of existing zones and computed zones will follow.

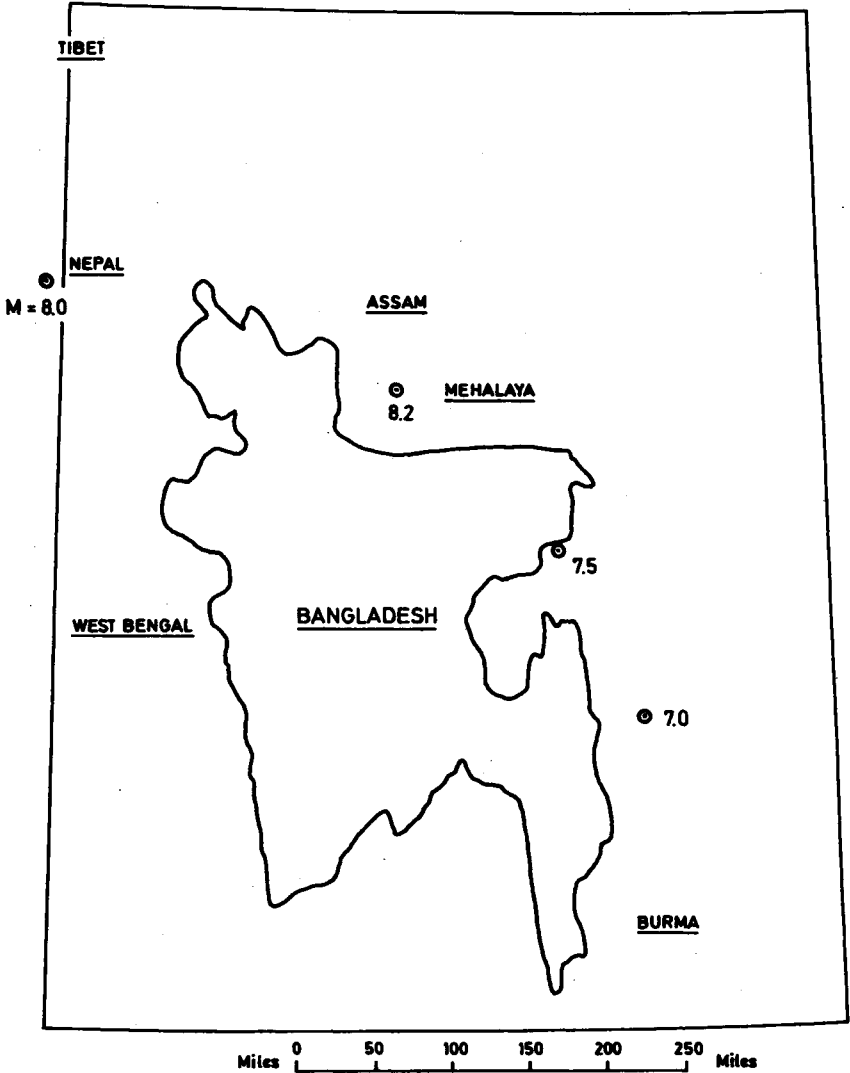
It will be found that good agreement is obtained.

Furthermore — and this is a more significant aspect of this study — the theory introduces quantitative structural design parameters which can be utilized in a straight-forward engineering design — analysis of structures. Because of the code-analysis correlation, these design parameter values can therefore be directly related to the zones of the Bangladesh code, thereby affording a rational engineering procedure (suitable for use by ordinary engineering design offices) for damage assessment and structural design.

* The author acknowledges the assistance of S. M. Shakiel and M. D. Kamal Shahid, graduate students of Civil Engineering at Stevens Institute of Technology, in gathering data for this section.

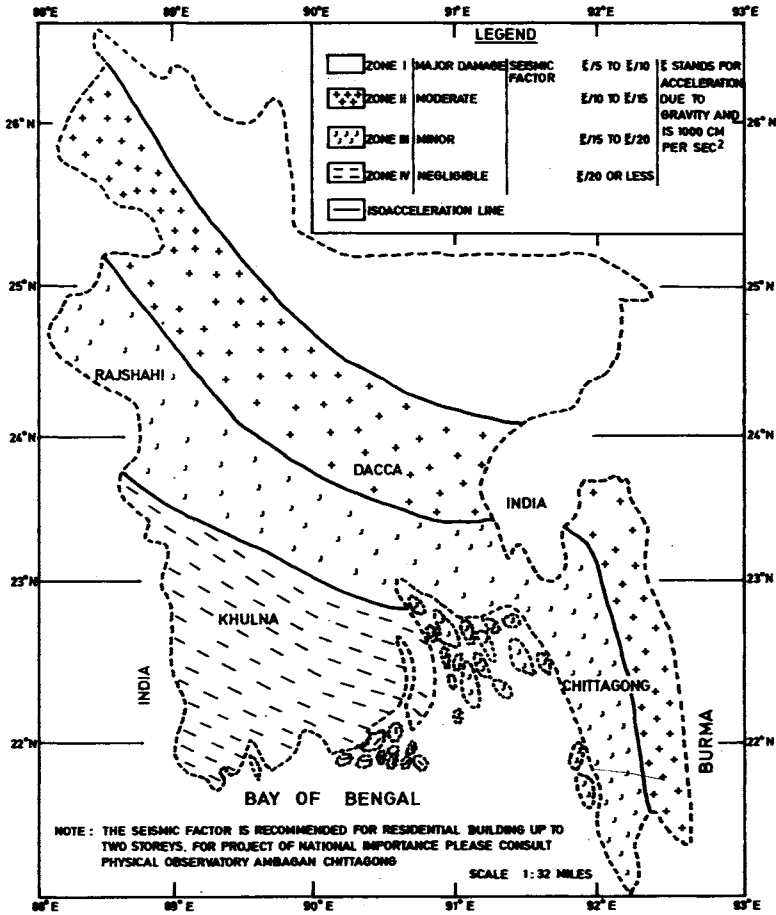


Map 1



Map 2 The Locations and Magnitudes of the Four Earthquakes Used in the Rational Analysis

SEISMIC ZONES OF BANGLADESH



Map 3

The Available Earthquake Data

The existing information on earthquakes that have affected Bangladesh is mostly contained in the records and memories of members of the Geological Survey of India. These include comprehensive qualitative descriptions of most major earthquakes that occurred on the sub-continent from the middle of the last century. Also included, when available, are instrumental data and earthquake analyses and observations collected from outside institutions such as the U. S. Geological Survey, U. S. Coast and Geodetic Survey, U. K. Institute of Geological Sciences, the India Meteorological Department and others. As might be expected most of these data are of geological (rather than engineering) import.

The major earthquakes that have affected Bangladesh since the middle of the last century are:

The Cachar Earthquake, January 10, 1869.

The Bengal Earthquake, July 14, 1885.

The Assam Earthquake, June 12, 1897.

The 'Great' Earthquake, July 12, 1897.

The Srimangal Earthquake, July 8, 1918.

The Dhubri Earthquake, July 3, 1930.

The Bihar-Nepal Earthquake, January 15, 1934.

The earthquake and available data which will be used in this study are (see Map 2) listed in Table 3.

Table 3

| Earthquake* | Date | Epicentre | | Reported Magnitude (Richter) |
|----------------|---------------|----------------|----------------|---------------------------------|
| | | N ^o | E ^o | |
| 1) Cachar | Jan. 10, 1869 | 24.3 | 92.2 | 7.5 |
| 2) Assam | June 12, 1897 | 25.7 | 90.4 | 8.2 |
| 3) Bihar-Nepal | Jan. 15, 1934 | 26.6 | 86.8 | 8 |
| 4) Dhubri | July 3, 1930 | 22.7 | 93.0 | 7.0 |

* No data concerning depths of foci available.

The locations of these earthquakes span the critical large earthquake region for Bangladesh in a manner which reasonably indicates probable earthquake damage over the entire country.

Thus, in a very general way, the four major earthquakes listed in Table 3 are of sufficient strength and destructive effect to serve as suitable code models for the entire country.

Otherwise stated — an engineering design of sufficient strength to withstand the destructive effects of these earthquakes would, by ordinary technical standards, very likely be considered as a responsible, professional engineering design.

The Zonal Regions of Bangladesh

Bangladesh has been (code) divided into three (or four) seismic zones (see Maps 1 and 3). The northwestern part which includes the towns of Sylhet, Mymensingh and Rangpur is in Zone 1, the most active seismic zone where earthquake shocks of maximum intensity IX of the Modified Mercalli scale may occur. Zone II includes the towns of Dinajpur, Bogra, Dacca and Chittagong where shocks of maximum intensity VIII (M.M.) are possible). Zone III covers the towns of Rajshahi, Pabna, Kushtia, Jessore, Faridpur, Khulna, Barisal, Patuakhali and Noakhali. Here the maximum earthquake intensity VII (M.M.) is possible. It is clear that the zonal designations of Maps 1 and 3 are not in complete agreement.

The Rational Analysis of the Seismic Zones

The procedure will be as follows:

1. Using Figure 4.5 of Chapter 4, which correlates the basic canonical isoseismal parameters $\Sigma(IS)_f$ and S_f with the earthquake magnitude and 'geology', the values of $\Sigma(IS)_f$ and S_f will be determined for the four earthquakes of Table 3, assuming they are single shock quakes and that they occur in an \mathcal{R}_2 geologic region.
2. Having $\Sigma(IS)_f$ and S_f , from the canonical isoseismal index relation the values of S_j will be determined as in Section A of this chapter. S_j is the radial distance from the epicentre of an earthquake to the mid-point of the circular band of intensity $I = j$.
3. From the values obtained in (2), the values of $S_{O.R.}$ will be obtained. $S_{O.R.}$ is the distance from the epicentre to the 'outer reach' of any constant intensity band. For any intensity, j , $S_{O.R.,j}$ will be given by (approximately), the sum of half the widths of adjacent regions.
4. Thus, the MID (magnitude, intensity, distance) curve will be known for each of the four key earthquakes.
5. We shall assume contour lines of equal-magnitude earthquakes running along the northern border and northern regions of Bangladesh, corresponding approximately to the four basic earthquakes and the acknowledged seismic history of the region. See Map 2.

6. From the data calculated in (3) and (4) and because of (5), it will be possible using superposition of canonical isoseismal maps to determine 'bands' of known intensity values throughout the entire country, as in Chapter 7.
7. In order to correlate our rational intensities (step 6) with those assumed in the Bangladesh code 'zones' we shall assume.

our I > IX ≡ Zone 1, 'Major damage'
 our IX > I > VI ≡ Zone 2, 'Moderate damage'
 our VI > I > IV ≡ Zone 3, 'Minor damage'
 our IV > I > III ≡ Zone 4, 'Negligible damage'

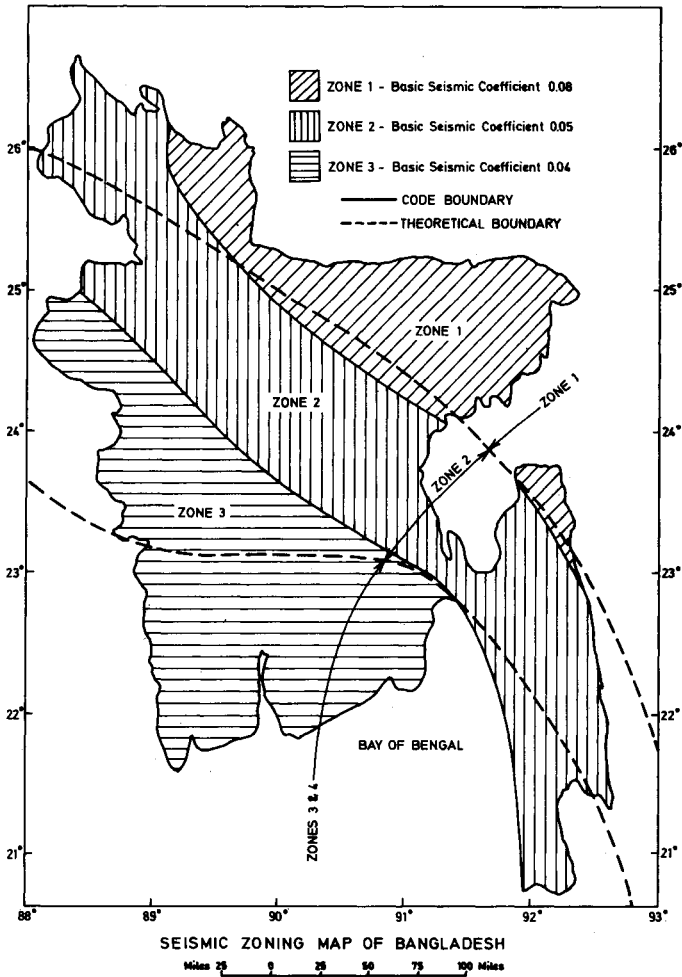
8. Our zones are compared to the Bangladesh code zones in Map 4. Note, there is generally good agreement between the two.
9. Of particular significance is the ground surface energy compatibility relation. In Figure 4.8 approximate values of the energy are given for the different intensity values. A smooth variation of these can be assumed over the intensity band and the corresponding energy at any point in any of the zones will be the key parameter in the structural analysis of the given structure under consideration. It should be noted that the surface energy is dependent upon the depth of earthquake focus, the geology of the earthquake region, local anomalous features and possibly other factors as well. Thus, it is possible that the isoseismal index relation (step 2) varies for different earthquake regions on the earth's surface. We are assuming in this report that the equation as determined in Chapter 3 applies to Bangladesh. If this is not so, the Bangladesh values may be adjusted accordingly and these will then be applicable — for all time. The same is true for any other earthquake region. It may be pointed out that analyses of many earthquakes, occurring all over the earth over many years, do indicate that the isoseismal equation of step 2 appears to be a universal relation.

The numbering in the analysis which follows will conform to that given above.

1. Figure 4.5 determines the data for the four earthquakes assuming an R_2 geology. In the present instance the values used are as shown in Table 3.
2. The canonical isoseismal equation has been programmed to solve for S_y values.
- 3., 4., 5., 6., 7. Tables 4 through 7 summarizes the MID data for the four earthquakes.
- 8., 9. Using the summary data of the Tables and the Zonal correlation of Step 7, we superpose our data on Map 1 and obtain Map 4.

Table 4

| Earthquake | Magnitude | $\Sigma(IS)_f$ | S_f (km) |
|---------------|-----------|----------------|------------|
| Cahar | 7.5 | 4,100 | 350 |
| Assam | 8.2 | 11,000 | 900 |
| Bihar - Nepal | 8 | 9,000 | 750 |
| Dhubri | 7.0 | 2,200 | 170 |



Map 4

Table 5 Cachar Earthquake, January 10, 1869: Magnitude = 7.5 (Richter)
 $S_f = 330$ km, $\Sigma(IS)_f = 4100$ km

| Magnitude | Intensity (M.M.) | S_{av} (km) | IS_{av} | $\Sigma(IS)_f$ | Distance to Outer Reach (km) |
|-----------|------------------|---------------|-----------|----------------|------------------------------|
| 7.5 | X | 3.6 | 36.0 | 4100 | 12.0 |
| | IX | 19.7 | 177.0 | | 28.0 |
| | VIII | 37.0 | 295.0 | | 49.0 |
| | VII | 41.0 | 425.0 | | 78.0 |
| | VI | 95.0 | 575.0 | | 122.0 |
| | V | 148.0 | 740.0 | | 185.0 |
| | IV | 224.0 | 895.0 | | 277.0 |
| III | 330.0 | 990.0 | 384.0 | | |

Table 6 Assam Earthquake, June 12, 1897: Magnitude = 8.2 (Richter)
 $S_f = 900$ km, $\Sigma(IS)_f = 11,000$ km

| Magnitude | Intensity (M.M.) | S_{av} (km) | IS_{av} | $\Sigma(IS)_f$ | Distance to Outer Reach (km) |
|-----------|------------------|---------------|-----------|----------------|------------------------------|
| 8.2 | X | 27.0 | 270.0 | 11,000 | 40.0 |
| | IX | 54.0 | 486.0 | | 73.0 |
| | VIII | 92.0 | 736.0 | | 126.0 |
| | VII | 160.0 | 1120.0 | | 207.0 |
| | VI | 254.0 | 1524.0 | | 327.0 |
| | V | 400.0 | 2000.0 | | 503.0 |
| | IV | 607.0 | 2428.0 | | 754.0 |
| III | 900.0 | 2700.0 | 1047.0 | | |

Table 7 Bihar-Nepal Earthquake, January 15, 1934: Magnitude = 8.0 (Richter)
 $S_f = 750$ km, $\Sigma(IS)_f = 9000$ km

| Magnitude | Intensity (M.M.) | S_{av} (km) | IS_{av} | $\Sigma(IS)_f$ | Distance to Outer Reach (km) |
|-----------|------------------|---------------|-----------|----------------|------------------------------|
| 8 | X | 18.0 | 180.0 | 9000 | 28.0 |
| | IX | 38.0 | 342.0 | | 58.0 |
| | VIII | 78.0 | 624.0 | | 102.0 |
| | VII | 126.0 | 882.0 | | 165.0 |
| | VI | 203.0 | 1218.0 | | 315.0 |
| | V | 326.0 | 1630.0 | | 409.0 |
| | IV | 492.0 | 1968.0 | | 621.0 |
| III | 750.0 | 2250.0 | 879.0 | | |

Table 8 Dhubri Earthquake, July 3, 1930: Magnitude = 7.0 (Richter)
 $S_f = 170$ km, $\Sigma(IS)_f = 2200$ km

| Magnitude | Intensity (M.M.) | S_{av} (km) | IS_{av} | $\Sigma(IS)_f$ | Distance to Outer Reach (km) |
|-----------|------------------|---------------|-----------|----------------|------------------------------|
| 7.0 | X | 4.02 | 40.2 | 2200 | 7.7 |
| | IX | 11.41 | 102.69 | | 15.9 |
| | VIII | 20.45 | 163.6 | | 26.8 |
| | VII | 33.09 | 231.63 | | 42.2 |
| | VI | 51.35 | 308.1 | | 64.7 |
| | V | 78.12 | 390.6 | | 97.6 |
| | IV | 117.02 | 468.08 | | 143.5 |
| III | 170.0 | 510.0 | 196.5 | | |

Conclusion for This Section B

The rational analytic earthquake engineering theory has been applied to the problem of determining code (damage) zones for a particular country for use by engineers and other professionals in their analysis of probable damage and also in structural design.

The data for Bangladesh was utilized. Four major earthquakes which have occurred in the region were used as the 'experimental data'. Locations of epicentres and magnitudes of earthquake were all that were available. However, by utilizing the results and techniques of the theory, it was possible to determine approximate zonal areas corresponding to those given in the 'Bangladesh Code'.

In general, good agreement was obtained — particularly when one realizes that data on earthquakes which occurred more than one hundred years ago must be considered as somewhat approximate.

The analysis indicates the feasibility of the proposed procedure and points out that one of the features of the theory — an energy compatibility relation — enables engineers to *quantitatively* analyze structures using a rational engineering-scientific base.

C) AN APPROXIMATE THEORETICAL METHOD FOR ANALYZING ROCK SLOPE STABILITY DUE TO EARTHQUAKES*

Introduction

Rock avalanches caused by earthquakes are catastrophic events which frequently result in serious loss of life and property. A report by D. K. Keefer in *Science* (Reference 3) summarizes the results of a review study of rock avalanches and identifies key geologic factors which affect the susceptibility of a rock slope to failure during seismic events. Keefer's report concludes that the most susceptible slopes are steeper than 25 degrees and higher than 150 metres. The slopes studied also were undercut by fluvial or glacial erosion and consisted of intensely fractured rock. Other geologic indicators of low strength or potential instability were identified and discussed in the report.

The purpose of this section is to explore a new method of analyzing and predicting rock avalanches like those described in Keefer's report. The basic approach will consist of applying seismic surface energy to the rock slope in accordance with methods of rational earthquake analysis. In essence, the change in slope stability caused by an input of seismic energy will be examined. This

* The author acknowledges the assistance of John Schuring in performing the analysis calculations for this section.

proposed method differs from the present state-of-the-art 'acceleration' approach for evaluating seismic stability which will be discussed briefly.

Background

The same factors which affect static stability of rock slopes are also important in evaluating seismic slope stability. These common factors include (Reference 4):

1. Type of rock and degree of weathering
2. Spacing and orientation of geologic discontinuities (joints, shear planes, for example)
3. Geometry of the slope (height, angle, undercutting, for example)
4. Distribution of porewater pressure
5. Past loosening of rock strata by manmade or natural occurring events

The four generic types of landslide/rockslides generally recognized are falls, rotational slides, translational slides and flows. Any given landslide/rockslide may consist of one or more of these fundamental mechanisms.

When evaluating the effect of earthquakes on rock slopes, it is clear that an allowance must be made for the disturbing forces induced by seismic energy. A method presently used to evaluate the influence of dynamic loading on rock slopes was developed by E. Hoek (Reference 5). It is a simple 'pseudo-static' analysis in which the accelerations applied by an earthquake are assumed to act horizontally towards the free face of the slope. By performing a number of trial calculations, Hoek developed the following empirical relationship:

$$F_d = F_s - 2.3a$$

where: F_d = factor of safety under dynamic conditions

F_s = factor of safety under static conditions

a = horizontal acceleration in terms of the acceleration g due to gravity

Proposed Energy Approach and Stability Criteria

The proposed new method for rock avalanche analysis consists of applying both horizontal and vertical surface energies to the slope under analysis to determine the stability criteria. In one approach to be tested, the applied seismic energy is assumed to 'dilate' the rock mass with the ultimate effect of reducing the particle interlocking and thus the shear strength (ϕ angle) of the rock mass. Two extreme limiting conditions of dilation and resulting stability criteria will be

considered. First, the entire slide mass will be assumed to dilate uniformly as a result of the input of seismic energy. Next, only a localized dilation will be assumed to occur in the vicinity of the failure surface.

In a second approach which differs from (although is not unrelated to) the first, the horizontal and vertical surface energies will be utilized in conjunction with the energy conservation requirement (and resulting divisions of kinetic and potential energies) to develop the stability criterion.

The actual response of a rock mass to seismic energy is highly complex, so for the purposes of the analysis, the following simplifying (and reasonable) assumptions were made:

1. The rock mass is intensely fractured and will behave as a cohesionless soil.
2. Any effects of pore water pressure are ignored.
3. The slide type will be assumed to be a combination of rotational-translational, and is considered to be shallow relative to its width and length.
4. The 'infinite slope' method will be used for determination of the stability factor of safety.
5. Conservatively, the entire energy generated by the earthquake is assumed as instantaneous input into the slope and as acting outward.

An important aspect of the analysis introduced in this report is that a complete rational quantitative theory is developed. This theory includes the earthquake variables and also the physical-stability parameters that should logically be included in any rational theory of landslide-rockslide stability mechanics. And finally, the method is simple, straightforward and capable of being applied by engineering design offices.

The method is developed in detail in the following pages. An avalanche from Keefer's report is then chosen for a check calculation. Although this is a first attempt at the development of the method, and additional work will have to be done to evaluate the accuracy of the approach, as will be seen the results of this initial check calculation are promising and appear to be sufficiently accurate for engineering analysis purposes.

1. Defining the Factory of Safety (See Figures 10.2 and 10.3):

Owing to the fact that these avalanches tend to be rotational-translational in nature (References 6, 7) the method of slope stability analysis chosen is the 'infinite slope' method (References 4, 10). In this method a unit block is analyzed without regard to the width or length of the slide, and the failure surface is assumed approximately parallel with the ground surface.

The derivation of the 'infinite slope' procedure for static conditions is given below:

$$\begin{aligned}
 \text{Factor of Safety} &= F.S. = \frac{\text{Resisting Forces}}{\text{Sliding Forces}} \\
 &= \frac{W \cos \alpha \tan \phi + C}{W \sin \alpha} \\
 &= \frac{W \cos \alpha \tan \phi}{W \sin \alpha} + \frac{C}{W \sin \alpha} \\
 F.S. &= \frac{\tan \phi}{\tan \alpha} + \frac{C}{W \sin \alpha}
 \end{aligned}
 \tag{1}$$

A further simplification can be made recognizing that an intensely fractured rock mass will behave as a cohesionless soil mass (Reference 6). Setting $C = 0$, we get

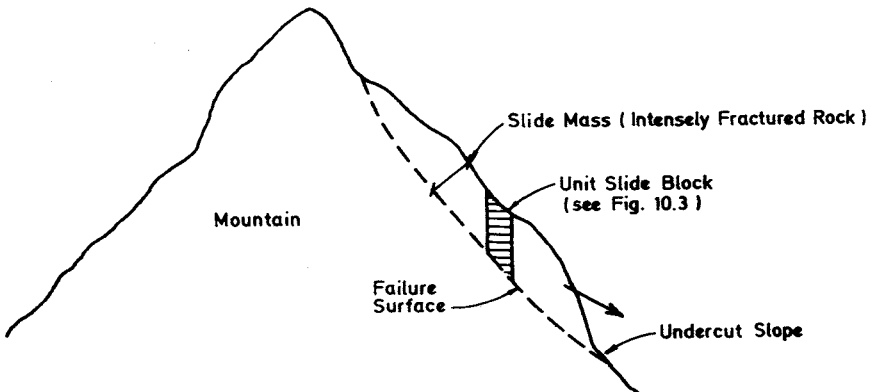


Figure 10.2

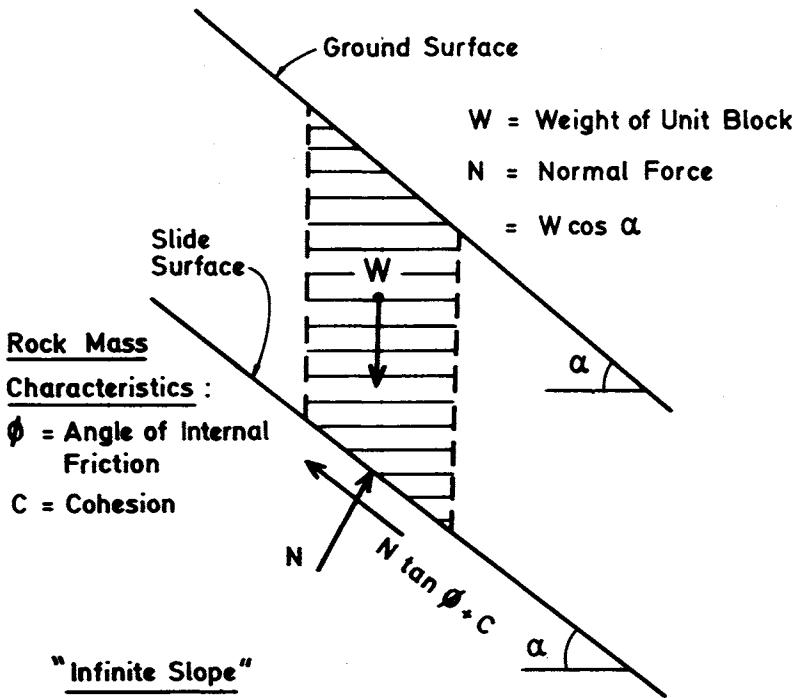


Figure 10.3

$$F.S. = \frac{\tan \phi}{\tan \alpha} \quad (2)$$

In applying the new method, two different (although not entirely unrelated) methods will be used to check the rock slope stability. Both methods are based entirely upon the ground energy concept introduced in earlier chapters, especially Chapter 4.

- A) In one approach, the 'dilation' of the rock mass by seismic energy will be determined. Two separate conditions will be considered as noted in the discussion following, Cases I and II.
- B) In the second approach, the earthquake ground energy will be considered in connection with the energy conservation requirement and the slope response in its kinetic and potential energy forms. This will be called Case III and although a factor of safety will not be determined directly, stability will be measured by an 'all or nothing' criterion. That is, if a

mantle of fractured rock is lifted clear of the mountain, failure (rock-slide) will be assumed. If not, the mass will be assumed as stable. The computations that follow will illustrate the procedure.

2. Dilation of Rock Mass by Seismic Energy:

Failure of the rock mass using this approach will be assumed to occur as a result of dilation caused by input of seismic energy. This dilation causes a reduced shear strength or ϕ , thus causing slope failure.

Two extreme limiting cases of dilation will be considered.

1. Uniform dilation of the entire slide mass.
2. Localized dilation in the vicinity of the failure surface. The rock above the failure surface will behave as a lumped mass.

These two cases are depicted in Figure 10.4.

The driving force for the dilation will be the horizontal and vertical ϵ_{t_f} from the present theory as outlined in Chapters 4 and 5.

In Case I, it is applied to each unit fragment in the mass. In Case II, it is applied to the lumped mass.

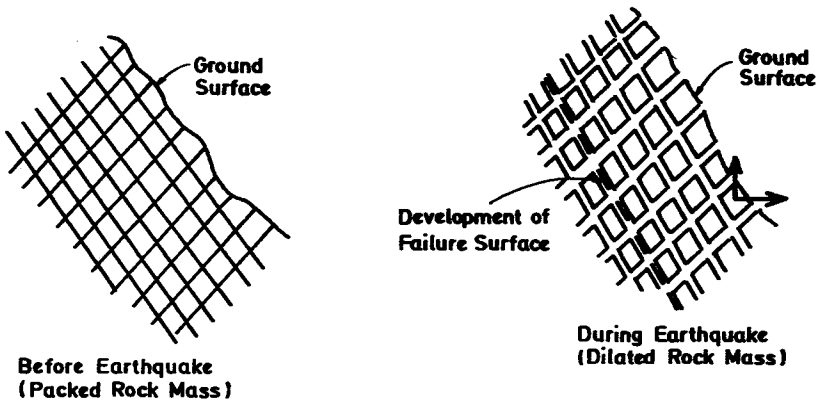


Figure 10.4 Case I Uniform Dilation

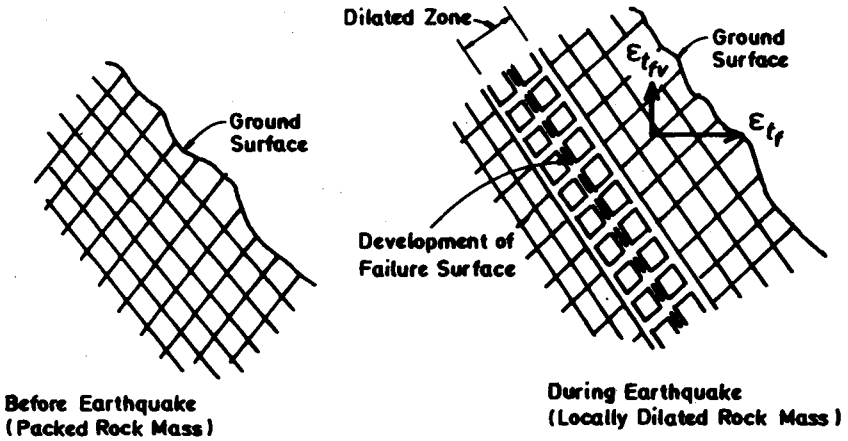


Figure 10.4 Case II Localized Dilation

3. Shear Strength (ϕ) Reduction Due to Dilation:

The amount of shear strength reduction caused by the dilation will be estimated by the established soil mechanics relationship shown in Figure 10.5 for soils (reproduced from Reference 7).

The intensely fractured rock mass may be assumed similar to a well-graded gravel (GW). For a GW soil, the approximate shear strength-dry density relationship from the Figure 10.5 can be approximated by the following linear equation,

$$\phi = 0.58 \gamma_D - 41 \tag{3}$$

where: ϕ = angle of internal friction (deg)
 γ_D = dry density (lb/ft³),

This relation will be used in the later check computations — see, typically, equations 5, 6, 13, 14, 15.

4. The Kinetic-Potential Energy Approach to Stability, Case III

This method can best be illustrated by its application to a specific avalanche. This will be done following the solutions to Case I and Case II which are now given in detail.

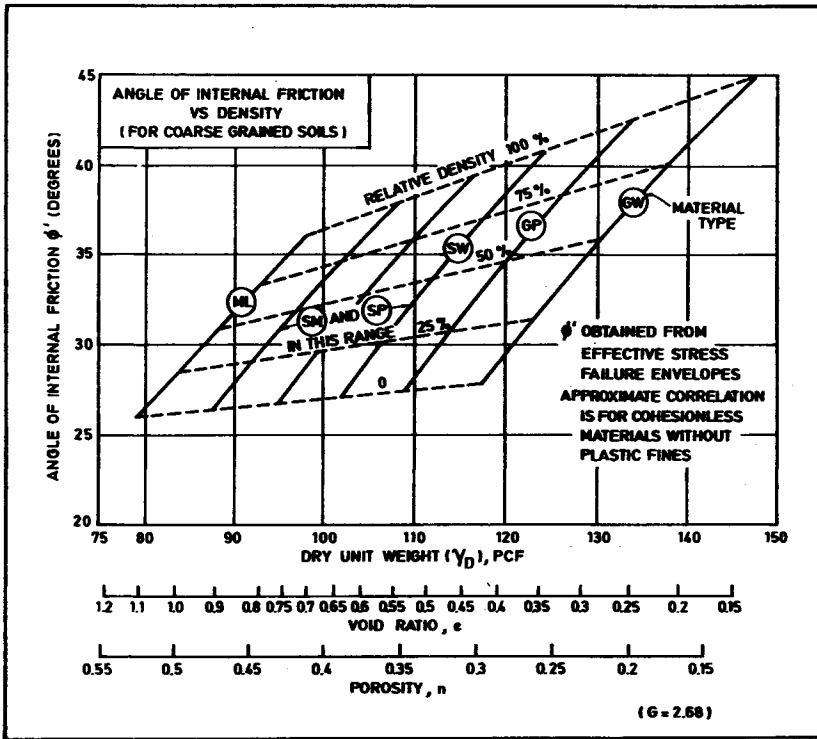


Figure 10.5 Correlations of Strength Characteristics for Granular Soils

Application of the New Approach to Past Rock Avalanches

In order to check the proposed approach, the rock avalanche data in Reference 3 will be utilized. The seismic rock avalanches discussed in the article *all* shared the following characteristics:

1. The slope consisted of intensely fractured rock with joint spacing 3 to 30 cm (1 to 10 in).
2. The slopes were undercut by fluvial or glacial erosion.
3. The slopes were steeper than about 25° and higher than 150 metres.

Other indicators of geologic instability encountered but which were not shared by all the slopes were:

1. Significant weathering
2. Planes or weakness dipping out of the slope
3. Weak cementation
4. Previous slide history

Of these other indicators, the presence of planes of weakness dipping out of the slope is considered to be a major flaw from a rock mechanics points of view. Such geologic continuities 'daylighting' the slope greatly weaken it, and the actual amounts of friction and cohesion available along these planes of weakness are difficult to determine even if detailed geologic data are available.

On account of their unpredictable nature, slopes described as having planes of weakness dipping out of the slope were disqualified for analysis using the new approach. The rock avalanches which were considered eligible for analysis are shown in Table 9 (from Reference 3). The cited references for these avalanches were searched, and further information was located for:

Shattered Peak, Alaska (South Face), 28 March 1964 (Reference 8).

Estancia De La Virgin, Guatemala, 4 February 1976 (Reference 9).

Rio Teocinte, Guatemala, 4 February 1976 (Reference 9).

These sources of information were reviewed and preliminarily analyzed. The Alaskan rock slopes were not selected for detailed analysis due to their extreme pre-slide slope angles of 55° and higher. Slopes as steep as this actually exceed the probable friction angle of the rock mass ($45-55^\circ$), thus indicating initial instability and the presence of some type of unusual cohesion in the rock mass. Considering the location and climate, permafrost may be providing this cohesion.

Two slopes in the Guatemalan earthquakes are considered ideal for a check of the new approach. The Estancia De La Virgin Rock Avalanche was chosen due to its significantly larger size.

Table 9

| Earthquake | Date | Magnitude |
|---|--------------|-----------|
| Khait, Soviet Union | 10 July 1949 | 7.6 |
| Lituya Bay, Alaska | 10 July 1958 | 7.7 |
| Shattered Peak Alaska, (South Face) | 28 Mar 1964 | 9.2 |
| Nevados Huascaran Peru | 31 May 1970 | 7.9 |
| Estancia De La Virgin Guatemala | 4 Feb 1976 | 7.5 |
| Rio Teocinte Guatemala | 4 Feb 1976 | 7.5 |
| Mt. Baldwin, Sierra Nevada, Cal. (2) | 25 May 1980 | 6.1 |

*Check Analysis: Estancia De La Virgin, Guatemala, 4 February 1976.
Using the Dilation Approach — Cases I and II*

STEP 1 Establish basic data and slide geometry (Vicinity map and Isoseismal map from Reference 9).

Earthquake and Slide Location Data:

1. $M = 7.5$ (as reported)
2. 170 km W.S.W. of epicentre.
3. Avalanche located in $I = VIII$ isoseismal zone
4. Surface faulting, assumed shallow focus, efficiency = 0.2. Assume \mathcal{R}_1 geology.
5. Slope faces E.S.E.

Geology

Rock type was andesitic volcanic rocks capped by discontinuous pumice layers ranging from 10–70 ft. in thickness.

Slope Failure Mechanism:

Rotational slump/rock fall avalanche.

Note: The photographs of the landslide in Reference 9 were examined and it appears to also have translational characteristics, i.e. the curved rotational surface has a very large radius. Application of the 'infinite slope' analysis is therefore reasonable, although it is suggested that a minor modification of the approach will account for curved surface failures if this assumption is made.

Slide Geometry:

The reported estimated volume of the slide debris is $6.0 \times 10^6 \text{ m}^3$ (presumed loose volume). The length and width of the slide estimated from the Figure 37 in Reference 9 as shown on Figure 10.6

$$\text{Avg. Length} = 600 \text{ m}$$

$$\text{Avg. Width} = 400 \text{ m}$$

Using a 25% swell for the debris, the average thickness of the slide can be estimated as follows: (The slide thickness is necessary to analyze the rock mass dilation caused by the seismic energy input and also for the application of method B previously discussed).

Then:

$$\begin{aligned} \text{Avg. Thickness} &= \frac{\text{Bank Volume}}{\text{Length} \times \text{Width}} \\ &= \frac{\text{Loose Volume}}{\text{Length} \times \text{Width} (1 + \text{Swell})} \\ &= \frac{6 \times 10^6 \text{ m}^3}{600 \times 400 (1 + 0.25)} = 20 \text{ m} = 66 \text{ Ft.} \end{aligned} \quad (4)$$

$$\text{Avg. Thickness} = 66 \text{ Ft.}$$

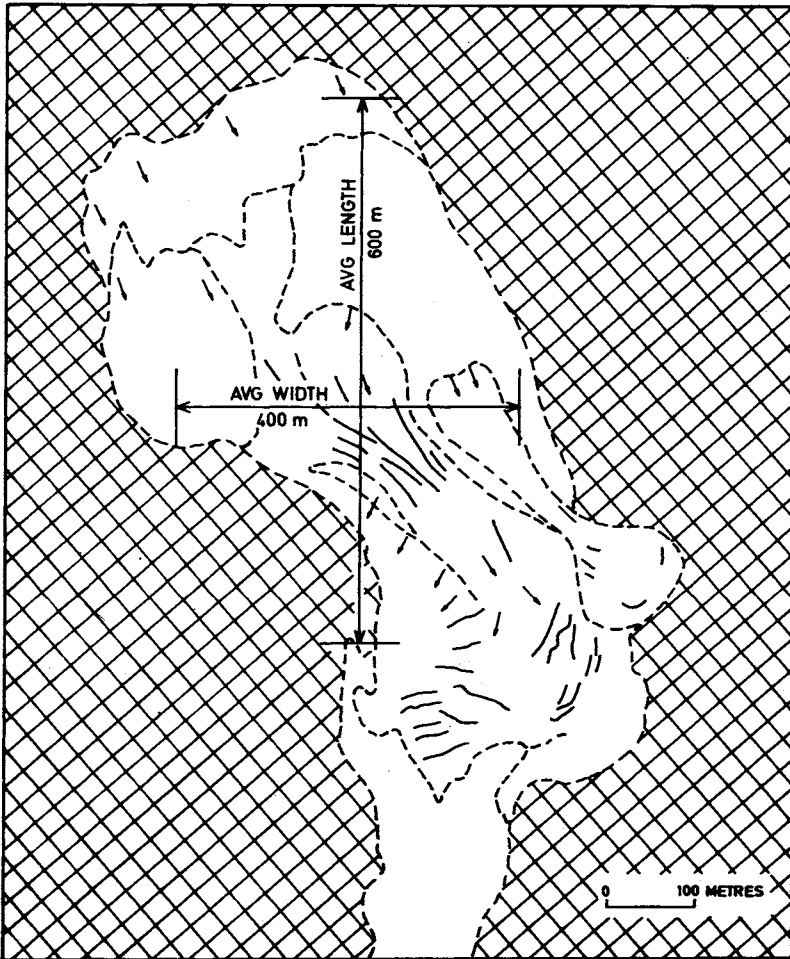


Figure 10.6
(Figure 37 From Reference 9)

The reported preslide slope was $\alpha = 23^\circ$.

Finally, the following slope geometry, Figure 10.7 is obtained.

Note: It must be recognized that the geometry shown is an average approximation of the very variable actual slope condition. However, if any attempt at a rational analysis is to be made, it is essential that such an averaging be used.

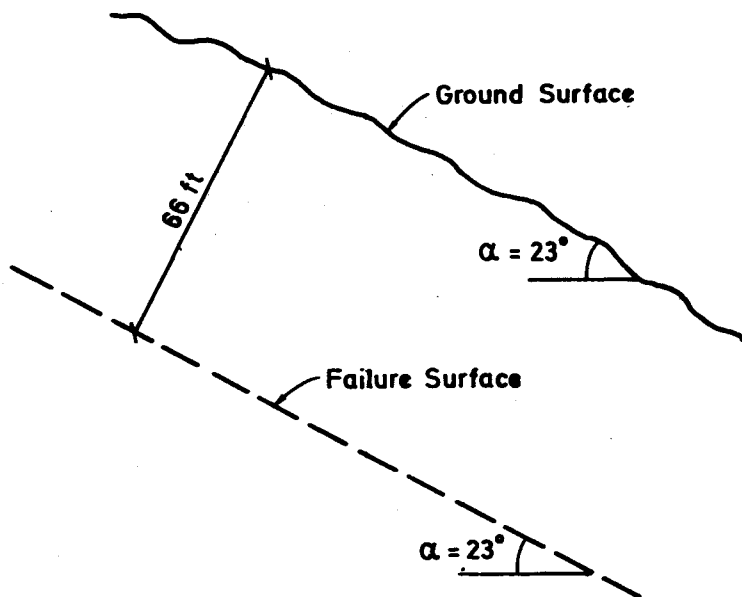


Figure 10.7

Rock Mass Properties:

1. Intense fracturing with joint spacing 3 to 30 cm (1" to 10"). Significant weathering also reported.
2. Use $\phi = 45^\circ$ for intact rock mass. This is estimated from the previously cited correlation between friction angle and density. The weathered and fractured rock mass would behave similar to a GW soil, which at 100% relative density has a $\phi = 45^\circ$. Refer to Figure 10.4.
3. Density:

For Andesite: $\gamma_D = 170 \text{ Lb/Ft}^3$

For Pumice: $\gamma_D = 100 \text{ Lb/Ft}^3$

Assuming a 60/40 mixture:

$$\left. \begin{array}{l} \text{Avg. } \gamma_D = 142 \text{ Lb/Ft}^3 \\ \text{Say } 145 \text{ Lb/Ft}^3 \end{array} \right\} \quad (5)$$

STEP 2 Estimate of Pre-Avalanche Factor of Safety

$$\text{Factor of Safety} = \frac{\tan \phi}{\tan \alpha} = \frac{\tan 45^\circ}{\tan 23^\circ} \tag{6}$$

$$F.S. = 2.36$$

Therefore, the slope is stable before the earthquake.

STEP 3 Estimate of horizontal and vertical energy, ϵ_{tf} and ϵ_{tfv} supplied by the earthquake. See Chapter 5 for definitions of the terms used.

Determine ϵ_{tf} :

The basic relationship for earthquake efficiency as derived in Chapter 5 is:

$$\eta = \frac{1}{2} \frac{V_4}{V_2} \frac{A_{4H}}{A_{4H} + A_{4V}} \tag{7}$$

When dealing with shallow earthquakes, $d = 0$, and

$$\left. \begin{aligned} A_{4V} &= \frac{1}{2} A_{4H} \\ \text{then,} \end{aligned} \right\} \tag{8}$$

$$\frac{A_{4V}}{A_{4H} + A_{4V}} = \frac{1/2}{1 + 1/2} = \frac{1}{3}$$

Therefore:

$$\text{Vert. } \eta = \frac{1}{2} \eta$$

The vertical surface energy is one-half the horizontal surface energy.

From Figure 4.8 we may estimate the value of ϵ_{tf} for the $I = VIII$ region (slide location) as

$$\begin{aligned} \epsilon_{tf} &= 5 \times 10^{17} \text{ ergs/km}^2 \\ &= 3425 \text{ ft lb/ft}^2 \end{aligned}$$

Therefore,

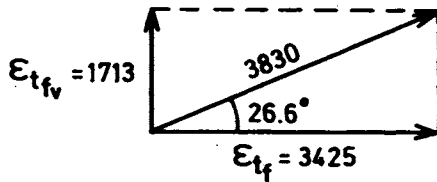
$$\left. \begin{aligned}
 \epsilon_{t_{fv}} &= \frac{1}{2} \epsilon_{t_f} \\
 &= (0.5) (3425 \text{ Ft/Lb/Ft}^2) \\
 \epsilon_{t_{fv}} &= 1713 \text{ Ft/Lb/Ft}^2 \\
 &\quad \text{Hor. Projection}
 \end{aligned} \right\} \quad (9)$$

Combining ϵ_{t_f} and $\epsilon_{t_{fv}}$ vectorally we get Figure 10.8a. Resultant ϵ_{t_f} is 3830 ft-lb/ft² acting at an angle of 26.6° off the horizontal.

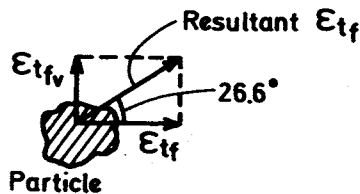
Note: The energies are essentially V^2 terms. Hence the vectoral combination is permissible.

STEP 4A Case I — Determine change in factor of safety due to uniform dilation of the slope.

Each rock mass particle in the slope will receive the following energies, Figure 10.8b.



(a)



(b)

Figure 10.8

For a unit column of soil inclined at 26.6° with the horizontal, the resulting total deformation and unit strain will be determined from Figure 10.9. Plane strain conditions are assumed.

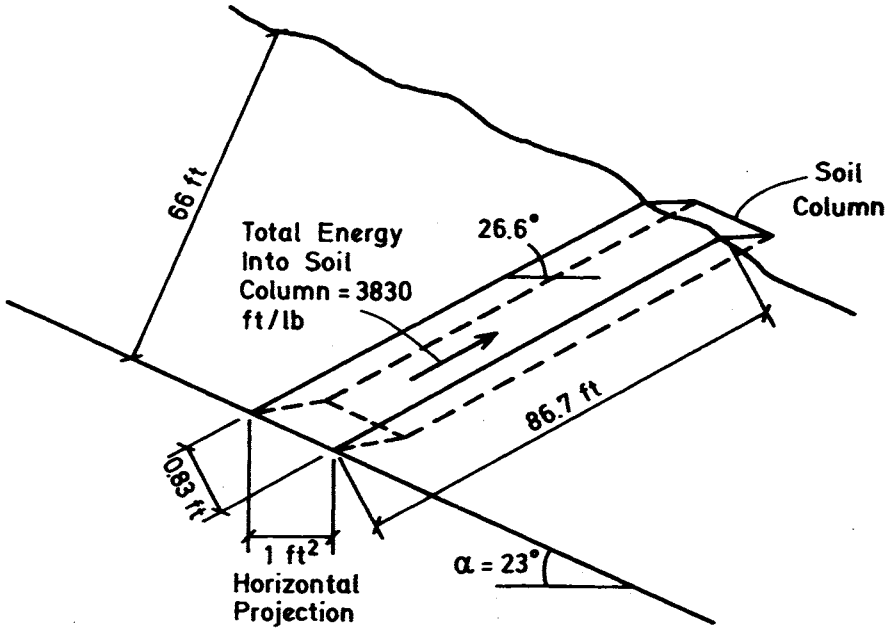


Figure 10.9

Then,

$$\begin{aligned} \text{Total Deformation} &= \frac{\text{Total Energy into Soil Column}}{\text{Total Weight of Soil Column}} = \frac{3830 \text{ Ft-Lb}}{(1.0 \text{ Ft})(0.83 \text{ Ft})(86.7 \text{ Ft})(145 \text{ Lb/Ft}^3)} \\ &= 0.37 \text{ Ft} \end{aligned}$$

and

(10)

$$\text{Unit Strain} = \frac{\text{Total Deformation}}{\text{Length of Soil Column}} = \frac{0.37 \text{ Ft}}{86.7 \text{ Ft}} = 0.0042 \text{ Ft/Ft}$$

Therefore each linear foot of soil in the column will be dilated or 'stretched' on an average of 0.0045 ft or 0.45%. This will change the density as follows:

$$\frac{145 \text{ Lb/Ft}^3}{1 + 0.0042} = 144.4 \text{ Lb/Ft}^3 \quad (11)$$

This slight change in density will have an almost indiscernable effect on the ϕ -angle of the rock mass. Stability will therefore not change if a uniform dilation of the rock mass is assumed. Therefore, insofar as Case I indicates, *a uniform dilation will not cause instability in this slope.*

Note: Although this slide mass was too thick to have become unstable due to a uniform dilation, this mechanism could be the cause of shallower rock slides. Using an assumed unit weight of rock, the critical depth at which uniform dilation would cause failure could be back-calculated. It would be interesting to check this surmise against some actual or laboratory induced shallow slides.

Now try Case II — Localized Dilation.

STEP 4B Case II — Determine the change in factor of safety due to localized dilation of the slope.

The 'lumped' mass of rock above the failure surface will received the following unit energy, Figure 10.10.

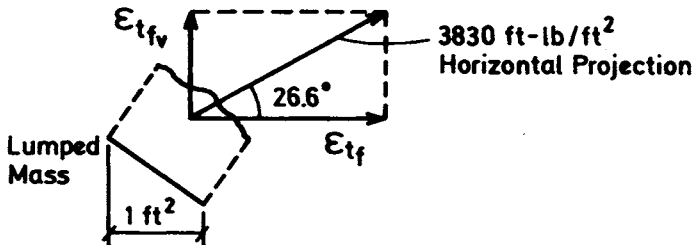
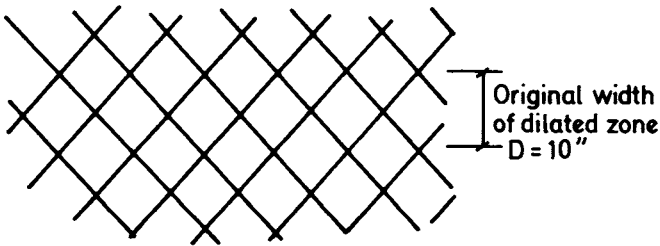


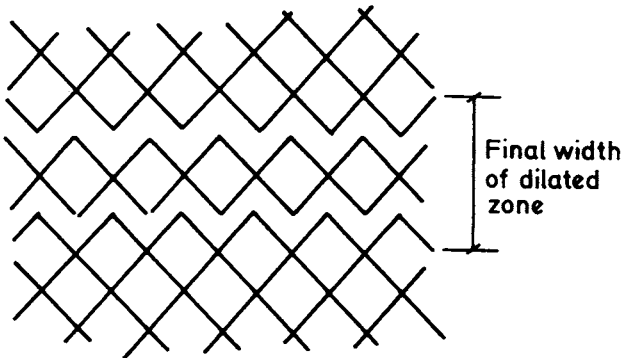
Figure 10.10

For a unit column of soil inclined at 26.6° with the horizontal, the resulting movement of the lumped mass will be as shown below

Note: A key assumption here is the thickness of the assumed localized dilation zone in the vicinity on the failure zone. Based on the 10'' maximum joint spacing of the intensely fractured rock mass, a minimum thickness for the dilated zone would be at least equal to the diameter of the maximum size particle to allow the particles to shear past one another. Using Max. $D = 10$ inches, we get, Figure 10.11



PACKED ROCK MASS



DILATED ROCK MASS

Figure 10.11

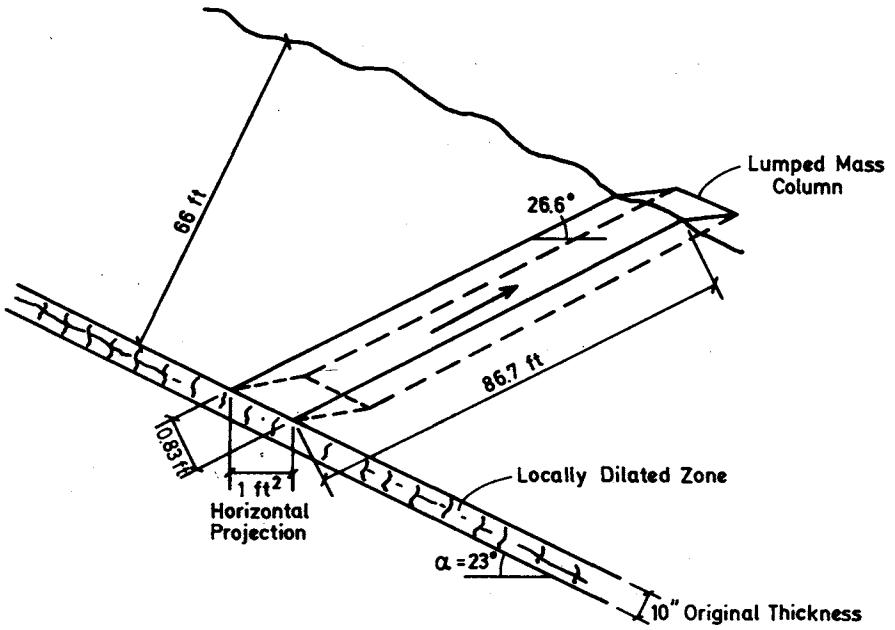


Figure 10.12

Then, from Figure 10.12

$$\begin{aligned}
 \text{Total Deformation} &= \frac{\text{Total Energy into Lumped Mass}}{\text{Total Weight of Lumped Mass}} \\
 \text{of Dilated Zone} &= \frac{3830 \text{ Ft-Lb}}{(1.0 \text{ Ft}) (0.83 \text{ Ft}) (86.7 \text{ Ft}) (145 \text{ Lb/Ft}^3)} \\
 &= 0.37 \text{ Ft}
 \end{aligned}$$

and

(12)

$$\begin{aligned} \text{Unit Strain} &= \frac{\text{Total Deformation}}{\text{Thickness of Dilated Zone}} = \frac{0.37 \text{ Ft}}{\frac{10 \text{ in}}{12 \text{ in/Ft}} \frac{1}{\cos 40.4^\circ}} \\ \text{in Dilated Zone} & \\ &= 0.34 \text{ Ft/Ft} \end{aligned}$$

Therefore, each linear foot of soil in the failure zone will be dilated or stretched on the average of 0.34 Ft or 34%. This will change the density as follows:

$$\frac{145 \text{ Lb/Ft}^3}{1 + 0.34} = 108.2 \text{ Lb/Ft}^3 \quad (13)$$

The resulting effect on the ϕ angle will be:

$$\phi = (0.59)(108.2) - 41 = 22.8^\circ \quad (14)$$

The modified factor of safety will be:

$$F.S. = \frac{\tan \phi}{\tan \alpha} = \frac{\tan 22.8}{\tan 23} = 0.99 \quad (15)$$

$$\begin{aligned} \text{Seismic Factor} &= 0.99 < 1.0 \\ \text{of Safety} & \end{aligned} \quad (16)$$

The slope is on the brink of failure.

It should be noted that this analysis is probably more realistic, physically, than the previous one.

*Check Analysis: Estancia De La Virgin, Guatemala, February 4, 1976
Using the Energy Conservation Approach — Case III*

STEP 5 In using this approach we again start with the earthquake surface energies ϵ_{t_f} and ϵ_{f_v} . As before these are applied to the rock column of Figure 10.9.

The total energy, 3830 Ft-Lb will impart a kinetic energy to the column, acting in the direction away from the slope. The geometry requires that the 'plug' or column rise and move sidewise. The rise reduces the vertical kinetic energy and increases the potential energy, with the sum of the two energies assumed to be constant and equal to 1713 Ft-Lb. (Damping is neglected during this first cycle which will determine whether or not failure occurs).

When all of the vertical kinetic energy has been dissipated, the upward column motion will have stopped, the column will have moved vertically a distance equal to Δ , where

$$\begin{aligned}\Delta &= \frac{\text{Vertical Energy}}{\text{Total Weight of Column}} \\ &= \frac{1713}{10000} \\ &= 0.19 \text{ ft.}\end{aligned}\tag{17}$$

This vertical distance corresponds to a distance X normal to the fracture plane given by

$$X = \frac{\Delta}{\sin 26^\circ} = 4\frac{1}{2}'' - 5'' \tag{18}$$

The 'characteric height' of the fractured stone is 3"—10" as noted in the earlier data section. Thus, the column (and the slope mantle) is lifted clear of (and away from) the main slope. Due to its induced potential energy it starts to fall (still moving horizontally) and the slide commences.

Just as for Case II the computation indicates the threshold for onset of failures. This may be related to the lower limit for slide angles reported in Reference 3 — i.e., about 25° which is close to 23°–26° angle used in the computations in this report.

Conclusion for This Section C

A 'mechanism' is developed to account for the occurrence of rock slides and landslides during an earthquake. The approach is based entirely upon plausible physical-engineering phenomena and utilizes a rational quantitative theory of

earthquake engineering, which includes within its format those physical-engineer-geologic parameters that should appear in any rational quantitative theory for the rockslide-landslide event.

In this first presentation of the method a rough check is made using data from a recent earthquake-rockslide in Guatemala*. The necessary reasonable quantitative approximations of the physical, geologic and earthquake data are made, and the computations do, indeed, check the actual behaviour for the single rockslide considered.

Two different, though related methods of analysis are utilized and these check each other satisfactorily. One is the so-called 'dilation' method and the second is a conservation of kinetic-potential energy approach.

Still to be done:

1. The suggested new approaches must be checked against additional rockslides in order to determine how accurate they are — or whether one or the other is more accurate.
2. The present check was an after-the-fact analysis. Much more convincing would be a 'prediction' of a particular happening at a given location. To do this, preliminary local geological data would be required and various earthquake data would have to be assumed.
3. It would be instructive to apply the new methods to check the various (27) rockslides considered in Reference 3 particularly insofar as the slope and height limits are concerned. It should be noted, however, that it is not clear that sufficient geologic and earthquake data is available to do this.
4. Finally, it appears likely that the same mechanism, suitably modified, can be utilized to analyze in a quantitative manner the four basic types of landslides mentioned previously. The key quantity, the driving element, in the happening is the ground surface energy (horizontal and vertical) which the earthquake supplies at the slope site and which the rock slope must absorb. The new theory develops an approximate analysis for the timewise and spacewise variations of ground energy due to an earthquake. In this section, the quantitative connections between the earthquake and the rockslide are forged.

D) THE MEXICAN EARTHQUAKE OF SEPTEMBER 19, 1985

Introduction

In this section we analyze the Mexican earthquake of September 19, 1985 with particular emphasis on various aspects of this earthquake and their connections

* It is interesting to note that superposition of canonical isoseismal maps was used to check the isoseismal map for this earthquake, see Chapter 7.

with the rational theories of this text.

Three particular behaviours of the earthquakes are considered.

1. The accelerogram-mechanism-magnitude correlation.
2. The accelerogram-period anomaly.
3. The anomalous damage — loss of life in Central Mexico City.

An additional exceedingly important aspect of the rational methods (and one which was essentially utilized in all parts of the book) will be introduced in this discussion of the Mexican earthquake. It involves the concept of 'average' conditions which is an essential assumption in a quantitative theory of earthquake engineering and which plays an important role in the rational analysis of the three items mentioned above. This will be discussed next.

The 'Average Case' or 'Averageness' Requirement

It is assumed that a reasonable engineering approach to the various earthquake phenomena requires (because of the *complexity* of the overall behaviour of the earthquake and its effects) that one assumes an 'average case' behaviour or an 'averageness' for the multiple parameters involved. Only then can usable quantitative engineering design data be developed. This includes — in the earthquake analyses — 'average case' assumption for

- a) the mechanisms
- b) the geologies
- c) the accelerograms (canonical)
- d) the isoseismal maps (canonical)
- e) the structural response

In all of the above, average *quantitative* behaviours are determined based upon reasonable physical-engineering, mathematical, dimensional considerations. In common with all engineering approaches, various pertinent physical parameters were introduced — most of which are uniquely (and solely) related to earthquake engineering. These parameters, once more in accordance with usual engineering practice, require calibration — a process that must be based upon experiments. In earthquake engineering, the experiment, in general, can only be the actual earthquake itself.

As pointed out previously, the fundamental parameter, the single over-riding physical entity which ties together all of the various timewise and spacewise elements of the complete, comprehensive, unified theory is *energy*. In developing the theory all of the items (a) through (e) previously listed were related to the

energy (within the scope of 'averageness') in one or another functional form and this is the basis for the approximate rational analyses discussed in this and all other chapters of the book.

Damage and Energy

Earthquake damage in many parts of the world is customarily related to an intensity-descriptive scale (similar to the Modified Mercalli, MM, scale used in the United States and other countries). The variation of intensity, I , over the surface of the earth affected by the earthquake, is shown on a contour-type map with regions of constant intensity shown between adjacent contour lines, see Chapters 3 and 4.

A more suitable intensity scale was developed which correlated the intensity number directly with the damage-producing parameter, namely the surface horizontal energy, Chapter 8. The present form of the curve is shown repeated in Figure 10.13. A number of applications to various earthquake engineering problems (Chapter 11) indicate that this chart gives numerical results which check actual earthquake damage data with acceptable engineering accuracy.

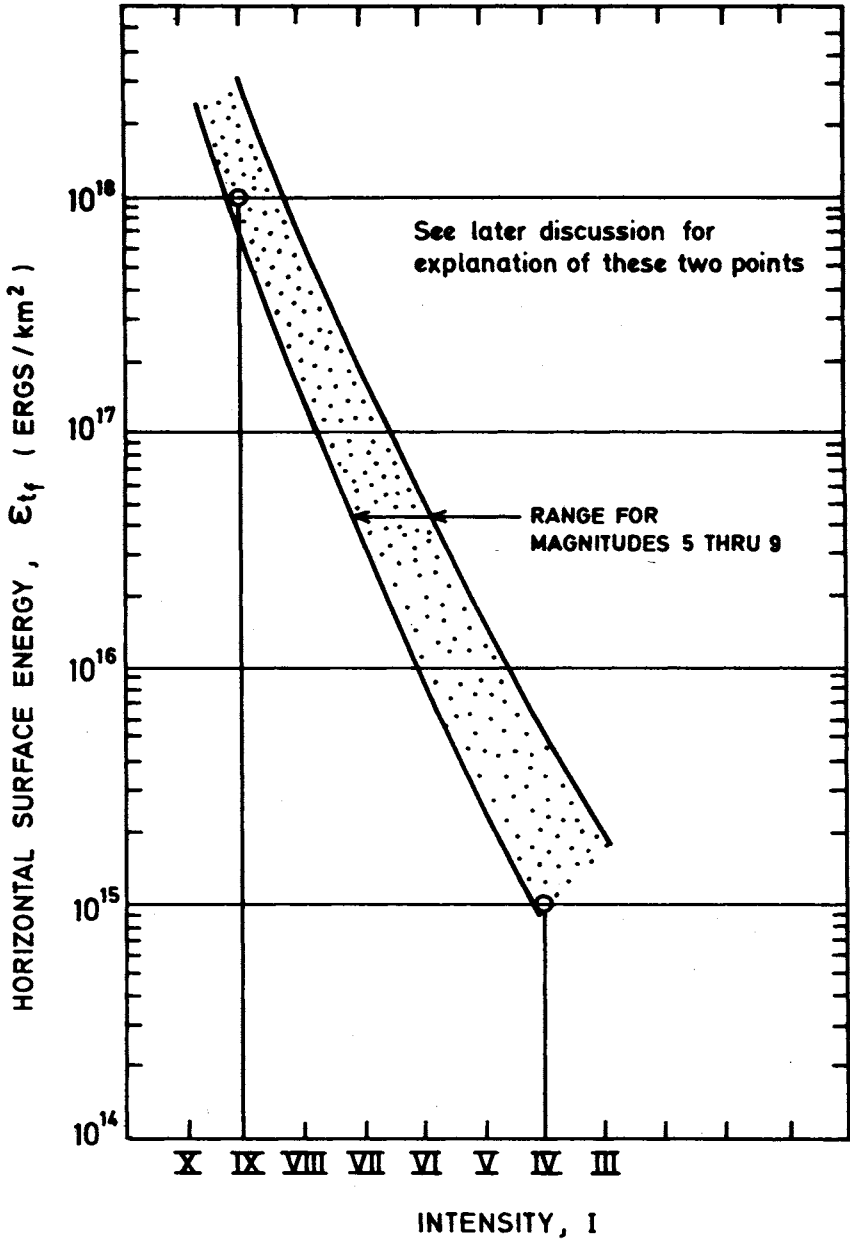
In developing Figure 10.13, it was postulated that — physically — a given intensity number or band should correspond to set values of ground energy, regardless of when or where the earthquake which generated the intensity occurred. Along these lines, several sets of after-the-fact earthquake data were used as calibrators which resulted in this presently used form of the energy-intensity curve.

Among the studies utilized in the calibration of the curve, several dealt with damage to particular building structures. These indicate that the 'area' term to be used as the multiplier of ϵ_{f_s} , in order to determine the energy which the given structures must absorb as strain energy, is the actual area of the foundation in contact with the ground.

The Mexican Earthquake of September 19, 1985

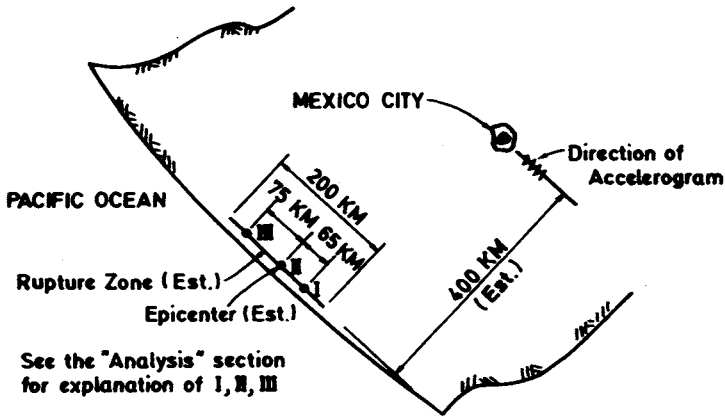
On September 19, an earthquake of Richter magnitude $M = 8.1$ struck Mexico. The epicentre was located near the town of Lazaro Cardenas as shown schematically in Figure 10.14. Also shown is the distance of the epicentre from Mexico City (estimated to be 400 km). An estimate of the rupture zone length, based upon a study of aftershock data, is that it was approximately 200 km, extending roughly from northwest to southeast.

A preliminary form of an accelerogram taken in the region of maximum devastation (the centre of Mexico City) is shown in Figure 10.15. We note that



Earthquake Intensity vs. Horizontal Surface Energy

Figure 10.13



NOT TO SCALE

Figure 10.14

although Mexico City is 400 km from the epicentre, the damage in Mexico City was greater than at any point between the epicentre and Mexico City. Furthermore, in Mexico City, the damage was largely confined to a relatively small area of Central Mexico City. It turns out that this region of anomalous behaviour — of catastrophic structural damage and loss of life — is on the bed of a filled-in lake.

We shall apply the rational theory of the text to an analysis of three different elements of the earthquake, as follows:

1. A superposition of canonical accelerograms (Chapter 6) is applied to the preliminary accelerogram (Figure 10.15) obtained in the lake-bed area of Central Mexico City.
2. The estimated earthquake magnitude, estimated epicentral location and estimated fault line geometry are correlated with (1) above and also with a superposition of a rational (mathematical) earthquake mechanism, founded on a tensile plate rupture instability, Chapter 1, and (1) and (2) are in turn correlated with
3. The anomalous devastation in the centre of Mexico City.

Some of the rational earthquake engineering parameters are, of necessity, assumed and the correlations are, similarly, hypothesized. In all cases, the values of the parameters and the hypothesized connections are physically reasonable.

The crucible for experimentally testing any rational theory of earthquake engineering is the earthquake itself. In the present case, the earthquake ‘experimental data’ which must be correlated with the (theoretical) analysis consists of

- a) A preliminary form of an accelerogram taken within the region of maximum devastation, Figure 10.15.
- b) The earthquake magnitude, epicentral location and geometry of the fault line — all of which are estimated.

The rational theory which will be utilized in the correlation analysis consists of

1. Canonical accelerograms and their fundamental parameters, t_f and $\Sigma(a\Delta t)_f$, see Chapter 2.
2. A superposition of canonical accelerograms, see Chapter 6 and Figure 10.16.

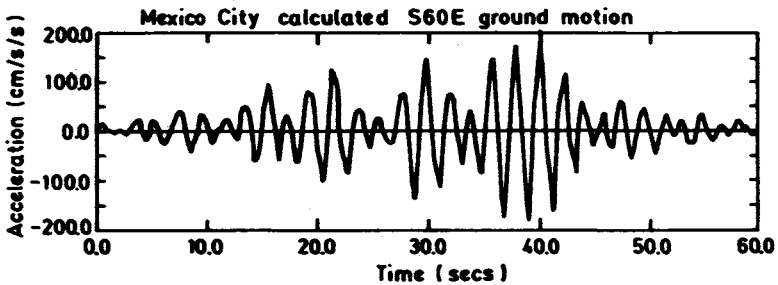


Figure 10.15

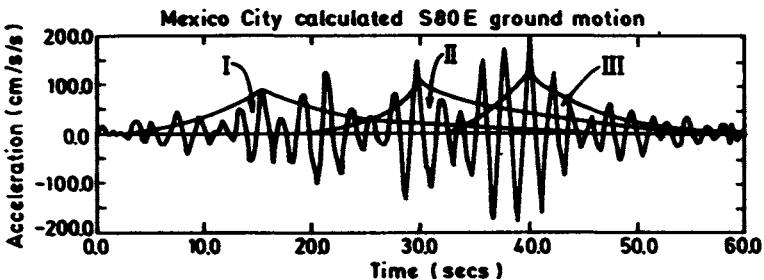


Figure 10.16

3. A mathematical model of an earthquake mechanism, see Chapter 1.
4. A damage chart which correlates the fundamental parameters of the canonical accelerogram (t_f and $\Sigma(a\Delta t)_f$) with the MM intensity number — the damage — as shown in Figure 10.17, and finally, the Intensity-Ground Surface Energy compatibility relation, shown in Figure 10.13, which determines the energy which the structure must absorb. If and when details of the structural design of the failed buildings (and also those nearby undamaged buildings) become available, this chart may be useful in accounting for the structural behaviour of the buildings.

The Three-Shock Analysis

According to the theory of this text, following is the sequence of events leading to the devastation of Central Mexico City:

1. Three major sequential shocks were involved as follows, see Figure 10.14 and Figure 10.16.
 - a) The first one, occurred at I on the fault line. For this shock — approximately — in Central Mexico City the accelerogram indicated (see Chapter 3)

$$t_0 = 4 \text{ sec}$$

$$t_A = 14 \text{ sec}$$

$$t_f = 44 \text{ sec}$$

from which,

$$\Sigma(a\Delta t)_{f_1} = 1.05 \text{ g. sec}$$

$$t_{f_1} = 40 \text{ sec}$$

and the intensity = VIII (Figure 10.17). We assume this is a plate rupture instability shock, and that the velocity of the rupture is approximately 5 km/sec.

- b) Thirteen seconds after (and 65 km distant from) the initiation of I, a second shock is triggered at II on the fault line. For this shock (Figure 10.16) — approximately in Central Mexico City, the accelerogram indicated

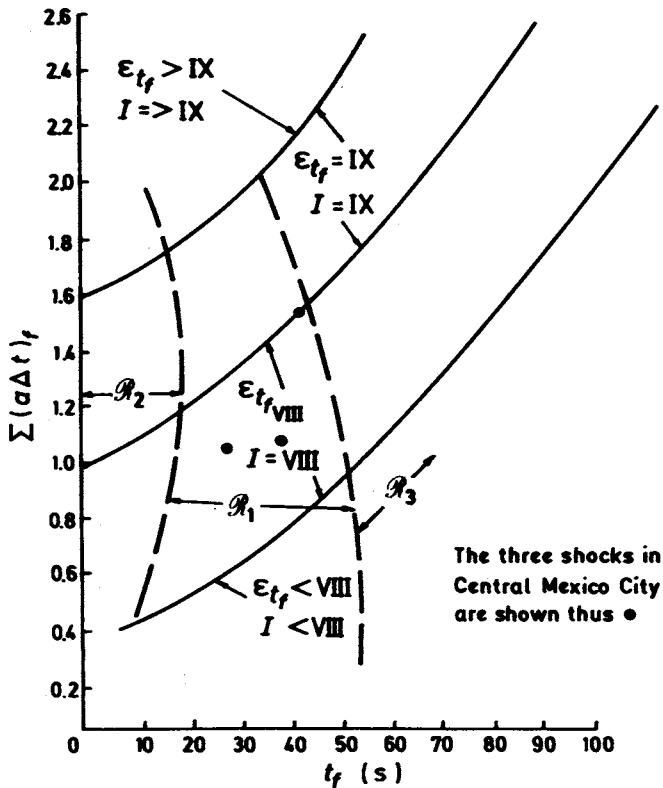


Figure 10.17

$$t_0 = 18 \text{ sec}$$

$$t_A = 29 \text{ sec}$$

$$t_f = 62 \text{ sec}$$

from which,

$$\Sigma(a\Delta t)_{f_{II}} = 1.47. \text{ sec}$$

$$t_{f_{II}} = 44 \text{ sec}$$

and the intensity = IX (Figure 10.17). This also is assumed to be a plate rupture instability shock whose rupture velocity is approximately 5 km/sec.

- c) Fifteen seconds after (and 75 km distance from) the initiation of shock II, a third shock is triggered at III on the fault line. For this shock (Figure 10.16) — approximately — in Central Mexico City the accelerogram indicated.

$$t_0 = 33 \text{ sec}$$

$$t_A = 40 \text{ sec}$$

$$t_f = 61 \text{ sec}$$

from which

$$\Sigma(a\Delta t)_{f_{\text{III}}} = 1.05 \text{ g. sec}$$

$$t_{f_{\text{III}}} = 28 \text{ sec}$$

and the intensity = VIII (Figure 10.17).

The damage caused by these three shocks — individually and cumulatively depending upon the energy-absorbing capacity of the structures — is not inconsistent with that reported for the lake-bed areas of Central Mexico City.

Two additional predictions may be made based upon the foregoing analysis. If we assume the energy is given by the following often used equation

$$\log_{10} E = 11.4 + 1.5 M \text{ ergs}$$

then for the reported single-shock magnitude, namely $M = 8.1$, we find

$$E = 10^{23.5} \text{ ergs}$$

For the three shocks postulated above by the present analysis, we find that for

$$M_{\text{I}} = 7.7, \quad M_{\text{II}} = 7.8, \quad M_{\text{III}} = 7.7$$

the *total* energy is approximately equal to the energy for the single $M = 8.1$ shocks.

A summary of the three-shock analysis is shown in Table 10 which follows:

Table 10

| | First Shock | Second Shock | Third Shock |
|--------------------------------------|-------------|--------------|-------------|
| M (Richter) | 7.7 | 7.8 | 7.7 |
| Time of onset, t sec | 0 | 14 | 29 |
| Duration of shock, t sec | 40 | 44 | 28 |
| a_{\max} , g | 0.10 | 0.12 | 0.13 |
| Max. Intensity (Central Mexico City) | VIII | IX | VIII |

The second prediction concerns the isoseismal map for this event based upon the three-shock postulate. In Chapter 7 a theoretical superposition procedure for multiple shocks is described. The map has been prepared (Figure 10.18) for the three shocks and may be compared with the still-to-be-determined isoseismal map for the actual event. The anomalous situation over the lake-bed area will not, of course be accounted for in this comparison.

The Two-Shock Analysis

Some investigators state that the earthquake consisted of *two* shocks, separated by 26 seconds, References 11 and 12.

The analysis of the preliminary form of the Central Mexico City accelerogram, discussed above, assumed that the earthquake was *three* shocks with the properties shown in Table 10. The same accelerogram can be considered as an approximate superposition of *two* shocks separated by 26 seconds. If this is done, the properties of the two shocks (assumed approximately of equal magnitude) are as shown in Table 11 which follows.

Table 11

| | First Shock | Second Shock |
|---|-------------|--------------|
| M , Richter | 7.9 | 7.9 |
| Time of Onset, t sec | 0 | 26 |
| Duration of Shock, t sec | 80 | 56 |
| a_{\max} , g | 0.1 | 0.15 |
| Maximum Intensity (Central Mexico City) | 9 | IX |

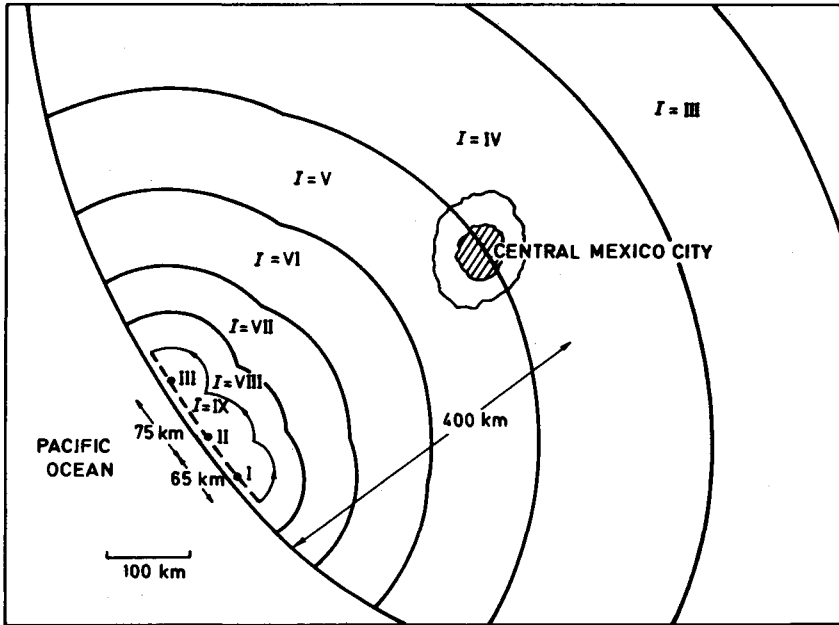


Figure 10.18 Isoseismal Map for the Three Shocks

The Averageness Assumption and the Mexican Earthquake

A superposition of the two-shock and three-shock isoseismal maps indicates that for an 'average' assumed Mexican geological condition, the intensity in Central Mexico City should be $I = IV$ or V . Furthermore, for typical 'average' accelerograms, the period should be about 0.05–0.1 seconds. The period indicated by the preliminary accelerogram in Central Mexico City is about 2 to 3 seconds and the intensity was estimated to be about $I = IX$, Reference 12.

The following questions raised by the above are fundamental and must be answered if one is to understand the earthquake event wherever it occurs, Reference 13, 14.

1. How to account for the devastation in Central Mexico City, 400 km distant from the epicentral tract, where an intensity of only $I = IV$ or V is indicated by the rational theoretical analysis?
2. How to account for the long period and relatively large accelerations in Central Mexico City whereas experience indicates a much shorter period in the (average) geological region of Mexico?

It will be shown in the next section that both questions can be answered by the approximate rational analyses of this text.

The Rational Analysis of the Damage in Central Mexico City

1. The 'Period-Damage' Connection

A very commonly stated correlation in earthquake engineering studies is that a period of ground motion resonant with the period of a structure is the crucial element in the building damage producing mechanism.

Furthermore, it is generally accepted that the period of vibration for a structure is given, approximately, by

$$p = 0.1 N \text{ sec} \quad (18)$$

in which N is the number of stories of the structure.

The preliminary accelerogram for the Central Mexico City location indicated a period of about 2+ seconds for the ground motion, indicating that maximum damage should have occurred in structures, say, over 15 stories high. However, Reference 13 which includes a preliminary damage study for Central Mexico City indicates that maximum damage, insofar as number of buildings is concerned, was sustained by buildings in the 5–10 story range. This would appear to raise some questions concerning either one or both of

- a) The approximate period-number of stories equation.
- b) The generally accepted damage correlation between ground motion period (as indicated by the accelerogram) and building period (as indicated by (a)). (Other conditions causing damage to buildings in Central Mexico City are described in References 11, 12, 14, 15.)

Our approximate analysis, described next, uses an entirely different approach for the period and damage effects.

2. The 'Average' Geology and the Central Mexico City Geology

Table 12 which follows, reprinted from Reference 16, indicates average moduli of elasticity for different soil conditions.

It will be assumed that the 'average' geology over the region in Mexico affected by the earthquake corresponds to 'rock, sound', with value of E (average) equal to say, 30,000 kg/cm². Also, we assume the average soil condi-

tion in Central Mexico City, over the lake-bed, corresponds to 'clay, plastic' with an E equal to 20 kg/cm^2 . Then*

$$\frac{E_{\text{Rock(Sound)}}}{E_{\text{Clay(Plastic)}}} \cong \frac{E_R}{E_C} \cong 1500 . \quad (19)$$

Table 12

| Compression Modulus of Elasticity, M_v | |
|--|-----------------------|
| Soil Material | $M_v, \text{kg/cm}^2$ |
| peat | 1 to 5 |
| clay, plastic | 5 to 40 |
| clay, stiff | 40 to 80 |
| clay, med. hard | 80 to 150 |
| sand, loose | 100 to 200 |
| sand, dense | 500 to 800 |
| gravel | 1000 to 2000 |
| rock, fissured, jointed | 1500 to 30000 |
| rock, sound | 30000 to infinity |

3. The Energy Magnification in Central Mexico City

In our approach, the load which an earthquake applies to a structure is an energy load, transmitted from the earth's surface through the foundation contact area to the building. The energy is transmitted through the earth's material by means of pressure. Energy transmission (and absorption) in the case of structural elements, including beams, plates and similar components such as volumes of deformable materials, is in the form of 'strain energy' and this is invariably inversely proportional to the tension-compression modulus of elasticity of the absorbing-transmitting material.

Thus, we assume,

$$\epsilon_{t_f} \sim \frac{1}{E}$$

in which, as noted earlier

ϵ_{t_f} = surface horizontal energy per unit area, Figure 10.13

E = modulus of elasticity of the ground material

* These are maximum bound values for the two moduli. See also the footnote on p. 206

Now, considering the special conditions present during the Mexican earthquake, we have the surface conditions as shown in Figure 10.19.

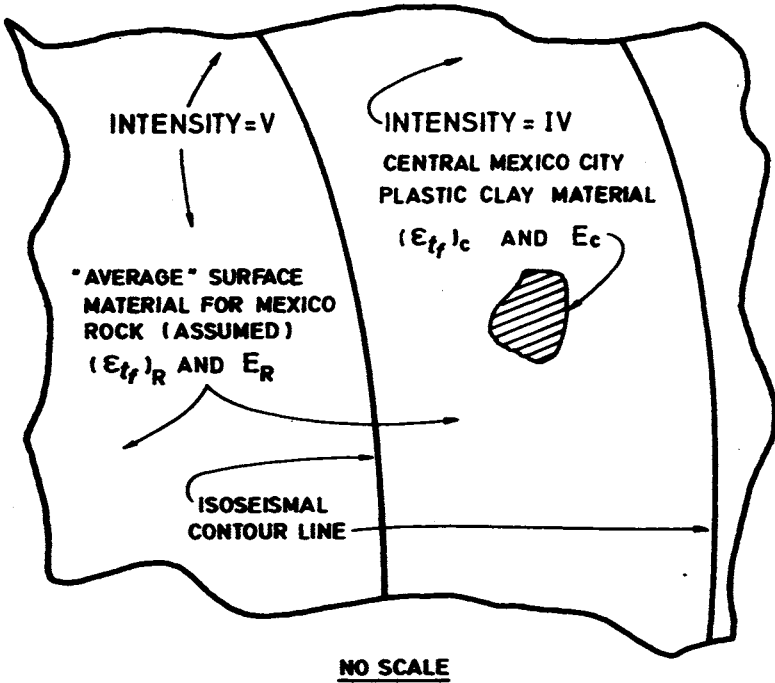


Figure 10.19 Plan View of Earth's Surface

As noted, the modulus for the average surface material is E_R and E_C for the clay of Central Mexico City. Then the energy which is *absorbed* and *transmitted* by the clay of Central Mexico City is related to the energy which is *absorbed* and *transmitted* by the adjacent 'average' rock material as

$$(\epsilon_{t_f})_c \cong (\epsilon_{t_f})_R \frac{E_R}{E_C}$$

Noting from Eq. 19 that

$$\frac{E_R}{E_C} \cong 0 (1500)$$

and from Figure 10.13, that for the 'average' Mexican geology,

$$\left(\epsilon_{t_f} \right)_{IV \text{ to } V} \cong 10^{15} \text{ ergs/sq km, say} \quad (20)$$

it follows that

$$\left(\epsilon_{t_f} \right)_C = 10^{15} (1500) = 1.5 \times 10^{18} \text{ ergs/sq km} \quad (21)$$

which indicates an *effective* intensity in Central Mexico City given by Figure 10.13 of

$$I_{eff.} = \text{Effective Intensity} \cong IX .$$

This checks the previously given value and, furthermore, corresponds to a devastating and near-catastrophic effect on structures — as indeed, did actually occur.

An additional significant behaviour pattern predicted by the rational analysis of this report which is subject to field checking, follows from the energy conservation principal basic to the analysis and is indicated in Figure 10.20.

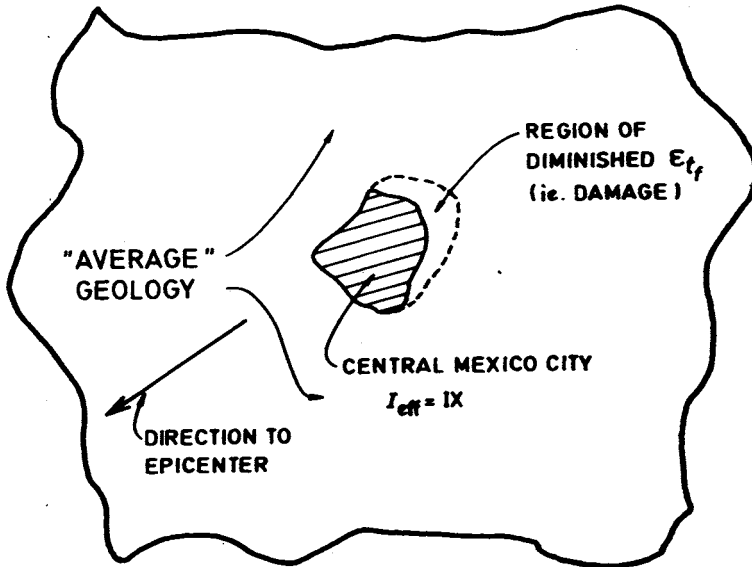


Figure 10.20

The clay pit area of Central Mexico City is an 'energy sink' absorbing energy from the 'average' geology adjacent to it and closer to the epicentre. This energy will therefore diminish the available energy adjacent to the clay pit on the far side and this effect should be observable as a region of lesser building damage, if a comparison of similar structures is made on both sides of the clay lake-bed.

4. *The Period Magnification in Central Mexico City*

As noted in the previous sub-section (3), energy absorption and transmission are the key to structural damage in our rational theory. Also, for beam, plates and other volume elements, the *period* of vibration is, in general, inversely proportional to the square root of the modulus of elasticity. Therefore, proceeding as in the last sub-section, we have

$$p_c \cong p_R \left(\frac{E_R}{E_c} \right)^{1/2} \quad (22)$$

and once more, assuming

$$\frac{E_R}{E_c} \cong 0 (1500) \quad (23)$$

we have

$$p_c \cong (38) p_r \quad (24)$$

so that if, for example, a typical value for the period in the 'average' geology is of the order 0.05–0.10 sec., then in the clay of Central Mexico City the period, p_c would be

$$2.0 \text{ sec} < p_c < 4.0 \text{ sec} \quad (25)$$

Obviously, other (field determined) values for 'average' geology and average clay values of the various parameters would give more accurate experimental values for $(\epsilon_{t_f})_c$ and p_c .*

* Thus, if it was assumed that the maximum shock magnitude was $M = 8.1$, then the 'average' intensity of the Mexico City region would be $I = V$. If, in addition, $E_R/E_c = 350$ then, see Figure 10.13, the effective intensity at the lake-bed would be $I_{eff} \cong IX$. Furthermore, the period p_c , would now be given by $p_c = 18 p_R$.

Furthermore, techniques and procedures have been developed (see Chapter 11) and applied to the structural analysis of buildings (and other elements) using the rational theories which involve all of the different parameters discussed in this section. An application of these methods to various structures (damaged and undamaged) in Central Mexico City would serve as an additional check on the theories.

Conclusion for This Section D

The rational quantitative theory has been applied to various aspects of the 19 September 1985 Mexican earthquake.

Among the results obtained in this study are

1. The original earthquake of published (single shock) magnitude 8.1 was probably either
 - a) two separate shocks each of magnitude about 7.9 separated by a 26 second interval, or
 - b) three separate shocks of magnitudes 7.7, 7.8 and 7.7, with time separations of 14 seconds between the first and second and 15 seconds between the second and third.

These results were based upon an analysis of a first preliminary form of accelerogram for Central Mexico City and may be revised based upon a later corrected accelerogram.

2. By assuming published values of ground material moduli for 'average' geology conditions in Mexico and for average soil conditions in the clay pit of Central Mexico City, it was possible to explain, quantitatively, two of the puzzling anomalous behaviours in Central Mexico City,
 - a) the long period of the accelerogram.
 - b) the great damage sustained by buildings.

Obviously, if more accurate field determined values can be obtained for the moduli these may be used to revise the numbers of (a) and (b) above.

3. The theory indicates that Central Mexico City is an energy sink and therefore predicts a region of lesser structural damage adjacent to the clay pit and further distant from the epicentre.
4. Finally, the theory predicts the strain energy which buildings in Central Mexico City should have been capable of absorbing. A study of the plans for buildings in the area would indicate, in conjunction with an elementary, straightforward strain energy analysis, whether this predicted damage agrees with the actual damage.

E) MONITORING UNDERGROUND ATOMIC BLASTS

Introduction

The rational earthquake engineering theory derived in this text determines expressions for obtaining the temporal and spacewise distribution of ground surface energy due to an underground earthquake.

If it is assumed that a dynamic mechanical energy St. Venant Principle is operative, it follows that the mechanical energy transferred from the ground surface to a superstructure (at some distance from the energy source) will be approximately the same for a) an atomic blast source and b) an actual earthquake source.

Based upon this premise, a procedure is outlined indicating how the previously obtained suitably calibrated charts, curves and equations — when used in conjunction with a relatively unsophisticated and inexpensive apparatus — will enable observers to determine the source and energy content of an atomic blast.

Notation

A_e = effective area of the structure

D = distance

I = intensity of earthquake (Modified Mercalli)

L = subscript, local

M = earthquake magnitude (Richter)

\mathcal{R}_j = designation for the major earthquake belts. The 'average' geology or geological region

S = distance from epicentre to midpoint of constant intensity band on isoseismal contour chart

E = the energy (due to the earthquake) which the structure and its contents must absorb

$$= \epsilon_{t_f} A_e$$

ϵ_{t_f} = surface horizontal energy (SHE) per unit effective area of structure at the location of the structure

a = acceleration indicated by the accelerogram

e = subscript, effective

f = subscript, final

j = subscript, a numeral

t = time

Discussion

In Figure 10.21 a schematic cross-section of the earth indicates the behaviour of the two different (but similar) phenomena:

- a) an underground atomic blast.
- b) an underground earthquake caused by, say, a rupturing plate.

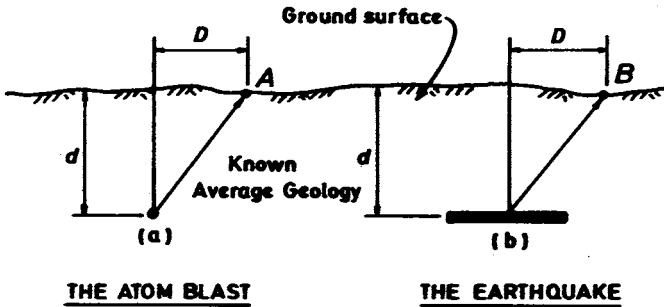


Figure 10.21

The energy content of the atomic blast consists of mechanical (stress related), chemical, heat, radiation and similar components. In this analysis we are concerned only with the *mechanical* energy and it is assumed that this (major) portion of the total blast energy can be determined for each blast. In what follows, when the world 'energy' is used in connection with the atomic explosion, it will be the 'mechanical energy' that is being referred to.

Although it is obvious that dynamic soil-rock conditions in the immediate neighbourhoods of (a) and (b) are very different from each other, if one assumes the St. Venant Principle (Ref. 17), is valid for dynamic mechanical energy phenomena (Ref. 18), then it may be assumed that mechanical energy conditions on the ground surface at A and B (each a 'large' distance r from the respective sources) will be approximately the same for the atomic blast at (a) and for the earthquake at (b), both of which have their foci at a depth d below the surface.

Thus, the energy transfer from soil to structure at A and B will be the same if the energy released at (a) is equal to the energy released by the rupturing plate at (b).

Therefore, the energy which will be absorbed by a 'structure' and the response of this structure at (a) will be the same as at (b).

The rational theory developed a series of equations and charts which predicted the surface horizontal energy (SHE) due to an earthquake that a structure would absorb in the form of kinetic and potential energy — subject, of course, to the fundamental conservation of total energy requirement.

Thus, if E is the SHE and if

$$E_a (= \text{Energy}_{(a)}) = E_b (= \text{Energy}_{(b)}) \quad (26)$$

then if $E_{(a)}$ can be determined in the field following an atomic blast at (a), we can determine the *amount* of energy of this blast by utilizing the expressions and charts obtained in the rational earthquake theory.

The detailed procedure for doing this will be described in the next section.

Procedure

A) *The Rational (Theoretical) Charts*

Four charts (which are representations of the theoretical rational equations — see Chapter 4) are the bases for the blast energy determinations. These are:

1) *The $\Sigma(IS)_f - S_f$ — Magnitude-Average Geology Chart* — typically shown in Figure 4.5 which is the current calibrated form of the chart. Knowing the average geology of the region in which the earthquake occurs, and the magnitude of the earthquake, the quantities $\Sigma(IS)_f$ and S_f may be obtained from this chart.

Having $\Sigma(IS)_f$ and S_f , then one may construct the

2) *MID Contour Chart* — This chart typically shown in Figure 4.6 represents contour areas of constant *Intensity* vs. *Distance* for a given earthquake magnitude in a region of given average geology. It is constructed by utilizing the procedure outlined in Chapter 4 using the values of $\Sigma(IS)_f$ and S_f as determined in (1) above.

A series of such charts (The MID Handbook) can be obtained from a single computer program for, say,

$$5 < M < 9$$

$$200 < \Sigma(IS)_f < 50,000$$

$$20 < S_f < 5,000$$

- 3) *The SHE/Unit effective area — Intensity Chart* — shown in Figure 4.8, will correlate the SHE at the measuring apparatus location with the intensity of the blast at the apparatus location. And finally, as a check, if an accelerogram has also been obtained at the apparatus location, then
- 4) *The $\Sigma(a\Delta t)_f - t_f$ — Intensity Chart* — Figure 4.7 may give a rough check on the intensity as determined in Step (3).

It should be emphasized — although all of the above charts are available in a quantitative form corresponding to the latest calibrations which appear to be suitable for earthquake engineering purposes (based upon many after-the-fact checks as described in this and the next chapter), as the author has pointed out several times it is desirable that a continuing calibration refinement be performed. This is strongly recommended in connection with the present applications. Indeed, it is not unlikely that much (if not all) of this calibration, assuming it is necessary, is available in the records and data of the blast tests already performed. Incidentally, because the blast sites are (presumably) in a relatively small area and the fixed apparatus sites located with reference to this blast area, the calibration could be determined fairly easily to a relatively high degree of accuracy.

B) The Apparatus

The purpose of the apparatus will be to determine ϵ_{t_f} and also the vertical energy per unit area at the apparatus site. The rational theory predicts an approximate value for this vertical energy and it would be worthwhile checking this prediction.

It would seem that a set of simple pendulums will be adequate. (Certainly, if desired or deemed necessary, quite elaborate forms of these could be used). A pendulum swinging East to West, a second pendulum swinging North to South and a third pendulum restrained to move vertically — all with suitable scribing devices will give the necessary quantitative data. These would be installed on suitably placed concrete pads of known based area, A_e . The geology of the blast region would be a relatively 'average' geology for the entire region.

The procedure then is as follows: (See Figure 10.22)

- a) The distances r_1 , r_2 and r_3 are to be determined in the 'average geology' region of the blast. This will then locate the blast site by triangulation.
- b) The SHE for each site, j , is determined from the measured (maximum) pendulum energy as

$$(\epsilon_{t_j})_j = \frac{\sqrt{(SHE_{E-W})_j^2 + (SHE_{N-S})_j^2}}{\text{Area of the Pad at } j} \quad (28)$$

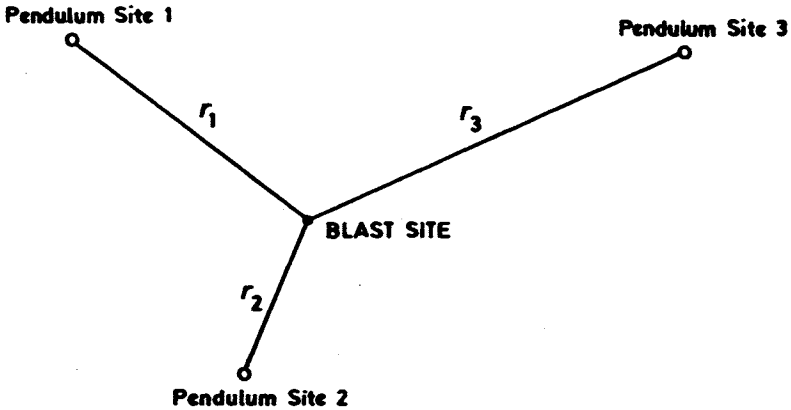


Figure 10.22 The Measuring Procedure (3 Pendulum Sites Shown)

For uniformly 'average geology' regions, these should have resultant directions approximately in the directions of r_j .

- c) From Figure 4.8 the given value of $(\epsilon_{t_j})_j$ will determine an intensity, I_j . Three values of I_j will be obtained.
- d) The problem now requires that these three values of I_j be correlated with r_j and M on an MID chart of step 2. At this point only I_j is known, as well as the locations of the three pendulum sites. From the Handbook of MID charts (Eq. 27) it should be possible to determine the value of M and the blast location such that:
 - 1) r_1, r_2 and r_3 correspond.
 - 2) The directions of $\epsilon_{t_{j_1}}, \epsilon_{t_{j_2}}, \epsilon_{t_{j_3}}$ correspond.
 - 3) As a rough check, the vertical energies at the three pendulum sites also check the approximate theoretical values, Chapter 5.
- e) Having the value of M we can determine the mechanical energy of the blast from one of the known energy-magnitude relations.
- f) Having the mechanical energy of the blast, from the known mechanical efficiency of the blast — i.e.,

$$\text{Mechanical Efficiency} = \frac{\text{Mechanical Energy of Blast}}{\text{Total Energy of Blast}}$$

we can determine the total energy of the blast.

Conclusion for This Section E

A sensor monitoring system is described for determining the energy of underground atomic blasts. The procedure utilizes two basic assumptions.

1. The applicability of a St. Venant Principle for dynamic loading phenomena, leading to
2. The assumption of the ground surface response equivalence of an underground atomic blast to an underground earthquake.

Based upon these assumptions, a simple theoretical-experimental procedure enables one to determine the energy of the blast utilizing rational earthquake theory developed in this text.

It is recommended that a continuing calibration of the rational curves and charts be performed, if necessary. It is possible that the dynamic St. Venant Principle in the form specified herein is only very roughly applicable. Under these circumstances actual field calibrations could determine charts similar to Figures 4.5–4.8 but with different numerical values.

CONCLUSION FOR THIS CHAPTER

The CONCLUSION for Chapter 11, p. 304, applies to this chapter as well.

REFERENCES FOR CHAPTER 10

1. Richard A. Kerr, *Earthquake Forecast Endorsed*, Science, Vol. 288, 19 April 1985.
2. Walter Sullivan, *Intricate Web of Sensors Enables Refined Quake Predictions*, The New York Times, April 16, 1985.
3. D. K. Keefer, 'Rock Avalanches Caused by Earthquakes: Source Characteristics', Science, Vol. 223, National Academy of Sciences, Washington, D. C. (1984), pp. 1288–1290.
4. A. R. Jumikis, *Rock Mechanics*, 2nd Edition, Trans. Tech. Publishers (1983).
5. E. Hoek, 'Rock Slopes', Proc. of Specialty Conference on Rock Engineering for Foundations and Slopes, ASCE, Univ. of Colorado, August 15–18, 1976, Vol. 2 pp. 157–171.

6. H. F. Winterkorn and H. Y. Fang, *Foundation Engineering Handbook*, Van Nostrand Reinhold (1975), Chapter 11.
7. *DM-7, Design Manual: Soil Mechanics, Foundations and Earth Structures*, U. S. Navy Navfac (1971).
8. G. Plafker, in *The Great Earthquake of 1964: Hydrology* (publication 1603, National Academy of Sciences, Washington, D. C. 1968).
9. E. L. Harp, R. C. Wilson, G. F. Wiczorek, U. S. Geologic Survey Professional Paper 1204-A (1981).
10. *Infinite Slope Analysis*, New York State Dept. of Transportation Soil Mechanics Bureau, 7.41-6, SEM 3/72, Feb. 1972.
11. Emilio Rosenblueth, *The Mexican Earthquake: A Firsthand Report*, Civil Engineering/ASCE, Jan. 1986.
12. Virginia Fairweather, *Rebuilding Mexico City*, Civil Engineering/ASCE, Jan. 1986.
13. Anon. *Research Agenda: Learning from the 19 September 1985 Mexican Earthquake*, a Joint Report Prepared by Panels from Consejo Nacional de Ciencia & Tecnologia, Mexico and Committee on Earthquake Engineering, National Research Council, USA, Jan. 1986.
14. William Stockton, *Lessons Emerge from Mexican Quake*, Science Times, N. Y. Times, Nov. 5, 1985.
15. Anon. *Mexican Quake Damage Update*, EERI Newsletter, Dec. 1985.
16. Alfredo R. Jumikis, *Soil Mechanics*, D. Van Nostrand Co., Inc. Princeton, N. J., 1962.
17. S. F. Borg, *Matrix-Tensor Methods in Continuum Mechanics*, D. Van Nostrand Co, Inc., Princeton, New Jersey, 1963 p. 143.
18. S. F. Borg, *On Saint Venant's Principle Under Dynamic Conditions*, Experimental Mechanics, Volume 1, Number 9, September 1961, p. 119.

CHAPTER 11

SOME STRUCTURAL APPLICATIONS OF THE RATIONAL THEORY

INTRODUCTION

In order to indicate the procedures and scope of the rational theory which was derived in the earlier chapters, six different structural analysis example-problems will be considered. They are:

- A) The earthquake engineering analysis of the supports for an offshore platform structure (OPS).
- B) The earthquake engineering analysis of a building with an open, ground level, column-supported parking area.
- C) The earthquake engineering analysis of a short, squat shear-type structure, $l/w \lesssim 1/2$.
- D) The earthquake engineering analysis of a low to intermediate height beam-column-girder energy absorbing structure.
- E) The earthquake engineering analysis of a tall building, $l/w \gtrsim 5$.
- F) A concrete dam earthquake analysis.

In all cases the essential theory has been developed earlier. This is used in conjunction with well-known relatively simple concepts of structural engineering. As in previous chapters, numbers are the ultimate aim — stresses, deflections, loadings etc. Having determined these, the structural engineer can proceed with the design of the structure being analyzed.

A) THE EARTHQUAKE ENGINEERING ANALYSIS OF THE SUPPORTS FOR AN OFFSHORE PLATFORM STRUCTURE (OPS)

Introduction

A series of design charts have been previously developed which relate the earthquake parameters and variables in a rational manner to the design of the pile

supported offshore structure. These include (but are not limited to)

1. The canonical accelerogram analysis and the fundamental accelerogram parameters.

An extended analysis of (1) leads to a *damage chart* at a point in terms of the accelerogram parameters, $\Sigma(a\Delta t)_f$ and t_f , as well as the *intensities* and the *geology* of the region.

2. The canonical isoseismal contour map analysis and the fundamental isoseismal parameters.

An extended analysis of (2) leads to a *damage chart* over the entire field in terms of the isoseismal parameters, $\Sigma(IS)_f$ and S_f as well as the *intensities*, the *geology of the region*, the *magnitude of the earthquake*, the *depth of the focus* of the earthquake.

For both (1) and (2), an essential *energy compatibility* relation has been obtained in which regions of a given intensity (regardless of how this is developed — i.e., magnitude of earthquake, geology etc.) have approximately the same values of ϵ_{t_f} , the energy per unit effective area (Ae) which must be absorbed by the structure.

All the above leads to rational damage assessment and also structural analysis procedures for given Code or Specification or engineering judgement values of say:

- a) A particular canonical accelerogram at a point (i.e., $\Sigma(a\Delta t)_f$, t_f), a given geological region, a given location of structure with respect to the epicentre or
- b) A given magnitude of an earthquake, with focus at a given depth, a given geological region, a given location of structure.

Other combinations of parameters may be utilized if deemed appropriate. See in this connection Chapter 8.

We shall apply these methods and concepts to the analysis of the platform support system for offshore platform structures subjected to earthquakes.

The Offshore Platform Structure (OPS)

We consider as typical, two related though different type of OPS, Figure 11.1. Both are firmly anchored to the sea-bed by means of pile supports. Thus, both structures may be assumed as 'fixed' at their lower ends.

Figure 11.1a has simple pile type supports. These may be steel sections, pipe sections filled with concrete or any other suitable structural arrangement.

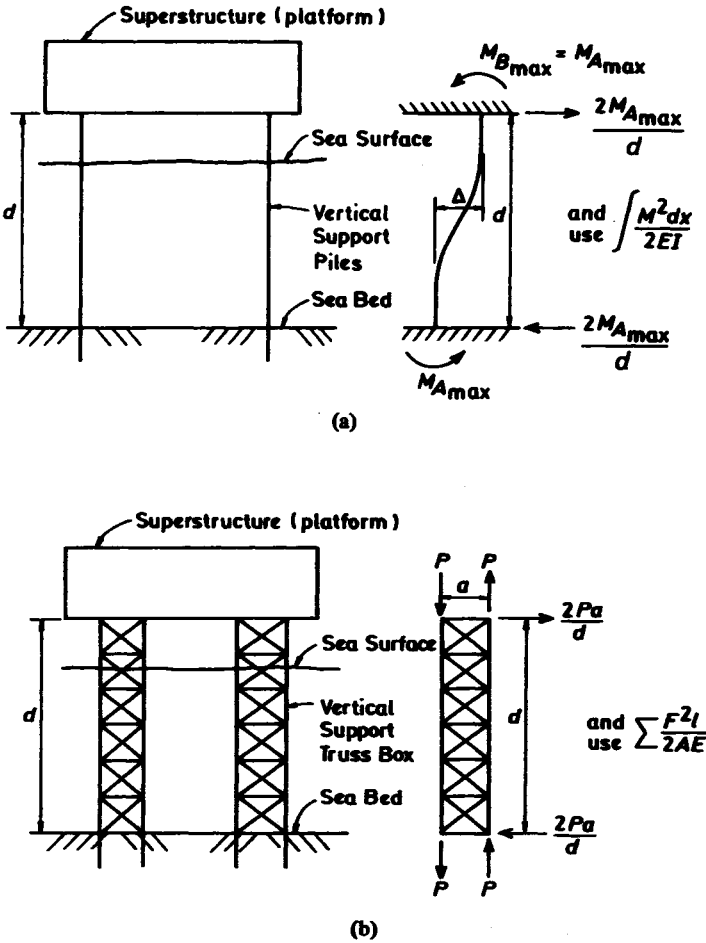


Figure 11.1 The Offshore Platform Structures (OPS)
(Full Fixity Conditions Shown)

Figure 11.1b has box-truss type supports as indicated.

For both types it is suggested, for the earthquake design condition, that at the junction of platform and vertical support members there be a network grillage of steel beams with essentially full-fixity type moment connections capable of absorbing and transferring energy to surrounding members. There will then be a small (but finite) rotation of the connection, a rotation which will carry structural deformation (and energy) away from the junction area out into the grillage and other supporting structures.

The fixity range, F , is given by the following condition

$$0 \leq F \leq 1$$

in which the lower limit assumes zero moment transmitted to the top grillage assembly and the upper limit assumes full fixity at the upper grillage. Neither limit can be achieved in practice.

It follows therefore that — approximately — and most conservatively, insofar as the vertical supports are concerned, we may consider the vertical support structure as built-in at both top and bottom when subjected to sea-bed horizontal energy inputs, as shown in Figure 11.1

Based upon the engineer-designer's judgement, intermediate values of fixity may be assumed and designed for without difficulty, using the data of Figure 11.2 and Table 1.

Table 1 Column Fixity Table

| $F = \frac{M_B}{M_A} = \text{FIXITY}$ | | | |
|---------------------------------------|--------------------------|----------------------|--|
| $\frac{M_B}{M_A}$ | $\frac{M_A}{M_{A \max}}$ | $\frac{E}{E_{\max}}$ | Strain Energy to Connecting Structure at Top |
| 1 | 1 | 1.0 | 0 |
| 3/4 | 4/5 | 0.52 | $0.48 E_{\max}$ |
| 1/2 | 2/3 | 0.33 | $0.67 E_{\max}$ |
| 1/4 | 4/7 | 0.27 | $0.73 E_{\max}$ |
| 0 | 1/2 | 0.25 | $0.75 E_{\max}$ |

These are the key points, in the development of the proposed analysis and when used in conjunction with the curves, charts and parameters discussed in Chapter 4 this leads to a relatively simple, straightforward, rational, easily visualized physical-engineering design analysis.

The Approximate Design Analysis

The parameters for a particular earthquake, such as magnitude, depth of focus, location of epicentre, geology, OPS location and preliminary structural design have been formulated by code, specifications, governmental agency or engineering designers.

Therefore, the total sea-bed horizontal energy which the structure must absorb can be determined. Call this total energy E . It is applied — timewise —

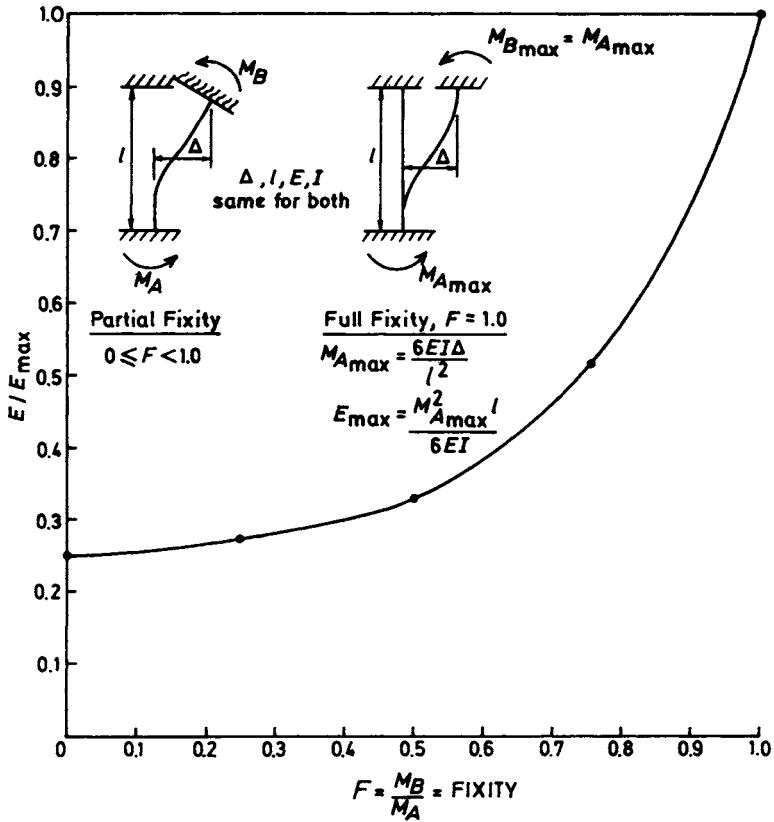


Figure 11.2

as indicated in Chapter 4. However, as pointed out there, the analysis suggests that practically all of the energy is applied in a relatively short time period following the onset of the earthquake effect. Thus conservatively, assume *all* the energy is applied to the structure in a single packet at time $t = 0$.

This energy — which must be absorbed by the structure — is transformed into kinetic (vibratory) energy and potential (strain) energy.

Also — because of the special construction and structural behaviour as given in the previous section, we shall assume that the response of the structure is as follows:

1. A known amount of energy (sea-bed, horizontal energy) E , is applied to the structure. For four support legs, each support is assumed to absorb $E_{\max} = E/4$.
2. This total energy per support is assumed (conservatively) to be applied in a single lumped package, timewise.
3. This energy is absorbed by the structure in a combined vibratory (moving)-deformation (stationary) response.
4. The movement of the structure — because of the special construction features and conservative assumption previously outlined consists of:
 - a) A deformation of the vertical support legs as the structure moves from side to side.
 - b) An assumed essentially *rigid body movement* from side to side of the platform.
5. The kinetic energy of the rigid body platform (4b) varies from a maximum (greatest velocity) when the legs are in their nearly undeformed vertical position to a minimum (zero velocity) when the legs and supporting grillage are in their maximum deformed position.
6. Assuming the major mode of vibration only is important (this also is probably a conservative assumption), the maximum kinetic energy may be equated to the maximum potential i.e. strain energy in any cycle.
7. From cycle to cycle energy is damped (i.e., removed) from the OPS by the water, internal friction and other similar damping mechanisms.
8. Thus — the *initial* cycle, which involves the total energy input, is the critical one and this will govern the design.
9. We consider the two commonly used vertical support systems, Figures 11.1a and 11.1b.

For Figure 11.1a, the vertical supports are in their maximum deformed (maximum strain energy) position when the platform is in its zero velocity position. As noted, we may, conservatively assume full fixity at the top (as well as at the bottom) and use an effective length of support equal to d . Knowing the energy which must be absorbed (assuming bending strain energy only — if shear is to be considered it can be included without difficulty) we have:

$$E_{\max} = \text{Strain Energy} = \int \frac{M^2 dx}{2EI} \text{ for each member.}$$

from which M can be determined and the additional stress in the pile support due to earthquake loading, calculated.

As stated earlier, the assumption of full fixity at the top is a conservative one since some portion of the platform structure will surely deform and absorb some strain energy. However, it is suggested that the platform grillage connecting structure and the connections be designed as energy absorbing mechanisms for full end fixity as a matter of sound engineering practice. The additional fail-safe factor will be significant for a modest economic outlay. However, if the engineer-designer desires, intermediate values for the required parameters may be assumed and the design performed accordingly, using Figure 11.2 and Table 1.

Figure 11.1b shows a typical truss box support structure and here again the maximum strain energy is known, and once more an equivalent full fixity condition (and corresponding grillage connection details) as well as effective depth d may be assumed as shown in the figure. The strain energy will be the usual simple tension — compression bar values or, if deemed necessary, secondary stresses (moments) in the truss members can be determined and the combined bending, normal and shear energy expressions can be used.

Conclusion for Section A

A rational procedure for the approximate structural design of an OPS subjected to earthquake loadings has been presented.

The method considers — as input data — the physical and engineering parameters directly related to the earthquake event, which terms should therefore be part of any rational analysis. Furthermore, the theory develops *quantitative* measures of the important earthquake loading factors.

The entire process is very strongly founded on engineering-physical reasoning and in common with all engineering design theories contains the equivalent of design 'allowables' which can only be determined by field or laboratory testing. These parameters, when evaluated for earthquake regions all over the earth, may then be utilized along with elementary engineering concepts to permit straightforward, routine application by ordinary engineering design offices.

In the meantime (and until these worldwide determinations have been made), an approximate form of all of the necessary terms is available. These have been checked in some preliminary analyses and can be utilized subject to the given approximation.

Obviously the procedure outlined in this section could also be used for *land-based* structures consisting of columns supporting nearly-rigid upper structures. Some computations for a typical building structure of this type will be presented in the next Section B of this chapter.

B) THE EARTHQUAKE ENGINEERING ANALYSIS OF A BUILDING WITH AN OPEN, GROUND LEVEL, COLUMN-SUPPORTED PARKING AREA*

Introduction

In this Section, we shall apply the rational method of earthquake analysis to a typical mid-height (~50 ft) reinforced concrete building with an open street-level area suitable for parking, see Figure 11.3.

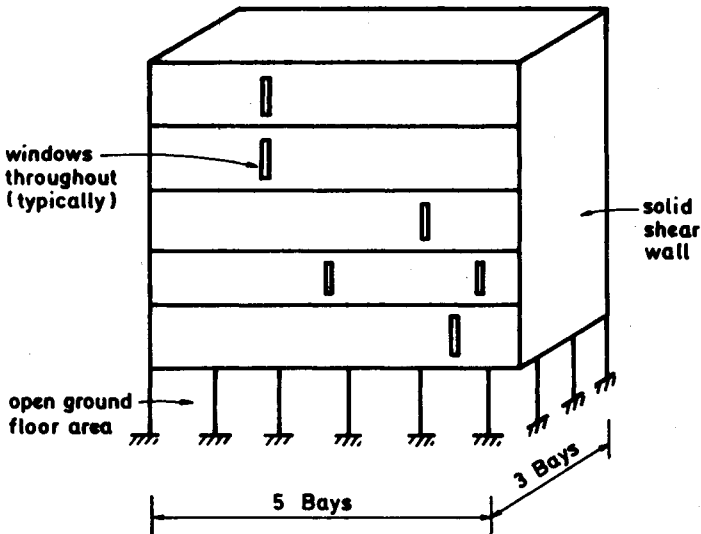


Figure 11.3 Schematic Sketch of Assumed Building

Because of its structural geometry, the upper floors behave essentially as a 'lumped mass' supported by the first story columns. With respect to the rational theory this simplifies the structural analysis, since as the building oscillates back and forth during the earthquake loading, because of energy conservation the strain energy in the first story columns can be determined at various intervals. The critical time is at the extreme end of the first oscillation, at which time the velocity of the column and superstructure is assumed to be zero, and all the energy is stored as strain energy in the column. At this point, damping has removed very little energy from the vibrating system. Hence, as a conservative assumption, the total energy supplied by the earthquake event will be assumed

* The author acknowledges the assistance of John Schuring in performing the analysis computations for this section.

to be input at this instant and will be assumed as absorbed by the columns and the adjacent structure — see the later discussion of ‘fixity’.

A number of reasonable assumptions regarding the dimensions of the building and its components will be made. These will be stated when they occur in the analysis.

All steps in the analysis will be shown in detail, including most of the computations. This is done in accordance with one of the three main purposes of this investigation, as follows:

1. To show, in detail, how one would apply the rational theory, from the instant the earthquake energy has reached the surface of the earth to the time that this energy has been absorbed by the structure.
2. To further calibrate several of the major parameters introduced in the new theory. In common with all theories in engineering, in this earthquake engineering theory certain ‘allowables’ and similar calibrations of fundamental parameters are needed before the engineer can apply the theory to actual design-investigation problems. In this section B a typical building is considered and the damage that it sustains, in the given earthquake, is similar to that which has occurred in a number of similar earthquakes to similar structures. Thus, the analysis is, in a sense, a calibration exercise for various parameters in the event. In particular, we shall use numerical values of the energy-intensity compatibility curve and also a numerical value for the ‘effective area’, A_e .
3. Finally, to indicate how the new theory accounts, to a suitable degree of accuracy, for some of the major behaviour and failure patterns for buildings of the type considered (Figure 11.3) when subjected to earthquakes of the given strength in the \mathcal{R}_3 geology.

In order to present the analysis in necessary detail, all computations, discussions and equations will be given in a step-wise form, more or less in the form which an engineering office might use in an actual design or investigation.

All of the methods, equations and procedures are either covered in earlier chapters and sections of the text or are included in elementary structural theories well known to structural engineers.

It should be noted that a number of geometric and physical property assumptions have to be made. Obviously other assumptions would lead to different results. But, the assumptions made are reasonable and realistic and the numerical results obtained are consistent with the behaviour of structures of the type considered when subjected to earthquake events as in this exercise.

The Analysis

We assume a single shock of strength $M = 6.4$ in an \mathcal{R}_3 geology. The building is as shown in Figure 11.3 and is assumed to be 10 km from the epicentre. Note, although, the basic earthquake parameters are assumed here for illustrative computational purposes only, the method to be described may be applied to an actual case.

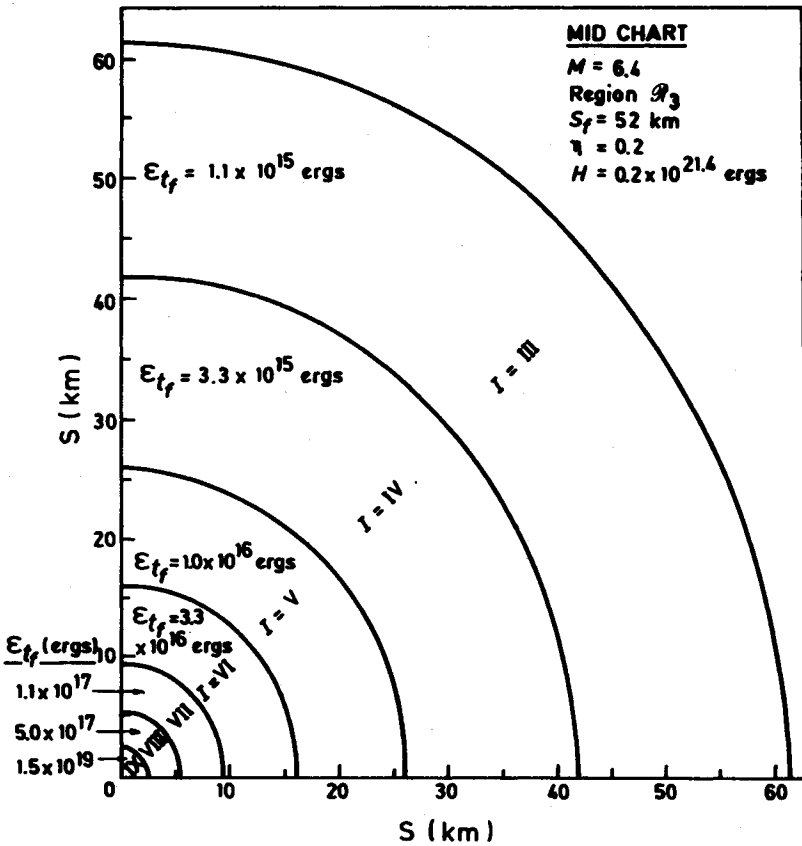


Figure 11.4

STEP 1 From Figure 4.5, we determine S_f and $\Sigma(IS)_f$. Then proceeding as in Chapter 4 we determine the MID diagram for this earthquake. This is shown in Figure 11.4. Also shown are the compatible ϵ_{f_f} values for the assumed magnitude-energy-intensity condition, see typically, Figure 4.8 and 10.2.

STEP 2 Estimate the moment capacity of the assumed reinforced concrete column, Figure 11.5.

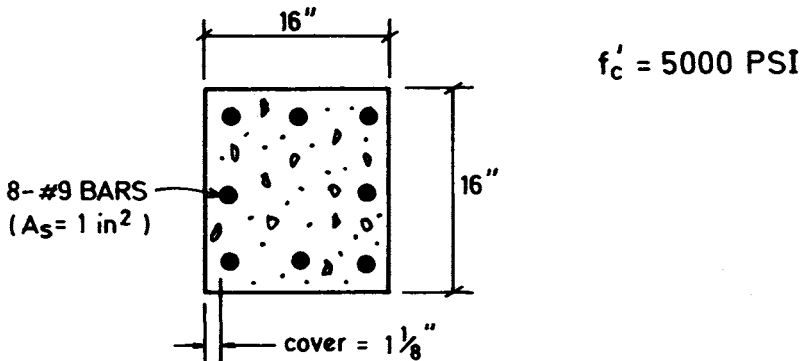


Figure 11.5

The column shown is a reasonable one for the given building.

The 'equivalent area' method will be used for the approximate analysis. We will assume the compressive stress due to the vertical service load is 2500 PSI. The assumed mode of failure will be compressive, i.e. the column will be assumed to begin to 'fail' when the concrete on the compression face crushes at its extreme fiber. This is considered the critical mode of failure since the steel on the tension side is capable of plastic elongation. The failure will begin when the compressive stress on the compression face reaches, say, 5000 PSI, or when the extreme fiber stress in bending due to the earthquake moment reaches 2500 PSI as shown on Figure 11.6. Although this is assumed to correspond to the onset of overstressing, it is considerably less than the value of the stress corresponding to the 'shattering' condition which seems to occur in some of the column failures due to earthquakes for buildings with this type of street-level construction. It must also be recognized that a failure or shattering stress for a vibrating structure is generally higher than the value for a stationary structure.

Analysis and Result:

Compute equivalent concrete A_{eq} and I for the steel:

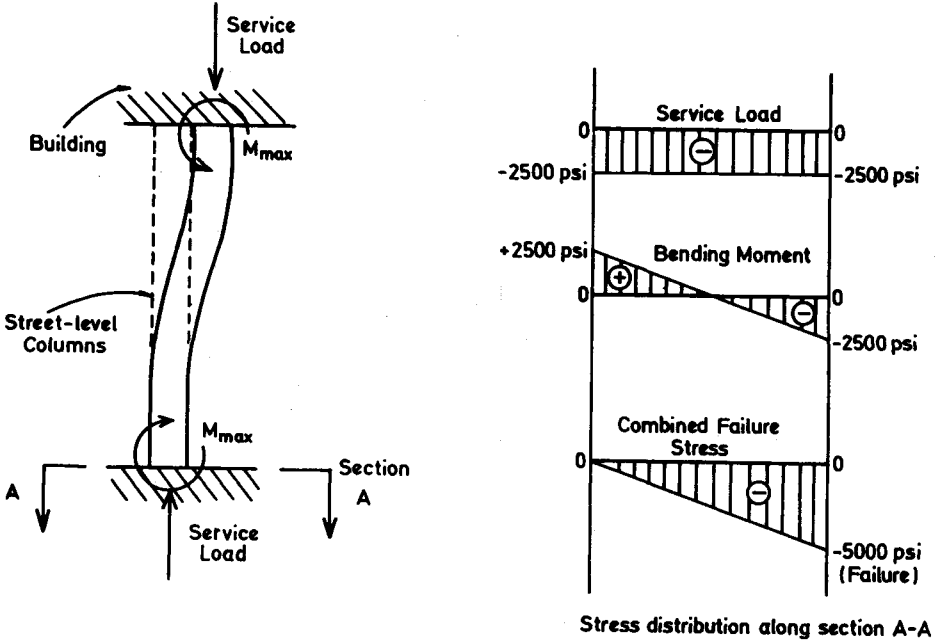


Figure 11.6

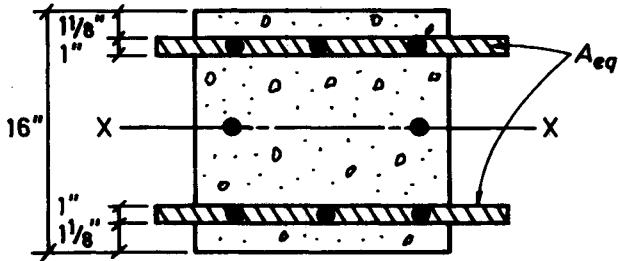


Figure 11.7

$$A_{eq} = (3 \text{ BARS}) (1 \text{ in}^2) \left(\frac{29,000,000}{2,900,000} \right) \quad (1)$$

$$= 30 \text{ Sq. In.}$$

$$\text{Total Equiv. } I_{eq} = 8000 \text{ in}^4, \text{ approximately} \quad (2)$$

Assuming crushing failure for the vibrating column starts when $f_b = 2500 \text{ PSI}$, we get:

$$M = \frac{f_b I_{eq}}{C} = \frac{2500 (8000)}{8} = 2,500,000 \text{ in-lb} \quad (3)$$

$$= 200,000 \text{ ft-lb}$$

Summarizing, we have:

$$\left. \begin{array}{l} \text{Moment Capacity} \\ \text{of Column} \end{array} \right\} = M_{cap} = 200 \text{ ft-kips} \quad (4)$$

which is the moment for the onset of crushing failure.

STEP 3 Determine the maximum moment delivered to the column by the earthquake assuming full fixity both top and bottom.

Method

Using the data developed in Step 1 the design value of ϵ_{tf} for this site will be determined. This will allow an estimate of the energy delivered to each column using the general strain in bending relationship:

$$\text{Strain Energy} = U = \int_0^l \frac{M^2 dx}{2EI} \quad (5)$$

Analysis and Result:

Find ϵ_{tf} :

For magnitude = 6.4, we get, assuming the energy-magnitude equation of the following form,

$$\left. \begin{aligned} \log_{10} E &= 15 + 1.0M = 21.4 \\ \text{or } H &= \eta E = (0.2)(10^{21.4}) \end{aligned} \right\} \quad (6)$$

Then, from Figure 11.4

$$\text{for } s = 10 \text{ km, } \epsilon_{t_f} \cong 4.8 \times 10^{16} \text{ ergs/km}^2$$

(This value could also have been obtained directly from Figure 4.8 using the intensity VI or VII at 10 km from Figure 11.4)

Estimate the Energy per Column:

We will assume only the areas of the footings are included in A_e . If one analyzes the physical factors involved, this emerges as a more reasonable assumption than the 'full building area' assumption which was recommended in *EE-DA&SD*.

To determine A_e :

The building will be assumed to be supported on spread footings. Since it was earlier stated that the stress in the 16 in. square column due to service loads was 2500 psi, the size of the footing can be inferred as follows:

$$\left. \begin{aligned} \text{Assumed Allowable} \\ \text{Soil Bearing Pressure} \end{aligned} \right\} \cong 10.0 \text{ KSF} \quad (7)$$

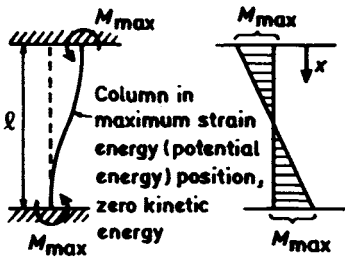
$$\text{Column Load} = (2500 \text{ psi})(320) \text{ in}^2 \cong 800 \text{ kips approx.} \quad (8)$$

$$\therefore \text{Footing Area} = \frac{800 \text{ kips}}{10} \cong 80 \text{ Ft}^2 = A_e \text{ per column} \quad (9)$$

$$\left. \begin{aligned} \text{Energy per} \\ \text{Column} \end{aligned} \right\} = \epsilon_{t_f} \times A_e \quad (10)$$

$$\cong 25,000 \text{ ft. lb.}$$

The strain energy in the column, in the full fixity top and bottom condition is obtained as follows:



Strain Energy in Bending

$$U = \int_0^l \frac{M^2 dx}{2EI}$$

$$= \int_0^l \frac{1}{2EI} \left[\frac{M_{\max} \left(\frac{l}{2} - x \right)}{l/2} \right]^2 dx \tag{11}$$

$$M_x = M_{\max} \frac{(\ell/2 - x)}{\ell/2}$$

$$U = \frac{M_{\max}^2 \ell}{6EI}$$

or

$$M_{\max} = \sqrt{\frac{6UEI}{\ell}}$$

Analysis and Results

Note: For the purposes of clarity, all moment capacities and delivered moments will be expressed as stresses using the Bernoulli-Euler relation

Extreme bending stress = $f = Mc/I$

Then $M_{\text{capacity}} = 200 \text{ ft-kips}$, as before, and

$$f_{\text{moment capacity}} = \frac{Mc}{I_{eq}} = 2500 \text{ psi},$$

or $f_{\text{ultimate}} = 2500 + 2500 = 5000 \text{ psi}$ (12)

and this is assumed to be the stress for the onset of failure.

Using $U = 25000 \text{ ft-lb}$ which is the previously obtained energy per column delivered by the earthquake we get:

$$M_{\max} = \sqrt{\frac{(6)(25,000)(2,900,000)(144)(8000)}{(10)(12^4)}} \cong 1400 \text{ ft-kips} \quad (13)$$

Moment delivered by the earthquake = $M_{\max} = 1400 \text{ ft-kips}$,

Note: Once more it is pointed out that this value of M_{\max} , the moment at the *base* of the column (and also the top assuming full fixity at both ends) is based upon the assumption that A_e , the effective area (and a fundamental parameter in this rational theory) is equal to the area of the foundations only. One of the important and significant results of this example analysis study is a strong indication that this assumption is a reasonable one.

It is assumed that all the columns and footings for the building are the same size. Actually, the interior columns and footings are probably larger than the outside ones since they support more load. This assumption is not unreasonable, however, since both the moment of inertia *and* footing size will increase as the load on the column is increased, thus maintaining some degree of proportionality.

Two final major assumptions must be made before the final computations are obtained.

The first has to do with the observed fact that in many cases (and this is true for the present example for the assumed magnitude and distance from the epicentre) there is a complete 'shattering' of the column requiring that the entire structure be torn down. We wish to make a 'reasonable' assumption concerning this — essentially — *modulus of rupture* or shattering stress. Clearly this is a subjective judgement assumption. However, from the known behaviour of concrete tested to complete shattering failure in compression, a reasonable value would appear to be of the order of about 15,000 psi as determined from the Bernoulli-Euler relation. Note, too, that the maximum stress is a transient value corresponding to the vibratory motion of the column. This would generally result in a higher value for the shattering stress.

Thus we shall assume that for stress larger than 15,000 psi, complete shattering occurs. For lower loads, although failure may result, various modes of less catastrophic behaviour occur.

The second major assumption involves the *fixity* of the columns.

Owing to the fact that the shear wall-column connections would be stiffer than the other top column connections, the fixity conditions shown below were assumed for the column connections.

The definition and development of the fixity factor 'F' as shown below in Figure 11.8 will be assumed. For a more complete discussion of the 'fixity' effect, see Section A of this chapter. For convenience we repeat below Table 1 of Section A.

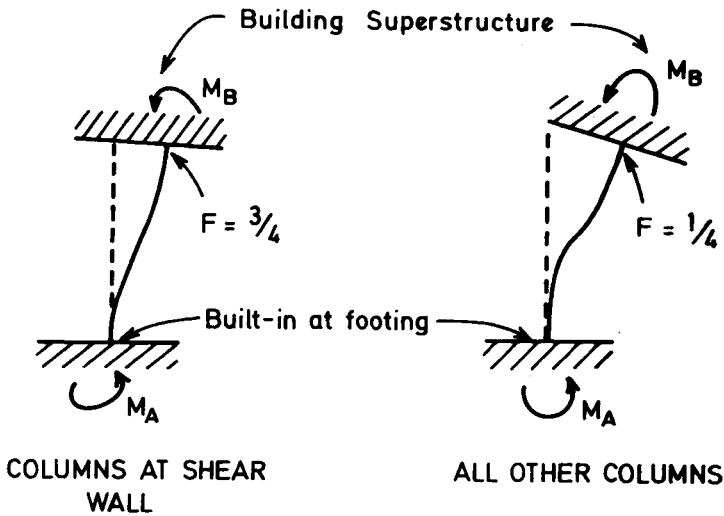


Figure 11.8

Table 1 Column Fixity Table

| $F = \frac{M_B}{M_A} = \text{FIXITY}$ | | | |
|---------------------------------------|--------------------------|----------------------|--|
| $\frac{M_B}{M_A}$ | $\frac{M_A}{M_{A \max}}$ | $\frac{E}{E_{\max}}$ | Strain Energy to Connecting Structure at Top |
| 1 | 1 | 1.0 | 0 |
| 3/4 | 4/5 | 0.52 | 0.48 E_{\max} |
| 1/2 | 2/3 | 0.33 | 0.67 E_{\max} |
| 1/4 | 4/7 | 0.27 | 0.73 E_{\max} |
| 0 | 1/2 | 0.25 | 0.75 E_{\max} |

The calculations for the moments follow:

Shear Wall Columns:

$$\text{Use } F = 3/4$$

$$\begin{aligned} \text{which leads to } M_A &= 0.80 M_{\max} = (0.80)(1400) = 1120 \text{ ft-kips} \\ M_B &= 0.75 M_A = (0.75)(1120) = 840 \text{ ft-kips} \end{aligned} \quad (14)$$

All other columns:

$$\text{Use } F = 1/4,$$

$$\begin{aligned} \text{which leads to } M_A &= 4/7 M_{\max} = (4/7)(1400) = 800 \text{ ft-kips} \\ M_B &= 0.25 M_A = (0.25)(800) = 200 \text{ ft-kips} \end{aligned} \quad (15)$$

Then using the Bernoulli-Euler equation to determine stresses we obtain the following Table 2 summarizing the final column stresses in psi:

Table 2 Column Stresses

| Location | Top | Bottom |
|------------|------------|------------|
| Shear Wall | 12,500 psi | 16,000 psi |
| Others | 4,900 psi | 12,000 psi |

The numerical values for the stresses in Table 2 are obviously merely an approximate measure of relative damage behaviour.

The table indicates that with our assumptions only the base of the shear wall column will shatter. This agrees with field observations for some earthquakes and buildings of this type.

Conclusion for Section B

The results of the foregoing analysis indicate that the moment capacity of the columns and the moment delivered to the failed columns by the earthquake are of the same order of magnitude. The 'calibration' performed in this respect is encouraging, but in view of the uncertainties in the analysis, these results will require further verification before the rational theory can be used in actual

design with complete confidence. As a first step, it would be helpful to obtain actual construction details of various shattered buildings of the type considered as well as the detailed post-earthquake damage reports.

It is ironic to note that according to this theory a contributing factor for the failure of the columns along the shear wall was the fixity afforded by the shear wall itself. The recently reported trends in earthquake regions of using more flexible, energy absorbing details seem appropriate.

The analysis indicates that for this type of building the key uncertainties which most affect the results are the intensity vs. ϵ_{t_f} relationship, the effective area, A_e , and the column fixities. Special efforts are being made to refine these variables by continued analysis of existing data.

C) THE EARTHQUAKE ENGINEERING ANALYSIS OF A SHORT SQUAT SHEAR-TYPE STRUCTURE, $l/w \lesssim 1/2$

Introduction

On March 20, 1984, a large earthquake occurred in the vicinity of Gazli, in Soviet Central Asia. A rather complete dispatch in the New York Times of March 21 described regions of various intensities, damage and similar after-the-fact data.

As another application of the rational theory of earthquake engineering of this text, a complete analysis is made of the earthquake event starting with the ground shaking (i.e. after the 'mechanism'). The theory predicts damage, regions of constant given intensity and furthermore leads to a method of structural analysis — based upon fundamental conservation of energy principles — that can easily and reasonably be applied to the region and structures in question.

The complete detailed analysis is given in this section, including the intensity regions, energy distribution and a structural analysis procedure. For approximate quantitative and illustrative purposes, only a very simplified short, squat (shear-type) structure will be considered and the effect of an earthquake on such a structure throughout the earthquake field will be determined. Obviously such an analysis can only give relative comparative values — a single simplified structure cannot be truly representative of the construction throughout a region of many thousands of square miles. However, it is still possible to obtain some approximate correlations between theory and the actual damage and this will be done. Furthermore, the computational procedure for any given earthquake

* The author wishes to thank S. M. Shankil and M. K. Shakid, graduate students in Civil Engineering at Stevens Institute of Technology for assisting in the computations involved in this analyses.

and similar shear structure will be given in some detail so that an analysis can be made for an actual event and structure.

Procedure

The given earthquake data upon which the analysis is based are:

1. A magnitude on the Richter scale, of 7.5 to 8. Although this fact is not expressly stated in the reports, it appears to be a reasonable assumption based upon the descriptive material average geology is R_3 .
2. The epicentre is near Gazli, about 50 miles northwest of Bukhara.

Using the rational procedures, charts and equations of Chapter 4 the effects of an earthquake corresponding to the above will be determined. Locations and extents of regions of given intensity will be determined. Surface ground energies over the entire region will be obtained and a typical rural type habitat will be assumed. This structure will be analyzed in various intensity-energy regions and a damage comparison will be made with the press reports. It will be seen that a qualitative-quantitative agreement between the two damage assessments is obtained for the assumed type of structure.

The Assumed Building

It will be assumed that a typical rural building in the region of the earthquake is as shown in Figure 11.9. In addition:

1. The structure is residential, of local masonry material. It is, clearly, for our purposes a short, squat, shear-type structure.

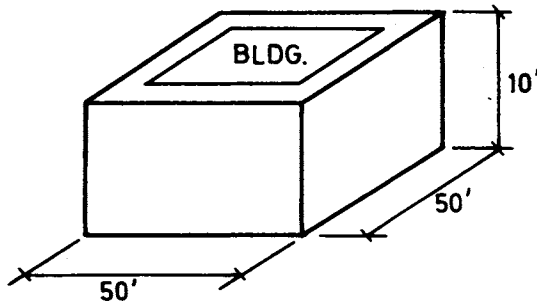


Figure 11.9

2. The wall thickness is 12" all around
3. Cross-sectional area of the wall is

$$\begin{aligned}
 A &= 50(50) - (48)(48) \\
 &\cong 200 \text{ sq. ft.}
 \end{aligned}
 \tag{16}$$

4. Base area is $50(50) = 2500 \text{ sq. ft.}$ (17)

5. Footing area, A_f , assuming 15" wall footings, is given by:

$$\begin{aligned}
 A_f &\cong 200(1.25) \text{ sq. ft.} \\
 &= 250 \text{ sq. ft} \\
 &= 22.5 \times 10^{-6} \text{ sq. km.} \\
 &= Ae
 \end{aligned}
 \tag{18}$$

6. Shear modulus $G = 2.5 \times 10^6 \text{ psi}$
 $= 3.6 \times 10^6 \text{ psf}$ (19)

7. It will be assumed that a computed shear stress,

$$\tau = \frac{V}{A}
 \tag{20}$$

which has a nominal value \lesssim about 3000 psi corresponds to a 'shattering' or catastrophic condition. We recall that the maximum stress condition is a transient stress caused by the vibratory to and fro motion.

Detailed Computations

1. Using the charts and procedures of Chapter 4, we obtain the following Table 3 for $M = 7.5$ and $M = 8$ earthquakes, for an R_3 region.

Table 3

| M | $\Sigma(IS)_f$ | S_f (km) |
|-----|----------------|------------|
| 7.5 | 4345 | 350 |
| 8.0 | 9000 | 600 |

This data was fed into the computer program representing the solution of the canonical isoseismal equation

$$\frac{\sum(IS)}{\sum(IS)_f} = e^{2[1 - (S_f/S)^{1/2}]} \quad (21)$$

giving the results which are summarized in Tables 4 and 5 for the given magnitudes.

Table 4

| | Intensity Region | S_{av} (km) | IS_{av} | $\Sigma(IS)_f$ | Distance to Outer Reach (km) |
|-----------|------------------|---------------|-----------|----------------|------------------------------|
| $M = 7.5$ | X | 3.83 | 38.30 | 4345 | 12 |
| | IX | 20.83 | 187.47 | | 30 |
| | VIII | 39.05 | 312.40 | | 52 |
| | VII | 64.48 | 451.35 | | 83 |
| | VI | 101.49 | 608.94 | | 129 |
| | V | 156.33 | 781.65 | | 197 |
| | IV | 237.29 | 949.16 | | 294 |
| III | 350.00 | 1050.00 | 463 | | |

Table 5

| | Intensity Region | S_{av} (km) | IS_{av} | $\Sigma(IS)_f$ | Distance to Outer Reach (km) |
|---------|------------------|---------------|-----------|----------------|------------------------------|
| $M = 8$ | X | 33.29 | 332.40 | 9000 | 47 |
| | IX | 59.67 | 537.03 | | 77 |
| | VIII | 94.85 | 758.80 | | 119 |
| | VII | 143.41 | 1003.87 | | 177 |
| | VI | 211.45 | 1268.70 | | 259 |
| | V | 306.80 | 1534.00 | | 372 |
| | IV | 436.80 | 1747.20 | | 519 |
| III | 600.00 | 1800.00 | 682 | | |

Figures 11.10 and 11.11 show the MID diagrams corresponding to Tables 4 and 5. The circles representing distances to outer reach for each intensity are obtained by taking half of the S_{av} values for adjacent intensities. Thus, for distance to outer reach of the $I = VIII$ band, we have (for $M = 7.5$),

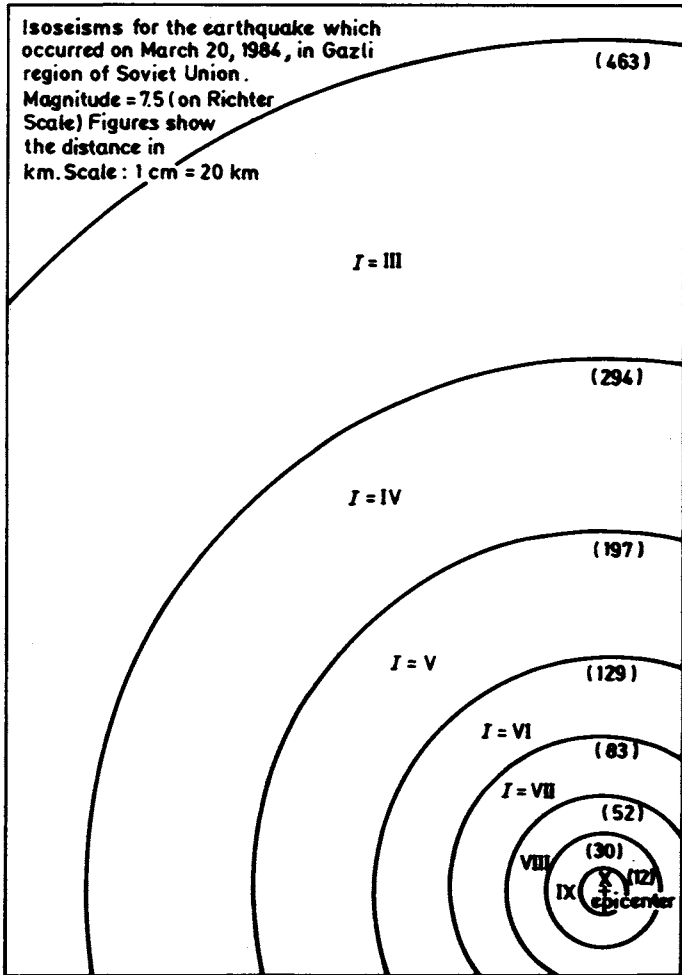


Figure 11.10

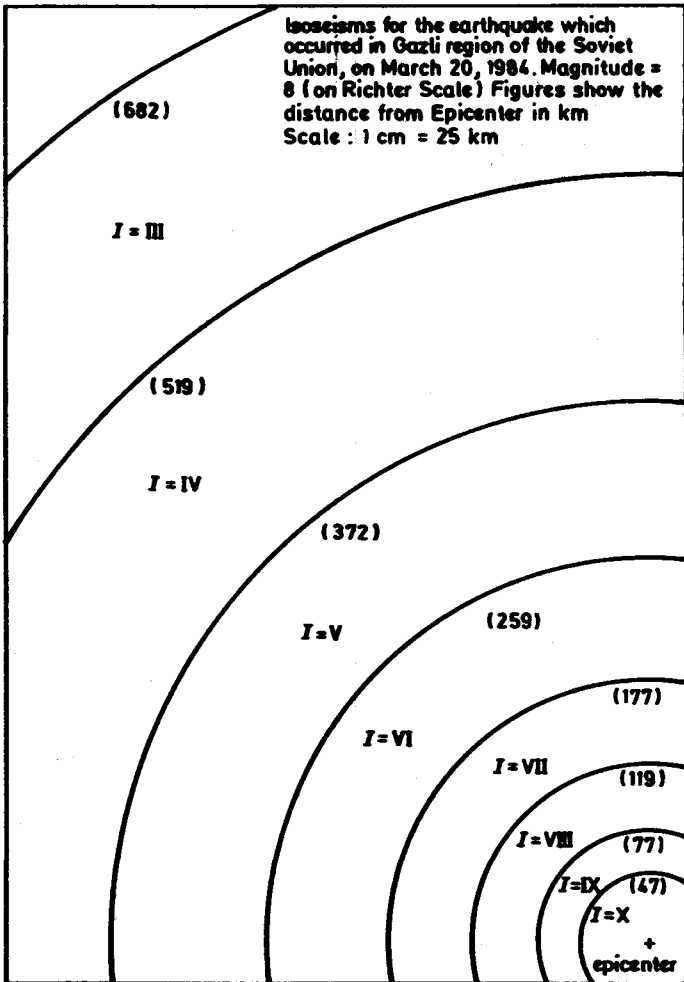


Figure 11.11

$$\begin{aligned}
 S_{\text{VIII Outer Reach}} &= S_{\text{VIII}_{av}} + \frac{S_{\text{VII}_{av}} - S_{\text{VIII}_{av}}}{2} \\
 &= 39 + \frac{64.5 - 39}{2} \\
 &= 52 \text{ km}
 \end{aligned}
 \tag{22}$$

Figure 11.12 shows the intensity-horizontal surface energy compatibility relations (repeated from Chapter 4, Figure 4.8). Using this chart, we obtain values as shown for the total strain energy the building must absorb at the different intensity values, Table 6.

As pointed out previously, the building will be analyzed as a short, squat structure. Hence all the energy must be taken as simple shear strain energy, and the maximum strain (and hence stress) will occur in one of the very early cycles. Thus, conservatively, we assume *all* the energies noted are to be taken as shear strain energy (damping effects neglected) and we have, see Table 6

$$U_{\text{total}} = K \int_0^{\ell} \frac{V_x^2 dx}{2AG}
 \tag{23}$$

where:

U_{total} = total energy to be absorbed by the structure in shear strain energy, equals $\epsilon_f A_f$

V_x = shearing force at any height x in the structure V_{max} will occur at the base

V_x = $x/\ell V_{\text{max}}$, assumed linear shear distribution

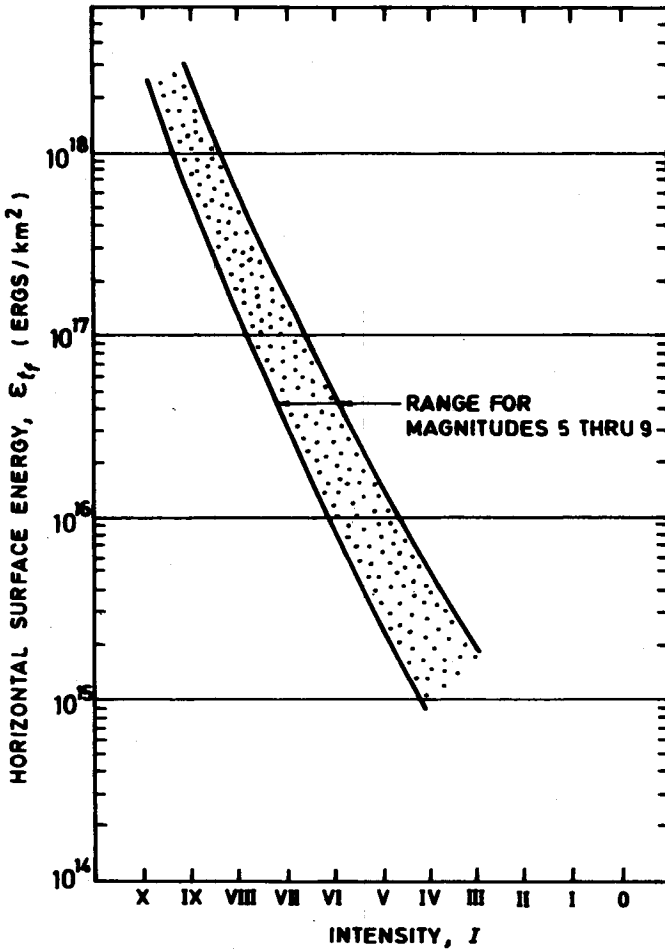
ℓ = height of the structure

A = area of the building wall

G = shear modulus

K = form factor, assumed equal to unity

Note, the effective area is the *actual* footing area — i.e., the area of the building which is in contact with the ground. Also ϵ_f values near the centre of the band are used for each intensity.



Earthquake Intensity vs. Horizontal Surface Energy

Figure 11.12 Earthquake Intensity vs. Horizontal Surface Energy

Table 6

| Intensity Region (MM) | ϵ_{tj} , ergs/km ² | $U_{\text{total}} = \frac{\epsilon_{tj} \times A_j}{10^7}$, ft lb |
|--------------------------|--|--|
| III | 1.8×10^{15} | 4×10^3 |
| IV | 4.5×10^{15} | 10×10^3 |
| X | 1.3×10^{16} | 29×10^3 |
| VI | 3.5×10^{16} | 8×10^4 |
| VII | 9.0×10^{16} | 20×10^4 |
| VIII | 3.0×10^{17} | 7×10^5 |
| IX | 1.3×10^{18} | 29×10^5 |
| X | 6.6×10^{19} | 14×10^7 |

Using the values in Table 6 we can obtain, from the elementary shear strain energy relation,

$$V_{\text{max}} = \sqrt{\frac{6AG}{\rho}} U_{\text{total}} \quad (24)$$

A typical computation for V_{max} , say at intensity = X would be

$$\begin{aligned} V_{\text{max}} &= \sqrt{\frac{(6)(200)(3.6 \times 10^8)(14 \times 10^7)}{10}} \\ &= 25 \times 10^8 \text{ lb} \end{aligned} \quad (25)$$

so that

$$\tau_{\text{nominal}} = \frac{V_{\text{max}}}{A} = \frac{25 \times 10^8}{200(144)} = 87,000 \text{ psi} \quad (26)$$

Proceeding in this manner for all the intensity values, we obtain Table 7. The last column has a general comment on the connection between the *nominal* computed 'shear stress' value indicated for given intensity (the previous column) as compared to 'devastating' or 'catastrophic' or 'high' or similar designations of a shear stress for a local masonry-type structure, as reported in dispatches from the area in question shortly after the earthquake.

Table 7

| Magnitude of Earthquake | Intensity Region | Nominal Computed $\frac{V_{\max}}{A}$, psi | Comment on Previous Column Values |
|-------------------------|------------------|---|-----------------------------------|
| 7.5 or 8.0 | III | 450 | some cracking |
| | IV | 700 | moderate |
| | V | 1200 | high |
| | VI | 2000 | high |
| | VII | 3200 | high-catastrophic |
| | VIII | 6000 | catastrophic |
| | IX | 12000 | devastating |
| | X | 87000 | devastating |

Discussion and Comments

From the results in Table 7, it is clear that up to the outer reaches of Intensity VII all ordinary shear-type masonry structures would be subject to dangerous structural overstressing, leading to complete failure for those in the highest intensity regions.

That is, from Tables 4 and 5, for a magnitude $M = 8.0$ earthquake up to 180 km and for the magnitude $M = 7.5$ earthquake up to 85 km, we have areas within which ordinary masonry structures would be expected to suffer high to catastrophic damage.

We may compare these conclusions with various statements from the N.Y. Times dispatch.

- A) 'According to Tass, the quake registered more than 9 near the epicentre at Gazli, a rating that on the 12 point Soviet scale is termed devastating'.

We may assume that our Intensity VIII is roughly equivalent to the Soviet '9', and from Tables 4 and 5 we see our Intensity VIII outer reaches are (for $M = 7.5$ and 8.0), 52 km and 120 km respectively.

- B) 'Quake today was rated 7 or 'very powerful' in Bukhara and the buildings in Gazli, Bukhara and other unidentified populated localities had been destroyed'.

Bukhara is about 50 miles from Gazli and from our MID diagrams, Figures 11.10 and 11.11, Bukhara is in the Intensity VIII and VII regions for $M = 8.0$ and 7.5 respectively. In these regions according to the descriptive damage scale, ordinary masonry buildings will be completely destroyed.

- C) 'Earthquake had been felt from Ashkhabad near the Iranian Border though Turkmenistan, Uzbekistan and Tadzhikistan to Tashkent'.

Also 'According to Tass, the quake today registered 7 or very powerful in Chardzhou in Turkmenistan and readings 6 or powerful in two other Turkmenistan cities, Mary and Tashauz and in the Uzbek city of Samarkand'. Also 'Tashkent and other Uzbek cities registered between 5 and 6 as did Ashkhabad'.

From a map of the earthquake area and from the results obtained in our rational analysis as indicated in the preceding section, we may summarize a general comparison of theory and 'experiment' as in the following Table 8.

Table 8

| City or County | Distance Approx. From Gazli (km) | Reported Effect — Intensity Registered | Intensity Region According to Present Analysis | | Comment |
|----------------------|--|---|--|----------|-----------------|
| | | | $M = 7.5$ | $M = 8$ | |
| 1) Ashkhabad | 484 | Felt | III | IV–V | Report Verified |
| 2) Chardzhou | 160 | 7 very powerful | V–VI | VII–VIII | Report Verified |
| 3) Samarkand | 242 | 6 powerful | IV–V | V–VI | Report Verified |
| 4) Tashkent | 484 | 5 & 6 | III | IV–V | Report Verified |
| 5) Bukhara | 80 | 7 very powerful | VII–VIII | VIII–IX | Report Verified |
| 6) Near Epicentre | — | 9 devastating | IX–X | IX–X | Report Verified |

Conclusion for Section C

This Section was written with two principal aims in mind —

1. To show — in detail — how the rational theory developed in previous chapters may be applied to a particular earthquake.
2. To show — in detail — how the data generated in (1) above may be applied to the problem of determining the stress (and resultant damage, if any) for a particular type of structure which is subjected to an earthquake. The structure in this case is a low, squat, local material shear structure — i.e. a structure which absorbs the energy of the earthquake in *shear* energy only. Using this structure as an 'average typical structure' for the entire earthquake

field, an approximate comparison analysis of damage could be made — in a sense, a comparison between ‘theory’ and ‘experiment’.

In order to accomplish these two aims, a correspondent’s report in the New York Times describing, in some detail, a recent severe earthquake in Central Asia, was utilized as the data (experimental) source.

The results obtained using the rational theory verified the reports of damage and related effects as given in the press report.

D) THE EARTHQUAKE ENGINEERING ANALYSIS OF A LOW TO INTERMEDIATE HEIGHT BEAM-GIRDER-COLUMN ENERGY ABSORBING STRUCTURE*

Introduction

This Section has two principal aims:

1. To obtain in some detail the structural analysis (shears and moments) using the rational methods of this text, for a low, squat reinforced concrete frame with beam, girder and column elements, which by virtue of continuity at their connections absorb the earthquake energy through their separate deformations. This differs from the analysis for the tall building which vibrates essentially as a single beam in shear and bending — an analysis which will be discussed in the next section. It also differs from the structure and analysis of the previous section in which shear alone predominates and bending effects need not be considered.
2. To compare the solution (i.e., the shears and moments in the frame elements of (1) above with the parallel solution for the same elements obtained using an earthquake ‘code’ typical of those used in countries throughout the world.

Elaborating on the above, the rational theory of earthquake engineering described in the previous chapters is based upon the transfer of energy from the ground to the structure, and utilizes in its formulation those earthquake engineering parameters that should enter into a rational theory of earthquake engineering

* The structure, the computations and the Turkish Code analysis are from Nazmi M. Talimcioglu, ‘A Comparison Analysis of a Concrete Building Structural Design Using the Turkish Earthquake Code and a New Rational Earthquake Engineering Theory’, Master’s Thesis, May 1985, Department of Civil and Ocean Engineering, Stevens Institute of Technology, Hoboken, N.J. 07030.

structural design. This procedure will be called the 'Rational Method' (RM), in this Section.

The commonly used methods of earthquake structural design — utilized in one or another quite similar form — is by empirical code. In this procedure, a number of factors are chosen, numerical values assigned to them and finally a string-multiplication determines an equivalent, empirical horizontal load which is applied to the structure. This procedure will be called the 'Code Method' (CM) in this Section.

The particular code to be used will be the earthquake code which is commonly used in Turkey. As will be seen in the detailed application that follows, this code, in common with other similar codes and in contrast to the RM, does not consider the basic earthquake parameters that obviously must be involved in the rational design process.

Because of this fundamental and critical difference in the basic analysis procedures, one can not expect that there will be agreement (except coincidentally) between results obtained using the two methods. This is borne out by the results of an actual analysis applied to a typical low, squat reinforced concrete frame structure as given in this section.

Particular values of shear and moment obtained in the two solutions differ for the various members by roughly a factor of three to twelve with the RM indicating the more critical condition for the overall structure. But this is dependent upon the assumed rational earthquake design parameters. For example, a different assumed location for the structure in the earthquake field would have given a different result. Also, the RM assumes the structure in its bare, framed-condition (which is critical in the RM) whereas the CM solution assumes the fully built and loaded structure (which is critical in the CM).

The procedure will be as follows:

1. The design structure will be described.
2. The assumed earthquake will be specified.
3. The Turkish earthquake code will be outlined.
4. The CM solution will be presented in outline form. The detailed computations and analysis are given in the footnote reference on page 244.
5. The RM solution will be presented in outline form. The details are covered in the same reference.
6. A tabular comparison will be made between the moments and shears as determined in (4) and (5).
7. A critical discussion of the tabular values will be presented.

The Assumed Structure

The specifications for the assumed structure are as follows:

Cover of the roof: Approximately 5cm. smooth concrete on the reinforced concrete slabs, 3cm. isolation material, 2.5 cm. concrete two layers of bitumen. Also a 40 cm. parapet wall surrounds the roof.

Slabs: Approximately 3 cm. smooth concrete on the reinforced concrete plates, mosaic cover.

Walls: All walls will be built of concrete block, wooden frames will be used for doors and window frames.

Spacing of the concrete structural frames: See Figure 11.13.

Material: Concrete B160, steel ST1 according to DIN (Turkish) codes.

Allowable bearing stress of the soil beneath the structure 2.5 kg/cm^2 .

External loads applied to the structure:

Weight of the structure

Additional loads at the top : Snow

Live loads

Earthquake

We shall consider, in detail, only the earthquake loads. The other loads will be assumed as given when used in the CM analysis.

Cross sectional areas of beams and columns: See Figure 11.14.

Specification of the Earthquake

1975 Lice, Turkey Earthquake

Magnitude = 6.40 (Approx. value)

Region : Mountain region, \mathcal{R}_2 . (assumed)

Distance from epicentre to centre of intensity region III at surface of the earth,

$S_f = 80 \text{ km}$, from Figure 4.5

Isoëismal Index, $\Sigma(IS)_f = 780 \text{ km}$ from Figure 4.5

Efficiency $\eta = 0.10$ (assumed)

Location of the structure (distance from epicentre) $S = S_f/2$ (assumed to give energy value corresponding approximately to empirical values assumed in the CM design).

The Turkish Earthquake Code

Following is a summary presentation of the Turkish earthquake code as it applies to the structural design aspects. It is quite similar to other earthquake codes (including USA codes) in use throughout the world. We consider loads per interior frame.

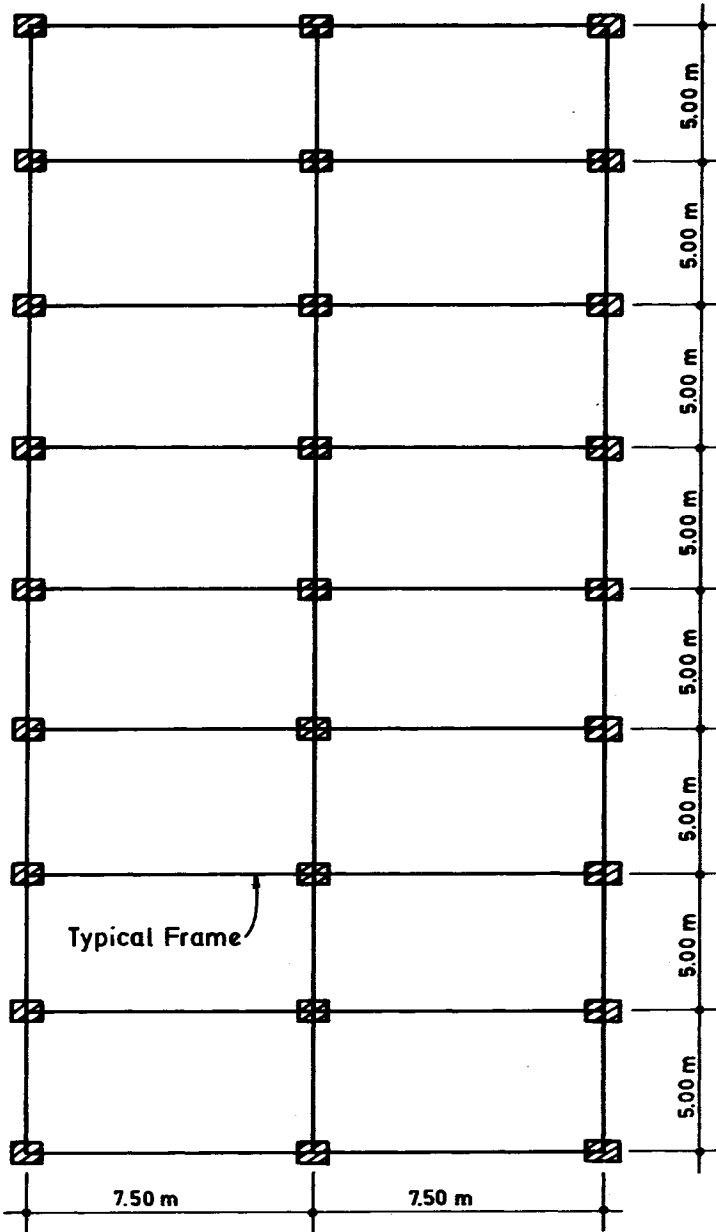


Figure 11.13 Plan View of Structure

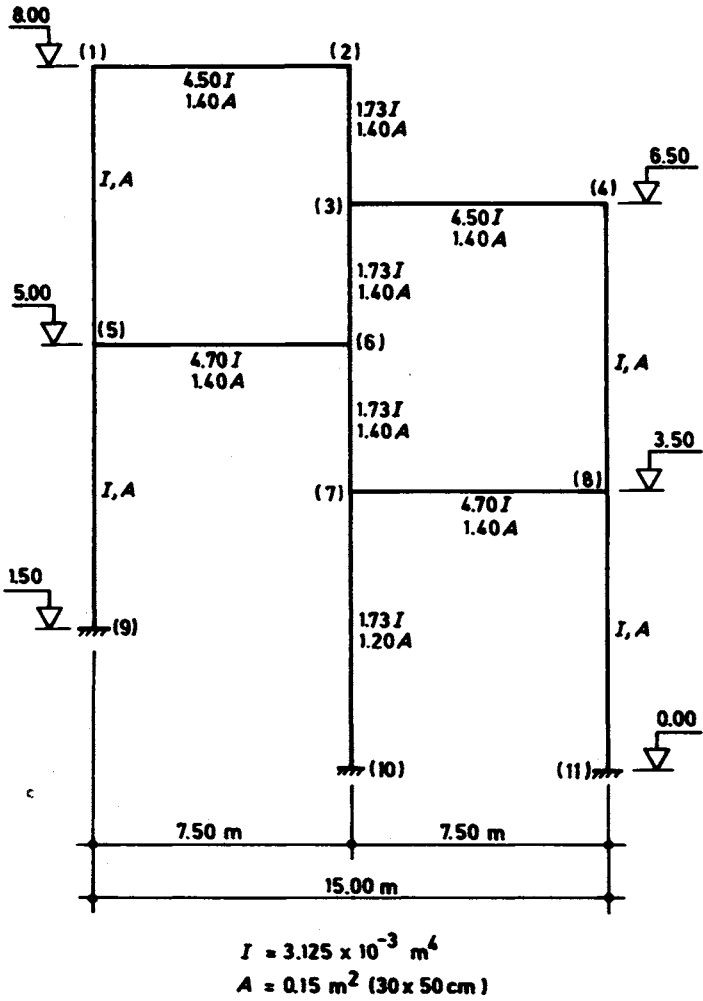


Figure 11.14 Typical Structural Frame Elevation
(8 bays in all — 7 interior frames and 2 end frames)

A) Summary of Turkish Earthquake Code

The total earthquake force per interior frame is given by the formula

$$F = C \times W \tag{27}$$

where

- F = total induced earthquake load
- C = earthquake constant
- W = total weight of the structure — i.e., per interior frame

Earthquake Constant (C)

C is given by the following

$$C = C_0 \times K \times S \times I \tag{28}$$

where

- C_0 = Earthquake region constant
- K = Type of structure
- S = Dynamic spectra constant
- I = Significance of the structure

These terms are more fully specified as follows:

Region Constant:

| Region | C_0 |
|--------------------------------------|-------|
| 1 st (highest seismicity) | 0.10 |
| 2 nd | 0.08 |
| 3 rd | 0.06 |
| 4 th (lowest seismicity) | 0.03 |

Type of Structure:

| Type | K |
|---------------------------------------|------|
| Ductile frames (Concrete or steel) | 0.80 |
| Non-ductile frames | 1.50 |
| Steel trusses | 1.50 |

Note that for all structures which consist of one or two stories, $K = 1$.

Dynamic Spectra Constant:

$$S \text{ is given by the formula } S = 1/[0.80 + T - T_0] \tag{29}$$

where

T = Natural vibrating period of the structure with respect to the first mode of oscillation (in seconds)

T_0 = Natural frequency of the ground (in seconds)

Note that T_0 is given by tables.

$$S_{\max} = 1.00 \quad \text{so that} \quad S \leq 1 \tag{30}$$

Significance of the Structure:

| Type of Structure | I |
|---|------|
| The most significant structures, i.e. hospitals, fire departments, post offices, etc. | 1.50 |
| Museums, banks, etc. | 1.50 |
| Schools, theaters, etc. | 1.50 |
| Others | 1.00 |

Loading Condition:

The total earthquake horizontal load F , must be distributed to each level of the structure with respect to the total weight. Then

$$F_i = (F - F_t) \frac{W_i \times h_i}{\sum W_i \times h_i} \tag{31}$$

where

F_i = Load acting on the i th elevation

W_i = Weight of i th floor

h_i = Height of i th floor measured from the ground surface

F_t = Load with respect to the second mode of oscillation

$$F_t \leq 0.15 \times F \tag{32}$$

and if $H/D < 3$ then $F_t = 0$ where H is the total height and D is the width of the structure.

The CM Solution

This solution will be given in bare outline form only. The details are presented in the footnote reference on page 244.

As noted above

$$\begin{aligned}
 F &= CW, \\
 C &= C_0 K S I
 \end{aligned}
 \tag{33}$$

For the building shown in Figures 11.13 and 11.14 the following values of the constants were used

$$\begin{aligned}
 T &= 0.38 \text{ sec} \\
 T_0 &= 0.42 \text{ sec} \\
 C_0 &= 0.10 \text{ sec} \\
 K &= 1.00 \text{ sec} \\
 I &= 1.00 \text{ sec}
 \end{aligned}
 \tag{34}$$

$$\text{and } S = 1/(0.80 + T - T_0) = 1/(0.80 + 0.38 - 0.42) = 1.32 > 1.00
 \tag{35}$$

so that $S = 1.00$

Substituting these values in the formula given below:

$$C = 0.10 \times 1.00 \times 1.00 \times 1.00 = 0.10
 \tag{36}$$

and noting that

$$W = W_1 + W_2 + W_3 + W_4$$

$$\begin{aligned}
 \text{then } W &= 34.45 + 36.14 + 36.98 + 36.98 \\
 &= 144.45 \text{ tons/frame}
 \end{aligned}
 \tag{37}$$

Since the height of the frame $H = 8$ m. and the width $D = 15$ m., $H/D = 8/15 = 0.53 < 3$, so that $F_t = 0.0$ (no effect of second mode, code requirement). Thus the total lateral load is as follows:

$$F = C \times W = 0.10 \times 144.55 = 14.46 \text{ tons/frame} \quad (38)$$

The load distribution is given by the formula:

$$F_i = (F \times W_i \times h_i) / (W_1 \times h_1) \quad (39)$$

where the subscript i indicates the elevation and h is the height of the corresponding story.

Distributed loads were then found to be as shown in Figure 11.15 for a typical interior frame.

$$\begin{aligned} F_1 &= 4.83 \text{ tons} \\ F_2 &= 4.12 \text{ tons} \\ F_3 &= 3.24 \text{ tons} \\ F_4 &= 2.27 \text{ tons} \end{aligned} \quad (40)$$

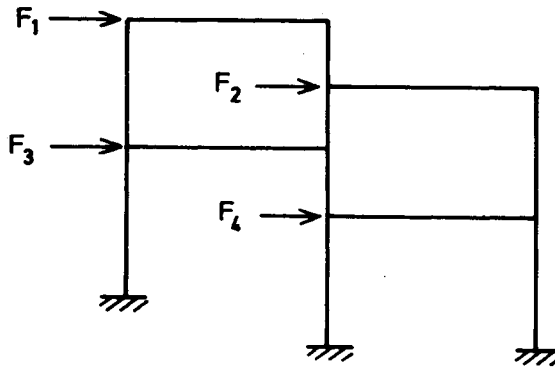


Figure 11.15

The rigid frame structure is solved for the loading shown and the resulting end moments are as indicated in Figure 11.16 for a typical interior frame.

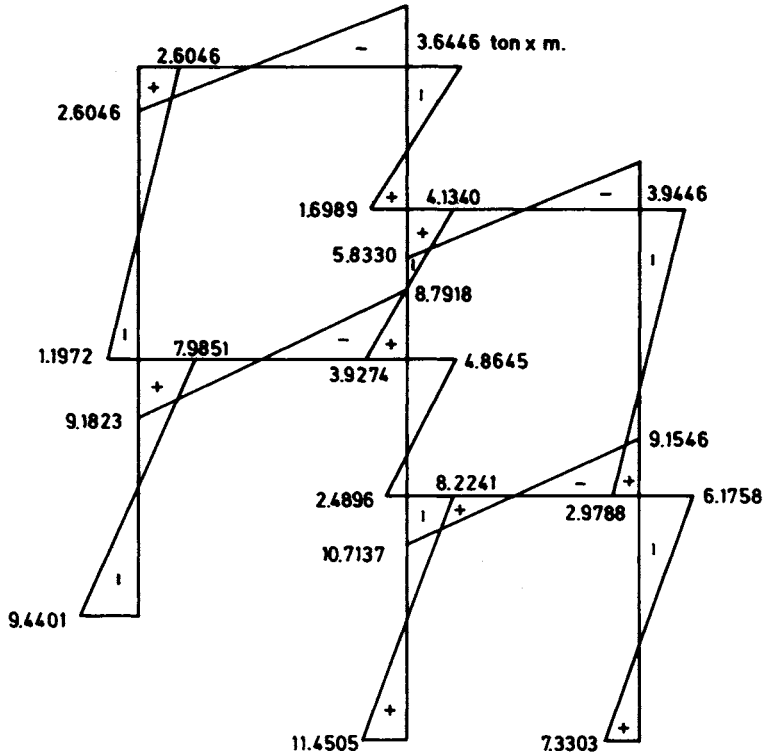


Figure 11.16 Moment Diagram for a Typical Interior Frame

The Solution by the RM

In this section, the rational approach to earthquake engineering design will be presented for the short, shear-bending type of structure shown in Figures 11.13 and 11.14. Most of the detailed calculations are obtained by computers. Hence only a brief outline and results will be given here. The complete details are in the footnote reference on page 244.

Corresponding to the data given in Chapter 4 the main assumption made in this analysis is the fact that a magnitude 6.4 Lice (Turkey) earthquake occurs while the building is being constructed. A second assumption which is needed is the distance of the structure from the epicentre. This is assumed as half of S_f , where S_f is the distance between the epicentre and the intensity III region defined by the Modified Mercalli Scale.

In agreement with the former calculations with respect to the Turkish earthquake code, the geology parameter will be taken as \mathcal{P}_2 which is specified as 'mountain region' in the RM.

From Figure 4.5 of Chapter 4 approximate values of S_f and the intensity index $\Sigma(IS)_f$ were determined as given below,

$$S_f = 80 \text{ km}$$

$$\Sigma(IS)_f = 780 \text{ km}$$

Following this, using the procedures detailed in Chapter 4 and shown in earlier sections of this chapter we can determine the MID (magnitude-intensity-dis-

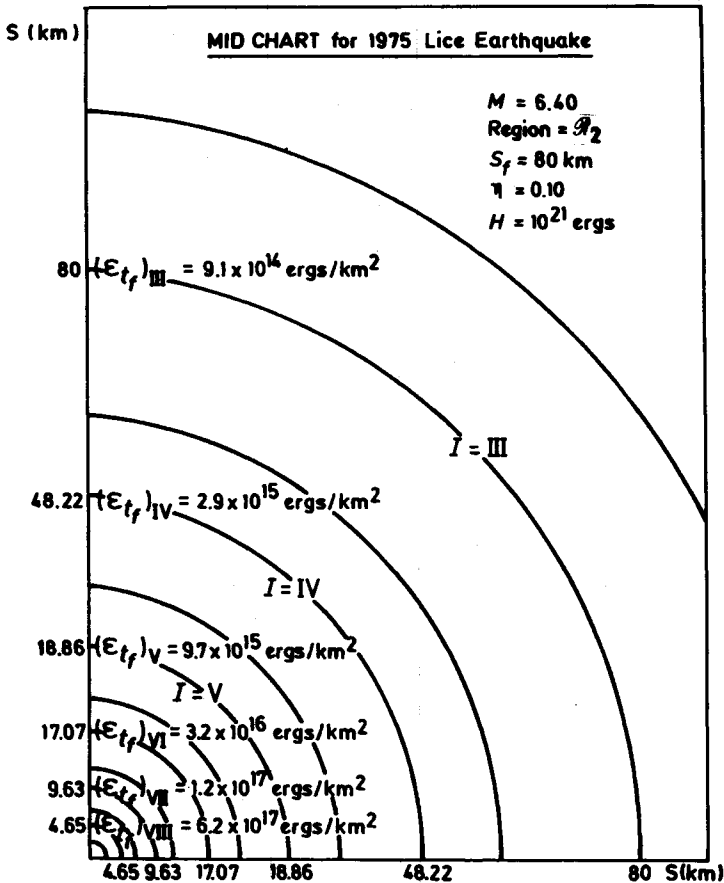


Figure 11.17

tance) chart and also the distribution of surface horizontal energy, ϵ_{tf} , throughout the field affected by the earthquake, up to and including the Intensity = III band.

These are as shown in Figure 11.7 and the values shown in the figure represent the basic structural design data as determined by the earthquake parameters.

Determination of ϵ_{tf} for the structure

Since the location of the structure was given to be at

$$S = S_f/2 = 80/2 = 40 \text{ km} \tag{41}$$

the building is in the intensity IV band (see Figure 11.17). From this figure we then find that, approximately,

$$\epsilon_{tf} = 3.0 \times 10^{15} \text{ ergs/km}^2 \tag{42}$$

This number could also have been obtained directly from Figure 11.12.

Determination of the total strain energy for the structure:

In accordance with a similar former project, the foundation plan for each interior frame was taken as shown in Figure 11.18.

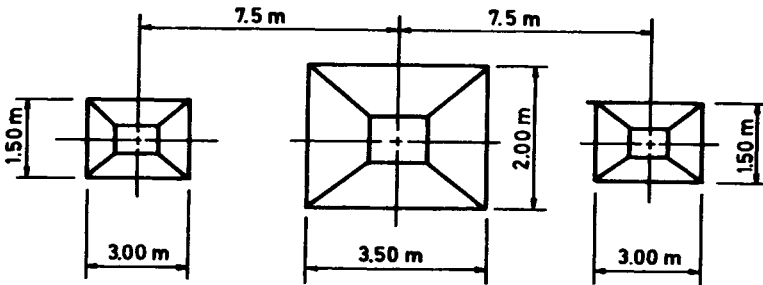


Figure 11.18

Since there are 8 similar bays the effective area of the entire structure is then the total foundation area of

$$A_f = 8 \times (2 \times 3 \times 1.5 + 3.5 \times 2) = 128 \text{ m}^2 = Ae \tag{43}$$

This assumes that the end frame foundations have half the area of the interior foundations. Then the total strain energy which all frames must absorb is given by

$$U_{\text{total}} = \epsilon_{t_f} \times Ae$$

$$U_{\text{total}} = 128 \times 10^{-6} \times 3 \times 10^{15} = 3.84 \times 10^{11} \text{ ergs} \quad (44)$$

Strain energy which each frame must absorb

There are 8 bays

or
$$U_{\text{frame}} = U_{\text{total}}/8 \text{ ergs}$$

so that
$$U_{\text{frame}} = (3.84 \times 10^{11})/8 = 4.80 \times 10^{10} \text{ ergs} \quad (45)$$

or
$$U_{\text{frame}} = 4.80 \times 10^4 \text{ kg-cm}$$

The strain energy will be absorbed by the frame as either

- a) Shear strain energy (very short, squat adobe or brick type building) — see the previous Section C.
- b) Shear plus bending strain energy (a beam, girder, column structure, for which shear and bending strain energy are of the same order of magnitude).
- c) Bending strain energy only (an intermediate to long structure, or a beam, girder column structure for which bending energy predominates).

It will be shown that the frames for this structure are of type c). Hence only bending strain energy of the frame elements will be considered.

This will be determined by introducing an initial, rigid horizontal deflection and then solving the structure by moment distribution. In the maximum deflection position all of the energy will be assumed as *strain* energy (in the zero deflection position all of the energy is *kinetic* energy). For the first (and most critical) cycle, damping is neglected and (conservatively) all of the energy is absorbed as strain energy.

The initial rigid horizontal motion is as shown in Figure 11.19.

A moment distribution solution of this frame, in terms of Δ is then obtained. Following this, an analysis of a typical member indicates that, for the members of this frame, with U the strain energy,

$$\frac{U_{\text{Bending}}}{U_{\text{Shear}}} \cong 20 \quad (46)$$

We will therefore neglect the shear strain energy in our solution. If desired it could, of course, be included without difficulty.

The moment distribution solution for Figure 11.19 is shown in Figure 11.20, in which the moments at the ends of all members are given in terms of Δ .

Using the moment values shown on Figure 11.20, it is now possible to determine the strain energy in bending for all members of the frame. This is as shown in Figure 11.21 and the computations pertaining thereto.

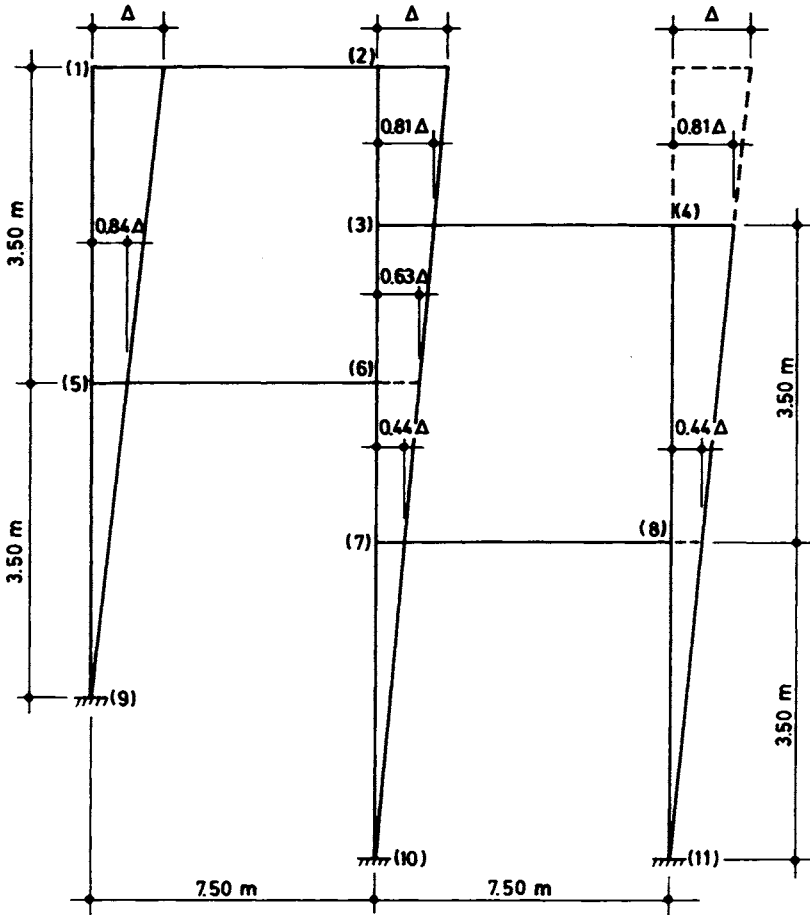


Figure 11.19

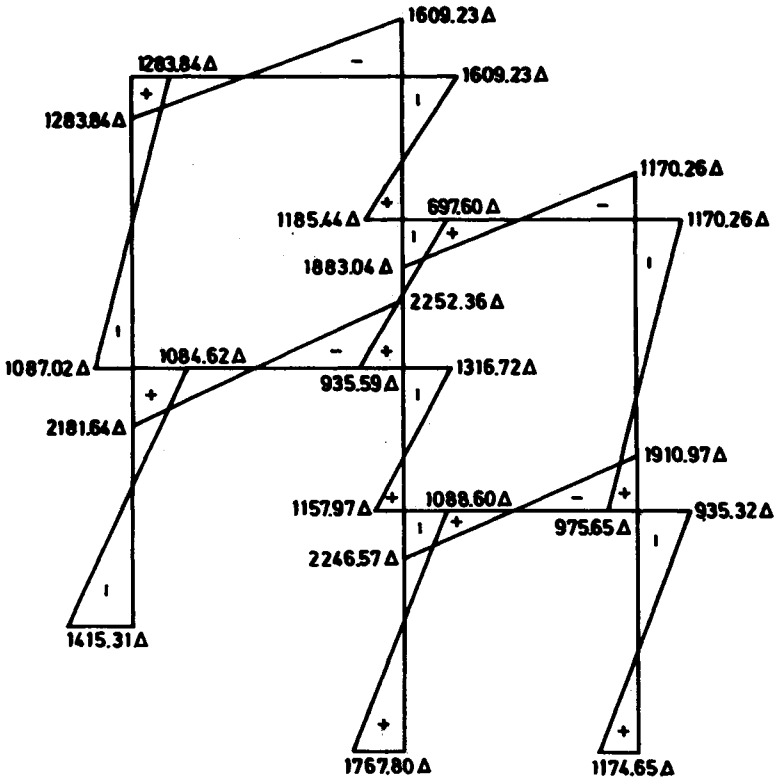


Figure 11.20

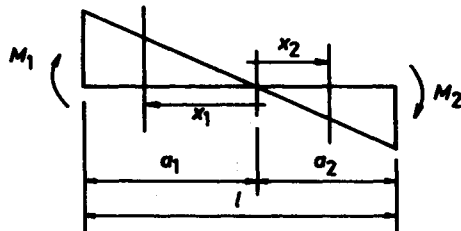


Figure 11.21

Since
$$U_{\text{bending}} = \int M^2 dx/2EI$$

$$U_{\text{member}} = \int_0^{a_1} \frac{1}{2EI} \left(\frac{M_1 x_1}{a_1} \right)^2 dx_1 + \int_0^{a_2} \frac{1}{2EI} \left(\frac{M_2 x_2}{a_2} \right)^2 dx_2 \tag{47}$$

or
$$U_{\text{member}} = \frac{1}{2EI} \left[\frac{M_1^2 \times a_1 \times M_2^2 \times a_2}{3} \right].$$

Adding all twelve strain energies, we obtain

$$U_{\text{frame}} = 1250 \Delta^2 \tag{48}$$

Determination of total deflection of the frame:

U_{frame} was also found to be the following:

$$U_{\text{frame}} = 4.80 \times 10^4 \text{ cm}\cdot\text{kg} = 4.80 \times 10^{-1} \text{ m}\cdot\text{tons} \tag{49}$$

Hence,
$$4.80 \times 10^{-1} = 1250 \Delta^2 \tag{50}$$

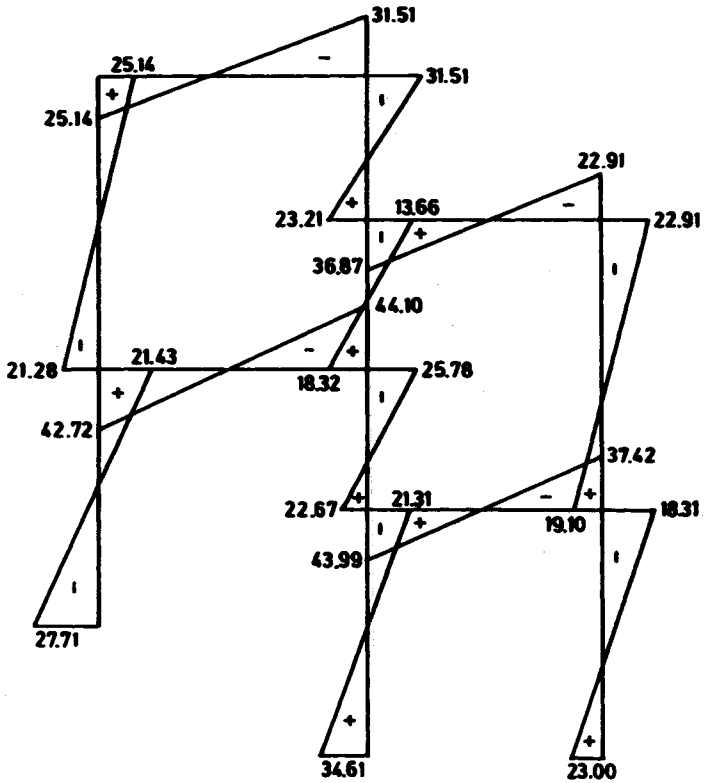
so that the total deflection (maximum deflection) at the top of the frame is

$$\Delta = 1.958 \times 10^{-2} \text{ m.} \tag{51}$$

or
$$\Delta = 0.77 \text{ in.}$$

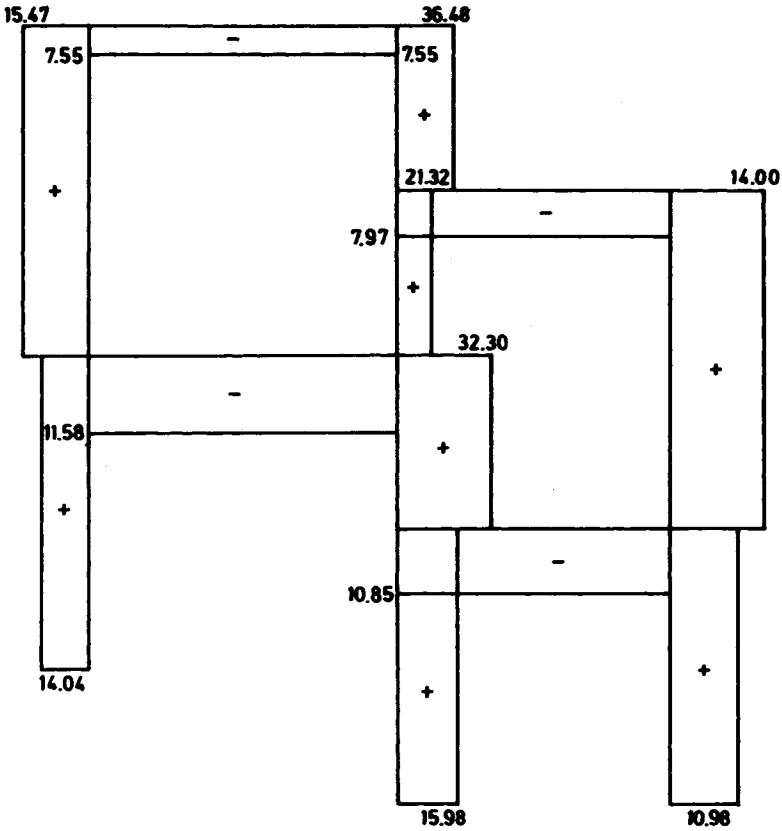
Moments are now obtained by substitution of the value of maximum deflection into the moment values given in Figure 11.20. The results obtained by this procedure are summarized in the moment diagram given in Figure 11.22. Shear forces can then easily be calculated by writing equilibrium equations at each node. The shear force diagram is given in Figure 11.23.

All results obtained by the rational solution of the frame due to the given earthquake will be compared with the results obtained in the previous analysis by the application of the Turkish earthquake code.



Maximum member end moments

Figure 11.22



Maximum member shears

Figure 11.23

Comparison of CM and RM Solutions

The following Table summarizes the results of the analysis.

Table 9

| BAR # (i-j) | Turkish Code | | | Rational Method | | |
|----------------|--------------|-------|----------|-----------------|--------|----------|
| | M_i | M_j | T_{ij} | M_i | M_j | T_{ij} |
| 1 2 | - 2.60 | -3.64 | -0.83 | -25.14 | -31.51 | - 7.55 |
| 3 4 | - 5.83 | -3.94 | -1.30 | -36.87 | -22.91 | - 7.97 |
| 5 6 | - 9.18 | -8.79 | -2.39 | -42.72 | -44.10 | -11.58 |
| 7 8 | -10.71 | -9.15 | -2.65 | -43.99 | -37.42 | -10.85 |
| 9 5 | - 9.44 | +7.99 | +4.98 | +27.71 | +21.43 | +14.04 |
| 5 1 | + 1.20 | +2.60 | +1.26 | +21.28 | +25.14 | +15.47 |
| 10 7 | +11.45 | +8.22 | +5.62 | +34.61 | +21.31 | +15.98 |
| 7 6 | + 2.49 | +4.86 | +4.80 | +22.67 | +25.78 | +32.30 |
| 6 3 | + 3.93 | +4.13 | +5.37 | +18.32 | +13.66 | +21.32 |
| 3 2 | + 1.70 | +3.64 | +3.56 | +23.21 | +31.51 | +36.48 |
| 11 8 | + 7.33 | +6.18 | +3.86 | +23.00 | +18.31 | +11.80 |
| 8 4 | + 2.88 | +3.94 | +2.31 | +19.10 | +22.91 | +14.00 |

where

M_i = Moment at node i (tons-m)

M_j = Moment at node j (tons-m)

T_{ij} = Shear (tons)

And also note that the positive sign convention is shown in Figure 11.24.



Figure 11.24

An indication of the maximum stress obtained by the RM can be obtained as follows:

The maximum moment is 44.10 m-tons at the end of bar numbered 5-6. For this bar,

$$\begin{array}{l}
 \text{where} \\
 \text{then}
 \end{array}
 \left.
 \begin{array}{l}
 I_{\text{equivalent}} = 4.70 \times I \\
 I = 3.125 \times 10^{-3} \text{ m}^4 \\
 I_{\text{eq}} = 1.469 \times 10^{-2} \text{ m}^4
 \end{array}
 \right\} \quad (52)$$

The cross-sectional area of the bar is 30×70 cm, and the approximate stress due to bending is given by the formula:

$$\left.
 \begin{array}{l}
 \sigma = M z / I_{\text{eq}} \\
 \text{where } z = (70 - 3) / 2 = 33 \text{ cm. approximately}
 \end{array}
 \right\} \quad (53)$$

Then the maximum stress is approximately

$$\left.
 \begin{array}{l}
 \sigma_{\text{max}} = (44.10 \times 10^5 \times 33) / (1.469 \times 10^6) \\
 \text{or } \sigma_{\text{max}} = 100 \text{ kg/cm}^2 = 1400 \text{ psi}
 \end{array}
 \right\} \quad (54)$$

Also note that $(\sigma_{\text{max}} = 100 \text{ kg/cm}^2) > (\sigma_{\text{allowable}} = 70 \text{ kg/cm}^2)$, a typical allowable value, so the indication is that the structure may have problems for an earthquake of the assumed magnitude, if it occurs while the structure is being built.

Conclusion for Section D

A comparison structural analysis is performed for a typical short, squat reinforced concrete frame using two fundamentally different procedures,

1. The Turkish Earthquake Code (the Code Method, CM) which is typical of earthquake codes currently used in various countries throughout the world.
2. A theoretical, rational method of earthquake engineering analysis (the Rational Method, RM) based upon the theory of the text.

The results indicate that for the structure assumed and subject to the given earthquake assumptions the two methods give shear and moment results which differ by factors of three to twelve for the various members. The RM gives the larger values in the example considered here.

The significant questions raised by the rational approach relate to a consideration as to which parameters are in fact, of importance in an actual earthquake engineering structural analysis. Thus,

- a) The magnitude of the earthquake is important.
- b) The distance of the structure from the focus of the earthquake is important.
- c) The depth of the focus is important.
- d) The type of geology between the focus and the structure is important.

Of the above parameters, none are implicitly considered in the CM but all are included as fundamental parameters in the RM.

However, as noted above, it is interesting that a rough equivalence of input data gives a generally equivalent response for this particular structure, considering the two fundamentally different methods of structural analysis.

Another factor of interest in the present comparison study, is that the structure considered for the CM was at its maximum weight — i.e., fully built with the total dead load and live load. This gave the more critical condition for the CM.

On the other hand, the structure considered for the RM was the bare beam-girder-column structure subject to a given energy input. If the full structure (i.e., walls, slabs, partitions, etc.) was considered, the beams and girders and columns would absorb less of the (same total amount of) applied energy since the slabs, walls and other elements would take some portion of the overall energy input and lower values of moments, shears and stresses for the frame elements would have been obtained, thereby closing the gap between CM and RM stresses.*

E) THE EARTHQUAKE ENGINEERING ANALYSIS OF A HIGH STRUCTURE, $l/w \gtrsim 5$

Introduction

In the previous Section C and D of this chapter, the rational methods of this text's theory were applied to the structural analysis of short ($l/w < 1/2$) building structures.

In this section, the methods are applied to a tall ($l/w > 5$, say) building. This corresponds to a tall high-rise or office or similar building. Physically, the

* A very approximate analysis indicates that the slabs, walls and other elements absorb about half of the applied energy, thereby indicating that the values of the RM moments and shears in Table 9 would be about 0.7 times the values shown. If, in addition, we consider the interior live loads, the final values would be roughly half the values of Table 9.

structure considered is one which — overall — behaves as essentially a beam-type structure insofar as vibrational affects are concerned. This is fundamentally different, for example, from the structure of Section D, in which the *elements* of the structure vibrated as beams, rather than the complete structure (the frame) behaving in this manner.

There are a number of key assumptions made in the structural procedure for tall buildings. They will be listed here and discussed more fully, as needed, when introduced in later parts of this Section E.

1. An effective length of structure must be determined. This is l .
2. An effective area of the base of the structure must be assumed which will determine the amount of energy that the structure must absorb. This is A_e , and as pointed out previously, analysis of several different earthquake engineering problems strongly imply that this is the actual foundation area — i.e., area of the foundations in contact with the ground surface.
3. The structure of length l will be assumed as a free-free beam insofar as bending response to the earthquake is concerned. Short, squat structures $l/w \leq 1/2$, are treated as shear responders or, depending upon the construction details, as beam, girder, column, frame elements. See the previous Sections C and D of this chapter.
4. For our present purposes, a uniform structure will be considered. In actual cases, the true shape of the structure will offer no complication. Computer programs are available for determining the required design data, such as node locations and principal periods. The approximate procedure does, however, require the assumption of symmetry about the mid-height plane.
5. Loadings and response will be assumed as separable into symmetric and anti-symmetric components and superposable by simple addition.
6. For structures built of different materials, such as a steel frame and brick facing or similar, it will be assumed that a division of energy between the separate parts is known or can be assumed. A uni-material analysis may be appropriate.
7. The earthquake magnitude-energy-efficiency relationships for different geologies will be assumed as known, see Chapter 4.
8. The temporal and spacewise variations of surface horizontal energy will be assumed as given in Chapter 4 pending collection of additional actual calibrating data on these items.

This Section E presents, in some detail, the procedure to be used in solving the complete approximate time-history response for a tall structure (in the elastic range) subjected to an earthquake loading. In the explanation of the

method, special attention is given to the physical interpretation of the various steps involved in the proposed solution. The physical explanation and significance of the proposed division between shear-wave effects and bending vibrational effects (which is the foundation of the proposed method) is covered in detail.

Methods of elastic analysis for the dynamic earthquake problem are given in the literature in very general terms, but actual numerical computations are quite rare. It should be noted that what is being discussed in this section is the solution for the shear, moment, and deflection — not the frequency solution. Many computations have been given for the frequency analysis — and this is an important physical quantity since resonant vibrations due to rotating machinery can cause very undesirable effects unless properly designed for — and this proper design requires a knowledge of the frequencies of the various modes of vibration. However, the present discussion is concerned only with the structural analysis of the effects of earthquake loadings. In particular, earthquakes can lead to a considerable increase in the critical bending moment in structures. An approximate method for calculating these added moments (and shears and resulting deflections) is presented in this Section E.

It must also be repeated that the method described is, admittedly, an approximate one. However, all methods which have been presented as solutions to this problem are approximate to some degree. Also, as the discussion in the Appendix indicates, existing methods of analysis are open to serious criticism with reference to the accuracy of the designs to which they lead.

Procedure

For purposes of simplicity only, the discussion will be referred to a constant section structure, Figure 11.25 and the load, initially, will be an assumed pulse-type load as shown in Figure 11.25. However, the method is a general one and can be applied also to variable section structures and to variable loadings. In the case of the variable section, a graphical method of analysis can be utilized. Any given alternating load can be approximated by a summation of alternating pulse-type loads.

The response of the structure-shear, moment, and deflection, due to elastic-dynamic effects caused by the loading, will be obtained starting with $t = 0$. Note the phrase 'elastic-dynamic effects': this means that we are not interested in the rigid-body motion of the structure. This could be obtained using Newton's equations and the combined effect is a simple superposition of rigid body plus elastic-body motions. In this discussion, however, we shall be concerned with the elastic-body effects only.

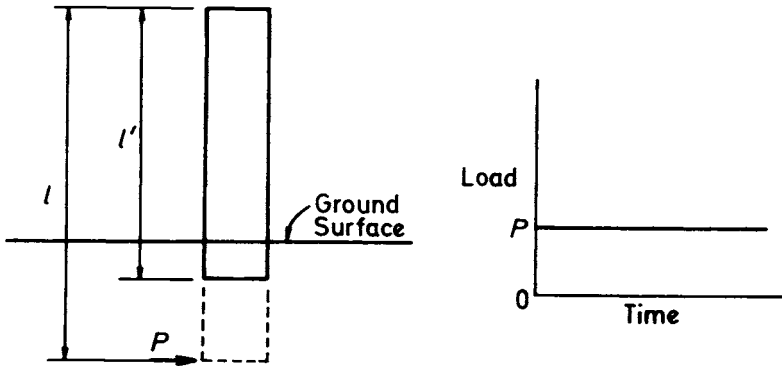


Figure 11.25

In Chapter 9 three separate time region were distinguished. We shall be concerned with the responses only in two of these namely: (a) the period of transition, and (b) the period of overall effect. The solution in the other region, the so-called period of localized effect, requires a detailed knowledge of the local structure in the neighbourhood of the point of application of the load and is of no interest here, although this could be critical.

The proposed method of solution is based primarily upon energy considerations insofar as (b), the period of overall effect is concerned. However, the response during the time period (a), the period of transition, is based upon the wave-transmission characteristics of the structure, and to some extent has its justification in the actual behaviour of a structure when subjected to earthquake loading. Before considering this point in greater detail, the question of symmetry, anti-symmetry, and unsymmetry will be discussed, particularly with reference to loading effects on the structure.

Symmetry, Anti-Symmetry, and Unsymmetry

For a uniform free-free beam section, the classical solution for the normal modes of vibration indicates alternating symmetrical and anti-symmetrical (or skew-symmetrical) shapes (see Figure 11.26). In our discussion, we shall be concerned only with the four modes shown. If additional modes are needed, they can be included. Or, if a more approximate (quicker) solution is desired, only the first two modes need be considered and in view of the inevitable approximations, we shall assume the two mode solution as acceptable for most cases.

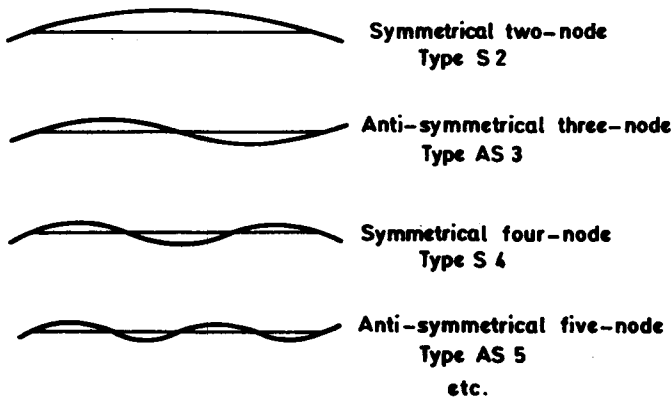


Figure 11.26

We shall assume, therefore, that in general S2 and S4 are the developed symmetrical modes of vibration, AS3 and AS5 are the developed anti-symmetrical modes of vibration, although for simplicity, S2 and AS3 only will be used in the detailed explanation of the method.

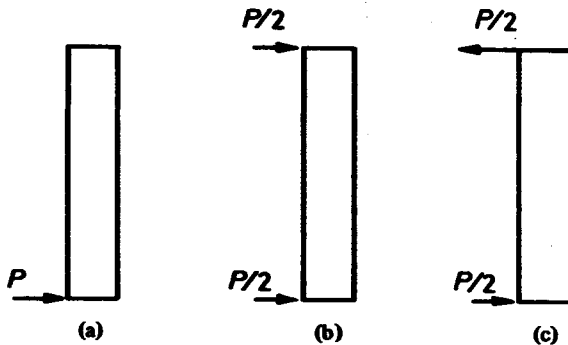


Figure 11.27

With reference to loadings, any arbitrary unsymmetrical load on a beam structure can be replaced by an equivalent pair of loadings, one of which is symmetrical, the second of which is anti-symmetrical. Thus, in Figure 11.27a, the arbitrary load is an unsymmetrical one. Figure 11.27b is a symmetrical loading, Figure 11.27c is an anti-symmetrical loading and, obviously, the sum of the cases (b) and (c) is equivalent to the case (a).

We shall assume that the loading and vibratory response can be analysed in terms of symmetry, anti-symmetry, and unsymmetry. This is fundamental in the proposed method of solution. Furthermore, it will be assumed that the overall effect can be approximated as a simple superposition of the separate symmetrical and anti-symmetrical effects.

Period of Transition

One participant's description of an earthquake effect on a tall building is that the initial awareness — immediately after the earthquake is felt — is of a 'shudder' going up the building. Shortly after that, the building begins to 'sway'. i.e. vibrate. The proposed method of solution is, physically, one which gives a response similar to that described. The equivalent of the 'shudder' is introduced by means of a shear wave travelling up the length of the building. This shear wave introduces required balancing inertia forces and introduces only shear deflections (although bending moments also are induced, but bending deflections have not had time to develop). The velocity of this shear wave is given by the known formula

$$V = k \left(\frac{Gg}{\rho} \right)^{1/2} \quad (55)$$

and the equilibrium conditions and loadings shown in Figure 11.28 are consistent with this velocity. Thus, Figure 11.28a is at a time $t = t_2$, where t_2 is within the period of transition defined earlier. Figure 11.28b shows conditions at the instant that the period of transition ends, and Figure 11.28c and 11.28d show Figure 11.28b in terms of the symmetrical and anti-symmetrical loadings.

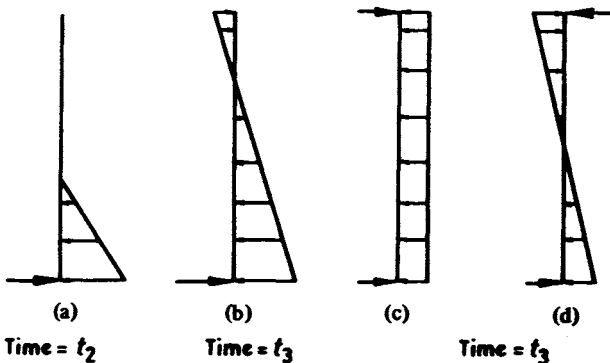


Figure 11.28

Figure 11.28a is assumed to be the period during which the 'shudder' is traveling up the building. Vibrations corresponding to Figure 11.28b have not as yet begun. The shear and moment at any point during this period can, however, be obtained. The balancing inertia loads are assumed as shown. The deflection and stress of the structure at any instant during conditions shown in Figure 11.28a or 11.28b are pure shear deflection and stress only, and may be obtained using the elementary relations for shear deformation and stress. Although there are bending moments acting on the structure, during this period of transition, it is assumed that these do not develop bending stresses since the bending deformation has not as yet developed.

It should be noted that the shear loading described above and the resulting bending strain energy described in the next section during the period of overall effect are introduced solely as a means for determining the division of strain energy into symmetrical and skew-symmetrical parts. Having determined these, the total energy that the structure must absorb is divided into symmetric and skew-symmetric portions having the same ratio as the corresponding energies described above. Because the structure is assumed as a uniform free-free structure it will vibrate in symmetrical and skew-symmetrical modes. The division of the symmetrical energy among the symmetrical modes and of the skew-symmetrical energy among the skew-symmetrical modes will be approximated on the assumption that they are additive for each set and also (as will be seen shortly) on an assumed simplified triangular inertia loading based upon the deflection configurations of the symmetrical and skew-symmetrical modes.

Period of Overall Effect

Figure 11.28b shows the loading on the structure at the instant the 'period of overall effect' begins, due to an earthquake pulse load P applied at the base of the 'equivalent length' structure. The loading shown is the equivalent (in the approximation used herein) to a suddenly applied load acting on the structure. This is an important statement in the explanation of the proposed method, because the fact that the loading shown in Figure 11.28b is a suddenly applied loading, when used in conjunction with the physical requirement that the structure is a free-free beam (and that therefore the required balancing inertia loading remains constant and the same as shown in Figure 11.28b as long as the load P is acting on the structure), enables us to introduce the vibratory effects as being caused by a suddenly applied energy input of known value. This will now be described in greater detail.

The strain energy is a laterally loaded beam element, for gradually applied loads is (bending effects only considered)

$$U_{\text{gal}} = \int_0^l \frac{M^2 dx}{2EI} \quad (56)$$

By 'gradually applied' we mean that the loads are applied so slowly that the beam will be in deflection equilibrium as well as statical force equilibrium at all times. This is, of course, only a theoretically-attainable state but for all practical purposes a slowly applied load approximates the condition of gradually applied load.

However, the condition shown in Figure 11.28b is just that corresponding to a 'suddenly applied load' because the beam has not had the time (it is assumed, and this very nearly so) to deform due to the bending effects. Under these circumstances the strain energy has the value

$$U_{\text{sai}} = \int_0^l \frac{M^2 dx}{EI} \quad (57)$$

Thus, at time $t = t_3$ with the loading shown in Figure 11.28b (which loading, as previously stated, remains constant), there has been an amount of strain energy introduced into the system of value

$$U = \int_0^l \frac{M^2 dx}{EI} \quad (58)$$

Of this strain energy,

$$\frac{U}{2} = \int_0^l \frac{M^2 dx}{2EI} \quad (59)$$

is required to account for the load of Figure 11.28b which therefore, corresponds to a quasi-static loading. The remaining energy

$$\frac{U}{2} = \int_0^l \frac{M^2 dx}{2EI} \quad (60)$$

goes into vibratory energy of the vibrating structure. It is just this energy which causes the structure to vibrate fore and aft about the vertical equilibrium position, and it vibrates in such a way that the sum of kinetic and strain energies is at all times equal to $U/2$ (less the amount damped from cycle to cycle).

In the present analysis, therefore, at all times $> t_3$, the condition on the structure due to the earthquake loading is:

1. The quasi-static balancing inertia loading of Figure 11.28b exists — in both directions as the accelerogram dictates.
2. The vibrating modes of Figure 11.26 exist and represent effects which superpose on those of (1). The amount of vibration (amplitude of oscillation) is determined by means of an energy balance: the total maximum strain energy of the vibrating structure is equal to $U/2$, which is just equal to the quasi-steady strain energy, or strain energy corresponding to the loading of Figure 11.28b.

Having described the state of the structural system during the period of overall effect, it is now necessary to explain how the vibrating strain energy is assumed apportioned among the different modes of vibration.

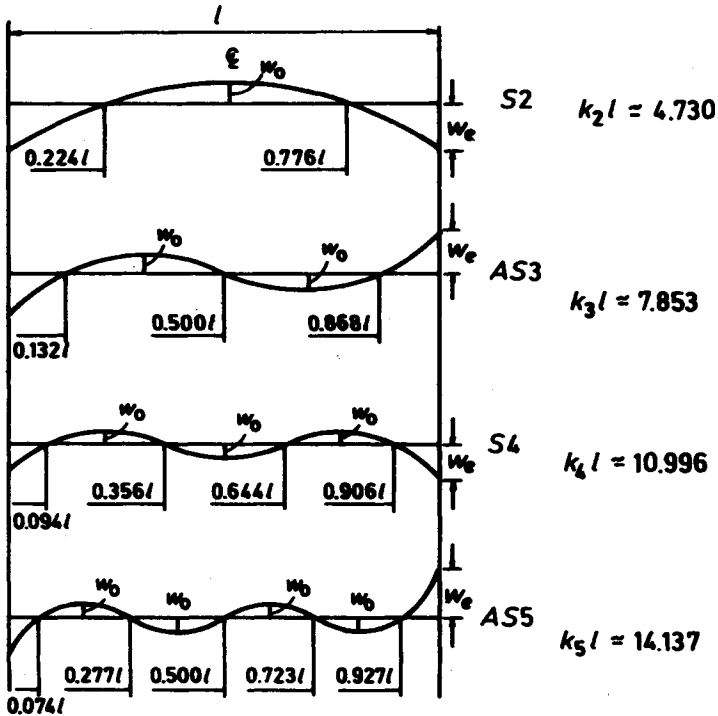


Figure 11.29

The Vibrating System

The configuration assumed for the four modes are indicated in Figure 11.29 shown rotated through 90° , for convenience. In this figure, the $k_n l$ terms refer to the free-free beam frequency solution

$$\omega_n = (k_n l)^2 (EI/ml^4)^{1/2} \text{ rad s}^{-1} \quad (61)$$

in which m = mass per unit length.

The following should be noted in connection with these configurations:

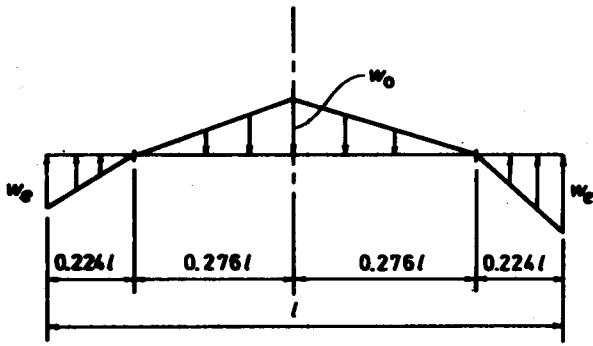
1. The node positions are those obtained in the solution of the classical laterally loaded free-free vibrating uniform beam problem.
2. The maximum oscillation is assumed to be the same for each internal loop for any mode.
3. It is assumed that each loop may be approximated by triangles as shown in Figure 11.30 for S2 and AS3 only.

The Deformation of the Vibrating Structure

The actual deformation mechanism for the structure is extremely complicated. It is initiated by the suddenly applied shear inertia loadings and consists of various (possibly) symmetric and anti-symmetric essentially non-superposable components deflecting from the vertical position. As an approximate approach, it will be assumed that the different modes are additive with each mode having its own period and frequency, and that the deformations start at time $t = 0$, from the vertical. If desired, the $t = 0$ time could be taken as t_3 , the end of the period of transition.

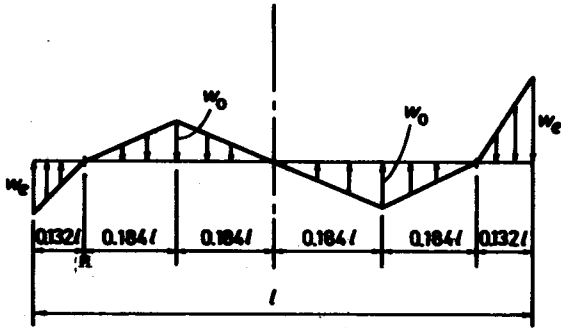
Consider typically, the S2 mode of vibration, in the maximum inertia load position as shown in Figure 11.31a. This will cause a deflection as shown in Figure 11.31b where zero deflection occurs at the points A, the nodes, w_{e_2} and w_{o_2} are assumed the loads on the structure causing the maximum deflection shown.

The applied earthquake load is a series of fore-and-aft short time pulses which cause the structure to vibrate on both sides of the vertical. The deflections δ_e and δ_o are assumed to be the deflection that would be caused by gradually applied loads w_{e_2} and w_{o_2} applied to an initially undeformed vertical structure. Therefore the actual deflections from the vertical, due to the inertia loadings of Figure 11.31a are assumed to be approximately the 'gradually applied' values corresponding to this load, with damping altering this as required.



S2

S2



AS3

AS3

Figure 11.30

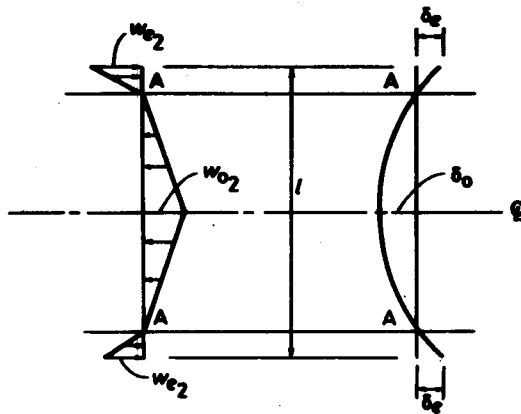


Figure 11.31

The various zero-deflection positions (the nodes) are set as closely as possible to the frequency analysis positions for these as shown in Figure 11.29.

The following preliminary data is collected and assembled in preparation for the deformation and structural analysis. The code or specifications or governing agency or engineer set the earthquake magnitude, location, and other data from which, using the equations and curves of Chapter 4, the ground energy per unit effective area can be determined. Based upon known data or the designing engineers' expertise and judgement, values are assumed for the effective base area, A_e , and the effective length, l . In this connection, the author recommends the following until such time as sufficient data and experience are gathered to suggest otherwise:

1. Assume a uni-material structure, with a single effective stiffness, EI .
2. For effective area, A_e , use the actual *foundation* area of the structure.
3. For effective length, l , use a value such that the two-node period of the structure (bending only considered) is equal to $0.1N$ as suggested by some observations. N is the number of storeys in the structure and the period is determined from the free-free vibration solution, Figure 11.29 and Eq. 61.
4. For the low, squat (shear) structure use the actual length of the structure and consider all energy as shear energy except for specially-designed steel or concrete rigid frames with moment connections at the joints (see Sections C and D of this chapter) and for large concentrated masses of equipment and similar items, for which mv^2 energies can be determined.

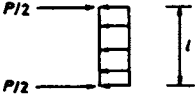
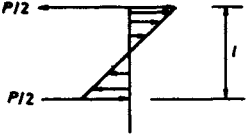
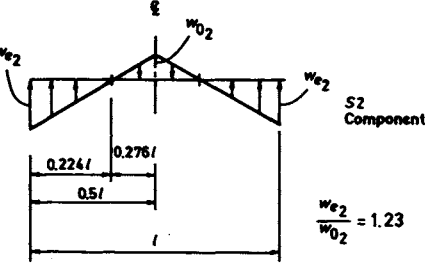
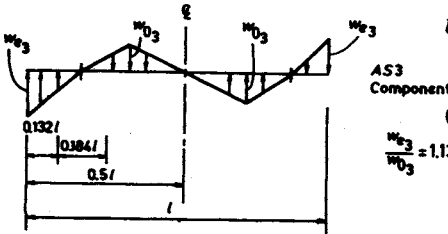
At this point, U_{total} is known, as are l , A_e , the period, and the dimensions, stiffness, etc.

The Division of Energy — See Table 10

The division of energy within the vibrating structure is determined in the following sequence and approximate manner:

1. We shall assume bending strain energy (and dynamic energy) only are involved. Shear effects will be important for short, squat structures, as in Section C of this chapter.
2. The total energy that the structure must absorb is $U_{\text{total}} = \epsilon_{t_f}(A_e)$, and the timewise application of energy to the structure is as shown in Chapter 4.
3. Because this energy is applied by the ground in an essentially smooth, continuous manner, with roughly equal alternating directional loads on the base, we shall assume that the quasi-static component of energy is not applied and all of the energy which the structure must absorb is taken in equal vibratory

Table 10 Energy Expressions

| Sketch and Loading | S = Symmetric AS = Anti-symmetric EI = Constant | Energy, U $U_{total} = \epsilon_{t_f}(Ae)$ |
|---|--|---|
|  | Symmetric Component | $U_{PS} = 0.00406 \frac{P^2 l^3}{EI}$ |
|  | Anti-symmetric Component | $U_{PAS} = 0.00059 \frac{P^2 l^3}{EI}$ |
| $\frac{U_{PS}}{U_{PAS}} = 6.82$ | | |
| $\therefore U_S = 0.87 U_{total}$ | | |
| $U_{AS} = 0.13 U_{total}$ | | |
|  | S2 Component | $U_S = 0.000259 \frac{w_{e2}^2 l^5}{EI}$ |
| $\frac{w_{e2}}{w_{02}} = 1.23$ | <p>CASE I</p> <p>U_{S2} and U_{AS3}, only</p> <p>$U_{S2} = 0.87 U_{total}$</p> <p>$U_{AS3} = 0.13 U_{total}$</p> <p>$U_{S4} = 0$</p> <p>$U_{AS5} = 0$</p> | |
|  | AS3 Component | $U_{AS3} = 0.0000374 \frac{w_{e3}^2 l^5}{EI}$ |
| $\frac{w_{e3}}{w_{03}} = 1.13$ | <p>CASE II</p> <p>U_{S2}, U_{AS3}, U_{S4}, and U_{AS5}</p> <p>$U_{S2} = 0.70 U_{total}$</p> <p>$U_{AS3} = 0.10 U_{total}$</p> <p>$U_{S4} = 0.17 U_{total}$</p> <p>$U_{AS5} = 0.03 U_{total}$</p> | |

(Table 10 continued on next page)

(Table 10 continued from previous page)

| Sketch and Loading | S = Symmetric AS = Anti-symmetric EI = Constant | Energy, U $U_{\text{total}} = \epsilon_{t_f} (Ae)$ |
|--------------------|---|---|
| | $U_{S4} = 0.0000192 \frac{w_0 e_s^2 l^5}{EI}$ | |
| | $U_{AS5} = 0.00000327 \frac{w_0 e_s^2 l^5}{EI}$ | |

(dynamic) and potential (strain) energies. At any point in the vibrating cycle, the energy is equal to the sum of dynamic and strain energies. The structure is assumed to vibrate on both sides of a vertical.

4. The maximum strain energy occurs when the structure is at its maximum deflected position, which occurs on both sides of the vertical (neutral) position of the structure. At these locations the dynamic energy is zero, since the velocity of the structure is zero.
5. The maximum dynamic energy occurs when the moving structure passes through the neutral vertical position, corresponding to zero strain energy and maximum velocity.
6. The maximum strain energy (step 4) is equal to the maximum dynamic energy (step 5) of the same cycle, less the loss due to damping.
7. The total energy is damped by an amount ΔU per cycle.
8. Referring to Table 10, in which the various strain energy quantities are shown, we see that

$$\frac{U_{PS}}{U_{PAS}} = 6.82 \quad (62)$$

We assume this determines the ratio of total symmetric to total anti-symmetric strain-vibratory energies. That is,

$$\frac{U_{\text{total}_S}}{U_{\text{total}_{AS}}} = 6.82 \quad (63)$$

From (2) above, we can now determine the total energies, U_{total_S} and $U_{\text{total}_{AS}}$ as follows

$$\begin{aligned} U_{\text{total}_S} &= 0.87 U_{\text{total}} \\ U_{\text{total}_{AS}} &= 0.13 U_{\text{total}} \end{aligned} \quad (64)$$

9. We consider only U_{S2} , U_{S4} , and U_{AS3} , U_{AS5} as the symmetric and anti-symmetric modes of vibration developed by the earthquake. Based upon the lengths of the loops developed and approximate strain and kinetic energy analyses, we assume

$$\frac{U_{S2}}{U_{S4}} \cong \frac{U_{AS3}}{U_{AS5}} \cong 4 \quad (65)$$

and therefore,

$$\left. \begin{aligned} U_{S2} &\cong 0.8 U_S \cong 0.70 U_{\text{total}} \\ U_{AS3} &\cong 0.8 U_{AS} \cong 0.10 U_{\text{total}} \\ U_{S4} &\cong 0.2 U_S \cong 0.17 U_{\text{total}} \\ U_{AS5} &\cong 0.2 U_{AS} \cong 0.03 U_{\text{total}} \end{aligned} \right\} \quad (66)$$

Obviously, if only U_{S2} and U_{AS3} are considered,

$$\left. \begin{aligned} U_{S2} &\cong 0.87 U_{\text{total}} \\ U_{AS3} &\cong 0.13 U_{\text{total}} \end{aligned} \right\} \quad (67)$$

10. It will be assumed that the combined effect of all four modes can be approximated by a simple superposition of effects. This includes shear, bending, and deflection as these are determined by the loading of Table 10 and the periods as determined by either a frequency analysis or by assuming the constant section free-free, effective length frequency values. Note that the w_e and w_o values are determined from the known U_{total} quantity and the expressions in Table 10.

Outline of the Design-Checking Procedures

We now outline, in step-wise form, a suggested design or checking procedure for a tall building using the methods and theory described. In this connection, it is emphasized that almost certainly refinements and modifications will be introduced as more experience is gained and additional data is collected. Also special structures such as bridges and dams may require different procedures, but in all cases these can be straightforward and logical extensions of the basic theory. In the next section a detailed application will be given for a particular structure.

As pointed out in the last section, the building has been located at a given point. The code or specifications or the engineers call for the design accelerogram or earthquake magnitudes and other data from which, assuming effective length and effective area are known, we can estimate the total energy which the structure must absorb. From Table 10 it is possible to determine the total energy for each mode of vibration.

Assume first the accelerogram is canonical. Then the energy can be assumed applied as either (a) a single total amount at $t = 0$, (b) continuously in accordance with Eq. 7 of Chapter 4 or (c) a series of energy packets, whose sum equals the total energy, at some predetermined frequency.

It would appear that method (a) is the most conservative and will lead to the maximum stress and deflection condition. We shall assume this is so and will describe the structural analysis corresponding to this method of loading. Consider the two-node mode only. The others are handled similarly with the obvious time variations corresponding to their frequencies.

1. At $t = 0$ (or $t = t_3$), the two-node free-free beam vibration is assumed to begin.
2. At the 1/4 cycle, the maximum deflection is reached and the values of w_e and w_o are determined from the known energy value, $U_{S2_{\text{equal}}} - U_{\text{damped}}$ in 1/4 cycle, see Table 10.
3. At the 3/4 cycle the maximum opposite deflection is reached and the values of w_e and w_o are determined from the remaining energy,

$$U_{S2_{\text{total}}} - U_{\text{damped in } 3/4 \text{ cycle}}$$

again using the expressions in Table 10.

4. Continue thus, going from maximum strain energy position to maximum strain energy position, decreasing the energy from half cycle to half cycle due to damping and computing the corresponding w_e and w_o values, until all the energy has dissipated.
5. Do this for the UAS3, US4, and UAS5 energies, Table 10 until all these energies have dissipated. Note that, because of the higher frequencies, these modes will dissipate to zero well before the U_{S2} mode, with U_{AS5} dissipating most quickly.
6. To find the approximate moment, shear, or deflection at any time, assume all four separate effects can be superposed, using times corresponding to the different frequencies.
7. If the energy is to be introduced in separate lump sums, as would be done, for example, for an accelerogram consisting of superposed canonical accelerograms, the same procedure is followed. We simply increase the amount of total energy at the appropriate times and calculate the corresponding w_e and w_o values at the maximum deflection positions of the vibrating structure in each of the four modes.
8. If only two modes, S2 and AS3, are used, the procedure is similar using the corresponding values of the energies, see Table 10.
9. If the structure contains significant (heavy) concentrated machine parts or similar objects, the energy which these absorb can be approximated from their locations in the structure and the corresponding mv^2 terms which can be estimated when the deformation is known. This energy must be subtracted from the total energy supplied by the ground. Or an equivalent distributed mass may be included in the mass of the structure.
10. If the structure is short and squat, then assume all the energy is absorbed as shear energy (less that amount taken by concentrated machines or by rigid frames in bending as in the last Section D).
11. In all of the foregoing, the maximum stress and deflection, for design purposes, should be less than specified code values. Failure will be indicated by excessively high values of stress and/or deflection.
12. If the building orientation with respect to a ray from the epicentre requires it, the energy may be decomposed into two perpendicular directions parallel to the principal axes of the structure and the response taken as a superposition of the two principal axes effects. This may be done because of the scalar identity $V^2 = V_x^2 + V_y^2$ and because the energy of the vibrat-

ing structure is given by the kinetic component $mV^2/2$. In the above, V = magnitude of velocity; V_x = magnitude of the velocity in the x principal direction; V_y = magnitude of the velocity in the y principal direction.

A TYPICAL DESIGN-ANALYSIS STRUCTURAL APPLICATION FOR A TALL BUILDING

Introduction

The previous section indicated, in general outline form, a suggested approximate design checking-analysis procedure for a building using the theory derived herein. In this section an actual application will be presented for a particular tall building. Most of the detailed calculations will be given. For those items which are best obtained using available (or easily prepared) computer programs, an outline only will be presented.

In a typical application, the code or specifications or the governing agency-engineer would specify:

1. Building dimensions, cross-section, materials.
2. Earthquake magnitude M , efficiency η , geology region \mathcal{R} .
3. Location of building, i.e. distance from epicentre.

From (2), we can determine,

4. $\Sigma(IS)_f$ and S_f and therefore the MID curve and ϵ_{t_f} , the total energy per unit area at the building location. See the last two paragraphs of the conclusion, p. 305.

From (3) and (4) as a check we can determine the approximate intensity at the building location and therefore from Figure 4.7 approximate values of $\Sigma(a\Delta t)_f$ and t_f and also ϵ_{t_f} , the total energy per unit area which must be compatible with the value determined in (4) and (2). Thus in (1), (2), and (3) all of the earthquake information needed for the rational design analysis of the structure is available using the chart, equations and methods developed in the text.

In addition, we require test data values or the engineers' judgement determined of l , the effective length, and of Ae , the effective area of the structure. We shall indicate in some detail how the design analysis is performed for a typical assumed set of conditions (1), (2), and (3).

In this connection, from the known ϵ_{t_f} and (assumed) $\Sigma(a\Delta t)_f$ and t_f values, packets of energy could be applied to the structure at predetermined times by using Eq. 7 of Chapter 4 and the stress-deflection behaviour of the structure obtained for this assumed input of energy. However, it should be noted that

according to Eq. 7 of Chapter 4 which is shown in Figure 4.3 of that chapter, a large part of the energy is introduced at small values of t . In other words, for practical design purposes, the assumption of total energy application at $t = 0$ is probably not excessively conservative for a single canonical accelerogram.

Therefore, for our present purposes (and very likely for most actual design situations) it will be sufficient to make the conservative assumption that all of the energy is applied at time $t = 0$, and furthermore this energy is apportioned to the S2 and AS3 modes only. The energy-packet design and the S4, AS5 contributions are handled in a similar manner if it is desirable or necessary to include these effects. For example, if a check on a particular actual response is desired, one could use the timewise variation of energy relation as well as the separate symmetric, anti-symmetric energy components and superposed canonical accelerograms, if desired. This will give a detailed representation of the stress and deflection response as determined by the present theory, including 'higher-order effects'.

It must be stated once more — the particular computations which follow are based upon the data available at this time. Various assumptions must be made (energy-magnitude, efficiency of earthquake, period of vibration, and others) and these will almost certainly be refined and will become more accurate as data are accumulated. The actual numerical results obtained must be evaluated and judged with this in mind. It is possible that these numbers are quite accurate. Or they may be somewhat approximate. The final determination of this must await the collection of additional experimental data, as is true in all fields of applied mechanics in which new approximate theories are introduced.

The technique which is used, however, is the one which will apply also when the additional data is at hand. Ultimately, it should be possible to prepare a 'handbook' in which all of the earthquake parameters are related to typical structures and the damage probability of structures is related to intensity and

ϵ_{t_f} .

It will now be shown, in some detail, how the various design and theoretical charts and equations of Chapter 4 are applied to a typical structural analysis. For the somewhat lengthy and complicated stress and deflection analyses, the general method only will be presented with a minimum of actual numerical computations. However, the detailed numerical solutions for these cases use elementary methods and are readily machine programmed. Also since at this point, the main purpose is to outline the procedure, a simplified cross-section (and general construction details) will be assumed for the illustrative structure.

The Design Analysis

The step-by-step procedure is as follows (the numbering of the actual computations will conform to these numbers):

1. The earthquake magnitude, geology, building dimensions, location, and materials of construction are specified.
2. From Figure 4.5, determine $\Sigma(IS)_f$ and S_f .
3. Prepare the MID diagram.
4. From one of the available magnitude-energy equations determine the total energy of the earthquake.
5. Assume an earthquake efficiency (specifications) and determine H , the total horizontal ground energy between S_i and $S_f = S_{III}$.
6. Using the energy-intensity chart (Figure 4.8) determine U_{total} , the total horizontal ground energy to be absorbed by the building. Assume the effective area, A_e , in this step. Note, in effect, the efficiency of step 5 can be related to the assumed value of S_f/S_i of Eq. 13 Chapter 4, so that the choice of S_f/S_i for any particular case will be determined by accumulated data and experience and will not be arbitrary. See also the last two paragraphs of the conclusions, p. 305.
7. Determine E , I , and m for the structure. [Note: In this computation we shall assume a uni-material concrete structure. As noted earlier, experience may indicate that a more accurate analysis can be obtained using separate framing (i.e. steel) and outer shell (i.e. brick or concrete) structures].
8. Compute the effective length, l , using the empirical relation

$$\text{period} = 0.1 N \quad (68)$$

and the major mode equation for the free-free vibrating structure,

$$\omega = (4.73)^2 \left[\frac{EI}{ml^4} \right]^{1/2} \text{ rad s}^{-1} \quad (69)$$

[Note: This introduces an approximation of the soil-foundation interaction effect. If, in the designing engineer's judgement, an adjustment is desirable, the value of l could be increased or decreased accordingly].

9. As a rough accelerogram compatibility check, when sufficient information is given, determine ϵ_{t_f} and check the value as given in the intensity-energy of step 6.

10. Determine U_{total_S} and $U_{\text{total}_{AS}}$ from

$$\left. \begin{aligned} U_{\text{total}_S} &= 0.87 U_{\text{total}} \\ U_{\text{total}_{AS}} &= 0.13 U_{\text{total}} \end{aligned} \right\} \quad (70)$$

11. Assume

$$\text{and} \quad \left. \begin{aligned} U_{S2} &= U_{\text{total}_S} \\ U_{AS3} &= U_{\text{total}_{AS}} \end{aligned} \right\} \quad (71)$$

12. Determine $w_{e_1}, w_{o_1}, w_{e_2}$, and w_{o_2} , using relations in Table 10.
13. Determine maximum shears and moments using the loads of step 12.
14. Determine deflections using the loads of step 12.
15. Using an assumed damping factor, determine shear, bending, and deflection time histories.
16. If a combined canonical accelerogram is to be used, the total energies corresponding to each of the separate canonical curves will be applied to the structure at the time corresponding to the assumed accelerogram.
17. If the structure is a short, squat shear structure then all the energy is to be taken in simple sliding shear

$$U_{\text{total}} = k \frac{V^2 l}{6AG} \quad (72)$$

in which, initially it is recommended that l be taken as the actual overall length of the structure, k be taken as unity, and Ae be taken as equal to the foundation area. Determine V and check the strength of the building. See Section C and D of this chapter.

The analysis-computation corresponding to the above now follows:

1. We will consider an earthquake roughly equivalent to an $M = 5.3$ in an \mathcal{R}_1 geology. Our building will be the one previously used for illustrative purposes and it will be assumed that it is located at $S = S_f/2$.
2. From Figure 4.5 this indicates that, approximately

$$\left. \begin{aligned} S_f &= 75 \text{ km} \\ \Sigma(IS)_f &= 850 \end{aligned} \right\} \quad (73)$$

3. We will determine the MID diagram as was done in several of the preceding sections of this chapter. See note in Step 6.
4. Assume the energy-magnitude equation is

$$\left. \begin{aligned} \log_{10} E &= 11.4 + 1.5 M \\ \text{so that } E &= 10^{20} \text{ ergs, approximately} \end{aligned} \right\} \quad (74)$$

5. If we assume an efficiency of 10 per cent, then

$$H = E\eta = 10^{19} \text{ ergs} \quad (75)$$

in which H is the total horizontal ground energy between S_i and S_f .

6. Using Eq. 14 of Chapter 4 noting the dimensions of the building is 100 ft \times 100 ft (= 0.03 km) and assuming this is the actual foundation (mat) area, then this is also the effective area, Ae , and we can determine the total energy to be absorbed by the building

$$U_{\text{total}} = \frac{(0.03)^2}{2\pi S} \frac{H}{9} \left[\left(\frac{S_f}{S} \right)^{1/3} - \left(\frac{S_f}{S + 0.03} \right)^{1/3} \right] \quad (76)$$

which, for $S_f = 75$ km, $S = 37.5$ km, H equals 10^{19} ergs gives

$$\left. \begin{aligned} U_{\text{total}} &\approx 10^{12} \text{ ergs} \\ &\approx 100,000 \text{ ft lbs} \end{aligned} \right\} \quad (77)$$

as the total energy to be absorbed by the building. Note, the value of U_{total} could have been obtained by using the MID diagram of Step 3 and $\epsilon_{t_f}(Ae)$ as was done in previous sections. This is preferable to using Steps 4, 5 and 6 as above. See the last two paragraphs of the conclusion, p. 305. The two values are approximately equal.

7. The concrete outer and inner walls are assumed to be 12" thick. There are 12-24 W 160 steel columns. We assume the neutral axis is at $d/3$, neglect tension in the concrete and assume the outside walls are 50 per cent effective because of window openings, etc. This is as shown in Figure 11.32. The principal axis of the building is assumed perpendicular to a ray from the epicentre.

Using dimensions, weights, and similar data, we obtain weight of building, $W = 92,000 \text{ lb ft}^{-1}$.

$$\begin{aligned}
 I_{NA} &= 186,000 \text{ ft}^4 \\
 E &= 2,500,000 (144) \text{ psf} \\
 A_{eq} &= 640 \text{ sq. ft} = \text{equivalent concrete area} \\
 m &= \frac{W}{g} = \frac{92,000}{32.2}
 \end{aligned}
 \tag{78}$$

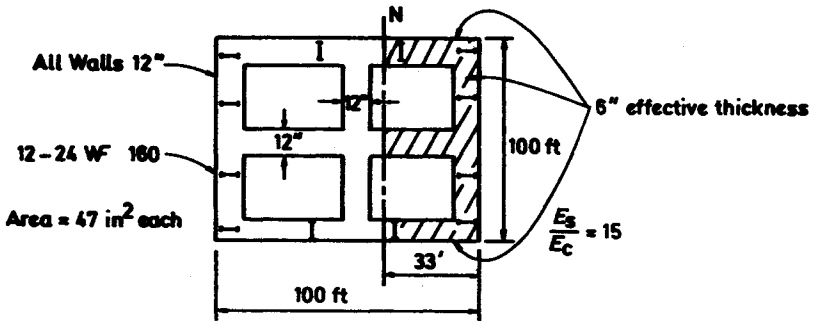


Figure 11.32

8. The empirical relation for the period of the building

$$\text{period} = 0.1 N s \tag{79}$$

gives, for $N = 40$ storeys

$$\begin{aligned}
 \text{period} &= 4s \text{ for a complete cycle} \\
 \omega &\cong 1.5 \text{ radians s}^{-1}
 \end{aligned}
 \tag{80}$$

or

Therefore, from Eq. 69 we have

$$l^2 = (4.73)^2 \left[\frac{EI}{W/g} \right]^{1/2} \quad (81)$$

and using the values in Step 7,

$$l = 1200 \text{ ft, say} \quad (82)$$

which indicates that the soil-interaction effect is assumed as approximately accounted for as shown in Figure 11.33.

As pointed out, if this value of l appears to warrant modification, this could be done by the designer.

9. This check requires additional data on the accelerogram.
10. Using the relations given in Table 10 and the value of U_{total} from Step 6, we determine

$$U_{\text{total}_S} = 0.87 U_{\text{total}} = 87,000 \text{ ft lb} \quad (83)$$

$$U_{\text{total}_{AS}} = 0.13 U_{\text{total}} = 13,000 \text{ ft lb}$$

$$11. \quad \left. \begin{aligned} U_{S2} &= 87,000 \text{ ft lb} \\ U_{AS3} &= 12,000 \text{ ft lb} \end{aligned} \right\} \quad (84)$$

12. From Table 10

$$\left. \begin{aligned} 87,000 &= \frac{0.000259 w_{e_2}^2 l^5}{EI} \\ 13,000 &= \frac{0.0000374 w_{e_3}^2 l^5}{EI} \end{aligned} \right\} \quad (85)$$

$$\frac{w_{e_2}}{w_{O_2}} = 1.23 \quad (86)$$

$$\frac{w_{e_3}}{w_{O_3}} = 1.13$$

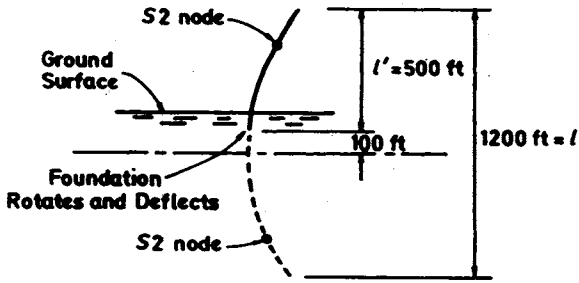


Figure 11.33

so that,

$$\begin{aligned}
 w_{e_2} &= 3100 \text{ lb ft}^{-1} \\
 w_{o_2} &= 2500 \text{ lb ft}^{-1} \\
 w_{e_3} &= 3000 \text{ lb ft}^{-1} \\
 w_{o_3} &= 2650 \text{ lb ft}^{-1}
 \end{aligned}
 \tag{87}$$

13. The ratio of

$$\frac{\omega_{AS}}{\omega_S} = \frac{61.6}{22.4} \sim 3
 \tag{88}$$

Therefore the w_2 and w_3 will combine to give the approximate maximum superposed effect when the symmetrical vibration is at the $1/4$ cycle and the anti-symmetrical vibration is at the $3/4$ cycle. The loadings will then be approximately as shown in Figure 11.34, and approximate values of maximum shear and maximum moments (due to the vibratory inertia loads) are

$$\begin{aligned}
 V_{1-1} &= w_{e_2} (0.112 l) + w_{e_3} (0.066 l) \\
 &= [3100 (0.112) + 3000 (0.066)] (1200) \\
 &= 650,000 \text{ lb}
 \end{aligned}
 \tag{89}$$

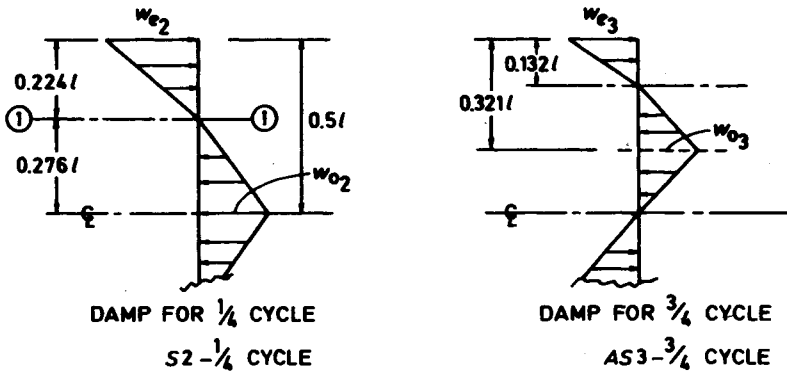


Figure 11.34

and

$$\left. \begin{aligned} M_{1-1} &= 545 (1200)^2 (0.15) \\ &= 117,700,000 \text{ ft lb} \end{aligned} \right\} \quad (90)$$

or

$$\left. \begin{aligned} M_{\bar{e}} &= \text{Approx. overturning moment} \\ &= 347 (0.43) (l)^2 - 2500 (0.276) l (0.092) l \\ &= 3.17 (0.43) (1200)^2 - 2500 (0.276) (0.092) (1200)^2 \\ &= 125,000,000 \text{ ft lb} \end{aligned} \right\} \quad (91)$$

Then

$$\left. \begin{aligned} \tau_{\max} = \text{shear stress} &= \frac{V}{A_{EQ}} \\ &\cong \frac{650,000}{640} \cong 1000 \text{ psf} \end{aligned} \right\} \quad (92)$$

$$\left. \begin{aligned} \sigma_{\max_{1-1}} &= \frac{Mc}{I} = \frac{(117,700,000) (30)}{186,00} \\ &\cong 200,000 \text{ psf} \\ &\cong 1400 \text{ psi} \end{aligned} \right\} \quad (93)$$

The above values will be modified by the effective eccentricity of the dead weight of the building, which will be dependent upon the actual spandrel and connection construction details.

14. The deflections will not be obtained. The actual determination of these offers no particular difficulty. Any of the elementary methods of deflection analysis can be utilized in this exercise, including available computer programs.
15. The deflections, shears, and moments may then be obtained timewise using the known frequency equations and an assumed damping factor.
16. Combined canonical accelerograms would require a simple superposition of effects previously obtained using the known (assumed) time phases and accelerogram shapes.
17. For a shear structure, say a building 15 ft high, steel columns 8 W 31, everything else being the same as the structure of Step 7, then the total energy, $U_{\text{total}} = 100,000$ ft lb is taken in shear strain energy and we have

$$U_{\text{total}} = \frac{kV^2l}{6AG} \quad (94)$$

with $k = 1$, assumed

$$l = 15 \text{ ft}$$

$$A = 12 (9.1) (15) + 400 = 2000 \text{ sq ft, equivalent concrete}$$

$$G = 1,000,000 (144) \text{ psf,}$$

So that

$$\begin{aligned} \tau &= \frac{V}{A} = \text{Shear stress} \\ &= \left[\frac{6 (1,000,000) (144) (100,000)}{(2000) (15)} \right]^{1/2} \\ &= 385 \text{ psi} \end{aligned} \quad (95)$$

which indicates that concrete stresses are high enough to be a cause for concern, particularly at corners where stress concentrations occur and cracks frequently initiate.

The above represents a typical macroscopic or overall analysis for a particular tall structure.

Following are some observations concerning connections, details of connections and similar items. According to a fundamental premise of this book, namely that energy is the earthquake effect that must be designed for, the most desirable characteristic of all beam connections and similar details is that they be capable of absorbing large amounts of energy, consistent with their ability to resist the imposed stresses. Friction, for example, as evidenced by tight, contiguous, moving surfaces is an effect that should be exploited. In all, the sum of the energy absorbing details enters into the 'damping' factor used for the vibrating structure. The optimum design of energy absorbing connection details (or, indeed, energy absorbing mechanisms for the entire building) represents an important aspect of the overall structural design in earthquake engineering.

Conclusion for Section E

In this Section a particular application was made of the rational theory — the analysis of a 'tall' building. A tall building in the context of this theory is one for which $l/w > 5$. This implies that the entire building vibrates as a beam unit in bending as against the previous Section D analysis in which the structural elements — separately — vibrated in bending as beams.

A fundamental assumption made was that the building vibrates in combined symmetric and anti-symmetric modes. This introduces key requirements as follows:

1. The building (i.e. beam) must have support (boundary) conditions that are consistent with symmetrical and anti-symmetrical modes of vibration and
2. There must be an approximate means for apportioning the basic parameter — the energy — among the various symmetric and anti-symmetric modes, and
3. It would be desirable that included in the solution is a translation and rotation of the actual base of the structure, corresponding to the known soil-foundation behaviour of actual tall buildings responding to earthquakes.
4. There should be included in the solution a dissipation of energy corresponding to soil-foundation interaction effects which are known to occur.

All four requirements, in fact, are inter-related and interact with each other.

Thus, requirement (1) was met by assuming the building is a free-free structure of constant section and one symmetrical about the mid-height. Requirement (2) was satisfied by utilizing elementary symmetry, anti-symmetry and unsymmetry considerations, which are frequently introduced in different fields of applied mechanics. Also involved was the assumption that the symmetrical and anti-symmetrical strain energies maintain the same ratios in their vibrating

phases as they do in their quasi-static generating phases. In addition, conservation of energy considerations (the invariance of the potential plus kinetic energy plus damping energy) and also beam mass inertia behaviour effects were introduced.

Finally — and not the least important — the observed empirical behaviour that the symmetrical principal mode period of the structure can be given approximately in terms of the numbers of storeys of the structure was called upon to tie all four requirements into a single unified packet for

- A) By using the known period-of-vibration equation for the free-free beam, it was possible to solve for an 'equivalent length' of the building.
The actual, above ground portion of the building then behaves as experience indicates that the building should behave in the event of an earthquake. Its shape and period are consistent with this behaviour.
- B) As noted, the free-free assumption satisfies the boundary condition requirements for symmetry and anti-symmetry. This in turn permits a division of the energy into symmetrical and anti-symmetrical parts, which is an essential requirement of this rational theory for all tall buildings, and
- C) By introducing an effective length, we permit a portion of the energy to dissipate corresponding to soil foundation interaction (damping), and
- D) By introducing this effective length parameter, the *actual* base of the structure rotates and translates from the equilibrium position as is required by known observed behaviour; and

these four extremely important aspects of the vibrating tall structure occur while the structure itself is vibrating at the required principal mode frequency and with the required principal mode shape. Therefore — insofar as the structure itself is concerned, it is behaving approximately in the manner that it should be.

A typical, very simplified structure was used primarily to illustrate the analytical procedure. In a given case, numerical values of shears, moments and deflections could be determined for any earthquake specified — as it should be — in terms of those parameters that must be involved in the earthquake event.

Clearly, for the 'tall' building analysis of this section, it is desirable that

1. We have more data relative to the effective base area assumption. Although the assumption that actual *foundation* area be used for this important parameter appears to give good results for the limited number of examples considered, the question must be asked — 'Is this true for *all* buildings in *all* geological environments?'

2. We have more data relative to the effective length assumption as made in the example. By satisfying the several different engineering-physical requirements noted above, it appears that a reasonable, approximate approach to some very difficult aspects of the problem is reached. But the questions arise — 'Is there a more accurate way to determine this effective length?' And — 'Can the results obtained using this concept be checked against actual behaviour for any case?'
3. We determine how the total energy applied to a building structure is absorbed by the separate parts such as the steel framing, the brick or concrete facing, and so on. Do we assume a uni-material based upon relative moduli of elasticity as is done in elementary strength of materials and reinforced concrete theory? Or do we separate the frame and steel (and interior machines, furniture and other objects) using a partial energy for each including an mv^2 term for the interior items? Or do we include these last items as equivalent parts of the main structure?
4. We check the equivalent soil-interaction damping (energy loss) as given by the approximate procedure developed here and the loss that actually occurs.

F) A CONCRETE DAM EARTHQUAKE ANALYSIS

Introduction

An after-the-fact theoretical damage analysis of the Koyna Dam in India due to an $M = 6.5$ earthquake on December 11, 1967 is presented.

The Koyna earthquake gave a rare example of the performance of a gravity dam during an earthquake. Major dams have infrequently been subjected to strong ground shaking so that there was little experience of earthquake performance for these structures.

Two seminal, early papers (listed below) are used as the basic data sources for the rational analysis of this Section. The first, in particular, was used for most of the physical-engineering information concerning the dam, the earthquake and the area in which it occurred. In addition, that paper presented the results only of a finite element stress and deflection analysis which the present Section uses for comparison purposes. We shall refer to the papers as CHOPRA and as GUPTA.

- a) Chopra, A. K., Chakraborti, P. *The Koyna earthquake and the damages to Koyna Dam*. Bulletin of the Seismological Society of America, Volume 63. No. 2, April 1973, p. 381–397.
- b) Gupta, H. K., Rastogi, B. K., Hari Narain, *The Koyna earthquake of December 11, 1967. A Multiple Seismic Event*. Bulletin of Seismological Society of America, Volume 61, No. 1, February 1971 p. 167–176.

The earthquake (surface-wave magnitude 6.5 is the generally accepted value although there are some questions about this) occurred on December 11, 1967 in the south-westerly region of India. The 2800 ft. long and 338 high Koyna Dam is a concrete gravity dam which was in the epicentral region of this earthquake, as a result of which it suffered structural damage.

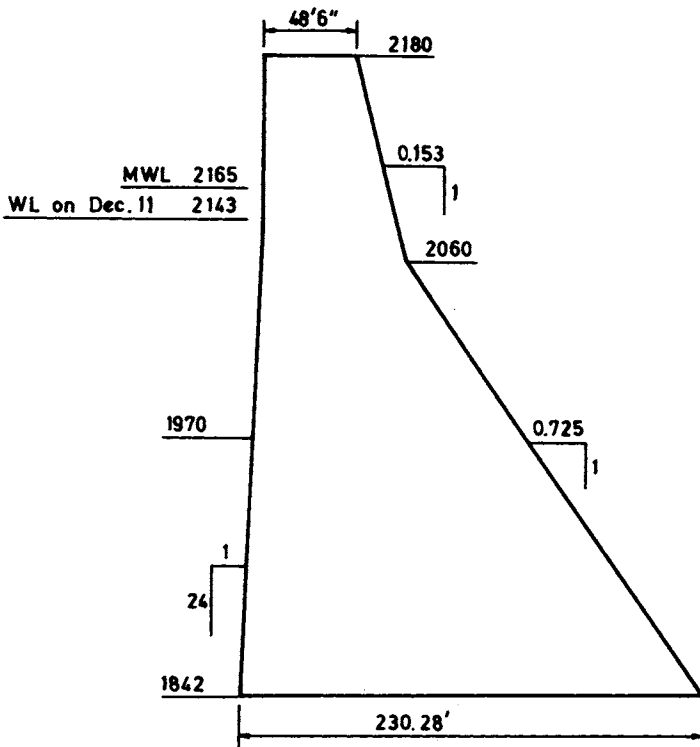
There are several aspects of this earthquake that need further elaboration. These are, in general, abstracted from the CHOPRA and GUPTA papers as are the earlier paragraphs in this Introduction.

1. Accelerogram records of the earthquake at the site are ambiguous and different interpretations of maximum conditions, including the magnitude, have been given by various investigators.
2. There is a stress concentration effect at the re-entrant corner of the dam at the critical station which will increase the stress above the value obtained in this Section. This effect will not be considered further although it is recognized as being a factor in the stress condition, and its value can be obtained quite simply using known stress concentration factors.
3. Values of assumed tensile and compression allowable stresses (CHOPRA) are about 200 psi and 900 psi respectively (tensile *strength* and compressive *strength* were taken as about 375 psi and 3500 psi respectively).
4. GUPTA analyzes the earthquake as a multiple event. An examination of the accelerogram in CHOPRA (his Figure 5) using the canonical accelerogram concept (Chapter 6) does indicate the strong likelihood that the earthquake consists of three separate shocks although it is not clear that the sequence and duration (as well as strengths of the separate shocks) are in agreement with GUPTA's conclusions. A more detailed analysis of this would be required.
5. GUPTA (his Figure 5) shows a map of the Koyna region, including the river and reservoir connected with Koyna Dam as well as an isoseismal map governing the event. Two points are of interest in connection with this figure:
 - a) As noted in (4) above as well as in GUPTA the earthquake in question was very likely a multiple event. It is possible, using the methods of Chapter 7, to prepare a superposition of canonical isoseismals which may then be compared with the map, Figure 5, from GUPTA.
 - b) The longitudinal axis of the dam appears to be at about 45° to the line of the main shock. This means that the energy absorbed by the dam in the transverse direction will be about 0.7 times the energy corresponding to the value shown on the energy-intensity chart, Figure 4.8.
 - c) GUPTA shows the dam located in an Intensity = VIII region about 4 km from one of several epicentres supposedly involved in this earthquake. In CHOPRA the dam is stated as being 'within eight miles of the epicentre'.

Also there is some question as to the magnitude of the earthquake, although a value of $M = 6.5$ is generally quoted. We shall use this value of the magnitude in our rational determination of the isoseismal map, and, in addition, we will use an average of the two distances (4 km and 12 km) to locate the dam. This will place the dam at, approximately, the junction of the rationally determined Intensity VIII and IX regions, giving the energy value later used in this analysis.

The Koyna Dam, (GUPTA)

Koyna Dam is a straight gravity structure with general sections as shown in Figures 11.35 and 11.36. Construction started in 1954 and was completed in 1963. The dam is about 2800 ft. long, 280 ft. high above the river bed, and 338 ft. high above the deepest foundation. It is constructed in 50 ft. wide monoliths and the contraction joints between the monoliths are provided with



NON-OVERFLOW SECTION, FOUNDATION ELEV 1842 TO 1900,
MONOLITHS 15 TO 17, 18/2

Figure 11.35

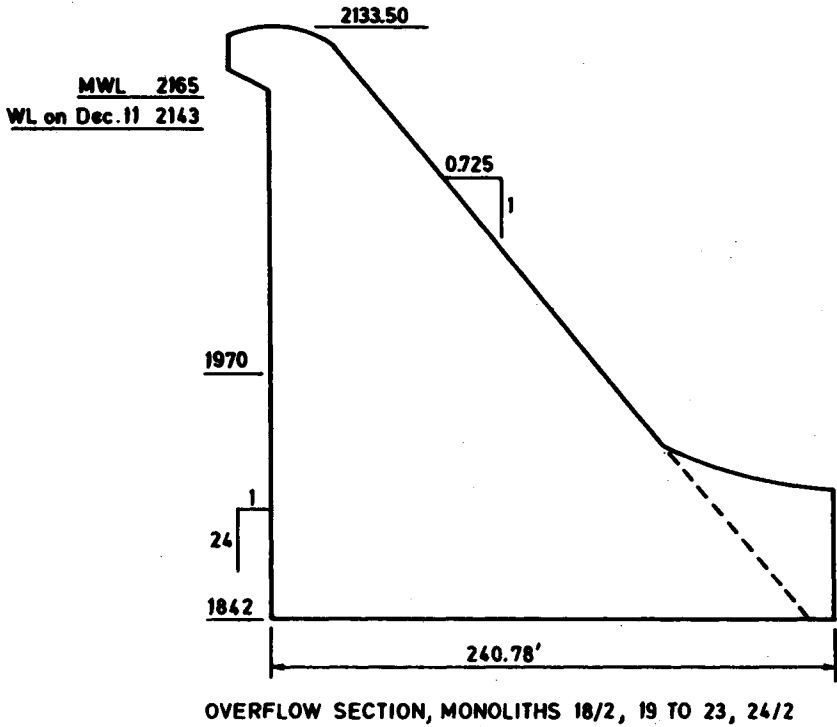


Figure 11.36

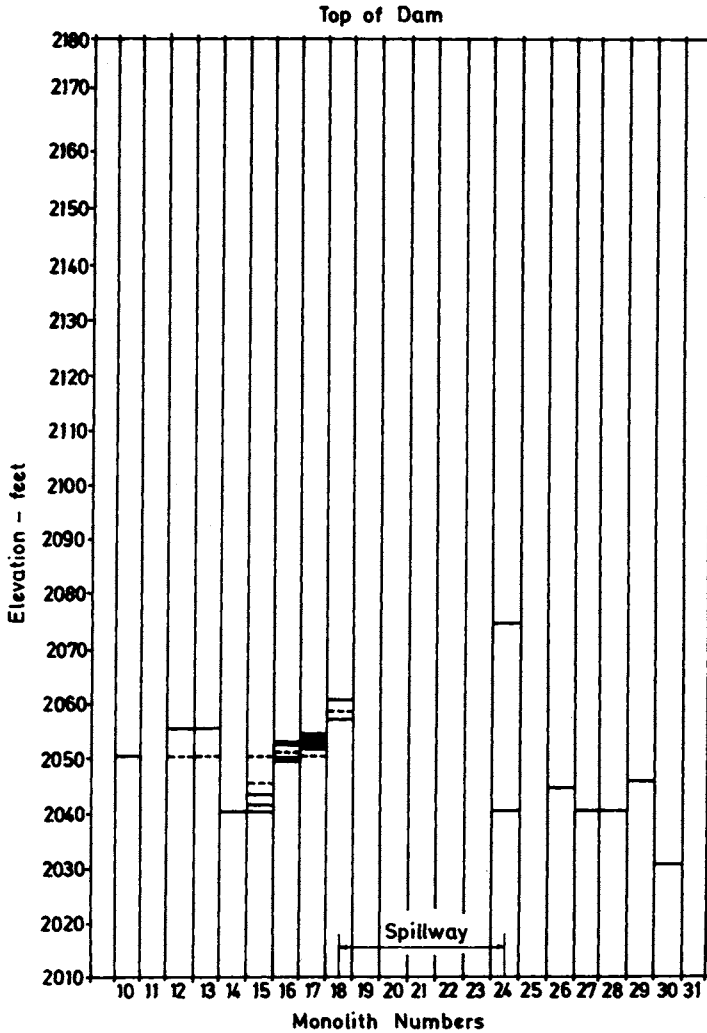
copper water seals. The spillway is about 300 ft. long. The dam is made of rubble concrete. To provide a more impervious zone, conventional concrete is provided for a 6 ft. thickness at the upstream face of all monoliths. The last six monoliths near the left bank are not made of rubble concrete but of hand laid rubble masonry.

The criteria adopted in designing the Koyna Dam section were (1) no tension in the section (2) the maximum compressive stresses to be less than the allowable stresses for the concrete used and (3) the shear friction factor is to be less than allowable values. See section (3) in the Introduction for assumed values of allowable stress and strengths.

Damage to the Koyna Dam

The most important structural damage to the dam were horizontal cracks on either the upstream or the downstream face or on both faces of a number of

monoliths. The locations of some of the cracks are shown on Figure 11.37. The cracks on the upstream face were located by divers using television cameras.



CRACKS IN UPSTREAM (—) AND DOWNSTREAM (---) FACES OF DAM

Figure 11.37

The MID (Iseismic Contour Map)

From Figure 4.5, the $\Sigma(IS)_f - S_f - \text{Average Regional Geology Chart}$ we obtain, for the single (canonical) $M = 6.5$ shock, Region \mathcal{R}_3 earthquake, the two values

$$\left. \begin{aligned} S_f &= 95 \text{ K} \\ \Sigma(IS)_f &= 1100 \text{ km} \end{aligned} \right\} \quad (96)$$

Then using the canonical isoseismic invariant equation, we determine the distances, S_j , to the centres of the various constant intensity j regions, as follows:

$$\left. \begin{aligned} S_{IV} &= 62 \text{ km} \\ S_V &= 39 \text{ km} \\ S_{VI} &= 25 \text{ km} \\ S_{VII} &= 15 \text{ km} \\ S_{VIII} &= 9 \text{ km} \\ S_{IX} &= 4 \text{ km} \end{aligned} \right\} \quad (97)$$

Thus, the Koyna Dam, located as noted in section (5c) of the Introduction, is at the junction of Intensity VIII and Intensity IX regions.

Now proceeding to the ϵ_{t_f} -Intensity Chart, Figure 4.8, we obtain the energy per unit foundation area which the vibrating dam must absorb in the forms of kinetic (moving) and potential (strain) energies, subject to the fundamental energy conservation principle.

The value obtained from the figure is

$$\epsilon_{t_f} \approx 3.5 \times 10^{17} \text{ ergs/sq. km} \quad (98)$$

It is now possible to proceed with the approximate plane strain structural analysis of the dam due to the earthquake. We analyse a one foot longitudinal strip of monolith as the vibrating element.

The Loading on the Dam

It will be assumed that the initial shock to the dam caused by the ground movement was a shear loading proportional to the cross-sectional shape of the dam.

properties are opaque so that one is interested in the Kerr effect where the angle mentioned above is known as the Kerr rotation.

The magneto-optic effects are produced when the indices of refraction for the right and left circularly polarized light are not the same.^{26,27} This is possible in a ferromagnet with non-zero-spin-orbit interactions. Thus, one must carry out fully-relativistic self-consistent spin-polarized electronic-structure calculations to understand and explain magneto-optic effects.

In the present discussion we consider the polar Kerr effect in which the light-propagation and magnetization directions are along the z-axis perpendicular to the surface of the sample, the most favorable configuration for maximum Kerr rotation. The Kerr rotation θ_k is given by²⁶

$$\theta_k = Re \left[\frac{N_r - N_l}{1 - N_r N_l} \right] \quad (17)$$

and the ellipticity (the ratio of minor to major axis)

$$\eta_k = Im \left[\frac{N_r - N_l}{1 - N_r N_l} \right] , \quad (18)$$

where *Re* and *Im* refer to the real and imaginary parts and N_r and N_l are the indices of refraction for right and left circularly polarized light respectively. N_r and N_l can be related to the conductivity tensor $\tilde{\sigma}$.

For a medium with three-fold or higher rotational symmetry about the z-axis, the conductivity tensor $\tilde{\sigma}$ has the form

$$\tilde{\sigma} = \begin{pmatrix} \sigma_{xx} & \sigma_{xy} & 0 \\ -\sigma_{xy} & \sigma_{xx} & 0 \\ 0 & 0 & \sigma_{zz} \end{pmatrix} . \quad (19)$$

Furthermore, the Onsager reciprocal relation $\sigma_{ij}(\vec{M}) = \sigma_{ji}(-\vec{M})$ gives $\sigma_{xy}(\vec{M}) = -\sigma_{xy}(-\vec{M})$ and $\sigma_{ii}(\vec{M}) = \sigma_{ii}(-\vec{M})$, where \vec{M} is the magnetization. Thus σ_{xy} and σ_{ii} have odd-power and even-power dependence respectively on \vec{M} .

Using Maxwell's equations one can write N_r and N_l in terms of σ_{ij} as follows:

$$N_{r,l}^2 = 1 - i \frac{4\pi}{\omega} (\sigma_{xx} \pm i\sigma_{xy}) \quad (20)$$

where ω is the frequency of the light. With the approximation $N_r \sim N_1 = N = (n + ik)$, we see that

$$(n + ik)^2 - (N_r^2 + N_1^2)/2 - 1 - i \frac{4\pi}{\omega} \sigma_{xx} \quad (21)$$

and

$$N_r - N_1 = \frac{4\pi}{\omega} \frac{\sigma_{xy}}{N} \quad (22)$$

so that

$$\theta_k = \frac{4\pi}{\omega} \operatorname{Re} \left[\frac{\sigma_{xy}}{(n + ik)[1 - (n + ik)^2]} \right]. \quad (23)$$

Thus, the Kerr rotation is determined by the off-diagonal component of the conductivity tensor and the indices of refraction of the medium.

σ_{xy} can be related to the electronic states by calculating the power P absorbed by the medium:

$$P = \frac{1}{2} \int \operatorname{Re} \vec{J}^* \cdot \vec{E} \, d\vec{V} \quad (24)$$

where \vec{J} , \vec{E} and \vec{V} are the current density, electric field and volume of the sample respectively.

Simplifying Eq. 24 one gets for right and left circularly polarized light

$$P_r = \frac{1}{2} V E^2 (\sigma_{1xx} \mp \sigma_{2xy}), \quad (25)$$

where subscripts 1 and 2 on σ_{ij} refer to the real and imaginary parts respectively.

Eq. 25 gives

$$\sigma_{1xx} = (P_r + P_1)/VE^2 \quad (26)$$

and

$$\sigma_{2xy} = (P_1 - P_r)/VE^2 \quad (27)$$

From quantum mechanics, the power absorbed at frequency ω is given by

$$P = \hbar \omega \sum_{\alpha\beta} W_{\alpha\beta} \delta(\omega_{\alpha\beta} - \omega), \quad (28)$$

where $W_{\alpha\beta}$ is the transition probability per unit time between electronic states α and β . The perturbation Hamiltonian H' due to the electromagnetic radiation responsible for these transitions is

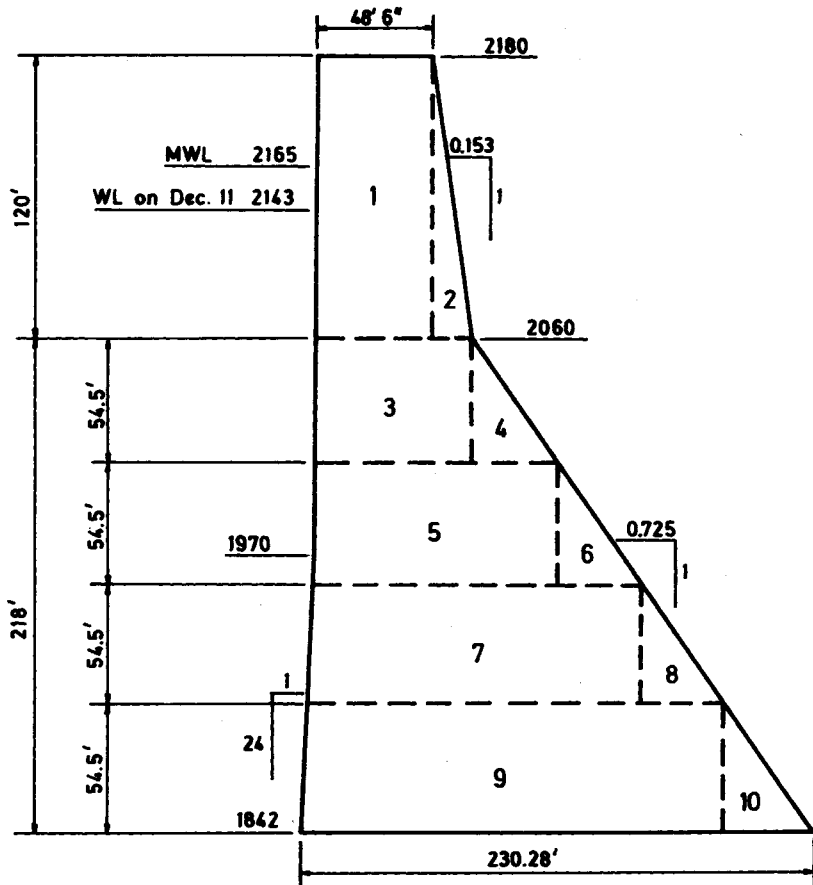


Figure 11.38 Block Division for Determining Transverse Earthquake Loading

Table 11

| Area Number | Total Shear V_{total} , lb | Average Shear V_{AV} , lb. | Average Area A_{AV} , sq. ft | l , Ft. | $\frac{U_s (2G)}{w^2 (10^4)}$ $G = 2 \times 10^4$ psi |
|-------------|---------------------------------|---------------------------------|-----------------------------------|-----------|--|
| 1 | 120 w | | | | |
| 2 | 23 w | 72 w | 58 | 120 | 1.1 |
| 3 | 78 w | | | | |
| 4 | 22 w | 193 w | 88 | 54.5 | 2.3 |
| 5 | 120 w | | | | |
| 6 | 22 w | 314 w | 128 | 54.5 | 4.2 |
| 7 | 164 w | | | | |
| 8 | 22 w | 478 w | 166 | 54.5 | 7.2 |
| 9 | 212 w | | | | |
| 10 | 22 w | 688 w | 208 | 54.5 | 11.4 |

From Figure 11.37 we see that major cracking occurs in the full height section in the neighbourhood of Elev. 2050–2060, on both upstream and downstream faces of the dam. We note first the design requirement previously stated that no tension occur in the concrete. Thus, at Elev. 2060 we have, approximately a D. L. + Hydraulic stress across the dam corresponding to

| <u>Upstream</u> | <u>Downstream</u> |
|------------------------|----------------------|
| El. 2060 0 psi tension | 240 psi, compression |

Due to the oscillating earthquake condition we have, on Elev. 2060, the moment and maximum stress,

$$\begin{aligned}
 M &= 120 (w) (60) + 3.5 (w) (40) \text{ ft lb.} \\
 &= 7340 w
 \end{aligned}
 \tag{105}$$

and

$$\sigma_{\max} \approx \pm \frac{Mc}{I} \approx \pm 960 \text{ psi}
 \tag{106}$$

on the upstream and downstream faces. The resultant maximum tensile stresses on the upstream and downstream faces, in the neighborhood of El. 2060, due to D. L. + Hyd. + Earthquake are, therefore

| | | |
|-----------------|-------------------|-------|
| <u>Upstream</u> | <u>Downstream</u> | |
| 960 psi tension | 720 psi tension | (107) |

indicating the very strong probability of tensile cracking on both faces. See section (3) of the Introduction for a statement concerning assumed allowable stresses.

Analysis at other elevations, in general, tend to confirm the cracking behaviour correspondings to the above.

The same type of analysis, applied to other monolith stations along the dam indicates similar cracking behaviours.

Note, also, the shear at El. 2060 is 143 w lb. so that the shear stress (nominal) on a plane through the monolith will be given by

$$\tau \approx \frac{145 w}{67 (1) (144)} \approx 210 \text{ psi} \tag{108}$$

indicating the strong possibility of shear distress within the dam.

Finally, a quick approximate check on the maximum bending deflection, Δ , of the crest with respect to the base (using elementary beam deflection formulas) determines a value for $\Delta = 1.3''$ as against a value for $\Delta = 1.23''$ obtained by CHOPRA.

Conclusion for Section F

The Koyna Dam, in India, was damaged during the $M = 6.5$ earthquake of Dec. 11, 1967.

The damage consisted of a large number of horizontal tension failure cracks on the upstream and downstream faces of the monolith sections which form the dam.

The theoretical rational methods which utilize previously obtained charts, curves and equations are applied-after-the-fact — to an analysis of the dam subjected to the given earthquake.

The analysis indicates the occurrence of excessive tensile stresses and cracks in the critical locations of the concrete monolith sections. In addition, large shear stresses within the dam are indicated.

For the purposes of this Section in which the application of the rational method to a dam analysis is discussed, it was deemed acceptable to assume a coarse subdivision of the dam cross-section as shown on Figure 11.38 and in Table 11. In spite of this, the results of the analysis indicate stresses which are in general agreement with those corresponding to the indicated damage.

For the design-analysis of dams before-the-fact, one may utilize a plane-strain solution using thin vertical slices of the dam cross-section with a unit longitudinal thickness of dam which can be very simply computer programmed. This will give a complete stress analysis of the cross-section at all stations.

The damage (characterized by horizontal-tension type cracks) appears to have been greatest in monoliths numbered 15, 16, 17. These three monoliths have the deepest and largest foundations (and hence the greatest earthquake energy loading). Thus, on the basis of the rational theory here utilized, one would expect these three sections to be more severely damaged than others.

Although the structural analysis procedure used in CHOPRA is entirely different from that used herein, the critical stresses and maximum crest deflections obtained in both methods are in general agreement.

CONCLUSION FOR THIS CHAPTER

It is important that accurate base values (calibrations) be determined for the various energy-intensity-accelerogram and isoseismal relations.

Also, the magnitude-energy and energy-efficiency relations (from which the surface horizontal energy is obtained) should be calibrated further. Although computations involving these relations have been used in several analyses (some of which are included in this and the previous chapter) and the results obtained appear to be reasonable, it would be desirable that additional checks and verifications be obtained for these important connections.

We should increase the calibration accuracy of the basic $\Sigma(IS)_f - S_f - M$ — geology curve, Figure 4.5. More points are needed for each of the three regions (and possibly for additional regions). At this time the MID curves and resulting ϵ_{t_f} values are approximate to (among other factors) the degree that Figure 4.5 is approximate. Because the actual reported magnitudes of most earthquakes are themselves approximate to various degrees, as noted in an earlier chapter, it is not unlikely that some discrepancies in the MID diagram and ϵ_{t_f} values are always going to be represent. However, it is obviously desirable to lower the amount of approximation.

New fundamental procedures have been recommended in these last chapters but as pointed out, they are subject to modification and revision as data are accumulated concerning the various correlations.

The basic theory, the fundamental ideas which integrate the accelerogram (timewise energy)-isoseismal (spacewise energy) concepts still apply. What is needed are the experimental data that will permit one to use the methods with a greater degree of confidence and certainty, although there is, at this time, sufficient design data available and listed in the text for preliminary design-

checking purposes and possibly even for actual designs. These were used in the six sections included in this chapter.

It is suggested that as more and more data of the required form is gathered and absorbed, the methods and procedures described herein will permit compilations of handbooks similar in every respect to those currently used in steel, concrete and other material design analyses. This will simplify the earthquake analysis problem to the point where its functions can be performed routinely by ordinary engineering design offices.

Finally, although in several of the sections of this chapter and the previous Chapter 10, the key energy quantity, ϵ_{t_f} was determined using the various intermediate relations which were used in the preparation of the fundamental ϵ_{t_f} -Intensity chart, it is not necessary, in general, to go through these intermediate steps. This was done to illustrate how the ϵ_{t_f} -Intensity chart can be generated, if necessary, for special conditions such as for $M < 5$, for underground blasts (see Section E of Chapter 10) and for other applications as well.

ϵ_{t_f} can always be obtained from a suitably calibrated chart similar to Fig. 4.8 and the MID diagram, Fig. 4.6.

APPENDIX

EARTHQUAKE ENGINEERING AND APPLIED MECHANICS

In this Appendix some further observations are made dealing with the basic content and form of the book. These will include statements concerning the place of earthquake engineering as a subsection of 'applied mechanics'. The following paragraph is a relevant introduction to the discussion.

In late 1981, a group of leading geologists, seismologists, and engineers gathered in Knoxville to discuss earthquakes within the eastern United States. (*Earthquakes and Earthquake Engineering; The Eastern United States*, Sept. 1981, Knoxville, Tennessee, Proceedings available from Earthquake Engineering Research Institute, 2620 Telegraph Ave., Berkeley, California 94704.) Richard A. Kerr, in *Science*, 9 October, 1981, summarized papers and talks presented. Quoting from his report, 'Henry Degenkolb of H. J. Degenkolb Associates . . . , a prominent seismic engineer for many years, held a sobering slide show during the meeting's final panel discussion . . . He showed the (1973) code-designed Imperial County Services Building that was torn down as a total loss following a moderate southern California earthquake in 1979 because its stylish open ground floor weakened it (*Science*, 29 August, 1980, p. 1006). The old masonry courthouse across the street suffered no damage. He showed several buildings in downtown Managua after the great earthquake there. All were still standing, but the one designed to resist the greatest shaking suffered the most damage, while the one with no seismic design suffered the least damage. 'Doesn't this tell us that perhaps we're on the wrong track?' Degenkolb said. 'The real guts of earthquake engineering is not contained in present codes. We don't fully understand the tie-in between what we measure (severity of shaking) and damage'.

This book presents a new and different 'track' dealing with the 'guts' of earthquake structural engineering. 'Shaking' is not the critical design parameter; 'energy' is the determining quantity.

Practically all current approaches to earthquake engineering analysis are straightforward applications and extensions of classical vibration and elasticity theory. The point of view taken herein is that the earthquake engineering phenomenon is a completely separate discipline in applied mechanics, just as elasticity and heat flow and others are separate fields. Therefore earthquake engineering has its own parameters, variables, constants, equations, invariants, and similar unique expressions.

A major corollary aim therefore was to uncover these quantities in the forms appropriate for earthquake engineering structural design purposes. It was expected that they might be different from the more familiar engineering terms and this is, in fact, the case.

In effect, it was assumed that insofar as earthquake engineering structural design was concerned, the fundamental engineering design method must find its source in the two sets of earthquake field (experimental) observables. These two basic sources of primary data which are the fountainheads of the methods described are

1. The accelerogram record.
2. The isoseismal (intensity) contour chart.

Invariants were looked for, these being quantities or relations that, *subject to the reality of the experimental accuracy*, appear to be approximately constant for all earthquakes, wherever and whenever they occur. Furthermore, these should be in a form that ultimately lends itself to structural engineering design applications — in as *simple* and *useful* a manner as possible — because engineers are practical workers in the market place and experience, over many years, indicates that the more complicated the analysis, the more suspect it is and the more likely it is to have errors and inconsistencies. Which is not to say that ‘simplicity’ itself is the be-all and end-all of analysis. However a reliance on physical reasoning (properly modified with engineering experience and intuition) does have a place in the more complicated engineering analyses, of which earthquake engineering surely is an outstanding example.

The situation being what it is in earthquake engineering, it was obvious that approximations of various orders were inevitable. But at some points the degrees of approximation would have to be tested, as indicated in the text.

The theory as developed and presented in the book is based upon field data, dimensional homogeneity, physical reasoning, and engineering experience and intuition. It assumes a ‘canonical’ form for the accelerogram (which many do, in fact, have approximately and those that do not can generally be represented by a superposition of canonical forms) and that isoseismal maps also may be

given in terms of canonical isoseismal maps (with circular contours) or in the case of clustered or sequential shocks as a summation of canonical isoseismal charts which corresponds to unsymmetrical isoseismal maps.

Following this the various parameters and invariants are utilized including (in addition to the basic accelerogram and isoseismal parameters) the magnitude of the earthquake M , the efficiency, η , and various temporal and spacewise energy variation terms.

All of these then converge naturally on, possibly, the most important of the parameters insofar as earthquake engineering is concerned, this being ϵ_f , the energy per unit area at any point on the surface of the earth in the earthquake field. The importance of this quantity becomes apparent when its position in the overall theory is examined; it is the key invariant quantity that binds together the temporal theory (as developed from the accelerogram record) and the spacewise theory (as developed from the isoseismal record). It is, in both theories, the surface energy per unit area, at a given intensity number regardless of how this intensity is generated. As such, it is a fundamental invariant term in any quantitative theory of damage or structural design and it is so used in the theories and applications throughout the previous chapters of the text.

Finally, and not the least important, there is the 'geology' which is related to focal depth as well as to the geology in a broad context and this is accounted for, at this time, by three different 'regions', \mathcal{R}_1 , \mathcal{R}_2 , and \mathcal{R}_3 . If more regions are needed, they can be introduced. This last, for example, might be the case for the effect of localized anomalous geological conditions which can be included without difficulty in the general theory, as shown, typically, in Chapter 10.

All of the above are shown on the different charts summarized in Chapter 4 and 5. There may be other charts that follow from the theory that will be useful in the design process but these will have to await the determination of actual numerical quantities for various earthquakes under different conditions, including the above noted 'anomalous geological conditions'.

Such an anomalous condition in fact appears to be involved in the very great damage and loss of life which occurred following the Sept. 19, 1985 earthquake in Mexico City. This earthquake, which is discussed in Section D of Chapter 10, occurred along the coast between Manzanillo and Acapulco. More than 3000 buildings in Central Mexico City were destroyed and more than 7000 people were killed. It is very likely that the major part of the building damage (which apparently occurred in a relatively small localized area) was caused by the particular sub-soil condition in the area in question. This would directly affect the accelerogram at the given location and would be further indicated by an anomalous isoseismal intensity region. In the present rational theory, the connection between $\Sigma(a\Delta t)_f - t_f$ -intensity and the geology is

accounted for in Figure 4.7 which — at this time — includes only the effects of the three major earthquake regions $\mathcal{R}_1, \mathcal{R}_2, \mathcal{R}_3$. Utilizing earthquakes similar to this Mexico City event as calibrators, it should be possible to correlate $\Sigma(a\Delta t)_f - t_f$ -intensity with particular geologies using the theory and methods described in Section D of Chapter 10.

To summarize, and in conclusion, it must be emphasized that

- a) even if the accelerograms are not canonical, they can almost always be represented by a superposition of canonical accelerograms and
- b) even if the isoseismal charts are not canonical (i.e., circular contours) they can almost always be represented by a superposition of canonical isoseismal maps

and for both (a) and (b) above the superposition corresponds to a physically reasonable superposition (i.e. cluster or sequence) of single 'canonical' shocks.

In other words, the assumptions of canonical accelerograms and isoseismal maps are not unreasonable from the engineering point of view. Also, the invariants which follow from the assumptions have been verified for a number of earthquakes that have occurred all over the world during the past 500 years. The energy relations (temporal and spacewise) also are physically and technologically reasonable and the entire development does then lead to a straightforward rational approximate design method which — when the design parameters have been firmly established — will enable the average engineering design office to design a structure for an earthquake loading with an acceptable degree of engineering accuracy and confidence using a procedure which includes all of the major earthquake engineering parameters that one should expect to be included in such a design. A similar statement applies for damage assessment analyses.

There will surely be some anomalous behaviours. There are 'renegade' phenomena in every field — unusual, unexpected, or unexplainable occurrences that are beyond the scope of known rational analyses. It can only be hoped that these will not occur or if they do that the design used will have a sufficient factor of safety to take care of any possible excessive stressing or tendency to fail. If they occur (and they almost certainly will occur because of localized pockets of special soil or geologic conditions. Note the previous discussion of the Mexico City, 1985 earthquake), the data they generate may be incorporated into the new theory and will thereby advance our understanding of the fundamental earthquake engineering processes.

In accordance with established engineering practice, code values may be assigned for the various terms considered, including factors of safety to account

for the inherent uncertainty of the available data, and the entire procedure can be programmed and used in consulting design offices.

The tabulations which follow compare earthquake engineering as developed herein with two of the familiar disciplines that are part of applied mechanics. The first, Table A.1, deals with a comparison of the theoretical formulations of earthquake engineering and linearized elasticity. In the Table, the correspondence is shown between the two sets of basic terms, equations, invariants, and similar quantities indicating the basic similarities and differences in the two formulations. In the second, Table A.2, a comparison is made between the application methods of the book's earthquake engineering theory and the application methods of a typical linearized elasticity (commonly called structural engineering) problem.

Table A.2 shows that a number of the design parameters must be assumed. Initially, the source of this data will be limited so that a greater burden will be placed upon the experience and judgement of the designing engineer. As more and more studies and designs are made, comparisons between design and actual behaviour will be possible and the code-field data bases will become more certain and more accurate for engineering use.

Table A.1 Comparison between the Theoretical Formulations of Linear Elasticity and Earthquake Engineering

| Theoretical Data Bases | Linear Elasticity | Earthquake Engineering |
|---|------------------------------|--|
| Basic measured quantities | Stress tensor | $\Sigma(a\Delta t)$, t (acceleration index, time) |
| | Strain tensor | $\Sigma(IS)$, S (intensity index, distance) |
| Restraints | Boundary conditions | Initial and final conditions |
| Measured experimental physical constants | E modulus of elasticity | \mathcal{P} the geology |
| | ν Poisson ratio | I the intensity S_f , $\Sigma(IS)_f$ t_f , $\Sigma(a\Delta t)_f$ |
| Compatibility conditions | In terms of strain or stress | ϵ_f vs. intensity curve |
| Equations connecting the basic quantities | Hooke's Law (invariant) | $\Sigma(a\Delta t)$ vs. t relation $\Sigma(IS)$ vs. S relation (invariants) |
| Other relations or equations | Equilibrium | Intensity vs. $\Sigma(a\Delta t)_f$, t_f , geology M vs $\Sigma(IS)_f$, S_f , geology |

Table A.2 Comparison between Application Methods of Earthquake Engineering and Ordinary Structural Engineering

| Design Data Bases | Ordinary Structural Engineering Design - Analysis | Earthquake Engineering Design - Analysis |
|--|--|--|
| Assumed known — code or specification data | Floor loadings, dimensions and materials, wind load, impact load and similar data | t_f = maximum time for canonical accelerogram a_{max} = maximum acceleration for canonical accelerogram M = magnitude of earthquake η = efficiency of earthquake \mathcal{R} = geology (depth of focus) S = location (and orientation of structure) δ = damping factor Dimensions and materials of structure |
| Known from experimental or field data or must be assumed | Allowable pile loads, soil conditions, allowable stresses for materials and similar data | ϵ_{t_f} -intensity relation (partly available) $M - \Sigma(IS)_f - S_f$ geology relation (experimental - partly available) $W/H - S/S_f$ relation (theoretical — available, to be verified) $\epsilon_t/\epsilon_{t_f} - t/t_f$ relations (theoretical — available, to be verified) Ae = effective area l = effective length |

INDEX

I — EARTHQUAKES REFERRED TO

Agadir, Morocco 56, 59, 73, 77, 80, 81, 83, 91
Al Asnam, Algeria (1980) 74, 79, 83
Alaska, Anchorage (1964) 74, 76, 83, 91
Alaska, Lituya Bay (1958) 179
Alaska, Shattered Peak (1964) 178, 179
Arboledos (1950) 59
Assam Earthquake (1897) 164, 167, 168

Bantarkawung (1971) 59
Benavente (1909) 59
Bengal Earthquake (1885) 160, 164
Bihar, Nepal Earthquake (1934) 164, 167, 169
Bucharest (1977) 33, 34, 44, 86, 87, 103, 114

Cacher Earthquake (1869) 164, 168
Cahar 167
Charleston (1886) 2, 59
Corinth (1981) 59, 73, 83

Dhubri Earthquake (1930) 164, 167, 169

El Alamo, Baja California (1956) 104, 116, 117

Faial (1926) 59
Friuli (1976) 52, 56, 58, 59

Gazli (1984), region of Soviet Union 233, 237, 238
Great Earthquake of 1897, Bangladesh 160, 164
Guatemala, Estancia De La Virgin (1976) 178, 179, 189
Guatemala, Guatemala (1976) 55, 74, 79, 83, 91, 127, 130, 131, 132
Guatemala, Rio Teocinte (1976) 178, 179

Hawke's Bay (1921) 59
Helena, Montana (1935) 104, 105, 116, 118

Imperial Valley (1940) 52, 59, 104, 106, 116, 119, 120
Indonesia 56

Khait, Soviet Union (1949) 179
Koyna (1967) 293

Lake behind a high dam 25
Lice (1975) 59, 73, 83, 246, 253, 254
Lima (1966) 33, 34, 42, 86, 87, 103, 113, 114
Lima, Peru (1970) 108, 110, 111, 112, 116, 123, 124, 125
Lisbon (1755) 59, 74, 81, 83
Long Valley Caldera, California 4, 14, 25

Madeira (1946) 59
Madjene (1969) 59
Managua, Nicaragua (1972) 74, 75, 83, 91, 104, 107, 116, 121
Messina (1908) 59, 74, 81, 83
Mexico (1985) xi, 59, 86, 114, 116, 156, 191, 193, 214, 308
Mt. Baldwin, Sierra Nevada (1980) 179

Nevados Huascarán, Peru (1970) 179
New Madrid (1811) 24, 25, 27
Noziriko 49

Olympia Washington (1949) 108, 109, 116, 122, 123
Orleanville (1954) 59, 73, 83

Parkfield (1988) 155, 156

Romania (1977) 39

S. Jorge (1757) 59, 73, 81, 83
S. Miguel (1522) 59
San Fernando (1971) 33, 34, 36, 43, 52, 56, 58, 59, 73, 80, 83, 86, 87, 103, 114
San Francisco (1906) 59, 73, 81, 83, 84
Santiago, Chile (1985) 74, 83, 91
Skopje, Yugoslavia (1963) 74, 77, 83, 91
Srimangal Earthquake (1918) 160, 164

Taft (1952) 33, 34, 41, 86, 87, 103, 114
Tangshan 57, 59, 73, 83
Tockaki-Oki (1968) 48
Tolmezzo (1976) 33, 34, 40, 86, 87, 103, 114

Udine (1873) 48, 49, 52, 58, 59
Under a Volcano 26

Valparaiso (1906) 59, 81, 83

Wairoa (1932) 59
Washington State (1872) 52, 59
Wewak (1946) 59

II — AUTHOR INDEX

Armbruster, J. 2
Austurias, J. 55
Ayala, J. 91, 126

Bakun, G. B. 73, 91
Bath, M. 56
Benioff, H. 4, 23
Berg, G. V. 91
Berlin, G. L. 56
Bolt, B. A. 23, 54
Bullen, K. E. 56

Chakraborti, P. 293
Chang, J. S. 91, 126
Chopra, A. K. 293

Degenkolb, H. 306
Donovan, N. C. 56

Espinosa, A. F. 48, 55, 132
Fairweather, V. 214
Fang, H. Y. 213
Fattal 39

Gayhart, E. L. 154
Gere, J. M. 57
Giorgetti, F. 56
Gupta, H. K. 293

Hari Narain 293
Harp, E. L. 214
Hoek, E. 171, 213

Idress, I. M. 39
Jumikis, A. R. 213, 214

Kamal Shahid, M. D. 160
Keefer, D. K. 170, 172, 213
Kerr, R. A. 23, 213, 306

Machado, F. 56
McLachlan, N. W. 154
Mott, N. F. 10, 23

National Academy of Sciences 56
Neumann, F. 56
Newmark, N. M. 2, 23, 45, 55, 91, 102, 154

Plafker, G. 214

Quesada, A. 55
 Ramirez, E. J. 56
 Rastogi, B. K. 293
 Richter, C. F. 45
 Rosenblueth, E. 2, 23, 45, 55, 91, 102, 154, 214
 Roussey, G. 100

Schuring, J. 170, 222
 Seeber, L. 2
 Shah, H. C. 57
 Shakid, M. K. 233
 Shakiel, S. M. 160, 233
 Steinbrugge, K. V. 56
 Stockton, W. 214
 Sullivan, W. 23, 213

Talimcioglu, N. M. 244

Wieczorek, G. F. 214
 Wiegel, R. L. 39, 56, 154
 Wilson, R. C. 214
 Winterkorn, H. F. 213

Zener, C. 154

III — TOPICS

Acceleration index 33
 frequencies of 30, 65, 88
 parallel representations 38
 record 135
 Accelerogram 29, 40
 canonical 29, 31, 36, 38, 47, 136, 196
 canonical curve 35
 period anomaly 192
 record ix, 307
 vertical 30
 Accelerograph record 38
 Actual length l' 141
 structure 141
 Added 'equivalent' structure 141
 Adobe construction 78, 79
 After-the-fact analyses xi
 experimental results 90
 Aftershocks 13, 76, 84
 Aleutian area 76
 Alpidic Belt 64, 79, 81
 Amplitude of vibration 144
 Analysis of building with an open, ground level, column-supported parking area 222
 Andesitic volcanic rocks 179

- Anomalous damage — loss of life in Central Mexico City 192
 - behaviours in Central Mexico City 207
 - devastation in the centre of Mexico City 195
 - geologies 88, 102
 - isoseismal intensity region 308
- Anti-symmetric 265
 - energy components 282
 - modes of vibration 278
- Anti-symmetrical loading 268
 - three-node 268
 - five-node 268
- Anti-symmetry 267, 269, 291, 292
- Application methods of a typical linearized elasticity problem 310
- Application methods of earthquake engineering theory 310
- Approximate analytical damage (intensive number) assessment procedures 133
- Approximate damage (intensity) estimates 135
- Area under the canonical accelerogram envelope 33
- Assessment-damage x, 29, 39, 48, 57, 61, 84
- Asymmetric isoseismal intensity chart 126
 - map 130
- Avalanche 179
- Average case or averageness requirement 192
- Average geology 30, 86, 92
 - region 96, 114
- Average of soil 53
 - typical structure 243
 - uni-material area of building 140
- Averageness xi
 - assumption and the Mexican earthquake 201

- Bangladesh Code 170
- Basic parameter for the canonical isoseismal analysis 50
- Beam elements 265
- Beam-girder-column structure 264
- Beam-type structure 265
- Belt-Alpide 64, 78, 81
 - circumpacific 64, 75
- Bending energy 152
 - response to the earthquake 265
 - strain energy 152, 220, 257
 - vibrational effects 266
- Bernoulli-Euler relation 229
- Border region fluid-solid 5
- Boundary layer 8
 - type solutions 23
- Boundary of stretched plate 24
- Building design (type of construction) 135
 - orientation 280
- Bukhara 234, 242

- Caldera 47
 - surface 15

- Calibration accuracy 304
 - process 72, 84
- California type earthquakes 75
- Canonical $\Sigma(I\dot{S})_f$ and S_f values 85
- Canonical accelerogram 29, 31, 36, 38, 47, 61, 136, 196
 - analyses 117
 - at a point 216
 - area under envelope 33
 - chart and parameters 63
 - curve 35
 - invariant 30, 31, 39
 - maximum effect 37
 - series (summation) of 136
 - superposed 87, 136, 280, 282
 - superposition theory for 30, 47
 - superposition of 100, 102, 196
- Canonical isoseismal equation 236
 - index or invariant 156
 - invariant 53, 69, 298
 - map 158, 308
 - parameters 165
 - and its parameters 45, 64, 92
 - chart 36, 47, 53, 55, 61, 64
 - map 48, 76, 84, 157
 - record 47
 - superposition of 49, 126, 166
- Catastrophic condition 235
 - damage 242
- Central Mexico City 308
- Central Mexico City geology 202
- Checking procedure for tall building 279
- Chile earthquakes 75
- Chopra 293, 294, 303, 304
- Circumpacific Belt 28, 64, 75, 76
- Cluster of earthquake effects 76
 - separate point-focus shocks 50
- Cluster or sequence of shocks 100, 114
- Clustered earthquakes 126
- Clusters and sequence earthquakes 115
- Code 279, 281, 309
- Code method 245
- Code models 164
- Code requirements 136
 - earthquake 244
 - empirical 245
 - makers 135, 138
 - Turkish 244, 246, 259, 263
- Column elements 265
 - fixity table 218, 231
- Combined bending, normal and shear energy 221
- Compatibility condition-stress 11
- Concentrated machine parts 280

- Concrete dam earthquake analysis 215, 293
- Concrete frame-reinforced 244
- Conservation of energy 92, 292
- Constant intensity region 48
 - section structure 266
- Contour chart ix
 - maps-isoseismal 79, 100
- Coordinate-similarity 8, 13
- Crack-fatigue 10
- Cracking behaviour 303
- Cracks 8
- Critical frequency 148
 - stress 14
- Crushing failure 227
- Crystallized magma 17, 19
 - band of 18

- Damage and energy 193
- Damage assessment x, 29, 39, 48, 57, 61, 84
 - analyses 37, 309
- Damage criterion 30
- Damage in Central Mexico City 202
- Damage to the Konya dam 296
- Damage zones 160
- Damage-probable 135
- Damping 139, 257, 273, 277, 280
 - factor 284, 291
 - mechanism 144, 220
 - of a structure 154
 - of the model 153
 - of the prototype 153
 - of vibrational building oscillations due to an earthquake 144
 - ratio 148
- Dead material-volume of 12
 - region of 17
- Deep earthquakes 4
- Deflection equilibrium 271
- Deflection of the frame 259
- Deflections 273, 284, 290
- Deformation of the vibrating structure 273
- Defusing an earthquake 23
- Depth of earthquake focus 166
- Depth of focus 30, 99, 264
- Depth-focal 61, 65, 78, 92, 93, 96, 102, 113
- Design accelerogram 279
 - engineers 135
 - parameters 310
 - procedures for a tall building 279
 - structural x, 84
- Design-analysis of dams 304
- Design-analysis process 48
- Details of connections 291

- Devastation of Central Mexico City 197
- Dilated rock mass 187
- Dilation and resulting stability criteria 171
- Dilation of rock mass 174
 - by seismic energy 175
 - uniform 186
- Dimensional homogeneity 51, 307
- Direction of the energy shock 135
- Dissipation of energy 291
- Dissipation of energy from a vibrating structure 144
- Distance from epicentre 135, 136
- Distributed shock 50
- Division of energy 275
 - strain 270
- Dynamic energy 275
- Dynamic mechanical energy St. Venant principle 208
 - scaling requirements 148

- Earthquake 'code' 244
 - design parameters 245
 - efficiency 183
- Earthquake engineering analysis of a building with an open, ground level, column-supported parking area 215
 - a low to intermediate height beam-column-girder energy absorbing structure 215
 - a low to intermediate height beam-girder-column energy absorbing structure 244
 - a short, squat shear-type structure 215, 233
 - a tall building 215
 - the supports for an offshore platform structure 215
- Earthquake engineering and applied mechanics 306
- Earthquake engineering of high structure 264
 - research institute 116
 - uniqueness of 138
- Earthquake induced modulus of rupture stresses 299
 - intensity vs horizontal surface energy 90, 240
 - magnitude decrement vs d/r 96
- Earthquake magnitudes 279
 - behaviour and parameters 14
 - Caldera type 24
 - Chile 75
 - clustered 126
 - deep 4
 - defusing an 23
 - energy of 11, 21, 26
 - energy released 19
 - events 23
 - focus of the 264
 - lifetime of 17
 - magnitude of 21, 26, 27, 63, 78, 79, 92, 113, 135, 216, 264
 - mechanism 47
 - plains type 24
 - prediction of 23
 - shock 29

- single point focus 50
- single shock 29, 126
- superposed 127
- swarms of 18
- tectonic 2, 24, 27
- the mechanism x
- triggering an 23
- Earthquakes-code zones of Bangladesh 155, 159
- Effective area 137, 265, 275
 - base area 139, 140
 - intensity in Central Mexico City 205
 - length 139, 140, 147, 275, 283, 292, 293
 - length of structure 265
 - 'actual length' effect 147
 - stiffness EI 275
- Efficiency 36, 54, 89, 92, 93
 - of earthquake 62
 - vs d/r vs v_s/v_p 95
- Efficiency-focal depth analysis 94
- El Alamo Quake accelerogram 104
- El Salvador 79
- Elastic requirements 148
- Elasticity theory-California type 75
 - linear 13
 - surface fault 126
- Empirical code 245
 - period of vibration relation 145
- Energy about major and minor axes 137
 - absorbing details 291
 - expressions 276
 - field produced by an earthquake 48
 - in ergs, of earthquake at the focus 62
 - compatibility relation 89
 - division of 275
 - dynamic 275
 - intensity compatibility relation 61, 88, 126
 - intensity curve 193
 - kinetic (vibratory) 219
 - lost in fracturing 13
 - of earthquakes 11
 - potential (strain) 219
 - quasi-static component of 275
 - shear 275
 - strain 92, 133, 257, 271, 275
 - vibratory 272
 - loss in the vibration cycle 145
 - lost per cycle 153
 - magnification in Central Mexico City 203
 - of underground atomic blast 213
 - released by ruptured plate 26
 - sink 206, 207
- Engineering design tools 61

- Experience and intuition 307
- Epicentre-distance from 135, 136
- Equilibrium-deflection 271
 - statistical force 271
- Equivalence of an underground atomic blast to an underground earthquake 213
- Equivalent area method 225
 - base area 139, 140, 142, 154
 - distributed mass 280
 - length 139, 140, 145, 154, 292
 - length (height) of the building 141
 - series of separate concentrated earthquakes 156
- Erupting volcanos 24
- Estancia De La Virgin Rock Avalanche 178

- Factor of safety 309
- Failure or shattering stress 225
- Fatigue crack 10
- Faults-local 84
- Field data 307
- First chart 71, 77, 78, 79
 - region-magnitude relationship 83
 - revised form 81
- Fixity factor 231
 - range 218
 - intermediate values 218
- Focal depth 61, 65, 78, 92, 93, 96, 102, 113
- Focus of the earthquake 264
- Footing area 234
- Foundation area 142
- Four earthquake types 26
- Four modes 267, 273
- Fracture 7, 8
 - region 17
 - energy lost 13
 - stress 13
 - velocity of 7, 9
- Fractured phenomena 6
- Frame elements 265
- Free-free beam 142, 265
 - frequency solution 273
 - section 267
 - vibration 279
 - modes of vibration 150
 - structure 291
 - vibrating uniform beam 273
 - vibration solution 275
- Frequencies of the accelerations 30, 65, 88
- Frequency analysis 266
 - equation 150
- Frequency of lateral vibration 148
 - the accelerogram record 102
 - vibration 153

- Froude members 147
- Full-fixity type moment connections 217
- Fundamental parameters 36, 86
 - of canonical accelerogram 30, 35, 86
- Gazli 234, 242
- Generalized tensors and matrices 56
- Geological conditions 37, 53, 54
 - profile 17
 - region 136, 216
 - survey of India 164
- Geologies anomalous 88, 102
 - 'average' '86
 - non-average regional 102
- Geology 264
 - effect 93
 - of a region 64, 102, 135
- Geometric requirements 148
- Geophysical Institute of Lima 110
- Girder elements 265
- Governing agency 281
- Gradually applied load 271, 273
- Gravity dam 293
- Grillage of steel beams 217
- Ground acceleration-horizontal 30
- Ground energy-timewise variation 30
 - vertical 30
- Ground surface energy compatibility relation 166
 - movements 28
- Growth curve 35, 53
- Gupta 293, 294

- Helena earthquake accelerogram 104, 105
- High building 140
- High rise building 264
 - condominiums 79
- Higher order effects 282
- Honduras 79
- Honolulu Tsunami Centre 75
- Horizontal ground accelerations 30
 - plate movements 77
 - rupture failure 47
 - surface energy 183

- Imperial county services building 306
- India meteorological department 164
- Inertia effects 146
 - loading on structure 140
- Infinite slope method 172
- Instability-plate rupture x
- Insurers 135, 138
- Intensity contour scale 45

- Intensity damage- $\Sigma(a\Delta t)_f - t_f$ chart 136
- Intensity index 50
 - number 50, 72
 - MM 48, 88
- Intensity- $\Sigma(a\Delta t)_f - t_f$ -geology chart 61, 86
- Intensity- $\Sigma(a\Delta t)_f - t_f$ chart 211
 - canonical accelerogram-geology chart 135
 - energy compatibility relations 156
 - ground energy compatibility 114
 - ground energy correlation curve 135
 - horizontal surface energy compatibility relations 239
 - quantitative measure of 88
- Intermediate beam and girder and column buildings 140
 - values of fixity 218
- Internal friction 145
- Invariant 38, 307
 - of the canonical earthquake accelerogram 33
 - of the canonical representation 51
 - relation 29, 135
 - canonical 39
- Isoseismal contour chart ix
 - (intensity) contour chart 45, 304
 - contour maps 100
 - contours 79
- Isoseismal map 77, 78
 - asymmetric 130
 - canonical 48, 76, 84, 157, 158
 - theoretical predicted 155
 - unsymmetrical 308
- Isoseismal superposition procedures 156
- Isoseisms 237, 238

- Kinetic (vibratory) energy 219
 - energy 133, 257
- Koyna dam 293, 294, 295, 298, 303

- Lake-bed area of Central Mexico City 195
- Landslides-during an earthquake 190
 - rockslides stability mechanics 172
- Landslides/rockslides-four generic types 171
- Lapped intensity regions 127
- Lateral deflection of structure 140
 - vibration damping 153
 - frequency of 148
 - wave (vibratory wave) characteristics of the building 147
- Layer-boundary 8
- Layered intensity regions 127
- Length-of-time effect 139, 154
 - for tall buildings 142
- Linear elasticity theory 13
- Load acting on base of building 140
- Loading on the dam 298

- Local anomalous features 166
 - faults 84
 - geological conditions 86
 - intensity-compatibility-damage 100
 - soil or geological conditions 37
- Localized anomalous geological conditions 308
 - dilation in the vicinity of the failure surface 175
 - dilation of the slope 186
 - pockets of special soil or geologic conditions 309
- Long Valley Caldera in California 14, 17, 21, 22
- Los Amates 127
- Low seismicity region 64
- Low, squat (shear) structure 275
- Lumped mass 222

- $M - \Sigma(IS)_f - S_f$ correlation 136
- Mach number 146
- Magnitude 93
 - chart 156
 - of earthquake 23, 54, 63, 72, 78, 79, 135, 216, 264
- Magnitude- $\Sigma(IS)_f - S_f$ -geology chart 61, 70, 73, 82, 135
 - average geology chart- $\Sigma(IS)_f - S_f$ 210
 - intensity-distance (MID) relation 156
 - intensity-distance (MID) chart 61, 84, 135
 - region relationship 73
 - richter 74, 75, 79
- Major mode of vibration 220
- Masonry material 234
 - structures 78
- Material-superplastic-type x
- Maximum allowable stress (modulus of rupture or yield stress) of the structure 147
 - canonical accelerogram effect 37
 - deflected position 277
 - deflection 279
 - dynamic energy 277
 - earthquake magnitude 27
 - member end moments 260
 - member shears 261
 - moment 262
 - oscillation 273
 - shears and moments 284, 288
 - strain energy 277
 - stress 262
 - stress and deflection condition 279
 - failure 280
 - stress in the structure 148
 - stress induced in the structure 147
 - velocity 277
- Mechanism 19
 - application of 14
- M_{eff} 96
- Mercalli (MM) scale 137

- Methods-rational xii
- MID 281, 298, 304
 - chart 85, 136, 137, 224, 254
 - contour chart 210
 - diagrams 236
- Mini-quakes 24
- MM intensity 48, 51
- Model prototype relations 139
 - scaling xi
 - scaling requirements 146
 - testing of structures 146
- Modes of vibration 272
- Modified mercalli (MM) intensity number 88
 - scale (MM) 45, 133
- Modulus of rupture (or yield stress) 148, 153, 230
- Molten magma-sphere 17, 18, 19
 - chamber 14
- Moment diagram 259
 - distribution 257
- Monitoring underground atomic blasts 208
- Monoliths 295
- Motagua fault 127
- Mountain region 65, 102
- Movements-ground surface 28
- Multifault slippages 100

- Node locations 265
 - positions 273
- Nodes 273
- Non-overflow section of the dam 299
- Non-structural applications 155
 - of the rational theory 155

- Packed rock mass 187
- Pacoima dam 35
- Parabolic area relation 136
- Parallel acceleration index representations 38
- Period magnification in Central Mexico City 206
 - of localized effect 143, 267
 - of overall effect 143, 267, 270, 272
 - of the building 141
 - of transition 143, 149, 267, 269
 - of vibration for structure 202
 - of vibration equation of the free-free beam 292
- Permafrost 178
- Phase transition 4
 - change 13
- Phenomena-fracture 6
- Physical (r, t) plane 7
 - profile 17
 - reasoning 307
 - variables 36, 53

- Pile supported offshore structure 216
- Plains region 65, 102
- Plane 10, 16, 17
 - membranes-rupture instability 23
 - strain structural analysis 298
- Plate and membrane theories 16
 - rupture instability x
- Platform structure 221
- Poisson ratio effect 9
- Potential (inertia) load 152
 - (strain) energy 219
- Predicability of earthquakes 115
- Predicted isoseismal field 156
- Prediction of a possible earthquake 23
- Prince William Sound 76
- Principal mode frequency 292
 - shape 292
 - periods 265
- Probable damage 135

- Quantitative connections between the earthquake and the rockslide 191
 - measure of intensity 88
 - structural design parameters 160
- Quasi-static loading 271
 - component of energy 275

- Ratio of compressibility effect to inertia effects 146
 - effects 146, 154
 - surface wave effects to inertial effects 147
- Rational analysis 92
 - analysis of the seismic zones 165
 - earthquake mechanism 22
 - method of structural analysis 36, 54
- Rational methods xii, 245
 - of damage assessment 54
 - solution 259
 - theories in earthquake engineering 45
- Region of dead material 17
 - diminished damage 205
 - superplasticity 5
 - mountain 65
 - plains 65
 - surface fault 65
 - the low seismicity 64
- Reinforced concrete column 225
 - frame 244
- Resurgent dome 17
- Revised form of first chart 81
- Reynolds number 146
- Richter magnitudes 74, 75, 79
- Richter scale 23

- Richter-Guttenberg equation 26
- Rigid body platform 220
 - horizontal deflection 257
- Rock avalanche data 177
- Rock mass properties 182
 - dilated 187
 - packed 187
 - weathered and fractured 182
- Rock slope stability 155, 170
- Rockslide 80
- Rockslides-during an earthquake 190
- Rockslides/landslides-four generic types 171
- Rotational slump/rock fall avalanche 180
- Rupture instability-of plane membranes 23
 - of solids 23
 - velocity 14
 - failure 47
 - instability 18
 - selfsustaining 18
- Ruptured area 5
- Ruptured plate-energy released by 26
- Rural building 234

- San Andreas fault 156
- Scaling parameter 146
- Scaling requirements for the tall structures 146
 - model prototype xi
- Sea-bed horizontal energy 220
 - energy inputs 218
- Secondary faulting 127
 - stresses 221
- Seismic activity code 160
 - factor of safety 189
 - slope stability 171
 - surface energy 170
 - zones of Bangladesh 163
- Sequence of earthquake effects 76
 - series shocks 87
- Series (summation) of canonical accelerograms 136
- Severity of shaking 306
- Shaking machine 148
- Shallower focus 47
 - rockslides 186
- Shattering condition 225, 235
 - failure in compression 230
 - stress 225
- Shear and bending energy 152
- Shear bending wave transmission characteristics of the building 147
 - deflection 147
 - energy 152, 275
 - force diagram 259
 - plus bending strain energy 257

- responders 265
- strain energy 239, 241, 257
- strength (ϕ) reduction due to dilation 176
- translation 149
- wall 233
- wave 269
 - effects 266
 - velocity of 140, 149, 269
- Shearing force 239
- Sheartype structure-short, squat 234
- Shock-clusters 35
- Short, squat buildings 140
 - structures 265, 284
- Short-pulse earthquake loading 147
- Similarity coordinate 8, 13, 17
 - mechanism-selfsustaining 24
 - solution x , 24
 - solutions in the engineering, physical-chemical, biological-medical and social sciences 39, 56
 - transformation 13
- Simple tension-compression 221
- Single canonical accelerogram 282
 - point-focus earthquake 50
 - shock 136
 - shock earthquake 29, 126
- Skew-symmetrical 267
 - energy 270
 - modes 270
- Slope stability analysis 172
- Slowly applied load 271
- Soil foundation interaction 135, 141, 142, 292
 - effect 283, 291
 - interaction damping 293
 - structure interaction 145
 - substructure interaction 144, 153
- Solids-rupture instability of 23
- Spacewise distribution of energy 47
 - theory 308
 - variation of energy over the entire field 61, 65
 - variation of SHE 54
- Specifications 279, 281
- St. Venant Principle 209
 - for dynamic loading phenomena 213
- Static stability of rock slopes 171
- Statistical force equilibrium 271
- Strain energy 92, 133, 257, 271, 275
 - absorbed by the structure 147
 - in the column 228
 - in the structure 148
 - stored 24
- Strain-division of 270
- Stress compatibility condition 10

- critical 14
- failure or shattering 225
- selfsustaining (continual) 17
- tearing 7
- Stretched plate-boundary of 24
- Structural analysis for combinations of specified earthquakes 126
 - applications for the rational theory 215
 - design x, 84
 - analysis 39
 - charts and curves 61
 - engineering design applications 307
 - problems 57
 - procedure 36
- Subsurface soil 145
- Successive shocks 35
- Suddenly applied load 271
- Superplastic 5
 - type material x, 13
- Superplasticity-region of 5
- Superposed accelerogram-damage correlation 113
 - canonical accelerograms 87, 136, 280, 282
 - earthquakes 127
- Superposition assumptions 91
 - hypothesis for canonical isoseismal maps 50
 - of canonical isoseismal contour maps 126
- Superposition of canonical isoseismal maps 49, 166, 191, 309
 - canonical accelerograms 100, 102, 196
 - canonical isoseismals 294
 - effects 279, 290
 - energy 158
 - single canonical shocks 309
 - theories for the canonical accelerograms and the canonical isoseismal charts 47
 - theory for canonical accelerograms 30
- Surface energy per unit area 308
 - horizontal 183
 - vertical 183
- Surface fault earthquakes 126
 - region 65, 102
 - slippages 127
- Surface horizontal energy 93
 - per unit area 31
- Surface rupture earthquake 156
- Surface verticle energy 93
- Symmetric 265, 267
 - energy components 282
 - modes of vibration 278
- Symmetrical energy 270
 - two node 268
 - four node 268
 - loading 268
 - modes 270
 - principal mode period 292

- Symmetry 265, 269, 291, 292
- Tall building 140
- Tearing stress 7, 13
- Tectonic earthquakes 2, 24, 27
- Temporal and spacewise variations of surface horizontal energy 265
 - theory 308
 - variation of energy per unit area at a point 61, 65
- Tensile cracking 303
 - fracture stress 17
 - rupture instability 18, 24
- Theoretical predicted isoseismal map 155
- Theoretical, rational method of earthquake engineering analysis 263
- Theoretical formulations of earthquake engineering and linearized elasticity 310
- Thickness on the assumed localized dilation zone 187
- Three-region classification 64
- Three-shock analysis 197, 200
- Time-loading history of the earthquake load 147
 - history response for a tall structure 265
- Timewise distribution of energy 47
 - variation of ground energy 30
 - variation of SHE at a point 37
- Total dead load and live load 264
 - deformation of dilated zone 188
 - energy application 282
 - energy supplied to the structure by the earthquake 147, 148
 - focal earthquake energy 36
 - surface horizontal energy 38, 39
- Transformation-similarity 13
- Transition-phase 4
- Translation and rotation of the actual foundation 145
 - rotation effect at the soil foundation junction 141
- Triangular inertia loading 270
- Triggering an earthquake 23
- Truss box support structure 221
- Turkish code 244
 - earthquake code 246, 259, 263
- Twelve (12) point Soviet scale 242
- Two mode solution 267
- Two-node mode 279
- Two-shock analysis 200
- Typical design-analysis structural application for a tall building 281
- Typical structural analysis 282

- U.K. Institute of Geological Sciences 164
- U.S. Geological Survey 164
- U.S. Coast and Geodetic Survey 164
- Underground atomic blast 156, 209
 - energy of 213
- Uni-material analysis 265
 - concrete structure 283

- structure 275
- Uniform dilation of the entire slide mass 175
 - of the rock mass 186
- Uniqueness of earthquake engineering 138
 - existence hypothesis 33, 35, 53
- University of Chile Seismology Institute 75
- Unsymmetrical isoseismal maps 308
 - load 268
- Unsymmetry 267, 269, 291

- Velocity of shearwave 140, 149, 269
 - small disturbances 14, 17
 - fracture 7, 9
 - maximum 277
 - plane 9
 - rupture 10, 14
 - sound 9, 14, 142
- Vertical accelerograms 30
 - ground energy 30
 - support piles 217
 - support truss box 217
 - surface energy 183
- Vibrating building 141
 - dam 298
 - strain energy 272
 - structure-deformation of 273
 - amplitude of 144
 - modes of 272
- Vibratory energy 272
 - inertial loading 153
- Viscous effects 146
- Volume of dead material 12
 - related partition of earthquake energy 93

- Wave-transmission characteristics 267
- Weathered and fractured rock mass 182
- Worst case approximate intensity 136

- Zero strain energy 277
 - deflection positions 275
- Zonal regions of Bangladesh 165

